

# Density Model for Sei Whale (*Balaenoptera borealis*) for the U.S. East Coast: Supplementary Report

## Model Version 10.1

Duke University Marine Geospatial Ecology Laboratory\*

2023-05-27


## Citation

When citing our methodology or results generally, please cite Roberts et al. (2016, 2023). The complete references appear at the end of this document. We are preparing a new article for a peer-reviewed journal that will eventually replace those. Until that is published, those are the best general citations.

When citing this model specifically, please use this reference:

Roberts JJ, Yack TM, Cañadas A, Fujioka E, Halpin PN, Barco SG, Boisseau O, Chavez-Rosales S, Cole TVN, Cotter MP, Cummings EW, Davis GE, DiGiovanni Jr. RA, Garrison LP, Gowan TA, Jackson KA, Kenney RD, Khan CB, Lockhart GG, Lomac-MacNair KS, McAlarney RJ, McLellan WA, Mullin KD, Nowacek DP, O'Brien O, Pabst DA, Palka DL, Quintana-Rizzo E, Redfern JV, Rickard ME, White M, Whitt AD, Zoidis AM (2022) Density Model for Sei Whale (*Balaenoptera borealis*) for the U.S. East Coast, Version 10.1, 2023-05-27, and Supplementary Report. Marine Geospatial Ecology Laboratory, Duke University, Durham, North Carolina.

## Copyright and License

 This document and the accompanying results are © 2023 by the Duke University Marine Geospatial Ecology Laboratory and are licensed under a [Creative Commons Attribution 4.0 International License](https://creativecommons.org/licenses/by/4.0/).

## Model Version History

---

| Version | Date       | Description  |
|---------|------------|--|
| 1       | 2013-05-08 | Initial version with climatological predictor variables. |

---

---

\*For questions or to offer feedback please contact Jason Roberts ([jason.roberts@duke.edu](mailto:jason.roberts@duke.edu)) and Tina Yack ([tina.yack@duke.edu](mailto:tina.yack@duke.edu))

(continued)

| Version | Date       | Description   |
|---------|------------|---|
| 2       | 2014-03-01 | Reformulated density model using a Horvitz-Thompson estimator. Eliminated GAM for group size (consequence of above). Added group size as a candidate covariate in detection functions (benefit of above). Added survey ID as a candidate covariate in NOAA NARWSS detection functions. Took more care in selecting right-truncation distances. Fitted models with contemporaneous predictors, for comparison to climatological. Switched SST and SST fronts predictors from NOAA Pathfinder to GHRSSST CMC0.2deg L4. Changed SST fronts algorithm to use Canny operator instead of Cayula-Cornillon. Switched winds predictors from SCOW to CCMP (SCOW only gives climatol. estimates.) Added DistToEddy predictors, based on Chelton et al. (2011) eddy database. Added cumulative VGPM predictors, summing productivity for 45, 90, and 180 days. Added North Atlantic Oscillation (NAO) predictor; included 3 and 6 month lags. Transformed predictors more carefully, to better minimize leverage of outliers. Implemented hybrid hierarchical-forward / exhaustive model selection procedure. Model selection procedure better avoids concurvity between predictors. Allowed GAMs to select between multiple formulations of dynamic predictors. Adjusted land mask to eliminate additional estuaries and hard-to-predict cells. |
| 3       | 2014-05-20 | Fixed bug in temporal variability plots. Density models unchanged.  |
| 4       | 2014-06-02 | Added Reclassification of Ambiguous Sightings section, which was accidentally omitted. Density models unchanged.  |
| 5       | 2015-01-17 | TODO: Describe changes.   |
| 6       | 2015-01-18 | Switched back to a four season model, using seasons from version 4.   |
| 6.1     | 2015-01-19 | Restricted Fall season model to the surveyed area of the northeast.   |
| 6.2     | 2015-03-06 | Updated the documentation. No changes to the model.   |
| 6.3     | 2015-05-14 | Updated calculation of CVs. Switched density rasters to logarithmic breaks. No changes to the model.  |
| 6.4     | 2015-09-28 | Updated the documentation. No changes to the model.   |
| 6.5     | 2016-04-21 | Switched calculation of monthly 5% and 95% confidence interval rasters to the method used to produce the year-round rasters. (We intended this to happen in version 6.3 but I did not implement it properly.) Updated the monthly CV rasters to have value 0 where we assumed the species was absent, consistent with the year-round CV raster. No changes to the other (non-zero) CV values, the mean abundance rasters, or the model itself. Model files released as supplementary information to Roberts et al. (2016).  |
| 7       | 2017-06-01 | Began update to Roberts et al. (2015) model. Introduced new surveys from AMAPPS, NARWSS, UNCW, VAMSC, and the SEUS NARW teams. Updated modeling methodology. Refitted detection functions and spatial models from scratch using new and reprocessed covariates. Switched to two-season spatial model. This version of the model was released to the Navy and federal agencies in fall of 2017. Model released as part of a scheduled update to the U.S. Navy Marine Species Density Database (NMSDD).   |
| 8       | 2018-04-22 | Discovered that model version 7 erroneously excluded ambiguous "fin or sei whale" sightings classified as sei whales. Refitted the models with them included. The resulting models and spatial predictions were very similar. Total summer abundance rose only 1% but CV dropped from 0.098 to 0.091. Model released as part of a scheduled update to the U.S. Navy Marine Species Density Database (NMSDD).  |
| 9       | 2022-02-10 | Unreleased experimental model.  |

*(continued)*

---

| Version | Date       | Description  |
|---------|------------|--|
| 10      | 2022-06-20 | This model is a major update over the prior version, with substantial additional data, improved statistical methods, and an increased spatial resolution. It was released as part of the final delivery of the U.S. Navy Marine Species Density Database (NMSDD) for the Atlantic Fleet Testing and Training (AFTT) Phase IV Environmental Impact Statement. Several new collaborators joined and contributed survey data: New York State Department of Environmental Conservation, TetraTech, HDR, and Marine Conservation Research. We incorporated additional surveys from all continuing and new collaborators through the end of 2020. (Because some environmental covariates were only available through 2019, certain models only extend through 2019.) We increased the spatial resolution to 5 km and, at NOAA's request, we extended the model further inshore from New York through Maine. We reformulated and refitted all detection functions and spatial models. We updated all environmental covariates to newer products, when available, and added several covariates to the set of candidates. For models that incorporated dynamic covariates, we estimated model uncertainty using a new method that accounts for both model parameter error and temporal variability. |
| 10.1    | 2023-05-27 | Completed the supplementary report documenting the details of this model. Corrected the 5 and 95 percent rasters so that they contain the value 0 where the taxon was assumed absent, rather than NoData. Nothing else was changed.  |

---

# 1 Survey Data

We built most of this model from data collected between 1998-2020 (Table 1, Figure 1). In keeping with our primary strategy for the 2022 modeling cycle, we excluded data prior to 1998 in order to utilize biological covariates derived from satellite ocean color observations, which were only available for a few months before 1998. We restricted the model to survey transects with sea states of Beaufort 5 or less (for a few surveys we used Beaufort 4 or less) for both aerial and shipboard surveys. We also excluded transects with poor weather or visibility for surveys that reported those conditions.

For the winter model for the region covering the Blake Plateau and off-shelf waters south of the north wall of the Gulf Stream, we expanded the temporal range back to the winter of 1991/92 in order to include the wintertime NOAA SEFSC OT-92 shipboard survey, which reported three “Bryde’s or sei whale” sightings. Rosel et al. (2021) investigated the extant evidence for Bryde’s whales along the U.S. east coast and concluded that “Overall, the evidence to date indicates Bryde’s whales are extremely rare in U.S. waters of the western North Atlantic.” They pointed out that passive acoustic monitoring has not recorded whale call types associated with any type of Bryde’s whale along the East Coast, but sei whales have been regularly recorded. Therefore, for the 2022 modeling cycle, we treated the ambiguous sightings reported by OT-92 as sei whales and not Bryde’s whales. Lacking any definitive sightings of Bryde’s whale, we considered the species absent from U.S. east coast waters and retired the Roberts et al. (2016) model for the species.

Table 1: Survey effort and observations considered for this model. Effort is tallied as the cumulative length of on-effort transects. Observations are the number of groups and individuals encountered while on effort. Off effort observations and those lacking an estimate of group size or distance to the group were excluded.

| Institution              | Program             | Period             | Effort       | Observations |              |                 |
|--------------------------|---------------------|--------------------|--------------|--------------|--------------|-----------------|
|                          |                     |                    | 1000s km     | Groups       | Individuals  | Mean Group Size |
| <b>Aerial Surveys</b>    |                     |                    |              |              |              |                 |
| HDR                      | Navy Norfolk Canyon | 2018-2019          | 11           | 3            | 4            | 1.3             |
| NEAq                     | CNM                 | 2017-2020          | 2            | 2            | 3            | 1.5             |
| NEAq                     | MMS-WEA             | 2017-2020          | 37           | 21           | 54           | 2.6             |
| NEAq                     | NLPSC               | 2011-2015          | 43           | 22           | 35           | 1.6             |
| NEFSC                    | AMAPPS              | 2010-2019          | 89           | 17           | 28           | 1.6             |
| NEFSC                    | NARWSS              | 2003-2020          | 484          | 1,245        | 3,204        | 2.6             |
| NEFSC                    | Pre-AMAPPS          | 1999-2008          | 46           | 9            | 11           | 1.2             |
| NJDEP                    | NJEBS               | 2008-2009          | 11           | 0            | 0            |                 |
| NYS-DEC/TT               | NYBWM               | 2017-2020          | 77           | 2            | 7            | 3.5             |
| SEFSC                    | AMAPPS              | 2010-2020          | 114          | 0            | 0            |                 |
| SEFSC                    | MATS                | 2002-2005          | 27           | 0            | 0            |                 |
| UNCW                     | MidA Bottlenose     | 2002-2002          | 17           | 0            | 0            |                 |
| UNCW                     | Navy Cape Hatteras  | 2011-2017          | 34           | 0            | 0            |                 |
| UNCW                     | Navy Jacksonville   | 2009-2017          | 92           | 0            | 0            |                 |
| UNCW                     | Navy Norfolk Canyon | 2015-2017          | 14           | 0            | 0            |                 |
| UNCW                     | Navy Onslow Bay     | 2007-2011          | 49           | 0            | 0            |                 |
| UNCW                     | SEUS NARW EWS       | 2005-2008          | 114          | 0            | 0            |                 |
| VAMSC                    | MD DNR WEA          | 2013-2015          | 16           | 0            | 0            |                 |
| VAMSC                    | Navy VACAPES        | 2016-2017          | 19           | 0            | 0            |                 |
| VAMSC                    | VA CZM WEA          | 2012-2015          | 21           | 0            | 0            |                 |
|                          |                     | <b>Total</b>       | <b>1,319</b> | <b>1,321</b> | <b>3,346</b> | <b>2.5</b>      |
| <b>Shipboard Surveys</b> |                     |                    |              |              |              |                 |
| MCR                      | SOTW Visual         | 2012-2019          | 9            | 6            | 10           | 1.7             |
| NEFSC                    | AMAPPS              | 2011-2016          | 16           | 18           | 23           | 1.3             |
| NEFSC                    | Pre-AMAPPS          | 1998-2007          | 14           | 7            | 10           | 1.4             |
| NJDEP                    | NJEBS               | 2008-2009          | 14           | 0            | 0            |                 |
| SEFSC                    | AMAPPS              | 2011-2016          | 17           | 0            | 0            |                 |
| SEFSC                    | Pre-AMAPPS          | 1992-2006          | 33           | 3            | 5            | 1.7             |
|                          |                     | <b>Total</b>       | <b>101</b>   | <b>34</b>    | <b>48</b>    | <b>1.4</b>      |
|                          |                     | <b>Grand Total</b> | <b>1,420</b> | <b>1,355</b> | <b>3,394</b> | <b>2.5</b>      |

Table 2: Institutions that contributed surveys used in this model.

| Institution | Full Name  |
|-------------|--|
| HDR         | HDR, Inc.  |
| MCR         | Marine Conservation Research   |
| NEAq        | New England Aquarium   |
| NEFSC       | NOAA Northeast Fisheries Science Center                                      |
| NJDEP       | New Jersey Department of Environmental Protection                            |
| NYS-DEC/TT  | New York State Department of Environmental Conservation and Tetra Tech, Inc. |
| SEFSC       | NOAA Southeast Fisheries Science Center                                      |
| UNCW        | University of North Carolina Wilmington                                      |
| VAMSC       | Virginia Aquarium & Marine Science Center                                    |

Table 3: Descriptions and references for survey programs used in this model.

| Program             | Description   | References  |
|---------------------|---|---|
| AMAPPS              | Atlantic Marine Assessment Program for Protected Species                                | Palka et al. (2017), Palka et al. (2021)                        |
| CNM                 | Northeast Canyons Marine National Monument Aerial Surveys                               | Redfern et al. (2021)   |
| MATS                | Mid-Atlantic Tursiops Surveys   |   |
| MD DNR WEA          | Aerial Surveys of the Maryland Wind Energy Area   | Barco et al. (2015)   |
| MidA Bottlenose     | Mid-Atlantic Onshore/Offshore Bottlenose Dolphin Surveys                                | Torres et al. (2005)  |
| MMS-WEA             | Marine Mammal Surveys of the MA and RI Wind Energy Areas                                | Quintana-Rizzo et al. (2021), O'Brien et al. (2022)             |
| NARWSS              | North Atlantic Right Whale Sighting Surveys   | Cole et al. (2007)  |
| Navy Cape Hatteras  | Aerial Surveys of the Navy's Cape Hatteras Study Area                                   | McLellan et al. (2018)  |
| Navy Jacksonville   | Aerial Surveys of the Navy's Jacksonville Study Area                                    | Foley et al. (2019)   |
| Navy Norfolk Canyon | Aerial Surveys of the Navy's Norfolk Canyon Study Area                                  | Cotter (2019), McAlarney et al. (2018)                          |
| Navy Onslow Bay     | Aerial Surveys of the Navy's Onslow Bay Study Area                                      | Read et al. (2014)  |
| Navy VACAPES        | Aerial Survey Baseline Monitoring in the Continental Shelf Region of the VACAPES OPAREA | Mallette et al. (2017)  |
| NJEBS               | New Jersey Ecological Baseline Study  | Geo-Marine, Inc. (2010), Whitt et al. (2015)                    |
| NLPSC               | Northeast Large Pelagic Survey Collaborative Aerial Surveys                             | Leiter et al. (2017), Stone et al. (2017)                       |
| NYBWM               | New York Bight Whale Monitoring Surveys   | Zoidis et al. (2021)  |
| Pre-AMAPPS          | Pre-AMAPPS Marine Mammal Abundance Surveys  | Mullin and Fulling (2003), Garrison et al. (2010), Palka (2006) |
| SEUS NARW EWS       | Southeast U.S. Right Whale Early Warning System Surveys                                 |   |
| SOTW Visual         | R/V Song of the Whale Visual Surveys  | Ryan et al. (2013)  |
| VA CZM WEA          | Virginia CZM Wind Energy Area Surveys   | Mallette et al. (2014), Mallette et al. (2015)                  |

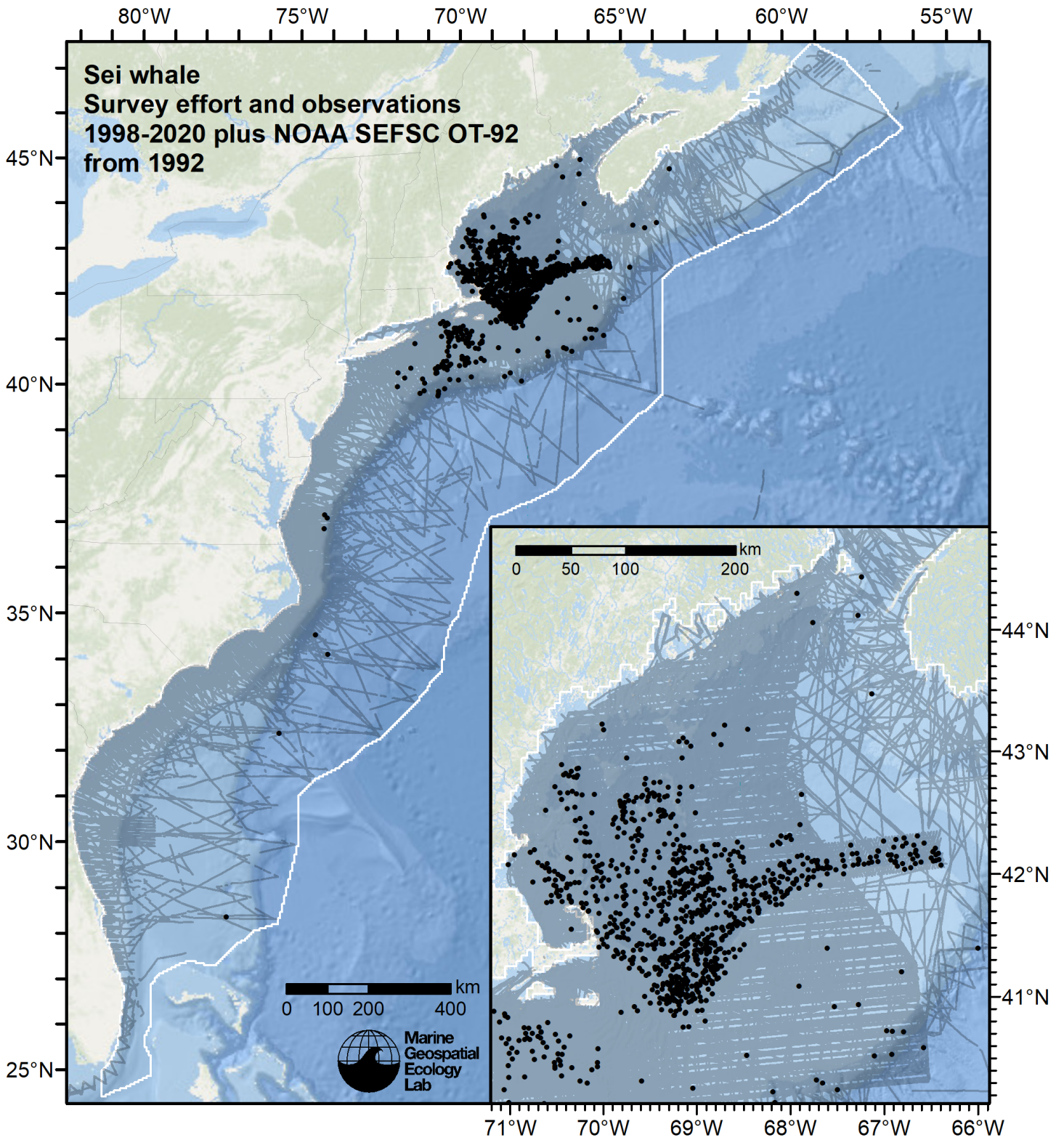


Figure 1: Survey effort and sei whale observations available for density modeling, after detection functions were applied, and excluded segments and truncated observations were removed.

## 2 Classification of Ambiguous Sightings

Observers occasionally experience difficulty identifying species, due to poor sighting conditions or phenotypic similarities between the possible choices. For example, observers may not always be able to distinguish fin whales from sei whales due their similar size and shape. When this happens, observers will report an ambiguous identification, such as “fin or sei whale”. In our density models, we handled ambiguous identifications in three ways:

1. For sightings with very generic identifications such as “large whale”, we discarded the sightings. These sightings represented a clear minority when compared to those with definitive species identifications, but they are uncounted animals and our density models may therefore underestimate density to some degree.
2. For sightings of certain taxa in which a large majority of identifications were ambiguous (e.g. “unidentified pilot whale”) rather than specific (e.g. “short-finned pilot whale” or “long-finned pilot whale”), it was not tractable to model the individual species so we modeled the generic taxon instead.
3. For sightings that reported an ambiguous identification of two species (e.g. “fin or sei whale”) that are known to exhibit different habitat preferences or typically occur in different group sizes, and for which we had sufficient number of definitive sightings of both species, we first fitted a predictive model that classified the ambiguous sightings into one species or the other and then included the resulting classified sightings in the density models for each of the two species.

This section describes how we classified the third category of ambiguous sightings reported as “Fin or sei whale” into one species or the other.

For the predictive model, we used the cforest classifier (Hothorn et al. 2006), an elaboration of the classic random forest classifier (Breiman 2001). First, we trained a binary classifier using the sightings that reported definitive species identifications (“fin whale” and “sei whale”). To increase the range of sampling of the classification model’s covariates, the training data may have included additional surveys not considered for the density model, as well as transects from outside the spatial and temporal extents of the density model. Only on-effort sightings were used. We used the species ID as the response variable and environmental variables as covariates.

We used receiver operating characteristic (ROC) curve analysis to select a threshold for classifying the probabilistic predictions of species identifications made by the model into a binary result of one species or another. For the classification threshold, we selected the value that maximized the Youden index (Perkins and Schisterman 2006). Then, for all sightings reporting the ambiguous identification, we classified each as either one species or the other by processing the covariate values observed for it through the fitted model. We then included the classified sightings in the detection functions and density models. The sightings reported elsewhere in this document incorporate both the definitive sightings and the classified sightings, unless otherwise noted.

### 2.1 Classification Model

MODEL SUMMARY:

=====

Random Forest using Conditional Inference Trees

Number of trees: 1000

Response: factor(OriginalScientificName)

Inputs: ClimChl, ClimDistToFront063, ClimeKE, ClimMnkEpi, ClimPP\_CAFE, ClimSST\_CMC, ClimTKE, DayOfYear, Depth, DistTo300m, DistToShore, Slope

Number of observations: 4256

Number of variables tried at each split: 5

Estimated predictor variable importance (conditional = FALSE):

Importance

ClimMnkEpi 0.03845

DayOfYear 0.03699

ClimSST\_CMC 0.03159

ClimPP\_CAFE 0.01901  
ClimEKE 0.01862  
Depth 0.01456  
DistToShore 0.01381  
DistTo300m 0.01144  
ClimChl 0.01138  
ClimDistToFront063 0.00799  
Slope 0.00751  
ClimTKE 0.00736

MODEL PERFORMANCE SUMMARY:

=====

Statistics calculated from the training data.

Area under the ROC curve (auc) = 0.949  
Mean cross-entropy (mxe) = 0.310  
Precision-recall break-even point (prbe) = 0.922  
Root-mean square error (rmse) = 0.307

User-specified cutoff = 0.565

Confusion matrix for that cutoff:

|                                 | Actual Balaenoptera physalus | Actual Balaenoptera borealis | Total |
|---------------------------------|------------------------------|------------------------------|-------|
| Predicted Balaenoptera physalus | 2823                         | 239                          | 3062  |
| Predicted Balaenoptera borealis | 240                          | 954                          | 1194  |
| Total                           | 3063                         | 1193                         | 4256  |

Model performance statistics for that cutoff:

Accuracy (acc) = 0.887  
Error rate (err) = 0.113  
Rate of positive predictions (rpp) = 0.719  
Rate of negative predictions (rnp) = 0.281  
  
True positive rate (tpr, or sensitivity) = 0.922  
False positive rate (fpr, or fallout) = 0.200  
True negative rate (tnr, or specificity) = 0.800  
False negative rate (fnr, or miss) = 0.078  
  
Positive prediction value (ppv, or precision) = 0.922  
Negative prediction value (npv) = 0.799  
Prediction-conditioned fallout (pcfall) = 0.078  
Prediction-conditioned miss (pcmiss) = 0.201  
  
Matthews correlation coefficient (mcc) = 0.721  
Odds ratio (odds) = 46.952  
SAR = 0.714  
  
Cohen's kappa (K) = 0.721



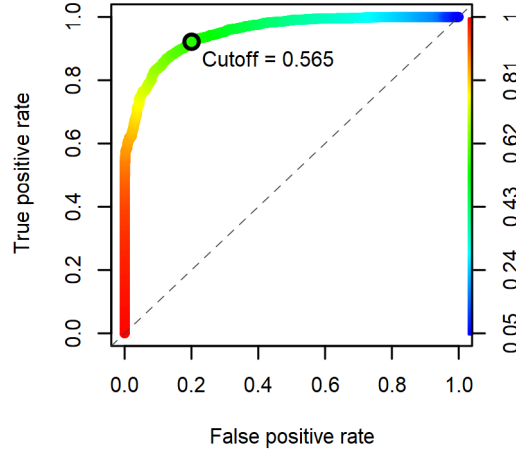


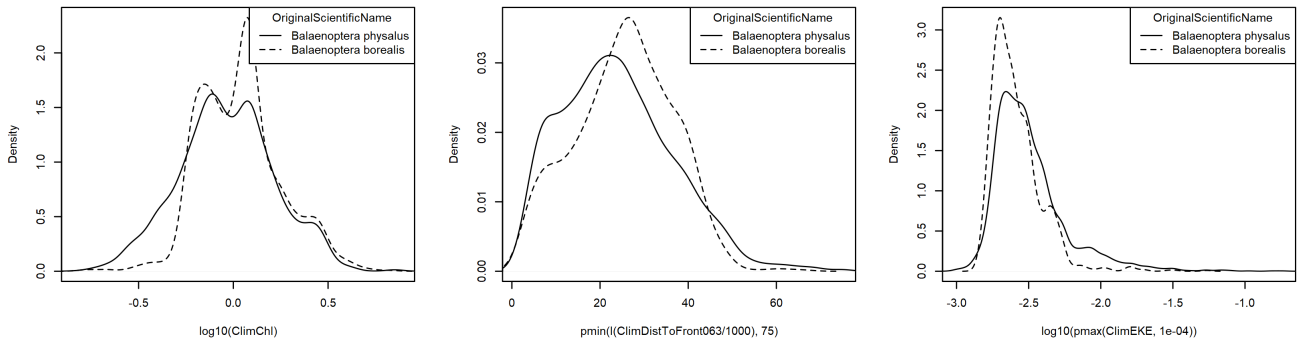
Figure 2: Receiver operating characteristic (ROC) curve summarizing the predictive performance of the ambiguous sighting classification model.

Table 4: Covariates used in the ambiguous sighting classification model.

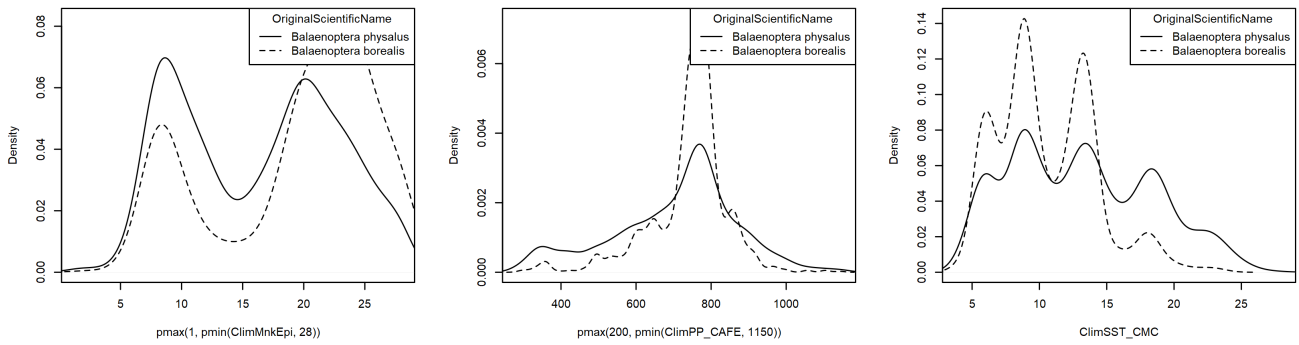
| Covariate          | Description  |
|--------------------|--|
| ClimChl            | Climatological monthly mean chlorophyll a concentration ( $\text{mg m}^{-3}$ ) from Copernicus GlobColour (Garnesson et al. (2019)), provided by E.U. Copernicus Marine Service (product OCEANCOLOUR_GLO_CHL_L4_REP_OBSERVATIONS_009_082)  |
| ClimDistToFront063 | Climatological monthly mean distance (km) to the closest sea surface temperature front detected in daily GHRSSST Level 4 CMC0.2deg and CMC0.1deg images (Brasnett (2008); Canada Meteorological Center (2012); Meissner et al. (2016); Canada Meteorological Center (2016)) with MGET’s implementation of the Canny edge detector (Roberts et al. (2010); Canny (1986))                                      |
| ClimEKE            | Climatological monthly mean eddy kinetic energy ( $\text{m}^2 \text{s}^{-2}$ ) derived from Aviso Ssalto/Duacs global gridded L4 reprocessed geostrophic currents, produced and distributed by E.U. Copernicus Marine Service. doi: <a href="https://doi.org/10.48670/moi-00148">10.48670/moi-00148</a>  |
| ClimMnkEpi         | Climatological monthly mean micronekton biomass available in the epipelagic zone, expressed as wet weight ( $\text{g m}^{-2}$ ), from SEAPODYM (Lehodey et al. (2008); Lehodey et al. (2015)), provided by E.U. Copernicus Marine Service. doi: <a href="https://doi.org/10.48670/moi-00020">10.48670/moi-00020</a> . Computed as the sum of the SEAPODYM mnkc_epi, mnkc_mumeso, and mnkc_hmlmeso variables. |
| ClimPP_CAFE        | Climatological monthly mean net primary productivity ( $\text{mg C m}^{-2} \text{day}^{-1}$ ) from the Carbon, Absorption, and Fluorescence Euphotic-resolving (CAFE) model (Silsbe et al. (2016))   |
| ClimSST_CMC        | Climatological monthly mean sea surface temperature ( $^{\circ}\text{C}$ ) from GHRSSST Level 4 CMC0.2deg and CMC0.1deg (Brasnett (2008); Canada Meteorological Center (2012); Meissner et al. (2016); Canada Meteorological Center (2016))  |
| ClimTKE            | Climatological monthly mean total kinetic energy ( $\text{m}^2 \text{s}^{-2}$ ) derived from Aviso Ssalto/Duacs global gridded L4 reprocessed geostrophic currents, produced and distributed by E.U. Copernicus Marine Service. doi: <a href="https://doi.org/10.48670/moi-00148">10.48670/moi-00148</a>   |
| DayOfYear          | Days elapsed since the start of the year   |
| Depth              | Depth (m) of the seafloor, from SRTM30_PLUS (Becker et al. (2009))   |
| DistTo300m         | Distance (km) to the 300m isobath, derived from SRTM30_PLUS (Becker et al. (2009))   |
| DistToShore        | Distance (km) to shore excluding Bermuda and Sable Island, derived from SRTM30_PLUS (Becker et al. (2009))   |

Table 4: Covariates used in the ambiguous sighting classification model. (*continued*)

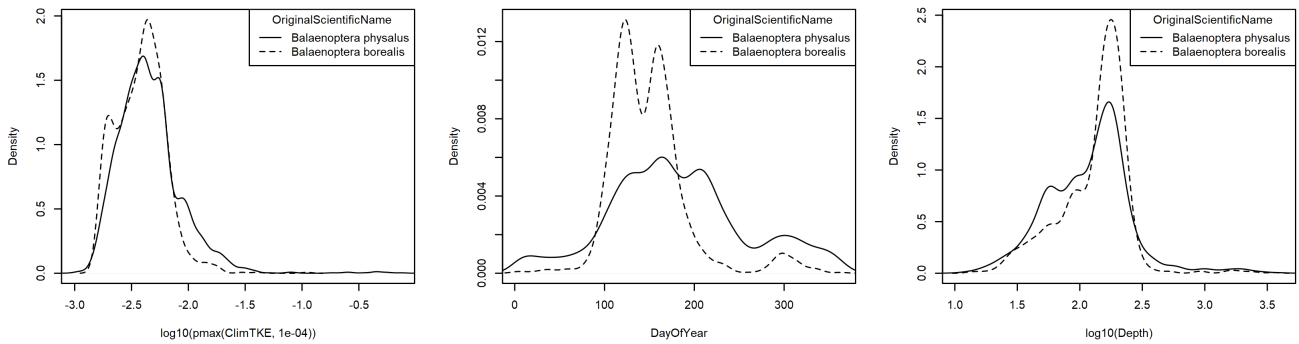
| Covariate | Description   |
|-----------|---|
| Slope     | Slope (percent rise) of the seafloor, derived from SRTM30_PLUS (Becker et al. (2009)) |



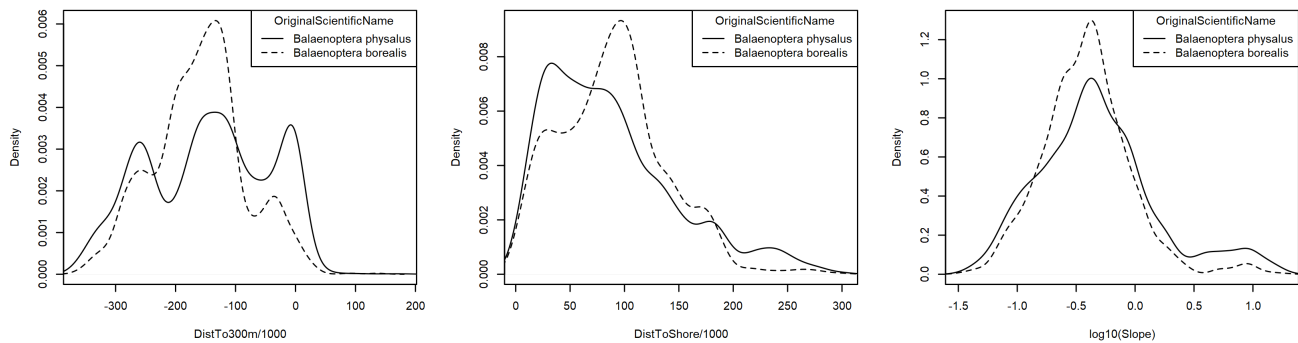
(a) Chlorophyll a concentration (mg m<sup>-3</sup>) (b) Climatological distance to SST front (km) (c) Climatological eddy kinetic energy (m<sup>2</sup> s<sup>-2</sup>)



(d) Climatological epipelagic micronekton biomass (g m<sup>-2</sup>) (e) Climatological net primary productivity (mg C m<sup>-2</sup> day<sup>-1</sup>) (CAFE model) (f) Climatological sea surface temperature (°C)



(g) Climatological total kinetic energy (m<sup>2</sup> s<sup>-2</sup>) (h) Day of year (i) Seafloor depth (m)



(j) Distance to 300m isobath (km) (k) Distance to shore (km) (l) Seafloor slope (percent rise)

Figure 3: Density histograms showing the per-species distribution of each covariate in the ambiguous sighting classification model. When a covariate exhibits a substantially different distribution for each species, it is a good candidate for differentiating the species. Transforms and other treatments are indicated in axis labels.  $\log_{10}$  indicates the covariate was  $\log_{10}$  transformed.  $\text{pmax}$  and  $\text{pmin}$  indicate the covariate's minimum and maximum values, respectively, were Winsorized to the values shown.  $/1000$  indicates meters were transformed to kilometers for interpretation convenience.

## 2.2 Classifications Performed

Table 5: Summary of the definitive sightings used to train the classification model, the ambiguous sightings to which the model was applied, and their resulting classifications. To increase the range of sampling of the classification model’s covariates, the training data may have included additional surveys not considered for the density model, as well as transects from outside the spatial and temporal extents of the density model. Only on-effort sightings were used.

| Institution              | Program             | Definitive   |              |            | Classified  |             |
|--------------------------|---------------------|--------------|--------------|------------|-------------|-------------|
|                          |                     | B. physalus  | B. borealis  | Ambiguous  | B. physalus | B. borealis |
| <b>Aerial Surveys</b>    |                     |              |              |            |             |             |
| FWRI                     | SEUS NARW EWS       | 3            | 0            | 0          | 0           | 0           |
| HDR                      | Navy Norfolk Canyon | 32           | 6            | 0          | 0           | 0           |
| NEAq                     | CNM                 | 16           | 2            | 0          | 0           | 0           |
| NEAq                     | MMS-WEA             | 51           | 24           | 6          | 4           | 2           |
| NEAq                     | NLPSC               | 68           | 21           | 10         | 9           | 1           |
| NEFSC                    | AMAPPS              | 110          | 15           | 29         | 26          | 3           |
| NEFSC                    | NARWSS              | 1,972        | 1,086        | 663        | 398         | 265         |
| NEFSC                    | Pre-AMAPPS          | 208          | 8            | 39         | 37          | 2           |
| NJDEP                    | NJEBS               | 1            | 0            | 0          | 0           | 0           |
| NYS-DEC/TT               | NYBWM               | 161          | 3            | 0          | 0           | 0           |
| SEFSC                    | AMAPPS              | 36           | 0            | 0          | 0           | 0           |
| SEFSC                    | MATS                | 6            | 0            | 0          | 0           | 0           |
| UNCW                     | MidA Bottlenose     | 1            | 0            | 0          | 0           | 0           |
| UNCW                     | Navy Cape Hatteras  | 9            | 0            | 0          | 0           | 0           |
| UNCW                     | Navy Norfolk Canyon | 9            | 0            | 0          | 0           | 0           |
| UNCW                     | Navy Onslow Bay     | 1            | 0            | 0          | 0           | 0           |
| UNCW                     | SEUS NARW EWS       | 12           | 0            | 0          | 0           | 0           |
| VAMSC                    | MD DNR WEA          | 16           | 0            | 0          | 0           | 0           |
| VAMSC                    | Navy VACAPES        | 1            | 0            | 0          | 0           | 0           |
| VAMSC                    | VA CZM WEA          | 11           | 0            | 0          | 0           | 0           |
| WLT/SSA/CMARI            | SEUS NARW EWS       | 2            | 0            | 0          | 0           | 0           |
|                          | <b>Total</b>        | <b>2,726</b> | <b>1,165</b> | <b>747</b> | <b>474</b>  | <b>273</b>  |
| <b>Shipboard Surveys</b> |                     |              |              |            |             |             |
| MCR                      | SOTW Visual         | 5            | 2            | 0          | 0           | 0           |
| NEFSC                    | AMAPPS              | 219          | 16           | 50         | 48          | 2           |
| NEFSC                    | Pre-AMAPPS          | 69           | 10           | 96         | 96          | 0           |
| NJDEP                    | NJEBS               | 26           | 0            | 0          | 0           | 0           |
| SEFSC                    | AMAPPS              | 7            | 0            | 0          | 0           | 0           |
| SEFSC                    | Pre-AMAPPS          | 11           | 0            | 0          | 0           | 0           |
|                          | <b>Total</b>        | <b>337</b>   | <b>28</b>    | <b>146</b> | <b>144</b>  | <b>2</b>    |
|                          | <b>Grand Total</b>  | <b>3,063</b> | <b>1,193</b> | <b>893</b> | <b>618</b>  | <b>275</b>  |

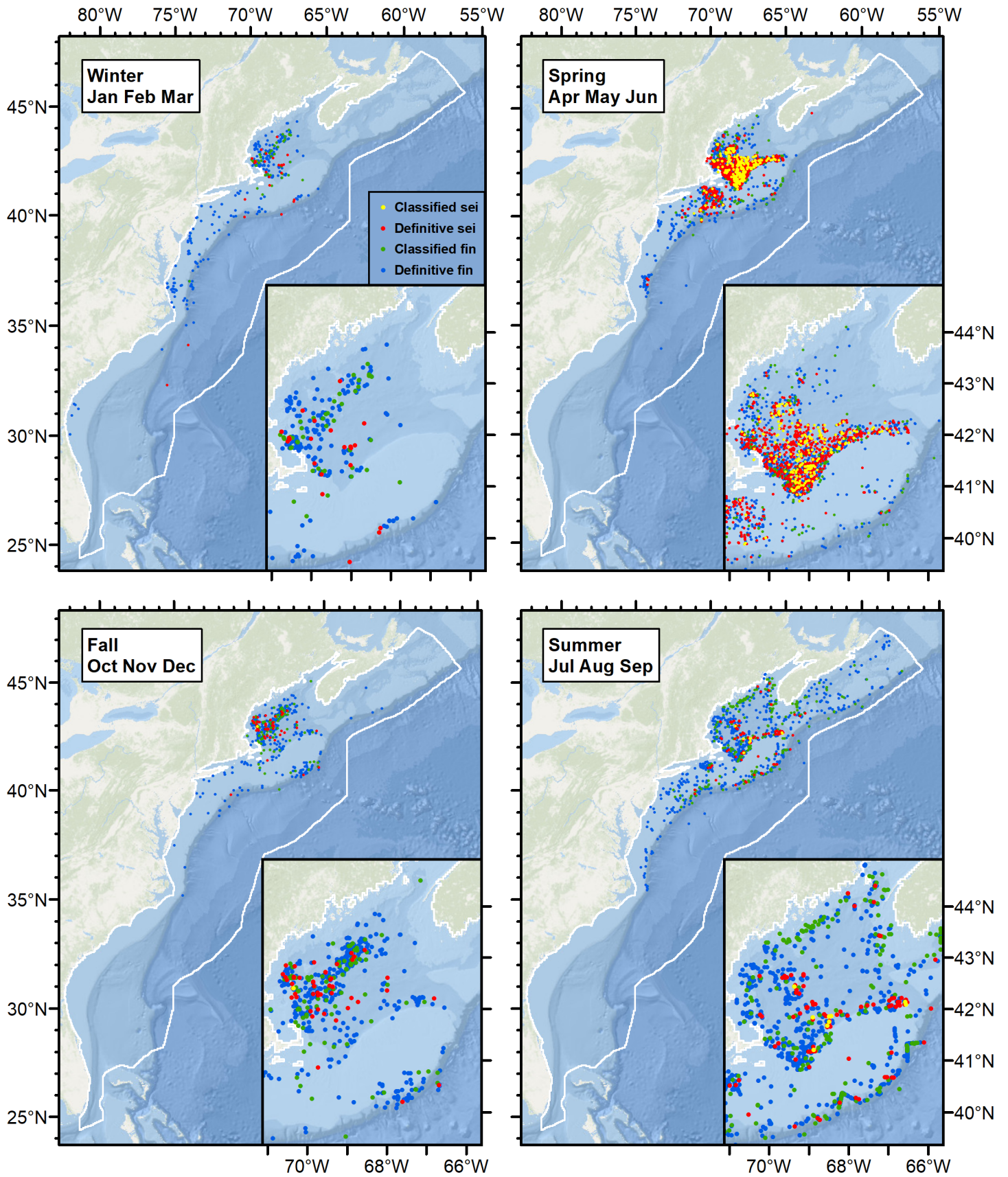


Figure 4: Definitive sightings used to train the model and ambiguous sightings classified by the model.

## 3 Detection Functions

### 3.1 With a Taxonomic Covariate

We fitted the detection functions in this section to pools of species with similar detectability characteristics and used the taxonomic identification as a covariate (ScientificName) to account for differences between them. We consulted the literature and observer teams to determine appropriate poolings. We usually employed this approach to boost the counts of observations in the detection functions, which increased the chance that other covariates such as Beaufort sea state could be used to account for differences in observing conditions. When defining the taxonomic covariate, we sometimes had too few observations of species to allocate each of them their own level of the covariate and had to group them together, again consulting the literature and observers for advice on species similarity. Also, when species were observed frequently enough to be allocated their own levels but statistical tests indicated no significant difference between the levels, we usually grouped them together into a single level.

### 3.1.1 Large Whales

#### 3.1.1.1 Aerial Surveys

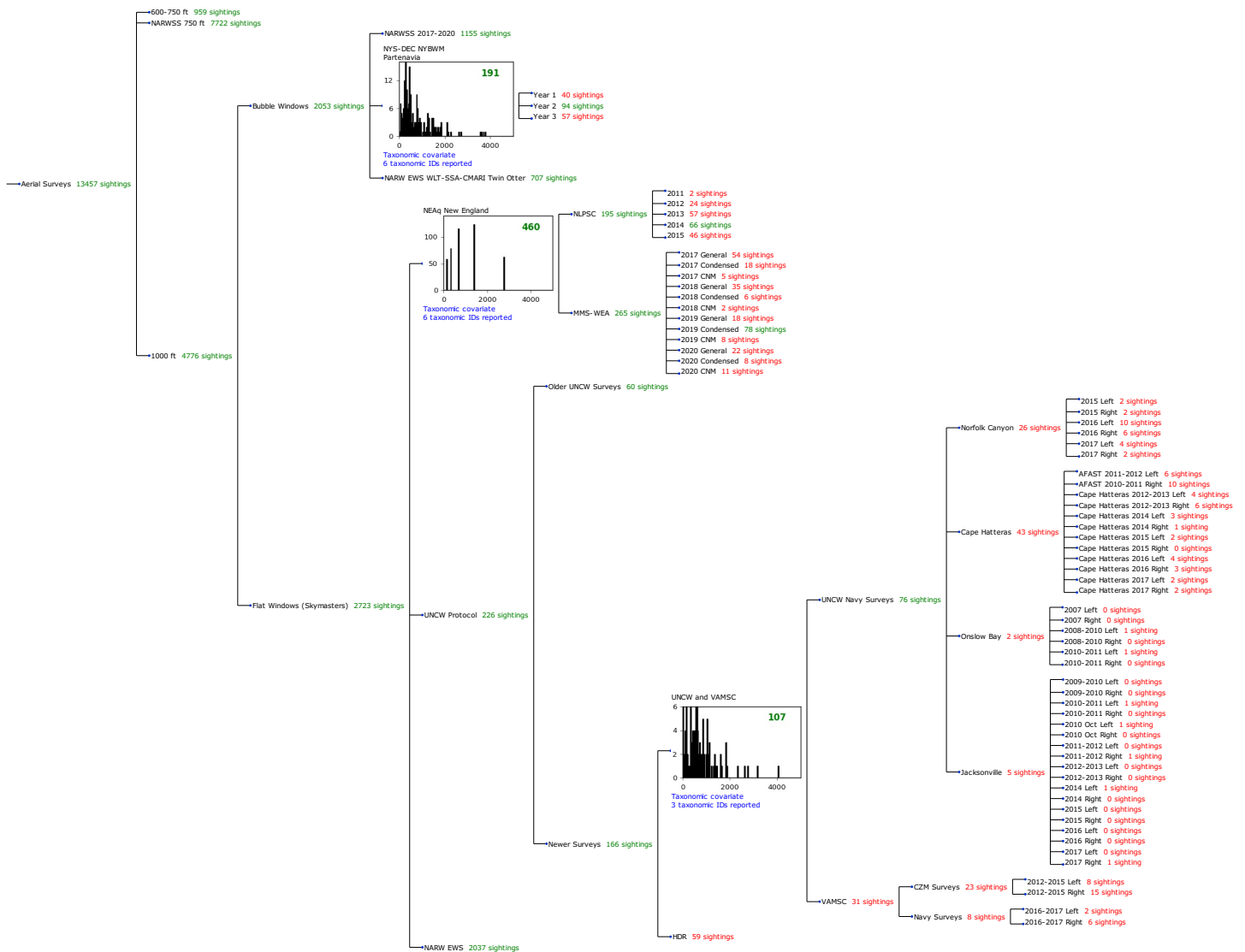


Figure 5: Detection hierarchy for aerial surveys, showing how they were pooled during detectability modeling, for detection functions that pooled multiple taxa and used a taxonomic covariate to account for differences between them. Each histogram represents a detection function and summarizes the perpendicular distances of observations that were pooled to fit it, prior to truncation. Observation counts, also prior to truncation, are shown in green when they met the recommendation of Buckland et al. (2001) that detection functions utilize at least 60 sightings, and red otherwise. For rare taxa, it was not always possible to meet this recommendation, yielding higher statistical uncertainty. During the spatial modeling stage of the analysis, effective strip widths were computed for each survey using the closest detection function above it in the hierarchy (i.e. moving from right to left in the figure). Surveys that do not have a detection function above them in this figure were either addressed by a detection function presented in a different section of this report, or were omitted from the analysis.

##### 3.1.1.1.1 NYS-DEC NYBWM Partenavia

After right-truncating observations greater than 2100 m and left-truncating observations less than 125 m (Figure 7), we fitted the detection function to the 172 observations that remained (Table 6). The selected detection function (Figure 6) used a hazard rate key function with OriginalScientificName (Figure 8), Season (Figure 9) and SurveyID (Figure 10) as covariates.

Table 6: Observations used to fit the NYS-DEC NYBWM Partenavia detection function.

| ScientificName         | n          |
|------------------------|------------|
| Balaenoptera borealis  | 2          |
| Balaenoptera musculus  | 2          |
| Balaenoptera physalus  | 82         |
| Eubalaena glacialis    | 12         |
| Megaptera novaeangliae | 57         |
| Physeter macrocephalus | 17         |
| <b>Total</b>           | <b>172</b> |

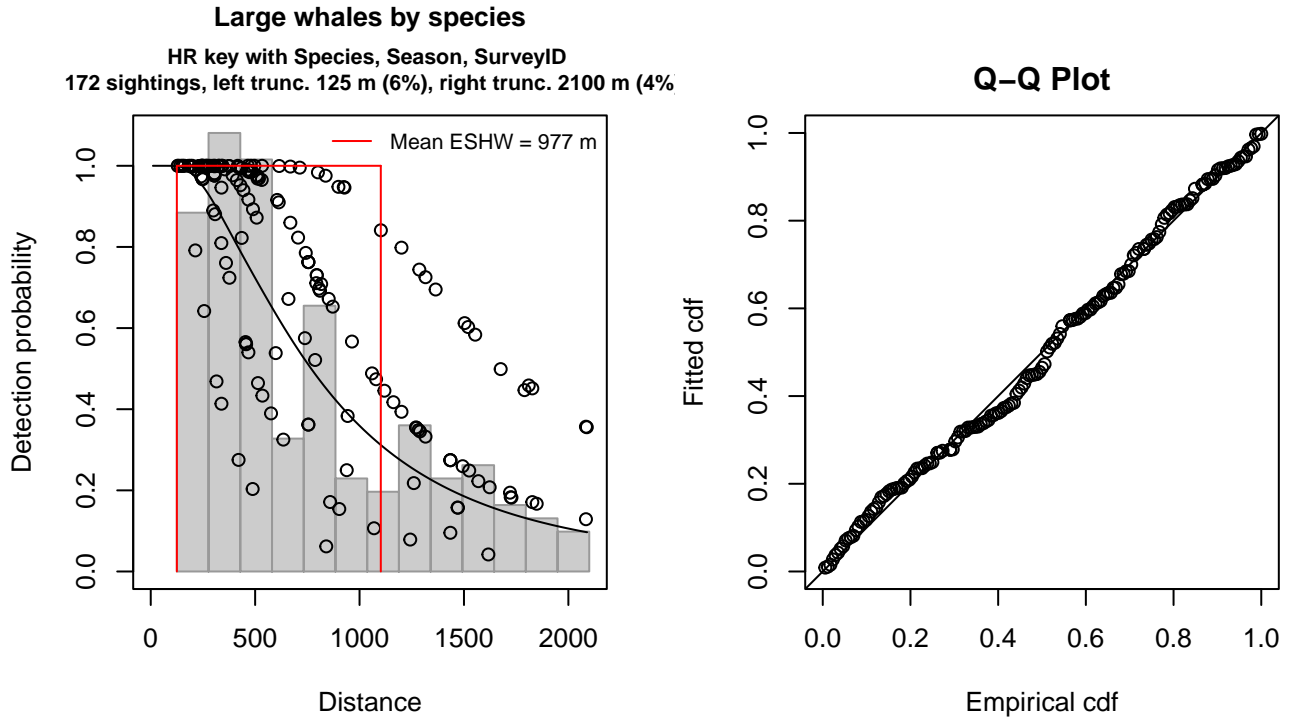


Figure 6: NYS-DEC NYBWM Partenavia detection function and Q-Q plot showing its goodness of fit.

Statistical output for this detection function:

Summary for ds object

Number of observations : 172  
 Distance range : 125 - 2100  
 AIC : 2521.205

Detection function:

Hazard-rate key function

Detection function parameters

Scale coefficient(s):

|                                       | estimate  | se        |
|---------------------------------------|-----------|-----------|
| (Intercept)                           | 5.5563867 | 0.3693793 |
| OriginalScientificNameHumpback, Right | 0.4977955 | 0.2125828 |
| SeasonSpring                          | 0.7279337 | 0.2896812 |
| SeasonSummer                          | 0.7542217 | 0.2477951 |
| SurveyIDYears 2-3                     | 0.4837030 | 0.2648931 |

Shape coefficient(s):



|             |           |          |
|-------------|-----------|----------|
|             | estimate  | se       |
| (Intercept) | 0.8485132 | 0.197714 |

|                     |             |             |           |
|---------------------|-------------|-------------|-----------|
|                     | Estimate    | SE          | CV        |
| Average p           | 0.4075964   | 0.06072428  | 0.1489814 |
| N in covered region | 421.9860458 | 68.23264910 | 0.1616941 |

Distance sampling Cramer-von Mises test (unweighted)  
 Test statistic = 0.068137 p = 0.763045

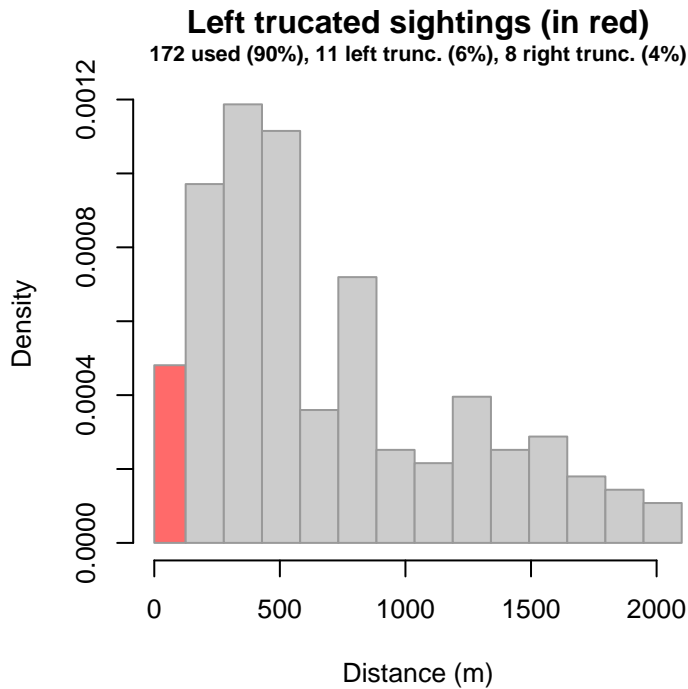


Figure 7: Density histogram of observations used to fit the NYS-DEC NYBWM Partenavia detection function, with the left-most bar showing observations at distances less than 125 m, which were left-truncated and excluded from the analysis [Buckland et al. (2001)]. (This bar may be very short if there were very few left-truncated sightings, or very narrow if the left truncation distance was very small; in either case it may not appear red.)

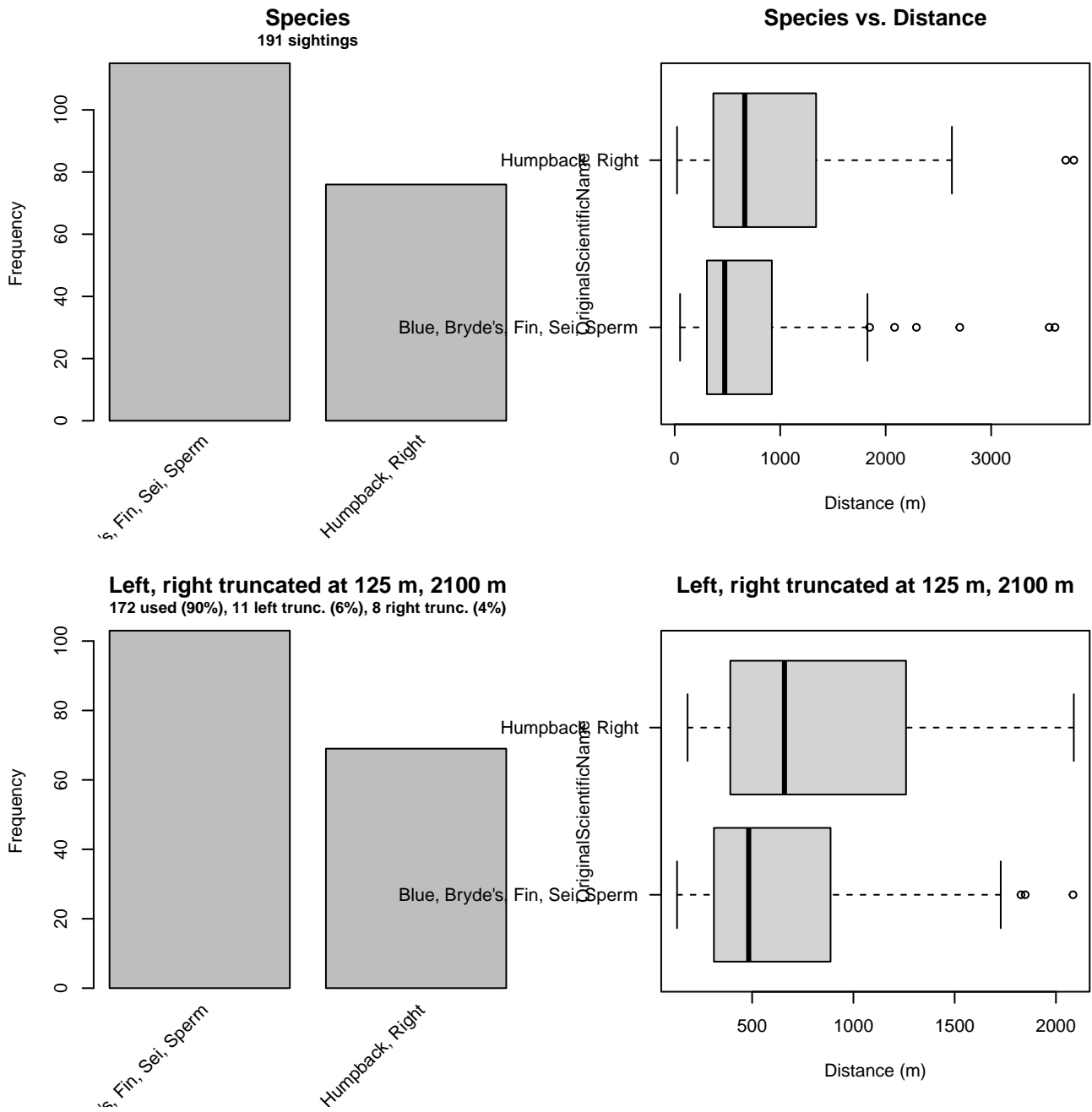


Figure 8: Distribution of the OriginalScientificName covariate before (top row) and after (bottom row) observations were truncated to fit the NYS-DEC NYBWM Partenavia detection function.

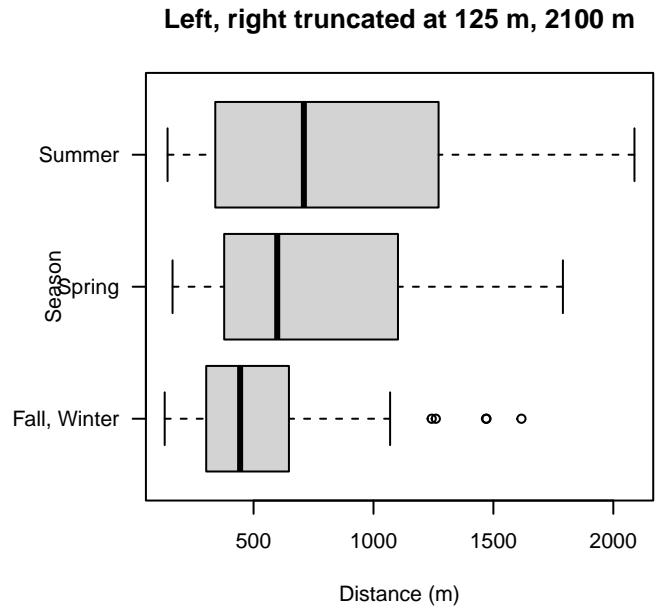
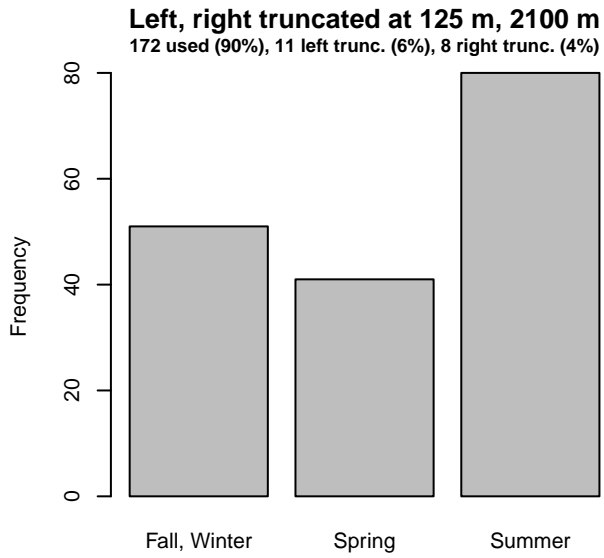
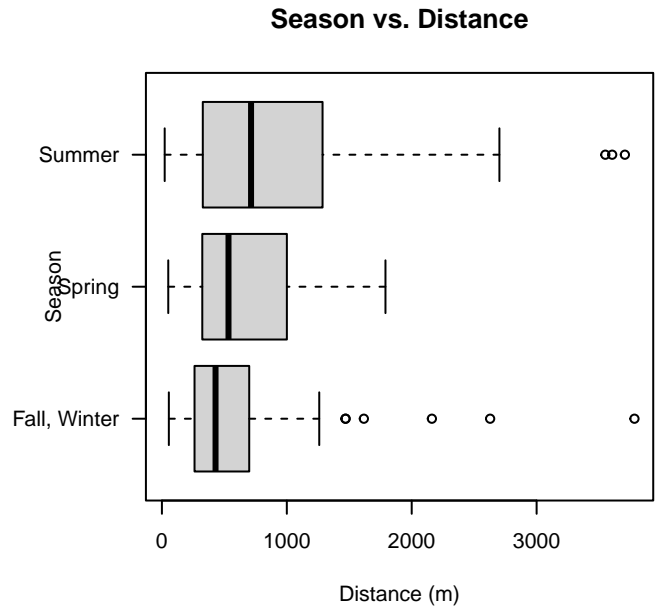
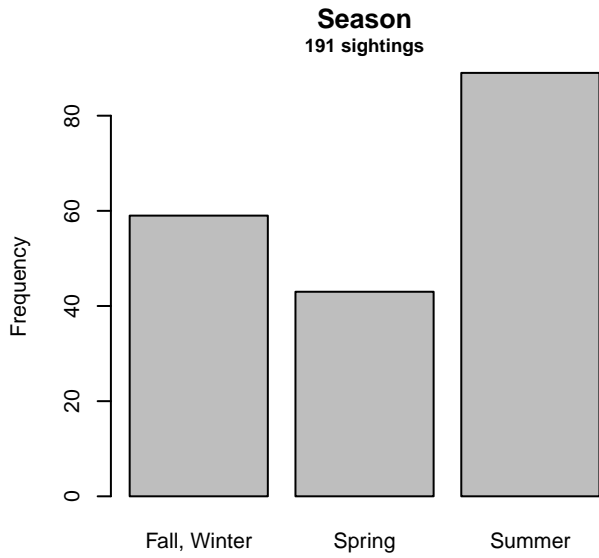


Figure 9: Distribution of the Season covariate before (top row) and after (bottom row) observations were truncated to fit the NYS-DEC NYBWM Partenavia detection function.

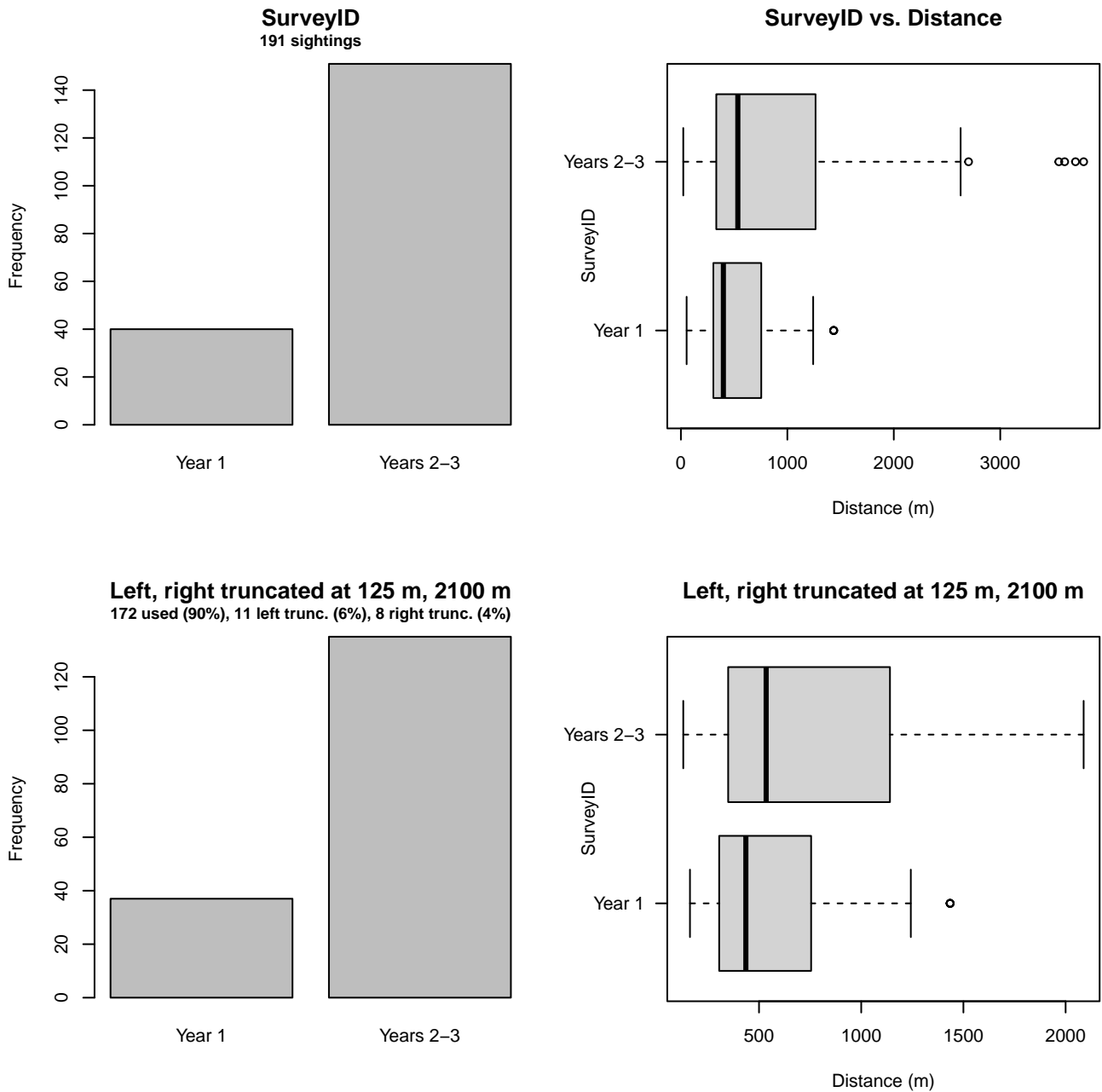


Figure 10: Distribution of the SurveyID covariate before (top row) and after (bottom row) observations were truncated to fit the NYS-DEC NYBWM Partenavia detection function.

### 3.1.1.1.2 NEAq New England

After right-truncating observations greater than 3704 m and left-truncating observations less than 71 m (Figure 12), we fitted the detection function to the 441 observations that remained (Table 7). The selected detection function (Figure 11) used a half normal key function with Beaufort (Figure 13), Glare (Figure 14) and OriginalScientificName (Figure 15) as covariates.

Table 7: Observations used to fit the NEAq New England detection function.

| ScientificName         | n          |
|------------------------|------------|
| Balaenoptera borealis  | 44         |
| Balaenoptera musculus  | 2          |
| Balaenoptera physalus  | 128        |
| Eubalaena glacialis    | 146        |
| Megaptera novaeangliae | 112        |
| Physeter macrocephalus | 9          |
| <b>Total</b>           | <b>441</b> |

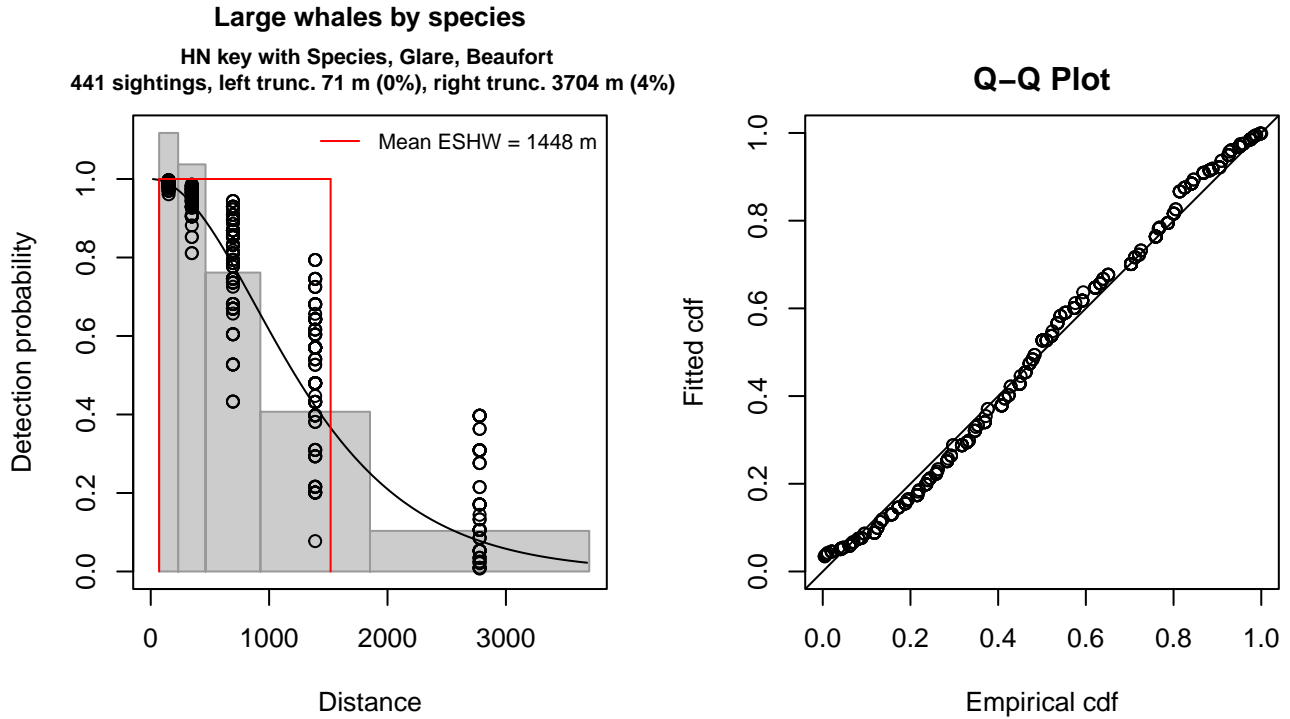


Figure 11: NEAq New England detection function and Q-Q plot showing its goodness of fit.

Statistical output for this detection function:

Summary for ds object

Number of observations : 441  
 Distance range : 71 - 3704  
 AIC : 1351.833

Detection function:

Half-normal key function

Detection function parameters

Scale coefficient(s):

|                                | estimate   | se         |
|--------------------------------|------------|------------|
| (Intercept)                    | 6.4199373  | 0.11956192 |
| OriginalScientificNameHumpback | 0.1198260  | 0.10455078 |
| OriginalScientificNameRight    | -0.1344891 | 0.09839291 |
| GlareSevere                    | 0.3449677  | 0.16999750 |
| GlareSlight, Moderate          | 0.3904627  | 0.09774396 |
| Beaufort2                      | 0.3680223  | 0.09867329 |
| Beaufort3-4                    | 0.6919932  | 0.12929768 |

|                     | Estimate     | SE          | CV         |
|---------------------|--------------|-------------|------------|
| Average p           | 0.3618698    | 0.01608762  | 0.04445694 |
| N in covered region | 1218.6704246 | 72.16746829 | 0.05921820 |

Distance sampling Cramer-von Mises test (unweighted)  
 Test statistic = 0.341945 p = 0.103421

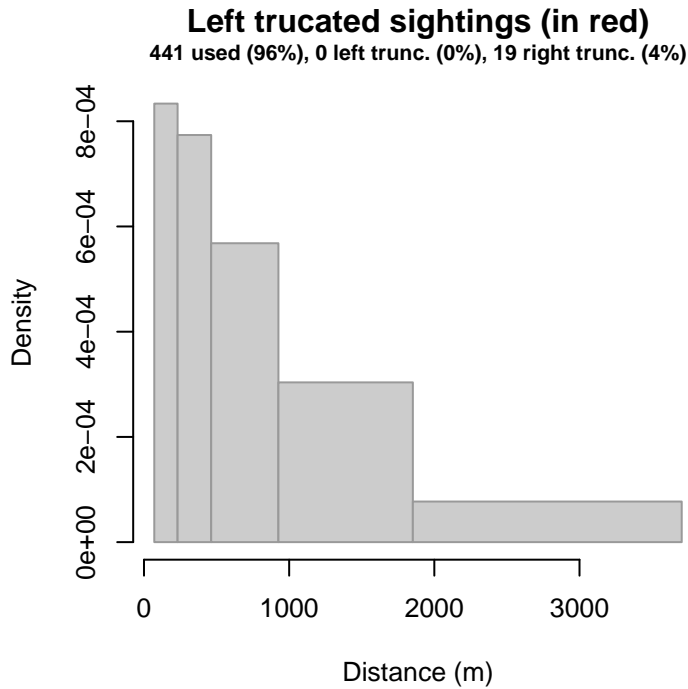


Figure 12: Density histogram of observations used to fit the NEAq New England detection function, with the left-most bar showing observations at distances less than 71 m, which were left-truncated and excluded from the analysis [Buckland et al. (2001)]. (This bar may be very short if there were very few left-truncated sightings, or very narrow if the left truncation distance was very small; in either case it may not appear red.)

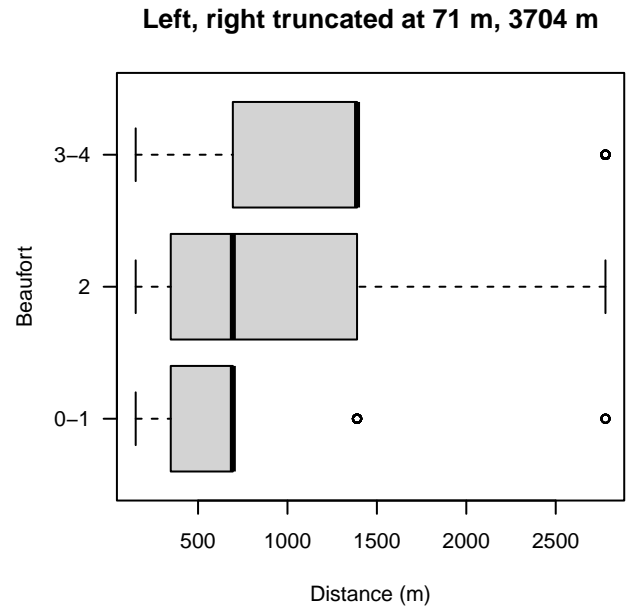
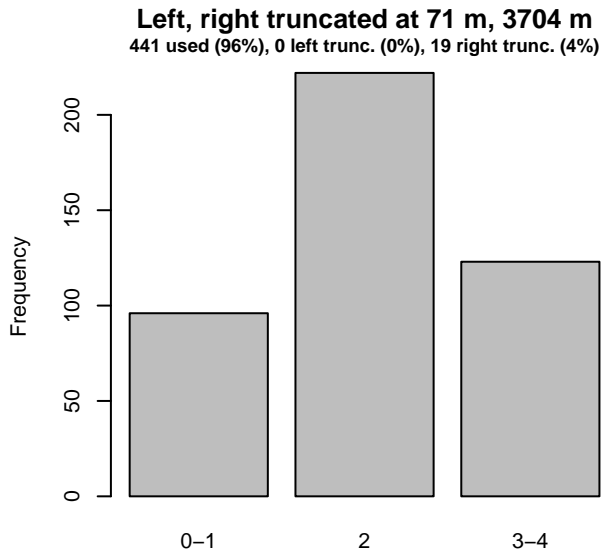
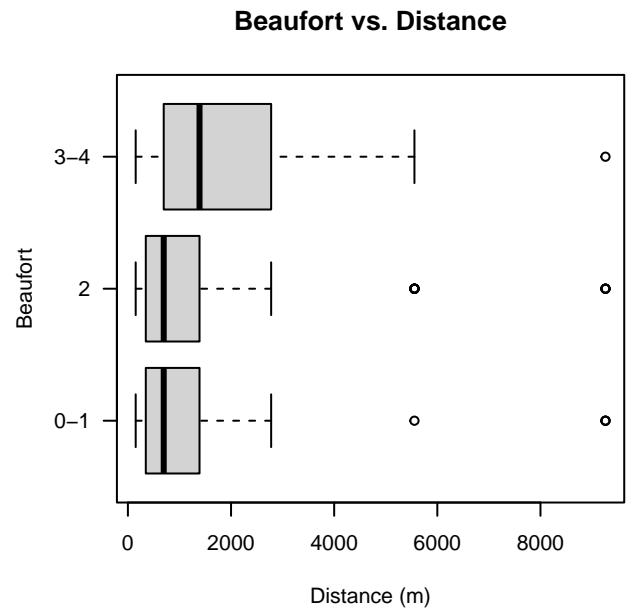
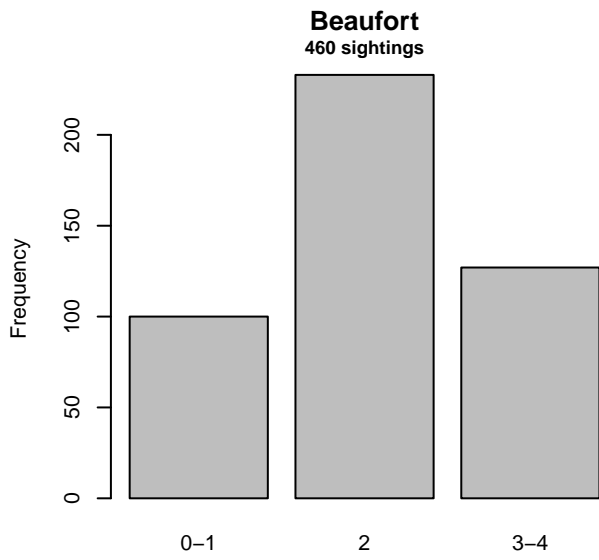


Figure 13: Distribution of the Beaufort covariate before (top row) and after (bottom row) observations were truncated to fit the NEAq New England detection function.

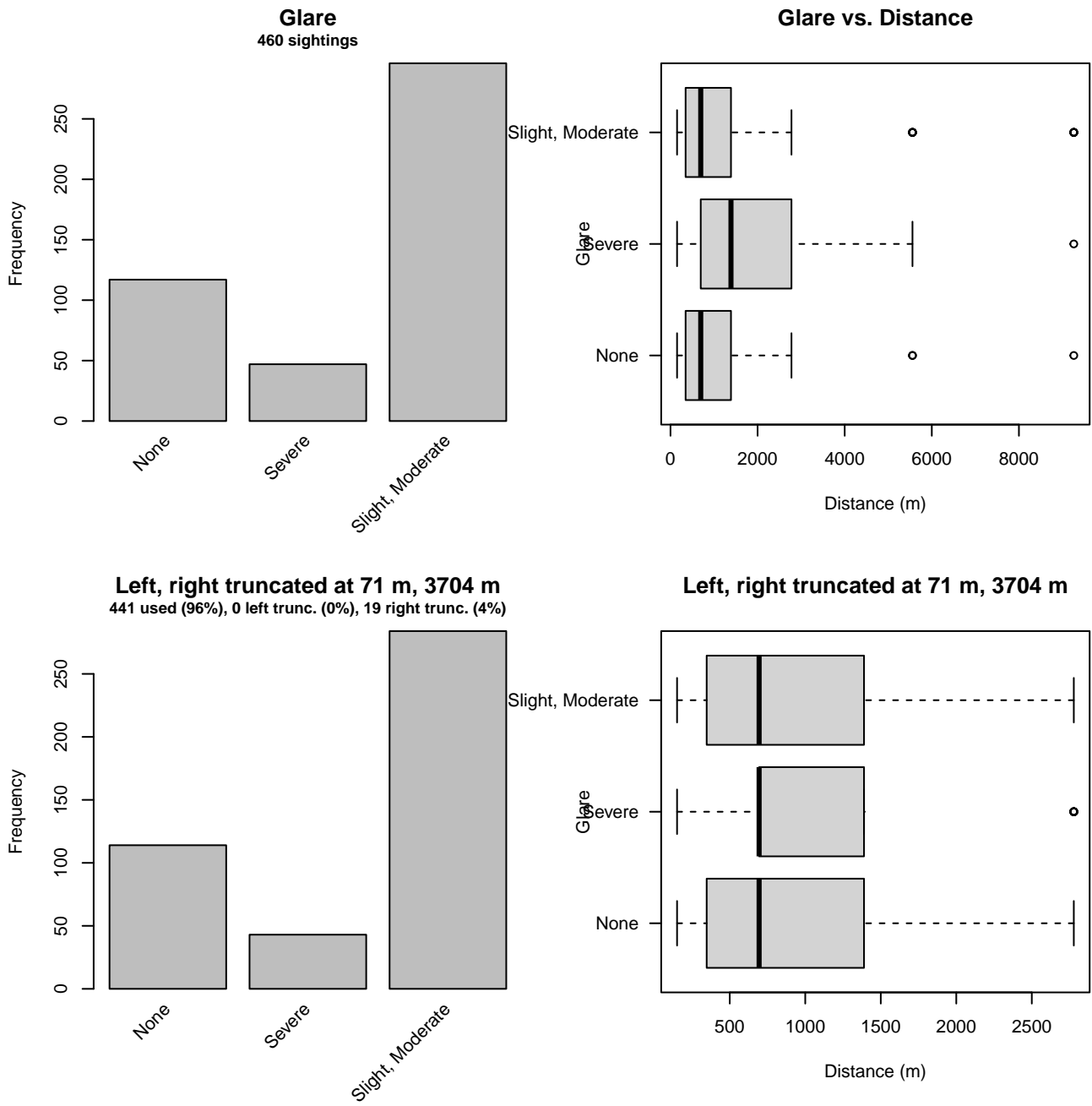


Figure 14: Distribution of the Glare covariate before (top row) and after (bottom row) observations were truncated to fit the NEAq New England detection function.



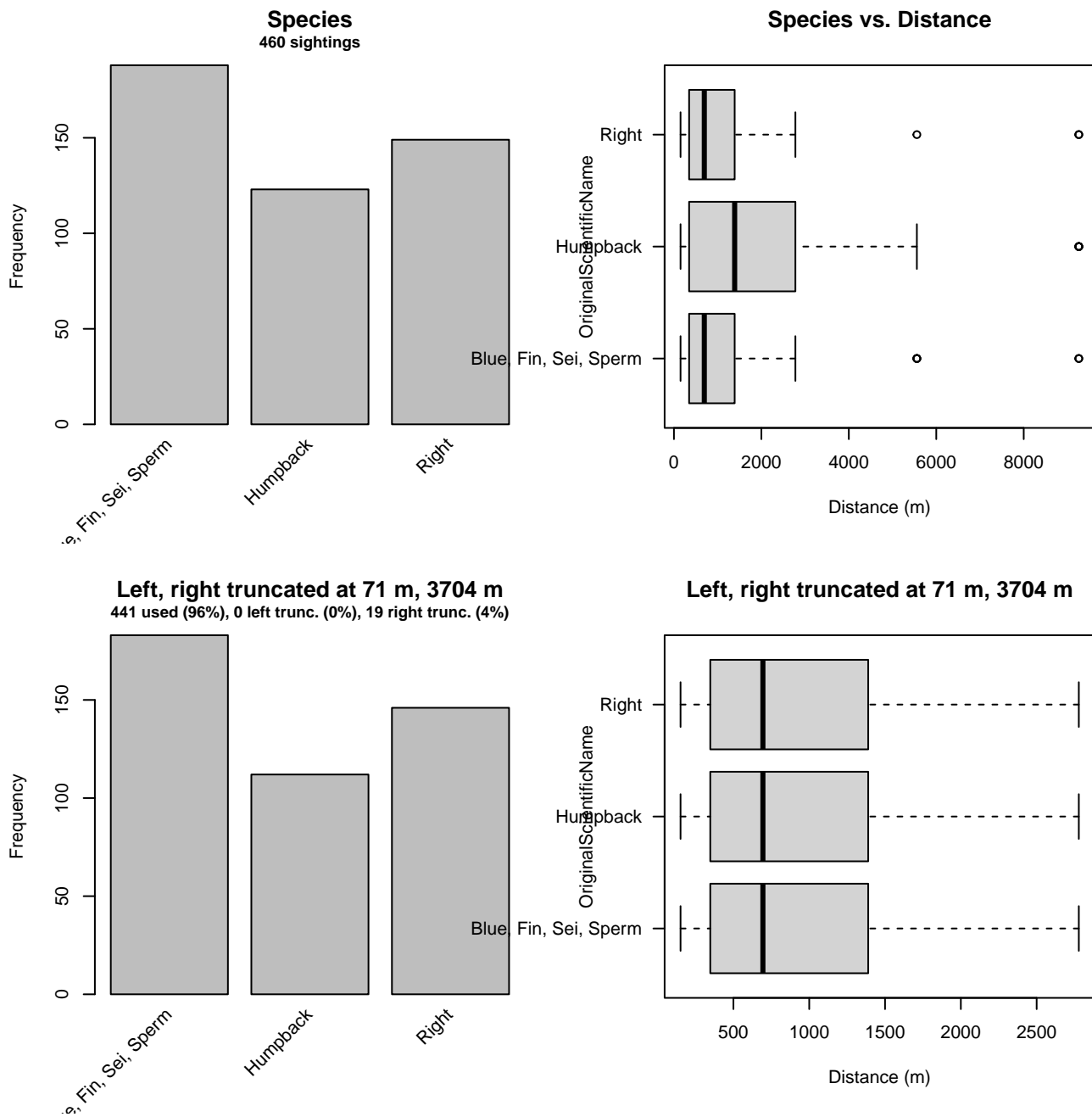


Figure 15: Distribution of the OriginalScientificName covariate before (top row) and after (bottom row) observations were truncated to fit the NEAq New England detection function.

### 3.1.1.1.3 UNCW and VAMSC

After right-truncating observations greater than 2000 m, we fitted the detection function to the 100 observations that remained (Table 8). The selected detection function (Figure 16) used a hazard rate key function with OriginalScientificName (Figure 17) as a covariate.

Table 8: Observations used to fit the UNCW and VAMSC detection function.

| ScientificName         | n          |
|------------------------|------------|
| Balaenoptera physalus  | 27         |
| Megaptera novaeangliae | 31         |
| Physeter macrocephalus | 42         |
| <b>Total</b>           | <b>100</b> |

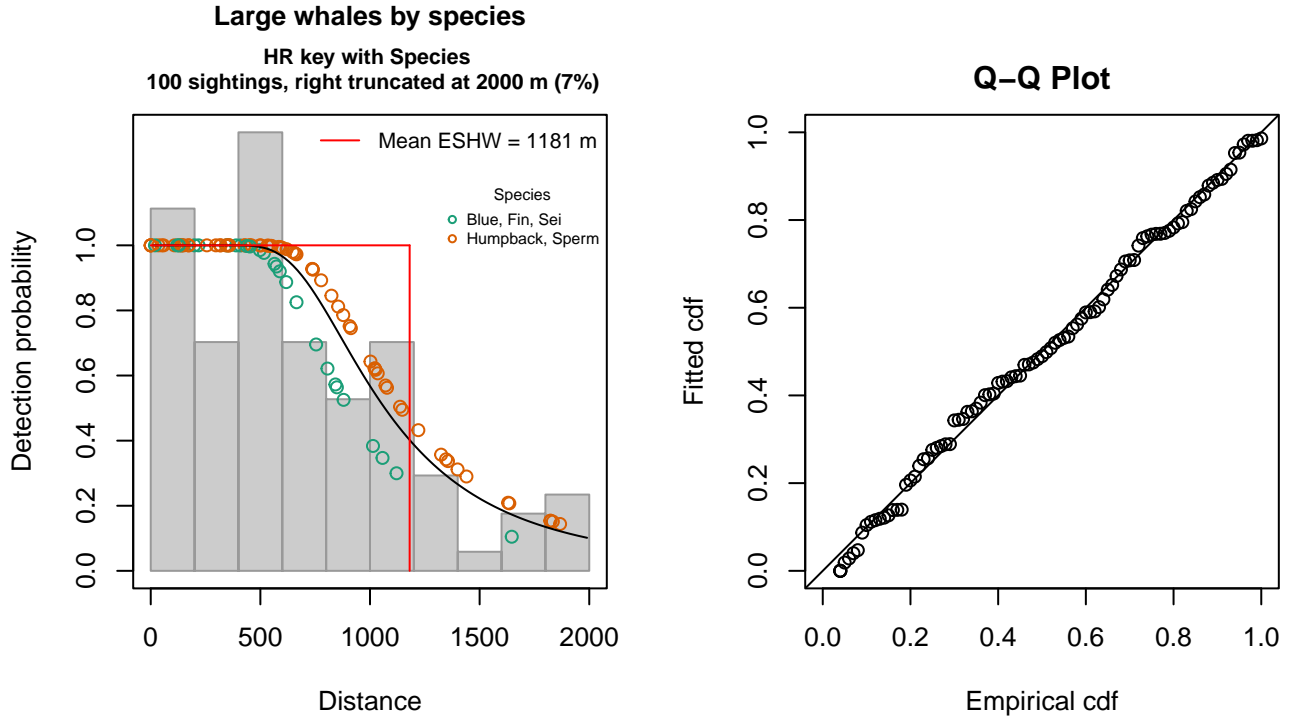


Figure 16: UNCW and VAMSC detection function and Q-Q plot showing its goodness of fit.

Statistical output for this detection function:

Summary for ds object

Number of observations : 100  
 Distance range : 0 - 2000  
 AIC : 1484.772

Detection function:

Hazard-rate key function

Detection function parameters

Scale coefficient(s):

|                                       | estimate  | se        |
|---------------------------------------|-----------|-----------|
| (Intercept)                           | 6.6826489 | 0.2197841 |
| OriginalScientificNameHumpback, Sperm | 0.2371163 | 0.2278764 |

Shape coefficient(s):

|             | estimate | se        |
|-------------|----------|-----------|
| (Intercept) | 1.11195  | 0.3071042 |

|                     | Estimate    | SE          | CV        |
|---------------------|-------------|-------------|-----------|
| Average p           | 0.5857436   | 0.05399642  | 0.0921844 |
| N in covered region | 170.7231622 | 19.23003142 | 0.1126387 |

Distance sampling Cramer-von Mises test (unweighted)  
 Test statistic = 0.036117 p = 0.952042

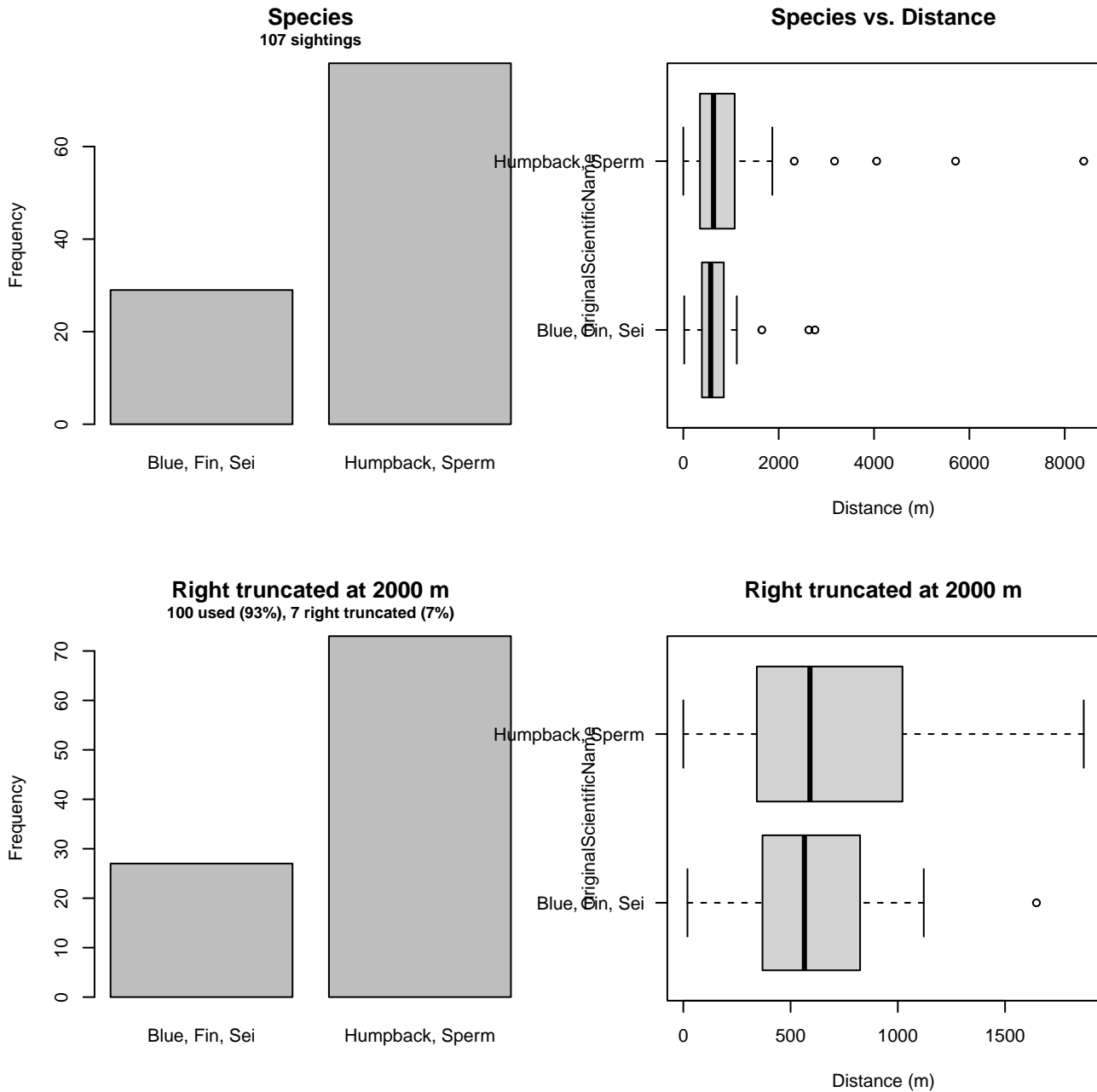


Figure 17: Distribution of the OriginalScientificName covariate before (top row) and after (bottom row) observations were truncated to fit the UNCW and VAMSC detection function.

### 3.1.1.2 Shipboard Surveys

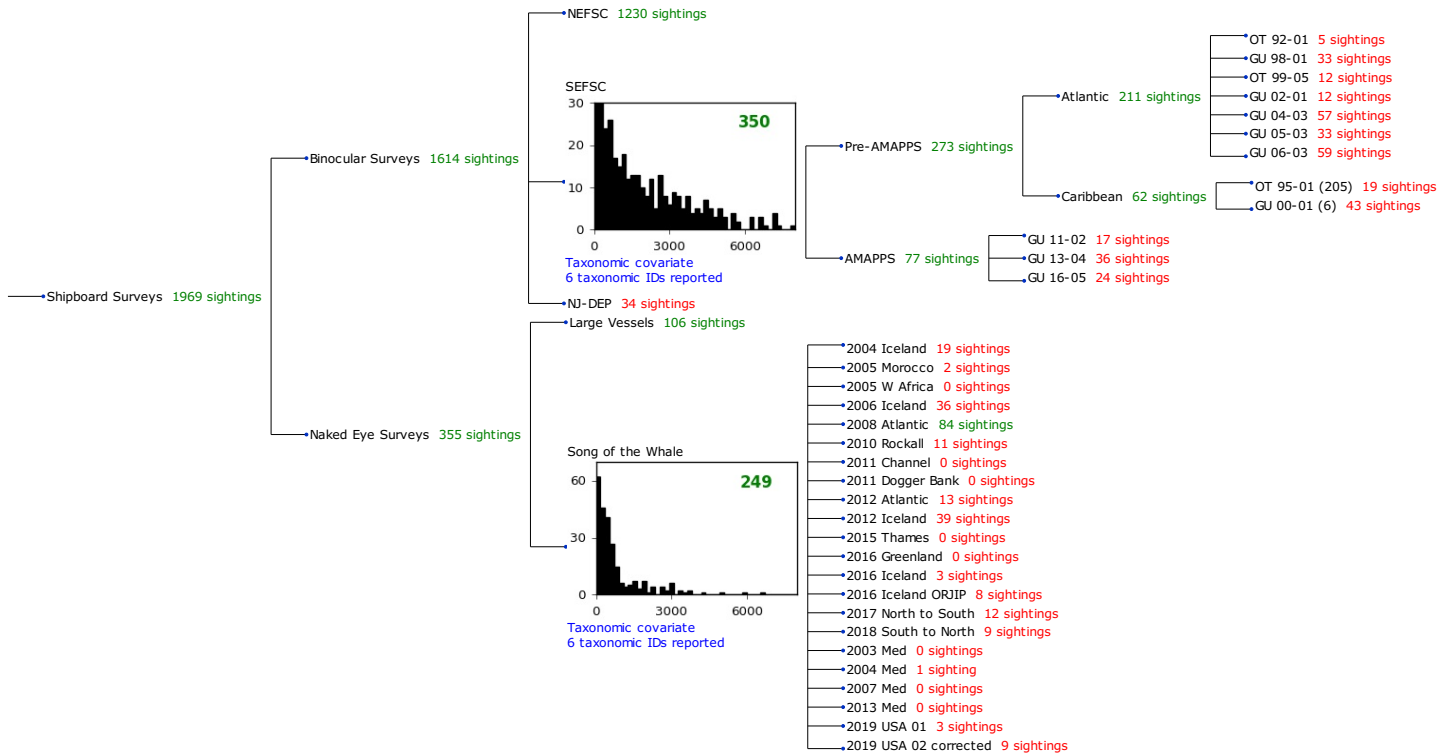


Figure 18: Detection hierarchy for shipboard surveys, showing how they were pooled during detectability modeling, for detection functions that pooled multiple taxa and used a taxonomic covariate to account for differences between them. Each histogram represents a detection function and summarizes the perpendicular distances of observations that were pooled to fit it, prior to truncation. Observation counts, also prior to truncation, are shown in green when they met the recommendation of Buckland et al. (2001) that detection functions utilize at least 60 sightings, and red otherwise. For rare taxa, it was not always possible to meet this recommendation, yielding higher statistical uncertainty. During the spatial modeling stage of the analysis, effective strip widths were computed for each survey using the closest detection function above it in the hierarchy (i.e. moving from right to left in the figure). Surveys that do not have a detection function above them in this figure were either addressed by a detection function presented in a different section of this report, or were omitted from the analysis.

#### 3.1.1.2.1 SEFSC

After right-truncating observations greater than 6000 m, we fitted the detection function to the 332 observations that remained (Table 9). The selected detection function (Figure 19) used a hazard rate key function with Beaufort (Figure 20), OriginalScientificName (Figure 21) and Program (Figure 22) as covariates.

Table 9: Observations used to fit the SEFSC detection function.

| ScientificName              | n          |
|-----------------------------|------------|
| Balaenoptera borealis/edeni | 3          |
| Balaenoptera edeni          | 10         |
| Balaenoptera physalus       | 17         |
| Eubalaena glacialis         | 2          |
| Megaptera novaeangliae      | 32         |
| Physeter macrocephalus      | 268        |
| <b>Total</b>                | <b>332</b> |

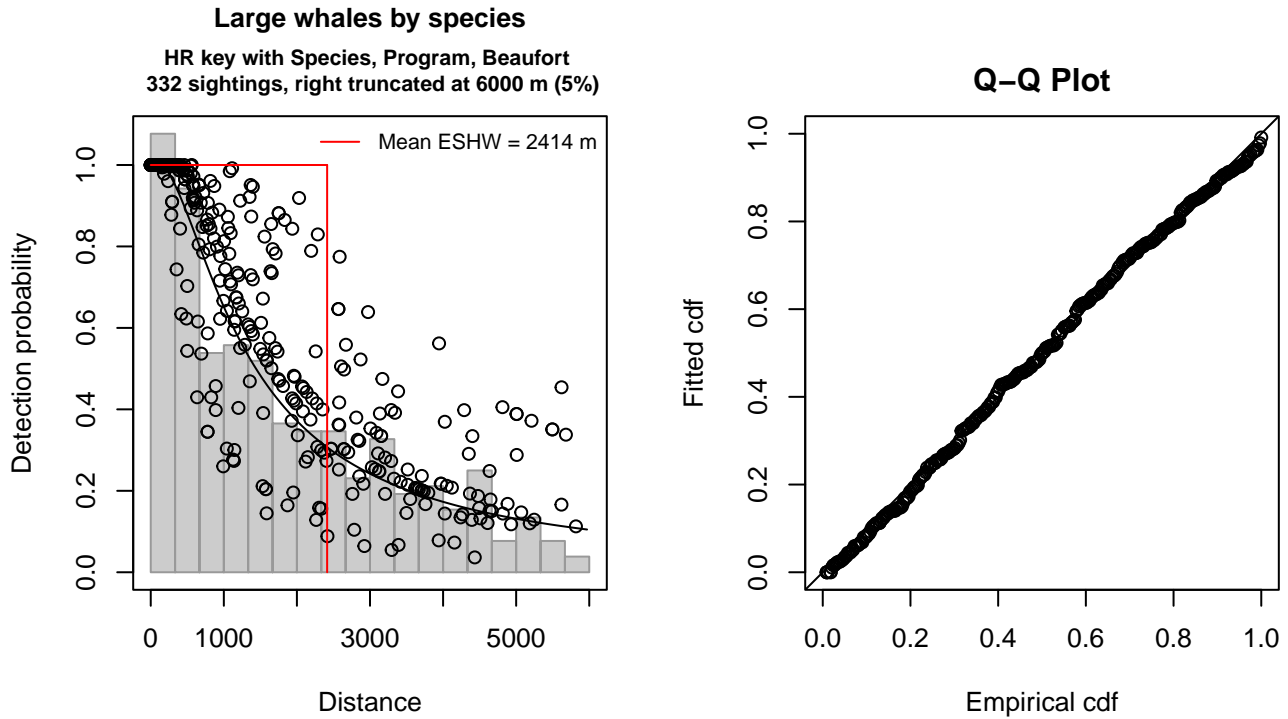


Figure 19: SEFSC detection function and Q-Q plot showing its goodness of fit.

Statistical output for this detection function:

Summary for ds object

Number of observations : 332  
 Distance range : 0 - 6000  
 AIC : 5604.674

Detection function:

Hazard-rate key function

Detection function parameters

Scale coefficient(s):

|                             | estimate   | se        |
|-----------------------------|------------|-----------|
| (Intercept)                 | 7.4794246  | 0.4929618 |
| OriginalScientificNameSperm | 0.7957413  | 0.3448895 |
| ProgramAtlantic Pre-AMAPPS  | -0.7295682 | 0.3154763 |
| ProgramCaribbean            | -0.7773443 | 0.4064337 |
| Beaufort                    | -0.1322436 | 0.1039800 |

Shape coefficient(s):

|             | estimate  | se        |
|-------------|-----------|-----------|
| (Intercept) | 0.3345999 | 0.1370809 |

|                     | Estimate    | SE           | CV        |
|---------------------|-------------|--------------|-----------|
| Average p           | 0.3546416   | 0.03786854   | 0.1067797 |
| N in covered region | 936.1563072 | 108.72789053 | 0.1161429 |

Distance sampling Cramer-von Mises test (unweighted)

Test statistic = 0.055285 p = 0.843624

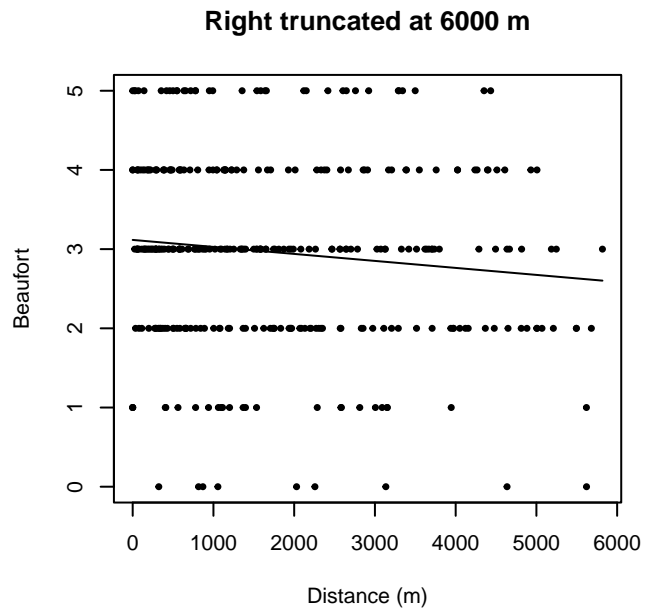
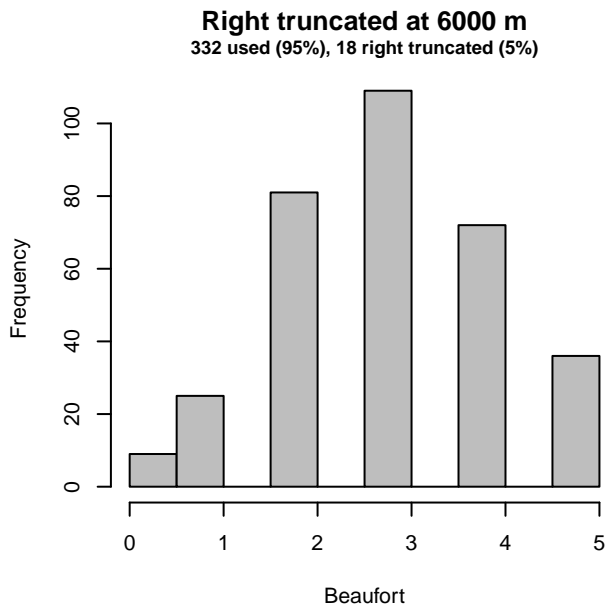
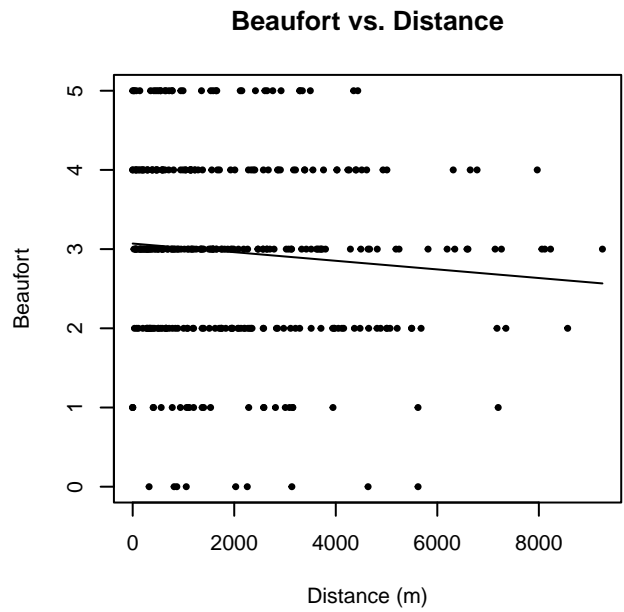
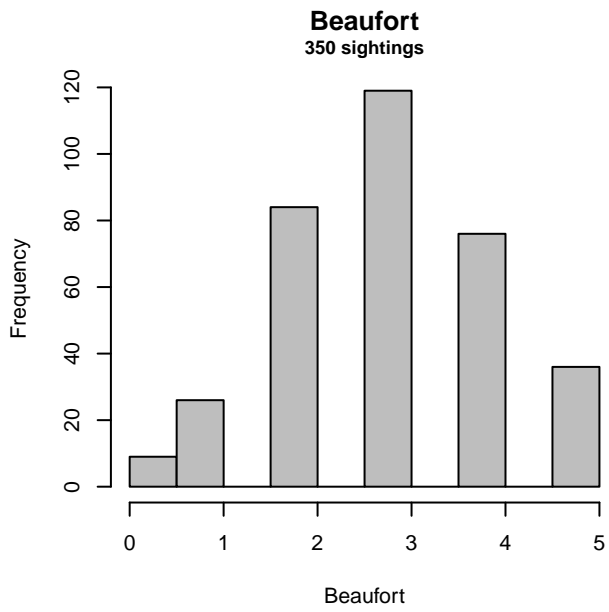


Figure 20: Distribution of the Beaufort covariate before (top row) and after (bottom row) observations were truncated to fit the SEFSC detection function.

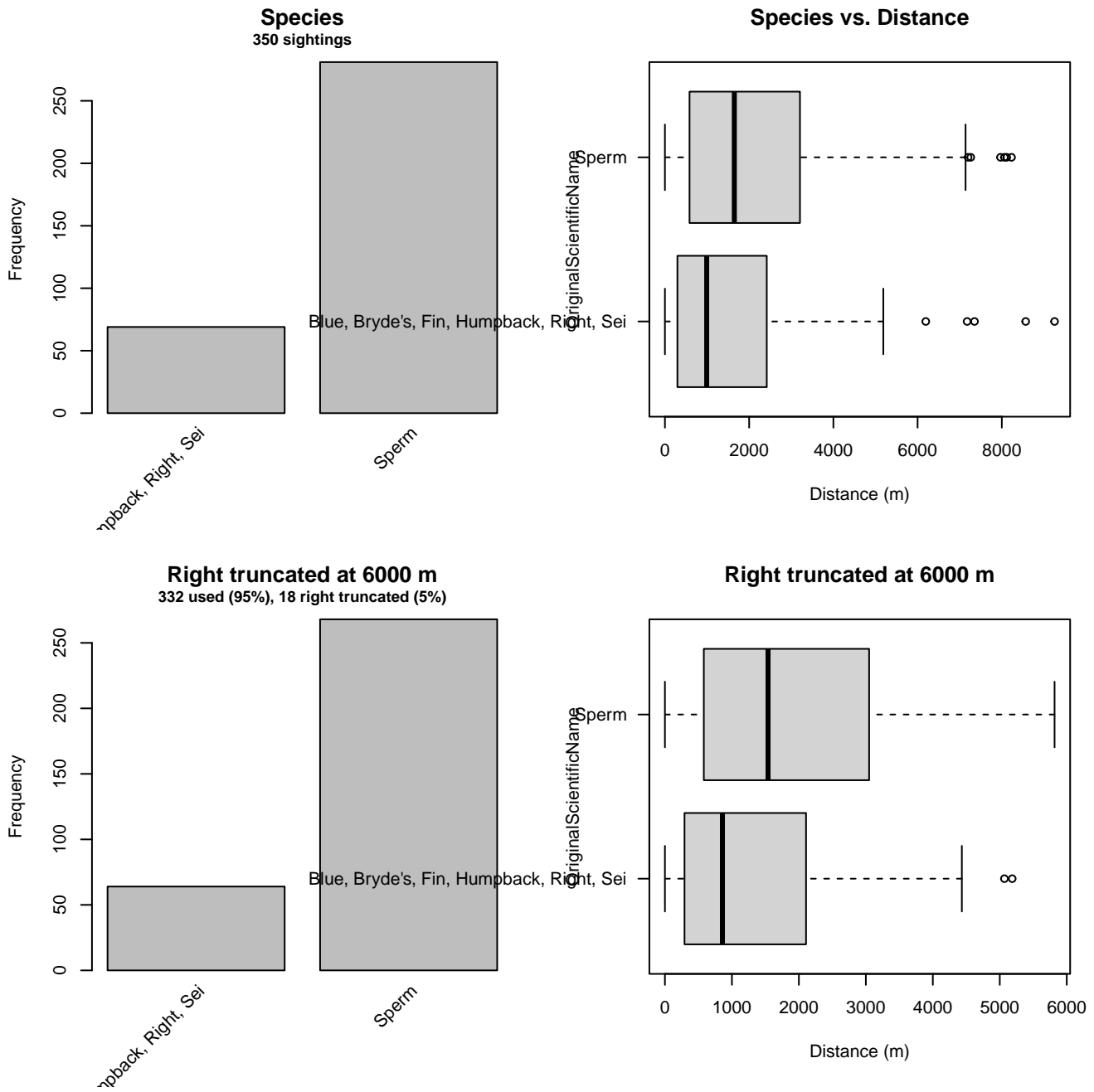


Figure 21: Distribution of the OriginalScientificName covariate before (top row) and after (bottom row) observations were truncated to fit the SEFSC detection function.

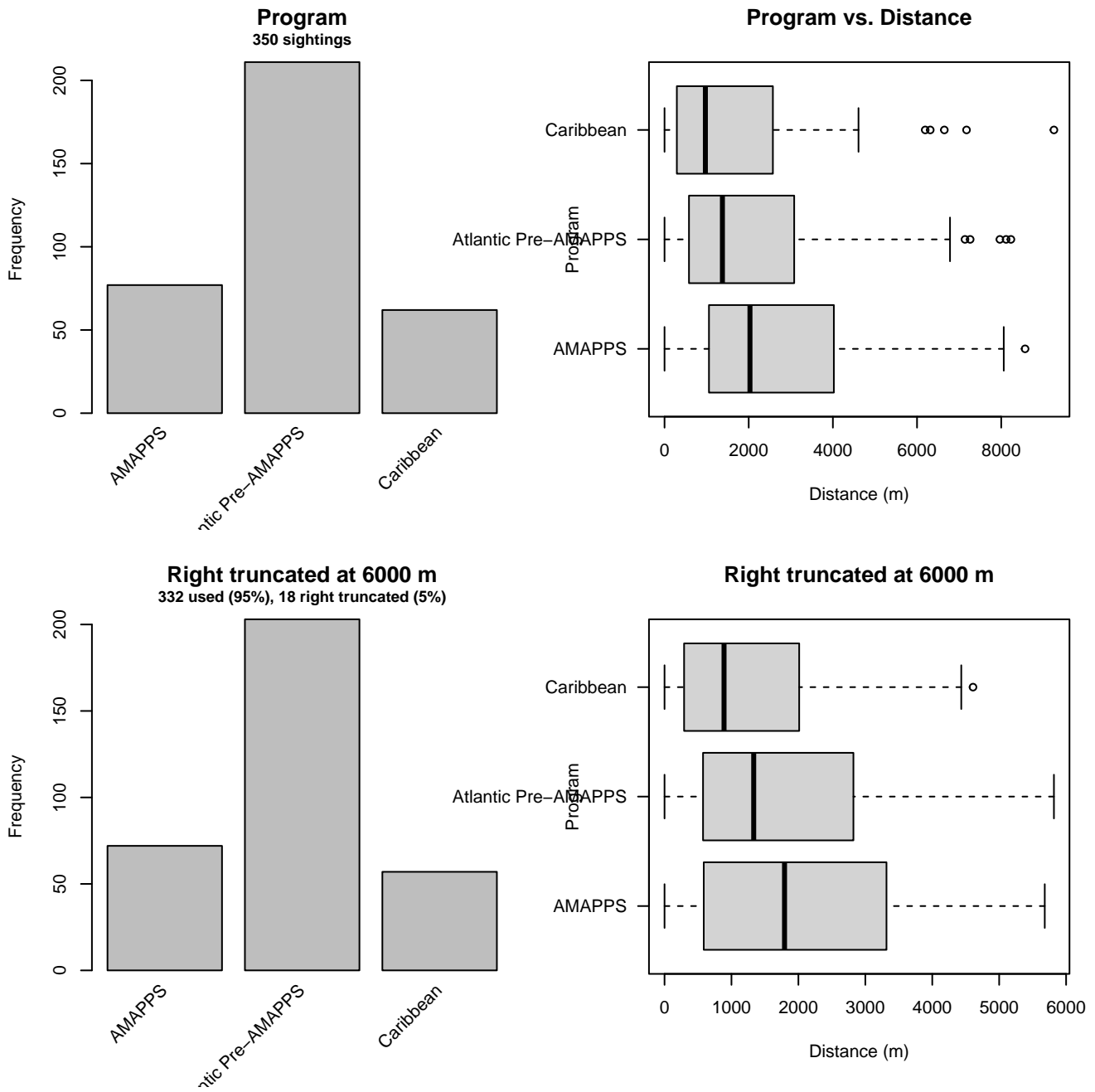


Figure 22: Distribution of the Program covariate before (top row) and after (bottom row) observations were truncated to fit the SEFSC detection function.

### 3.1.1.2.2 Song of the Whale

After right-truncating observations greater than 3000 m, we fitted the detection function to the 239 observations that remained (Table 10). The selected detection function (Figure 23) used a hazard rate key function with Glare (Figure 24), OriginalScientificName (Figure 25) and WeatherCode (Figure 26) as covariates.



Table 10: Observations used to fit the Song of the Whale detection function.

| ScientificName         | n          |
|------------------------|------------|
| Balaenoptera borealis  | 13         |
| Balaenoptera edeni     | 7          |
| Balaenoptera musculus  | 8          |
| Balaenoptera physalus  | 27         |
| Megaptera novaeangliae | 69         |
| Physeter macrocephalus | 115        |
| <b>Total</b>           | <b>239</b> |

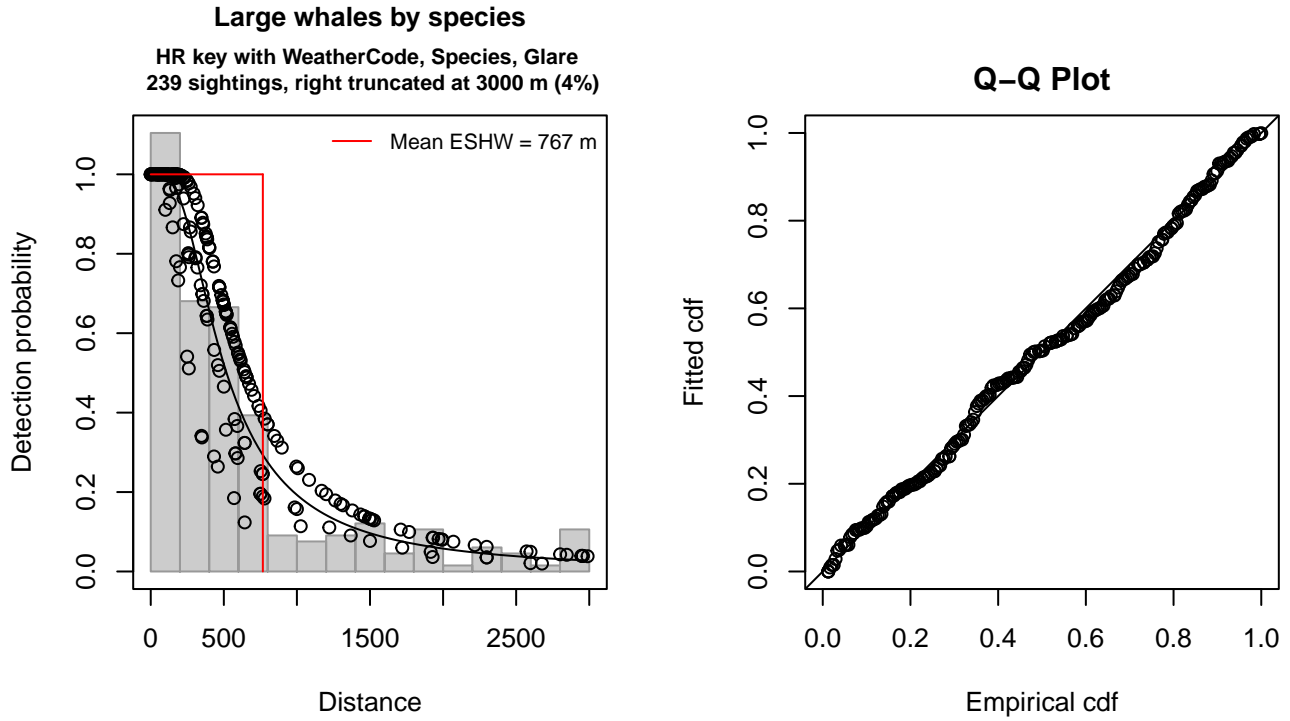


Figure 23: Song of the Whale detection function and Q-Q plot showing its goodness of fit.

Statistical output for this detection function:

Summary for ds object

Number of observations : 239  
 Distance range : 0 - 3000  
 AIC : 3547.931

Detection function:

Hazard-rate key function

Detection function parameters

Scale coefficient(s):

|                                       | estimate   | se        |
|---------------------------------------|------------|-----------|
| (Intercept)                           | 5.9647631  | 0.2274130 |
| WeatherCodeHaze                       | -0.8889445 | 0.5747918 |
| OriginalScientificNameHumpback, Sperm | 0.3084029  | 0.2238350 |
| GlareSevere                           | -0.4670165 | 0.2579856 |

Shape coefficient(s):

| estimate | se |
|----------|----|
|----------|----|

(Intercept) 0.6276528 0.09675212

|                     | Estimate    | SE           | CV       |
|---------------------|-------------|--------------|----------|
| Average p           | 0.2409962   | 0.02414927   | 0.100206 |
| N in covered region | 991.7170380 | 114.27753421 | 0.115232 |

Distance sampling Cramer-von Mises test (unweighted)  
Test statistic = 0.073160 p = 0.732317

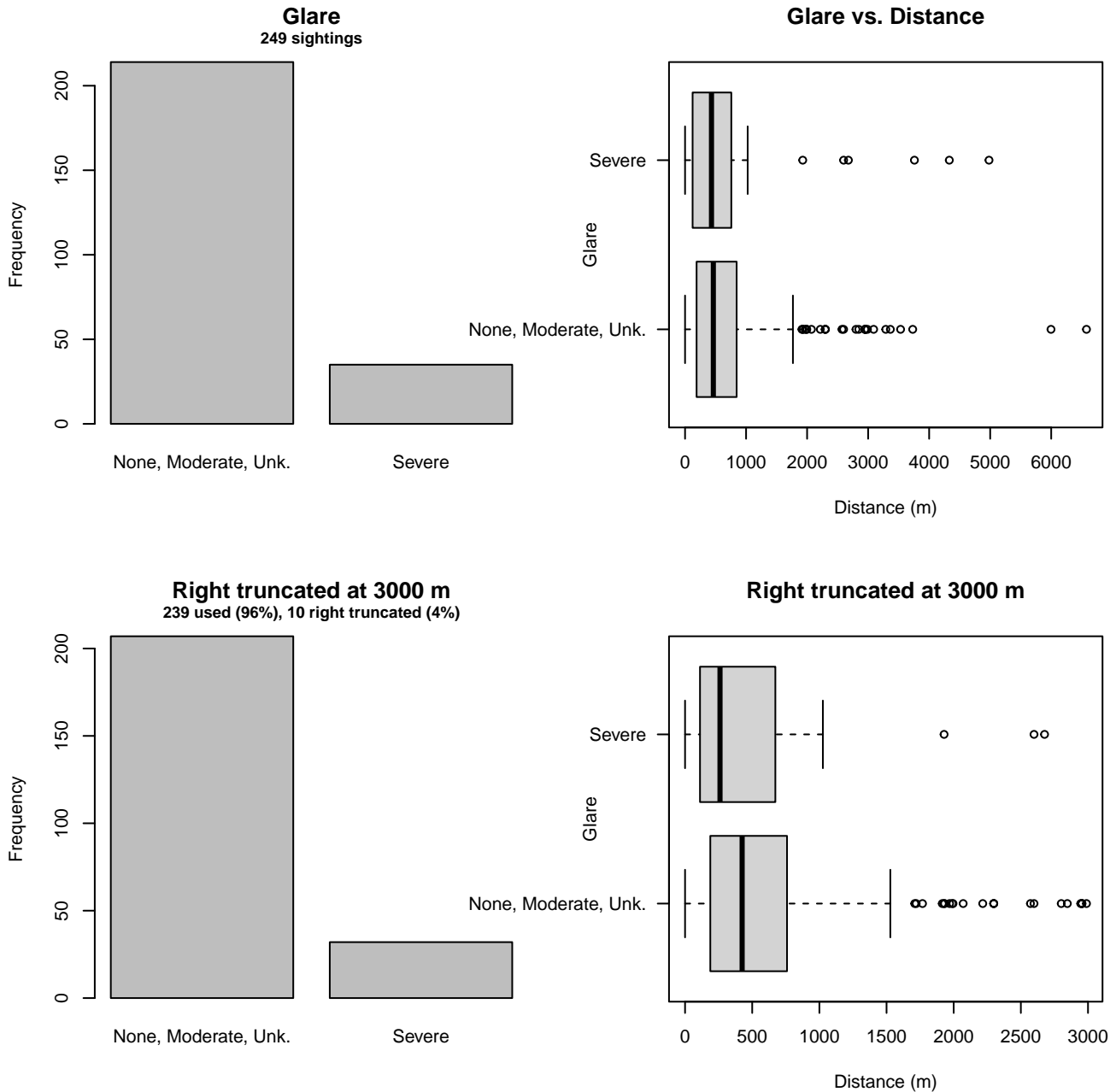


Figure 24: Distribution of the Glare covariate before (top row) and after (bottom row) observations were truncated to fit the Song of the Whale detection function.

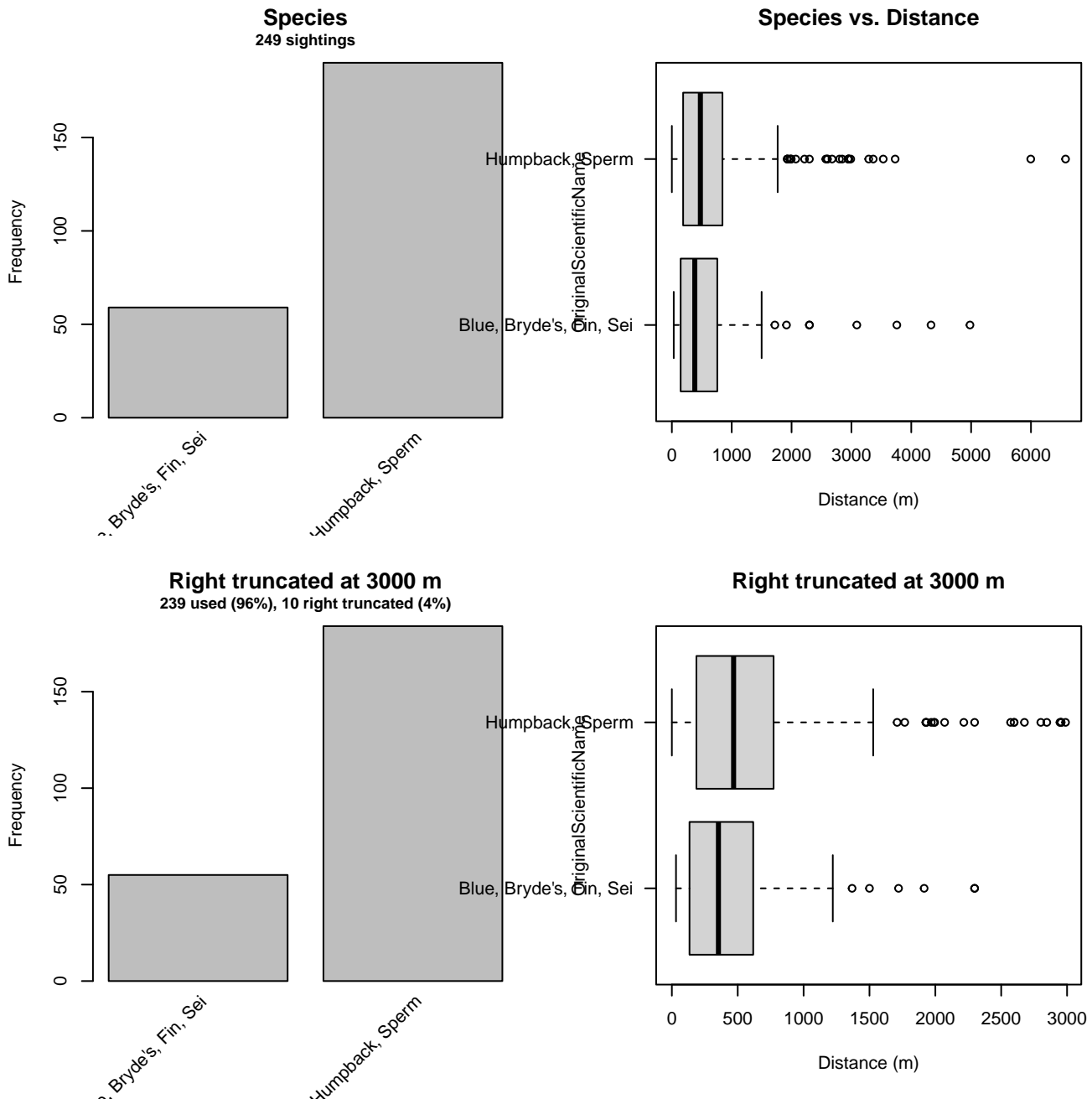


Figure 25: Distribution of the OriginalScientificName covariate before (top row) and after (bottom row) observations were truncated to fit the Song of the Whale detection function.

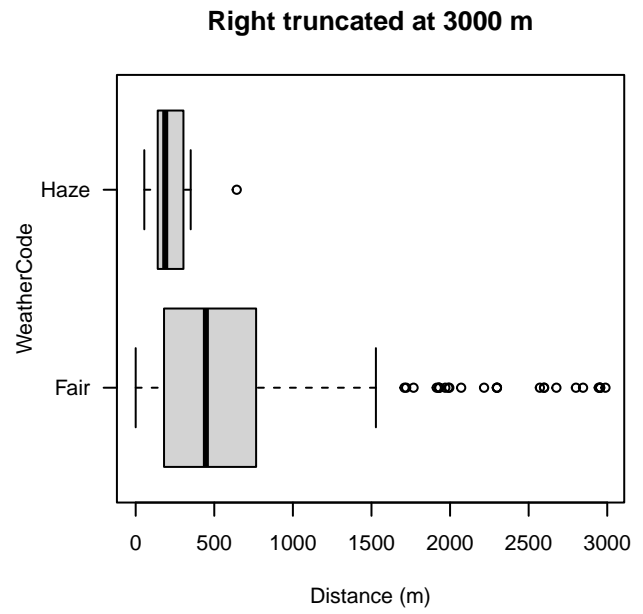
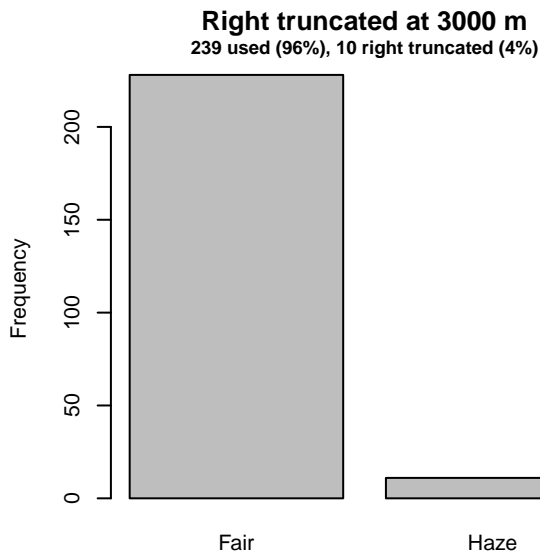
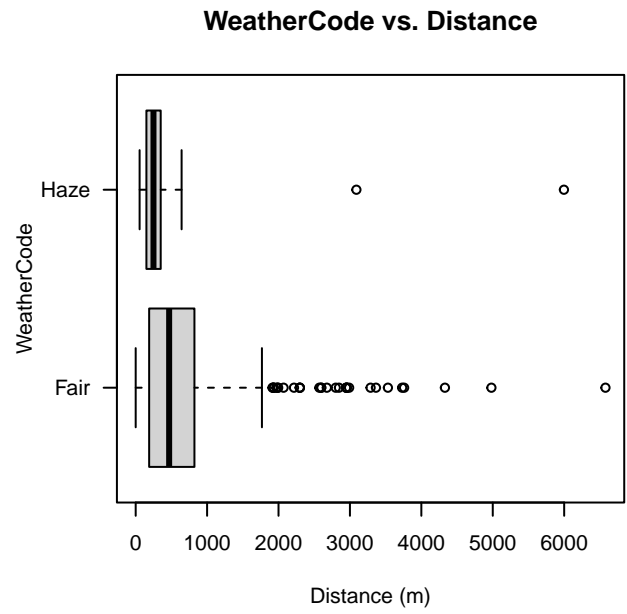
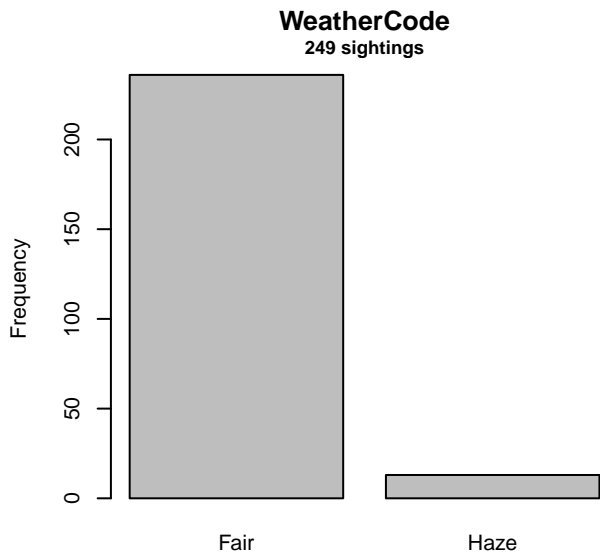


Figure 26: Distribution of the WeatherCode covariate before (top row) and after (bottom row) observations were truncated to fit the Song of the Whale detection function.

### 3.1.2 Large Whales (second group)

#### 3.1.2.1 Aerial Surveys

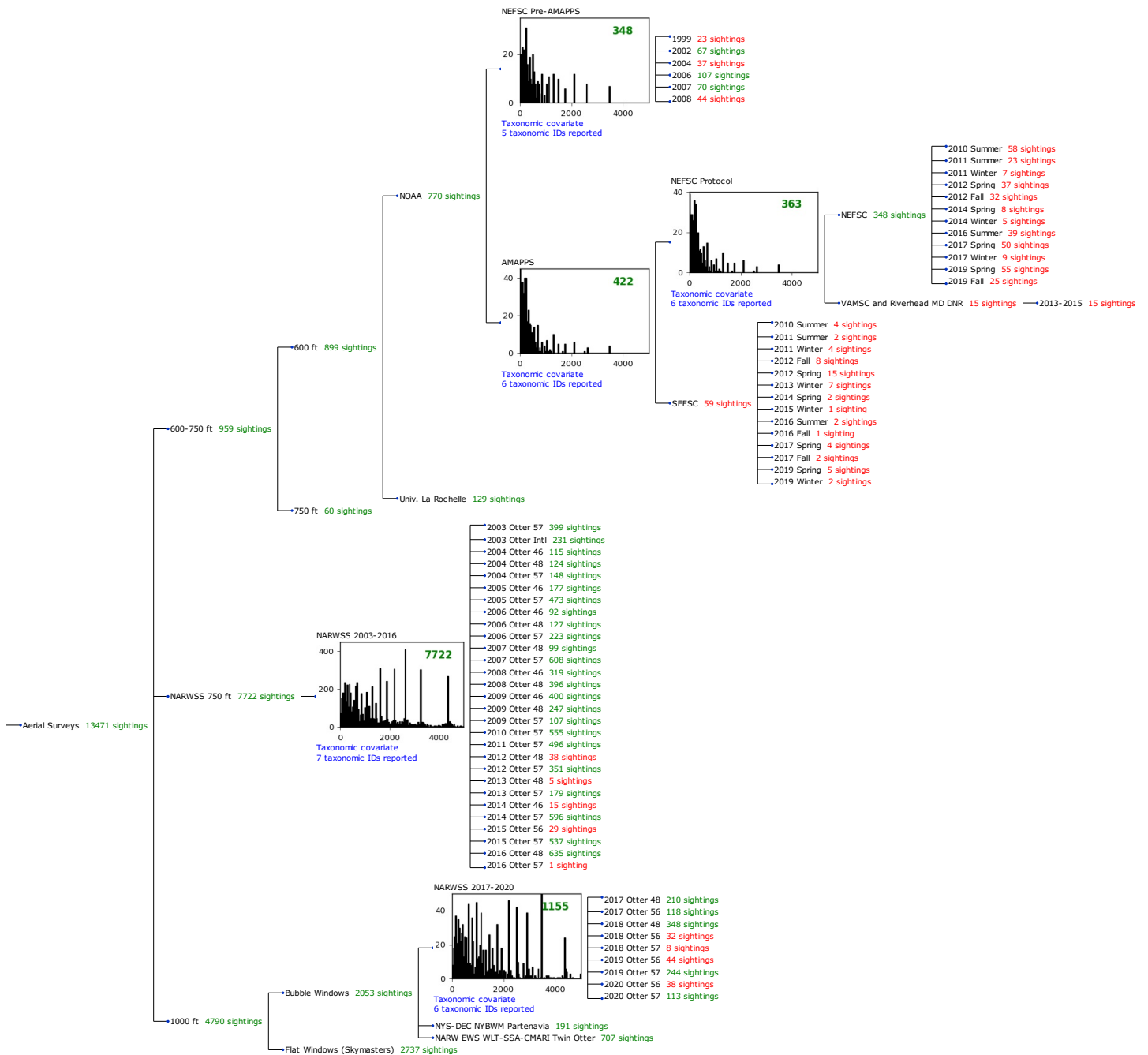


Figure 27: Detection hierarchy for aerial surveys, showing how they were pooled during detectability modeling, for detection functions that pooled multiple taxa and used a taxonomic covariate to account for differences between them. Each histogram represents a detection function and summarizes the perpendicular distances of observations that were pooled to fit it, prior to truncation. Observation counts, also prior to truncation, are shown in green when they met the recommendation of Buckland et al. (2001) that detection functions utilize at least 60 sightings, and red otherwise. For rare taxa, it was not always possible to meet this recommendation, yielding higher statistical uncertainty. During the spatial modeling stage of the analysis, effective strip widths were computed for each survey using the closest detection function above it in the hierarchy (i.e. moving from right to left in the figure). Surveys that do not have a detection function above them in this figure were either addressed by a detection function presented in a different section of this report, or were omitted from the analysis.

### 3.1.2.1.1 NEFSC Pre-AMAPPS

After right-truncating observations greater than 1500 m, we fitted the detection function to the 312 observations that remained (Table 11). The selected detection function (Figure 28) used a hazard rate key function with Beaufort (Figure 29) and ScientificName (Figure 30) as covariates.

Table 11: Observations used to fit the NEFSC Pre-AMAPPS detection function.

| ScientificName        | n          |
|-----------------------|------------|
| Blue, Fin, Sei, Sperm | 170        |
| Humpback, Right       | 142        |
| <b>Total</b>          | <b>312</b> |

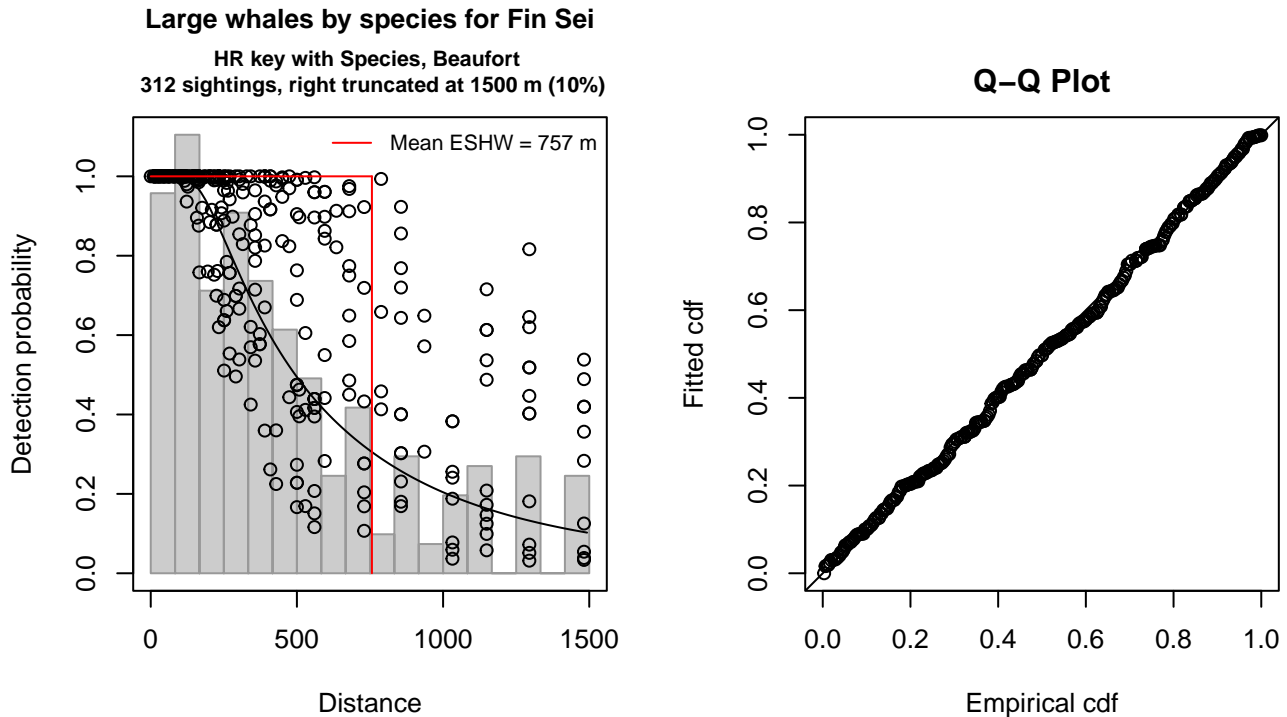


Figure 28: NEFSC Pre-AMAPPS detection function and Q-Q plot showing its goodness of fit.

Statistical output for this detection function:

Summary for ds object

Number of observations : 312  
 Distance range : 0 - 1500  
 AIC : 4376.913

Detection function:

Hazard-rate key function

Detection function parameters

Scale coefficient(s):

|                               | estimate  | se         |
|-------------------------------|-----------|------------|
| (Intercept)                   | 5.1153004 | 0.25110719 |
| ScientificNameHumpback, Right | 0.8493800 | 0.16417511 |
| Beaufort                      | 0.3206412 | 0.08719038 |

Shape coefficient(s):

estimate se  
 (Intercept) 0.7821505 0.1268451

|                     | Estimate    | SE         | CV         |
|---------------------|-------------|------------|------------|
| Average p           | 0.4255304   | 0.0322576  | 0.07580562 |
| N in covered region | 733.2025745 | 64.9225054 | 0.08854648 |

Distance sampling Cramer-von Mises test (unweighted)  
 Test statistic = 0.034598 p = 0.958737

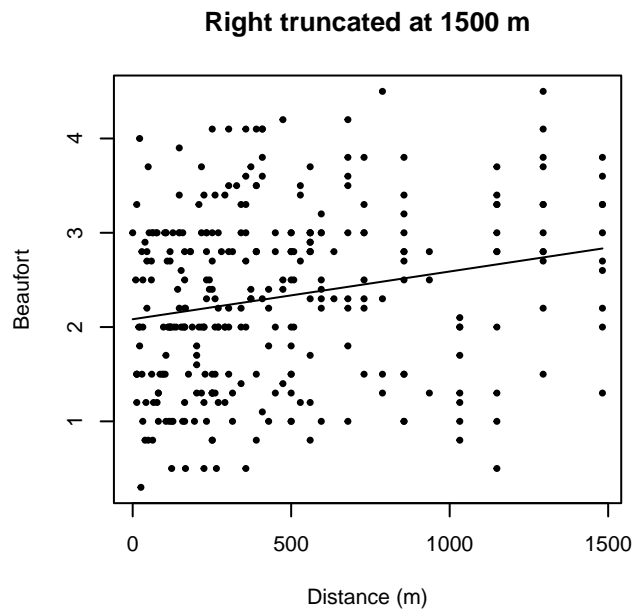
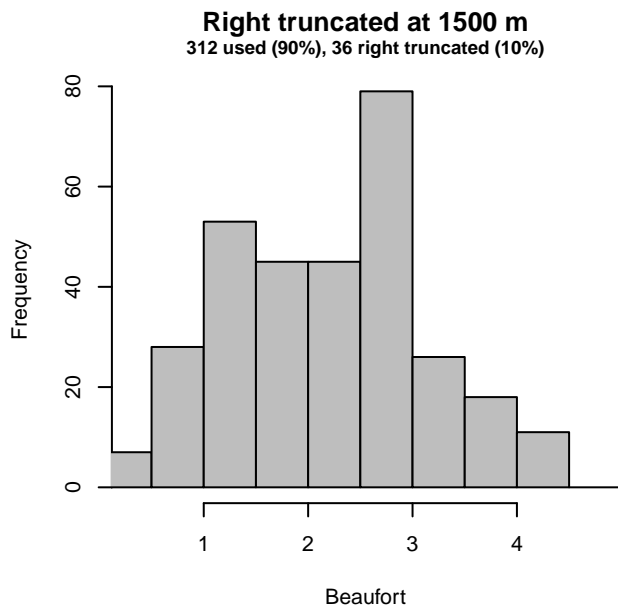
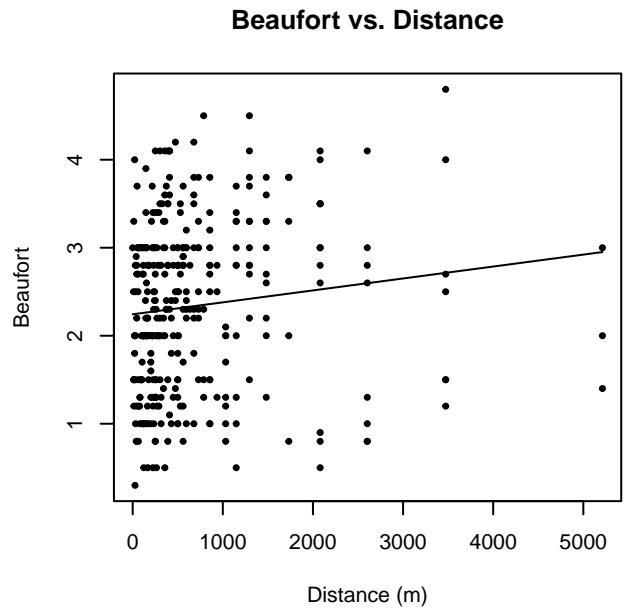
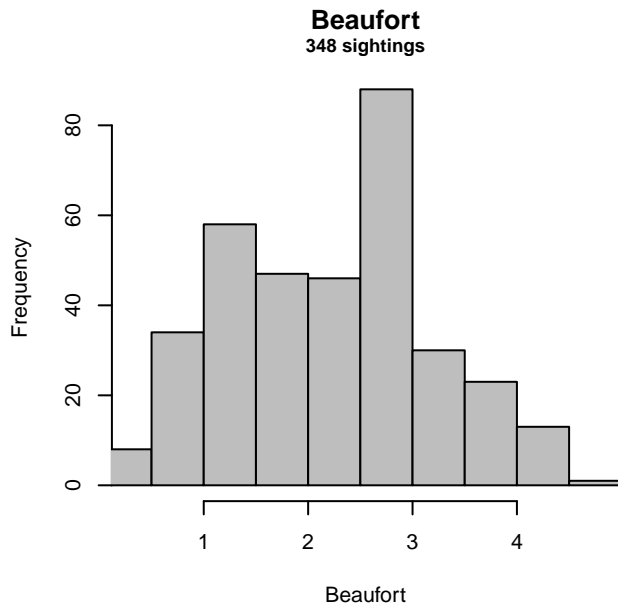


Figure 29: Distribution of the Beaufort covariate before (top row) and after (bottom row) observations were truncated to fit the NEFSC Pre-AMAPPS detection function.

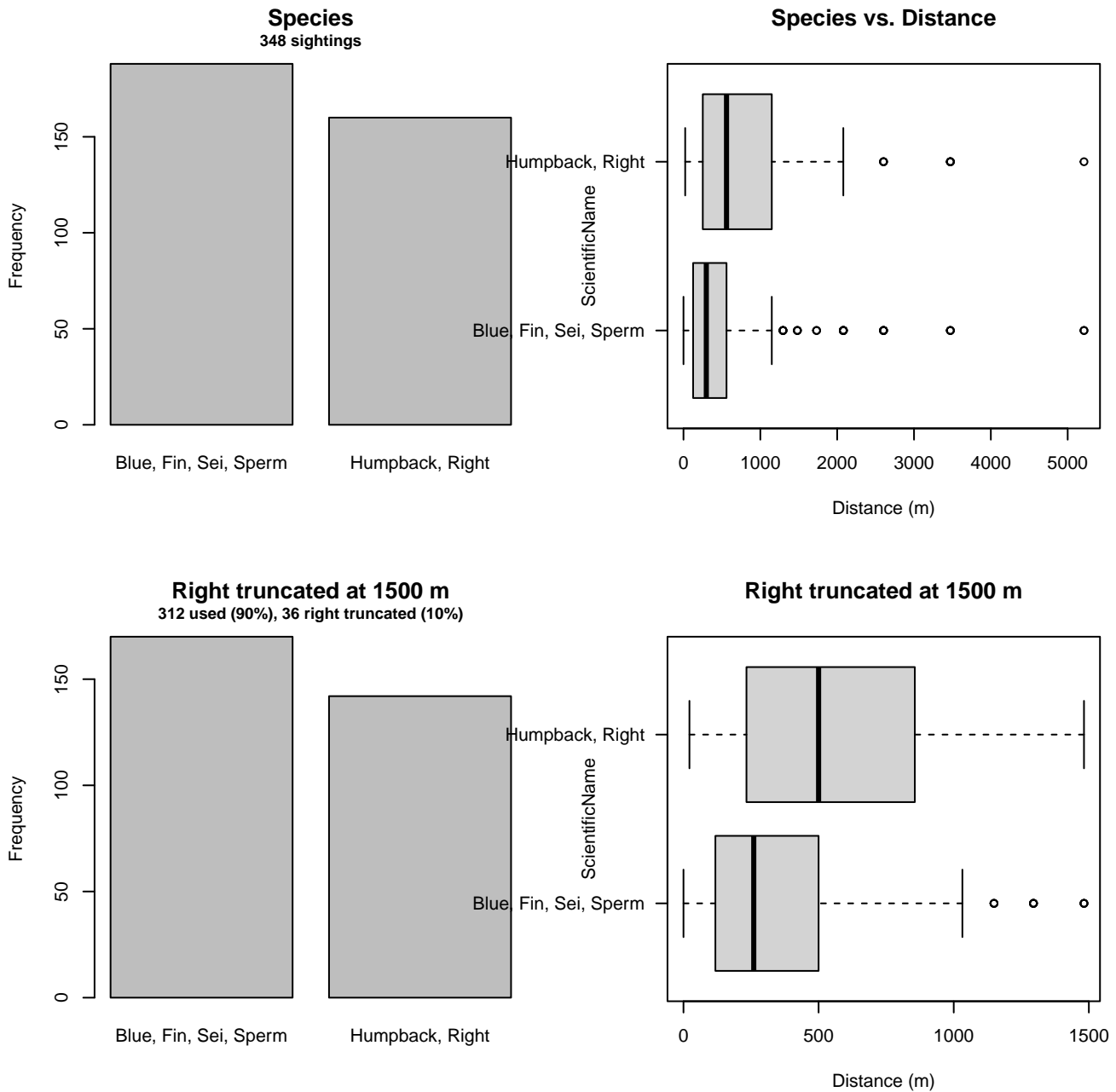


Figure 30: Distribution of the ScientificName covariate before (top row) and after (bottom row) observations were truncated to fit the NEFSC Pre-AMAPPS detection function.

### 3.1.2.1.2 NEFSC AMAPPS Protocol

After right-truncating observations greater than 1500 m, we fitted the detection function to the 342 observations that remained (Table 12). The selected detection function (Figure 31) used a hazard rate key function with Beaufort (Figure 32), ScientificName (Figure 33) and Season (Figure 34) as covariates.

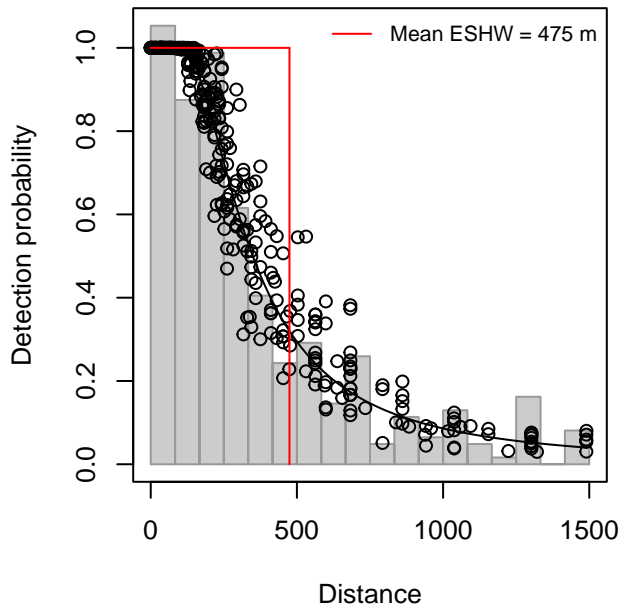
Table 12: Observations used to fit the NEFSC AMAPPS Protocol detection function.

| ScientificName        | n          |
|-----------------------|------------|
| Blue, Fin, Sei, Sperm | 169        |
| Humpback, Right       | 173        |
| <b>Total</b>          | <b>342</b> |



### Large whales by species for Fin Sei

HR key with Season, Species, Beaufort  
342 sightings, right truncated at 1500 m (6%)



### Q-Q Plot

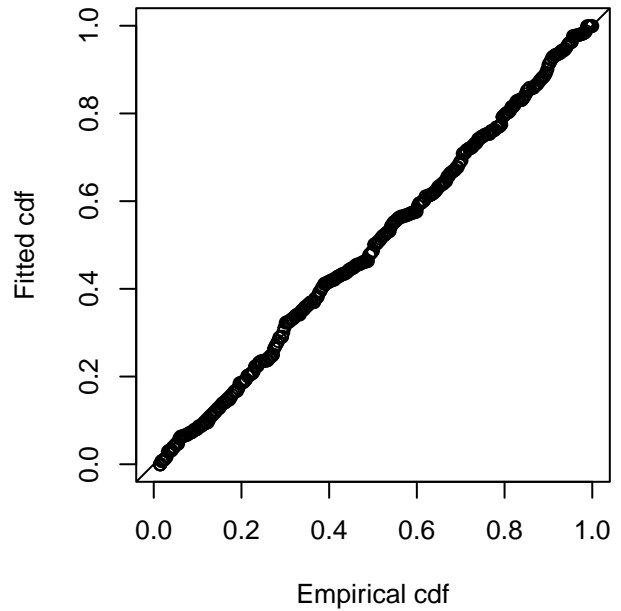


Figure 31: NEFSC AMAPPS Protocol detection function and Q-Q plot showing its goodness of fit.

Statistical output for this detection function:

Summary for ds object

Number of observations : 342  
Distance range : 0 - 1500  
AIC : 4680.051

Detection function:

Hazard-rate key function

Detection function parameters

Scale coefficient(s):

|                               | estimate   | se         |
|-------------------------------|------------|------------|
| (Intercept)                   | 5.4141136  | 0.28874273 |
| SeasonSummer, Fall, Winter    | -0.2958446 | 0.16505718 |
| ScientificNameHumpback, Right | 0.1935469  | 0.15017530 |
| Beaufort                      | 0.1447199  | 0.08488516 |

Shape coefficient(s):

|             | estimate  | se         |
|-------------|-----------|------------|
| (Intercept) | 0.6850132 | 0.09386195 |

|                     | Estimate     | SE          | CV         |
|---------------------|--------------|-------------|------------|
| Average p           | 0.3078245    | 0.02296861  | 0.07461592 |
| N in covered region | 1111.0225351 | 96.96112333 | 0.08727197 |

Distance sampling Cramer-von Mises test (unweighted)

Test statistic = 0.052545 p = 0.860677

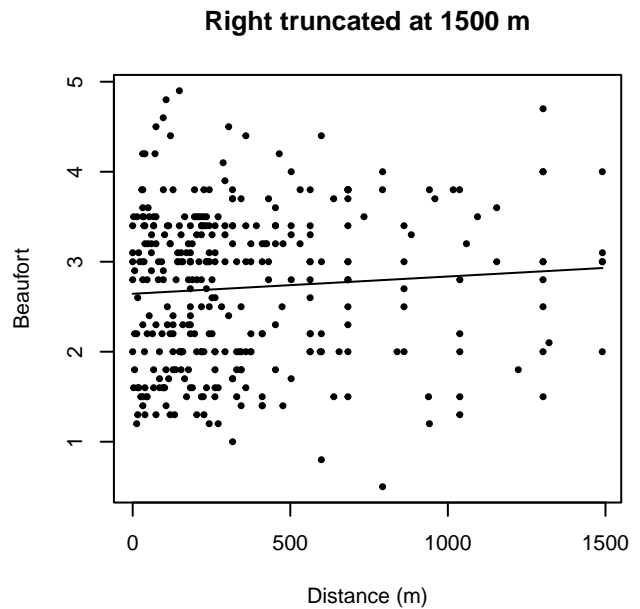
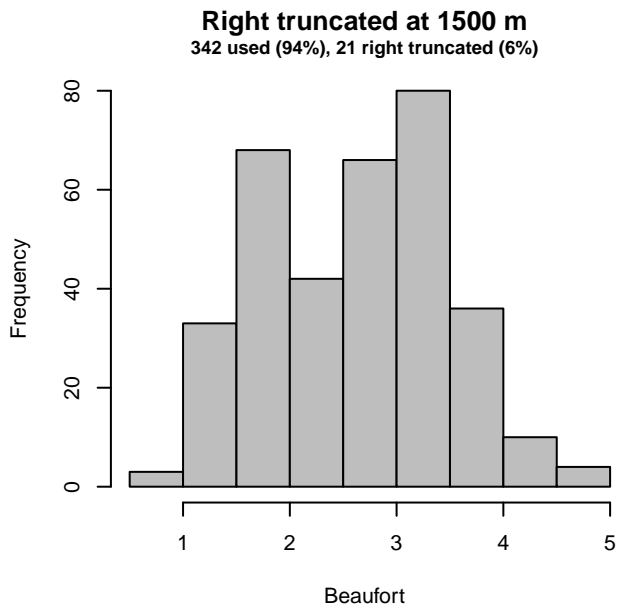
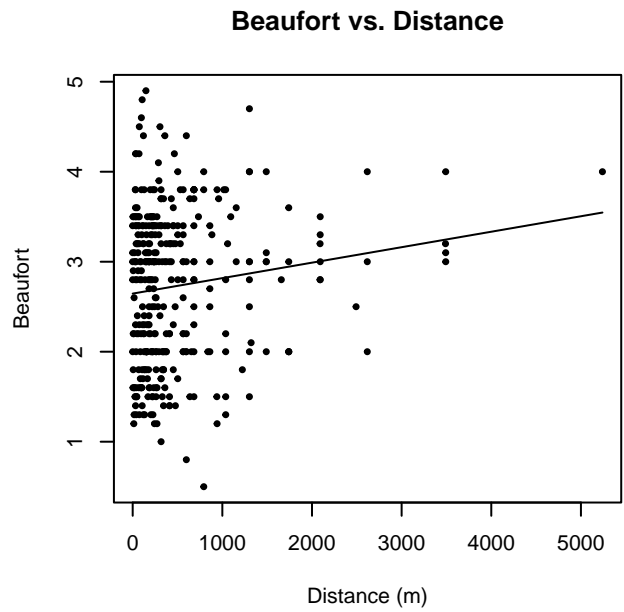
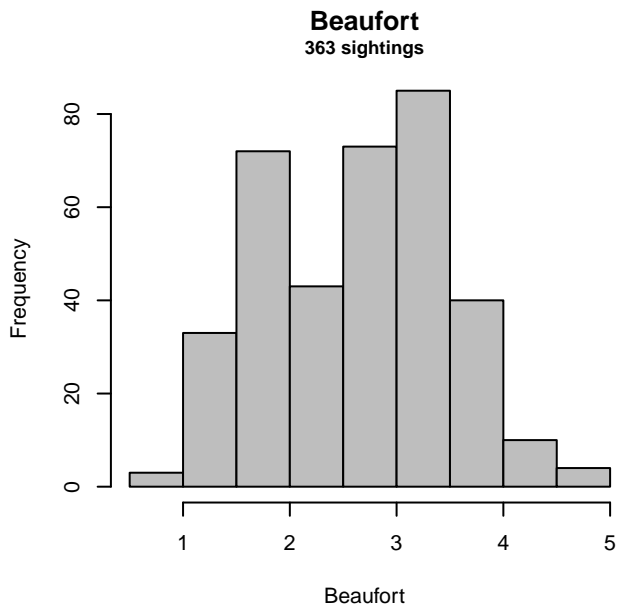


Figure 32: Distribution of the Beaufort covariate before (top row) and after (bottom row) observations were truncated to fit the NEFSC AMAPPS Protocol detection function.

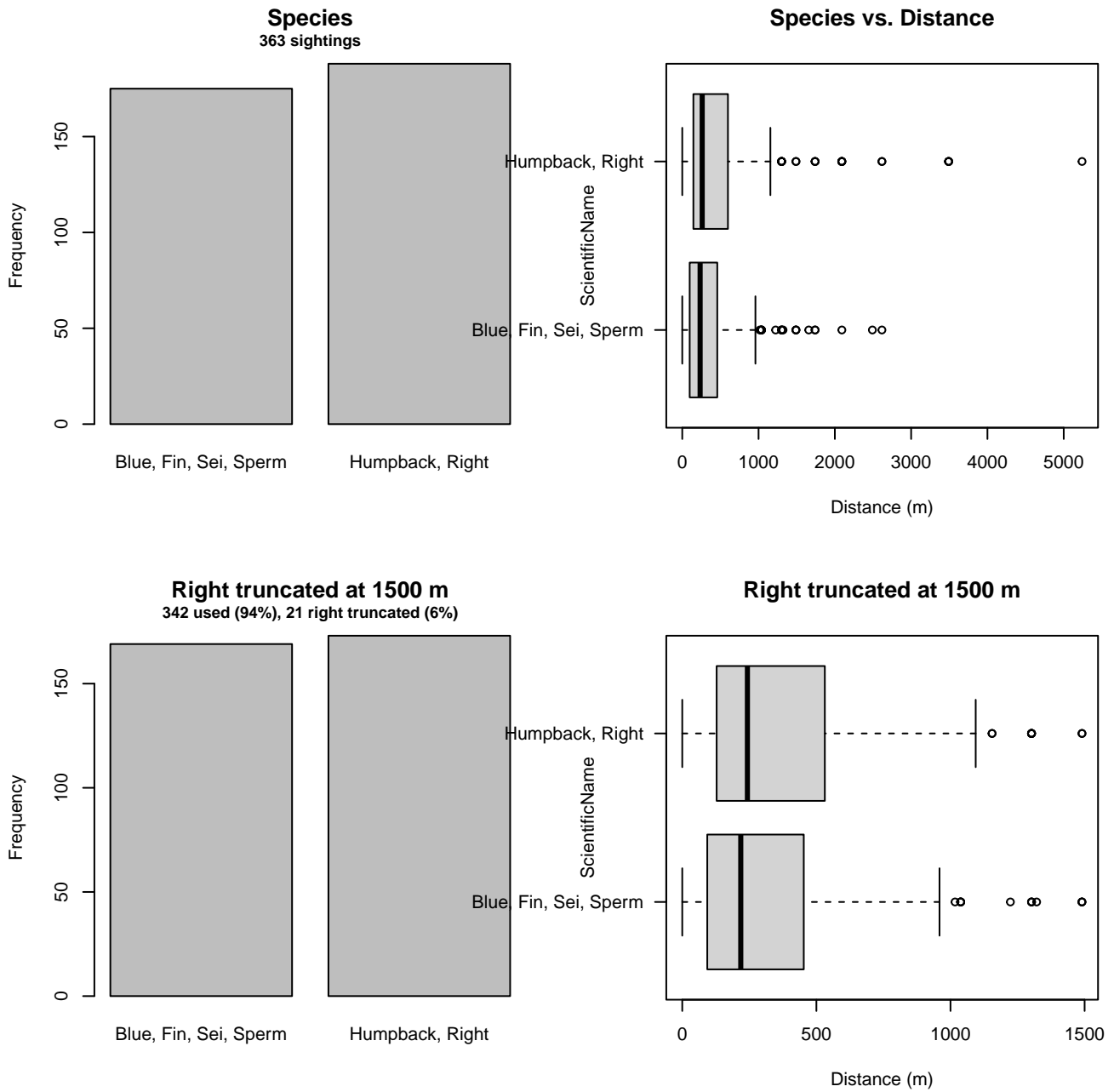


Figure 33: Distribution of the ScientificName covariate before (top row) and after (bottom row) observations were truncated to fit the NEFSC AMAPPS Protocol detection function.

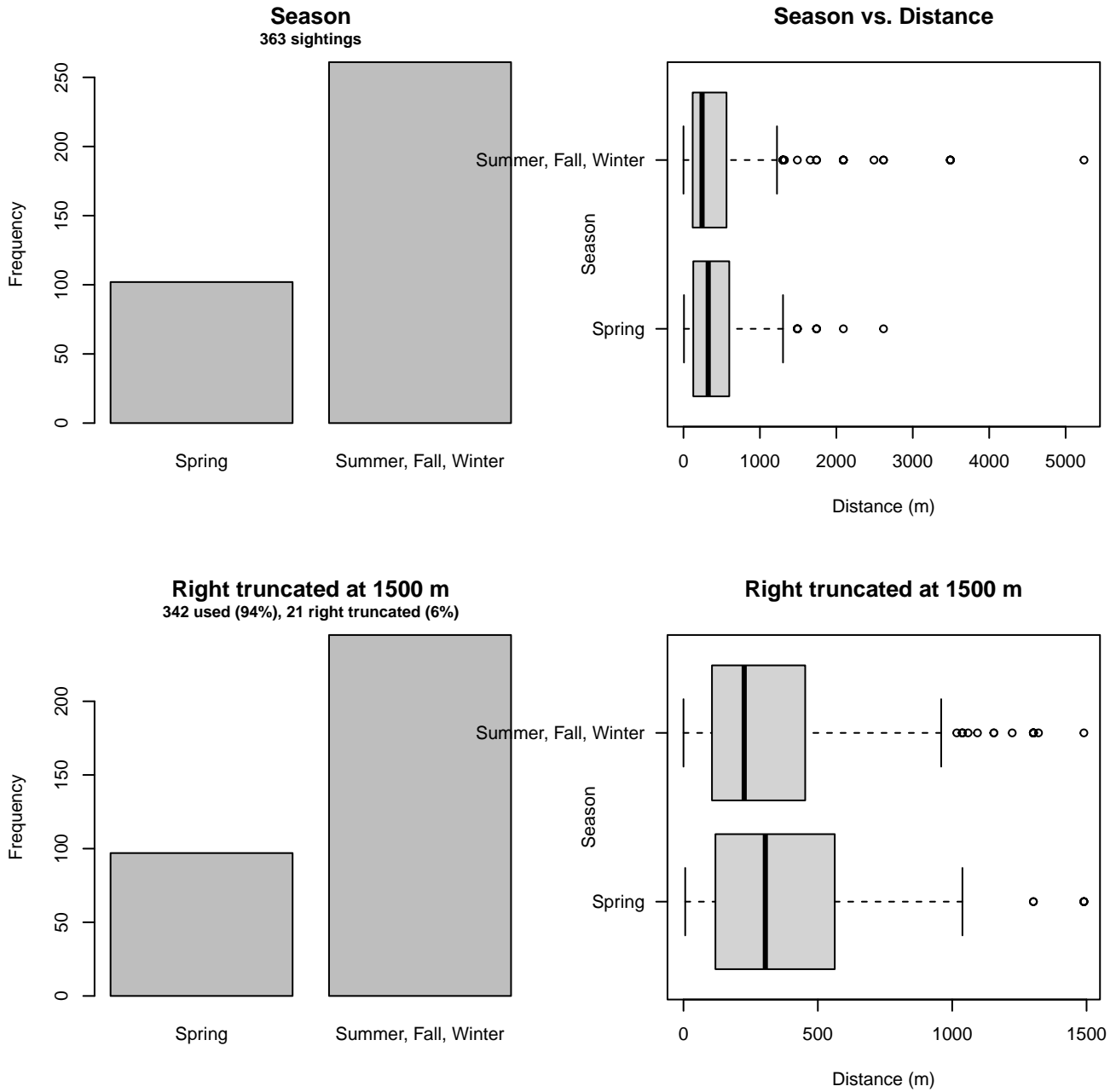


Figure 34: Distribution of the Season covariate before (top row) and after (bottom row) observations were truncated to fit the NEFSC AMAPPS Protocol detection function.

### 3.1.2.1.3 AMAPPS

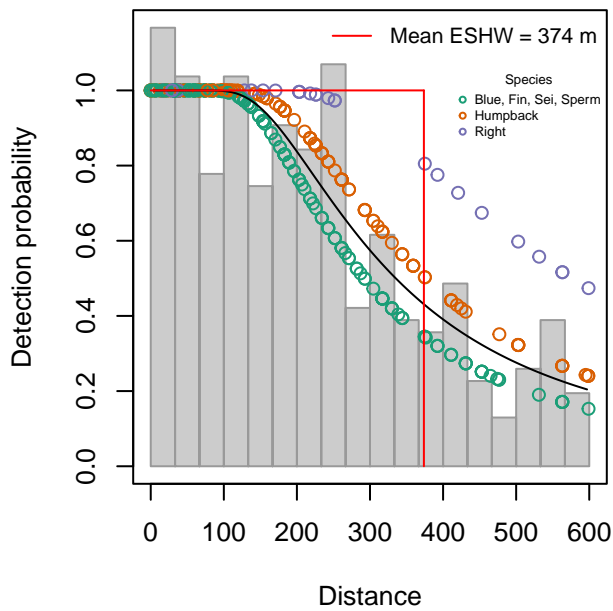
After right-truncating observations greater than 600 m, we fitted the detection function to the 341 observations that remained (Table 13). The selected detection function (Figure 35) used a hazard rate key function with ScientificName (Figure 36) as a covariate.

Table 13: Observations used to fit the AMAPPS detection function.

| ScientificName        | n          |
|-----------------------|------------|
| Blue, Fin, Sei, Sperm | 178        |
| Humpback              | 137        |
| Right                 | 26         |
| <b>Total</b>          | <b>341</b> |

## Large whales by species for Fin Sei

HR key with Species  
341 sightings, right truncated at 600 m (19%)



## Q-Q Plot

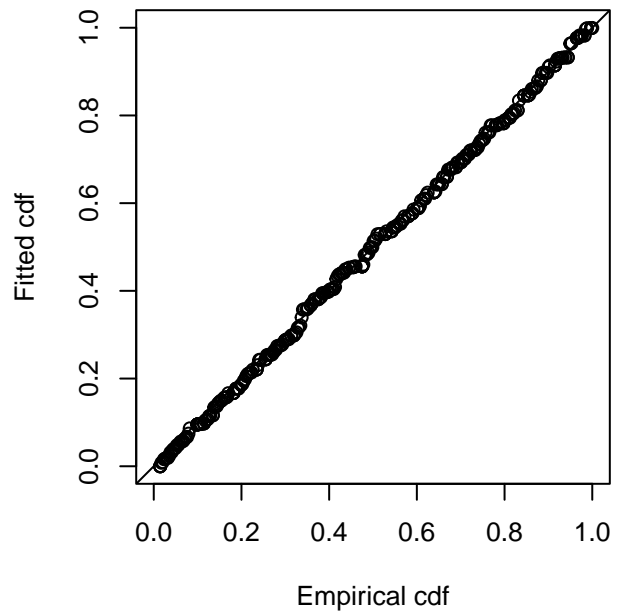


Figure 35: AMAPPS detection function and Q-Q plot showing its goodness of fit.

Statistical output for this detection function:

Summary for ds object

Number of observations : 341  
Distance range : 0 - 600  
AIC : 4284.044

Detection function:

Hazard-rate key function

Detection function parameters

Scale coefficient(s):

|                        | estimate  | se        |
|------------------------|-----------|-----------|
| (Intercept)            | 5.4948745 | 0.1470359 |
| ScientificNameHumpback | 0.2526859 | 0.1796647 |
| ScientificNameRight    | 0.6784369 | 0.3879710 |

Shape coefficient(s):

|             | estimate  | se        |
|-------------|-----------|-----------|
| (Intercept) | 0.6905331 | 0.1975579 |

|                     | Estimate    | SE          | CV         |
|---------------------|-------------|-------------|------------|
| Average p           | 0.6139761   | 0.04048736  | 0.06594289 |
| N in covered region | 555.3962176 | 41.21446559 | 0.07420732 |

Distance sampling Cramer-von Mises test (unweighted)

Test statistic = 0.027885 p = 0.982585

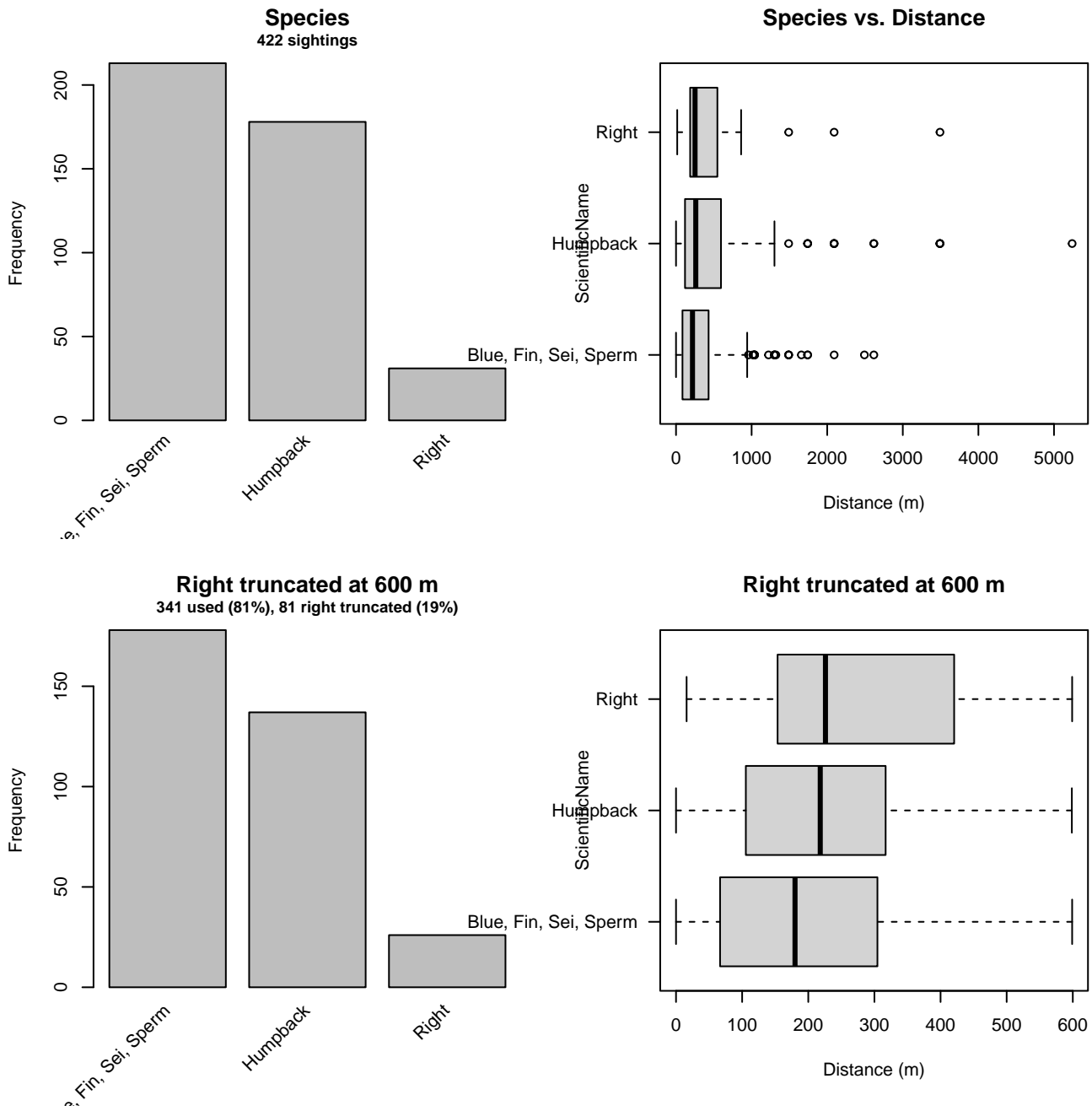


Figure 36: Distribution of the ScientificName covariate before (top row) and after (bottom row) observations were truncated to fit the AMAPPS detection function.

#### 3.1.2.1.4 NARWSS 2003-2016

After right-truncating observations greater than 5236 m, we fitted the detection function to the 7315 observations that remained (Table 14). The selected detection function (Figure 37) used a hazard rate key function with Beaufort (Figure 38), Glare (Figure 39), ScientificName (Figure 40) and Visibility (Figure 41) as covariates.

Table 14: Observations used to fit the NARWSS 2003-2016 detection function.

| ScientificName        | n           |
|-----------------------|-------------|
| Blue, Fin, Sei, Sperm | 3084        |
| Humpback              | 2890        |
| Right, Bowhead        | 1341        |
| <b>Total</b>          | <b>7315</b> |

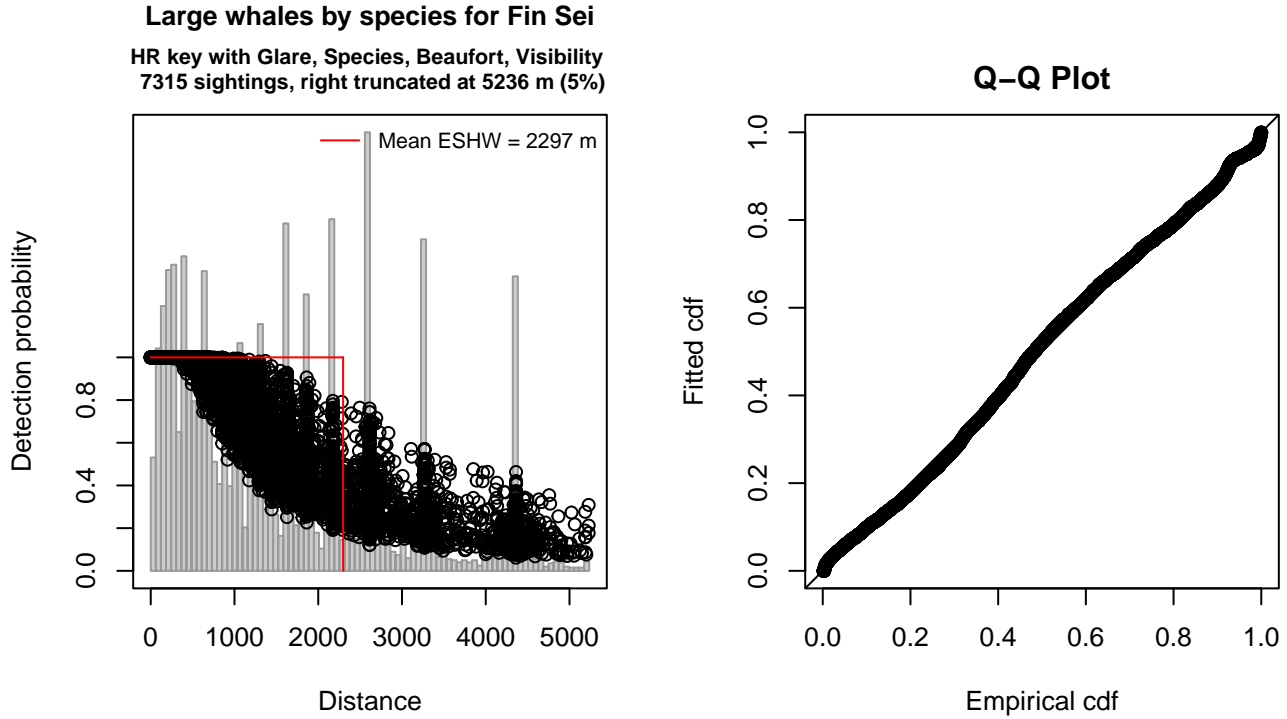


Figure 37: NARWSS 2003-2016 detection function and Q-Q plot showing its goodness of fit.

Statistical output for this detection function:

Summary for ds object

Number of observations : 7315  
 Distance range : 0 - 5236  
 AIC : 121560.3

Detection function:

Hazard-rate key function

Detection function parameters

Scale coefficient(s):

|                              | estimate    | se          |
|------------------------------|-------------|-------------|
| (Intercept)                  | 6.532231399 | 0.095753398 |
| GlareSevere                  | 0.418817117 | 0.059020446 |
| ScientificNameHumpback       | 0.392288899 | 0.046225103 |
| ScientificNameRight, Bowhead | 0.123395135 | 0.057328635 |
| Beaufort                     | 0.099396384 | 0.022096321 |
| Visibility                   | 0.007659624 | 0.002242667 |

Shape coefficient(s):

|             | estimate  | se         |
|-------------|-----------|------------|
| (Intercept) | 0.4861478 | 0.03138397 |

|                     | Estimate     | SE           | CV         |
|---------------------|--------------|--------------|------------|
| Average p           | 4.220665e-01 | 7.456216e-03 | 0.01766597 |
| N in covered region | 1.733139e+04 | 3.437425e+02 | 0.01983352 |

Distance sampling Cramer-von Mises test (unweighted)  
 Test statistic = 1.731302 p = 0.000052

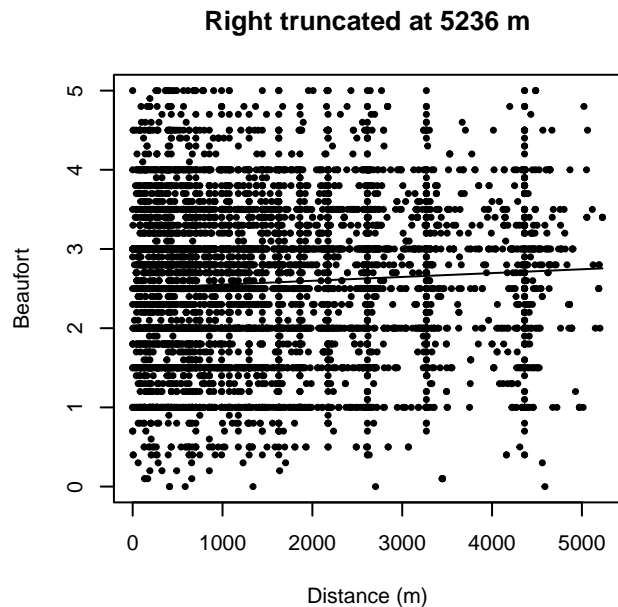
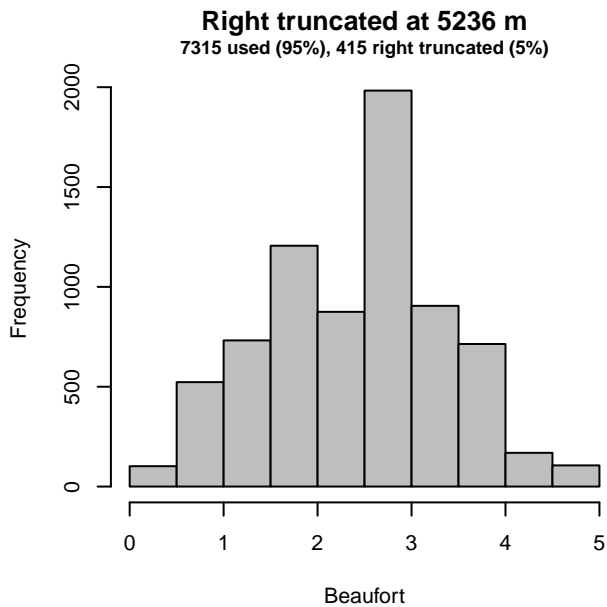
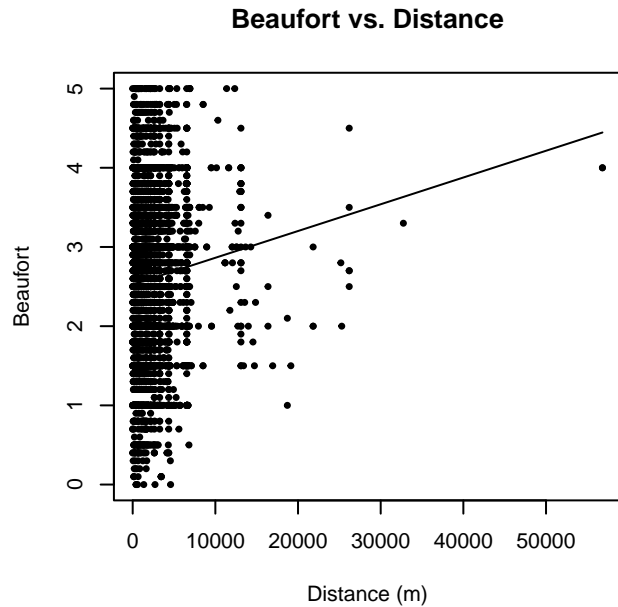
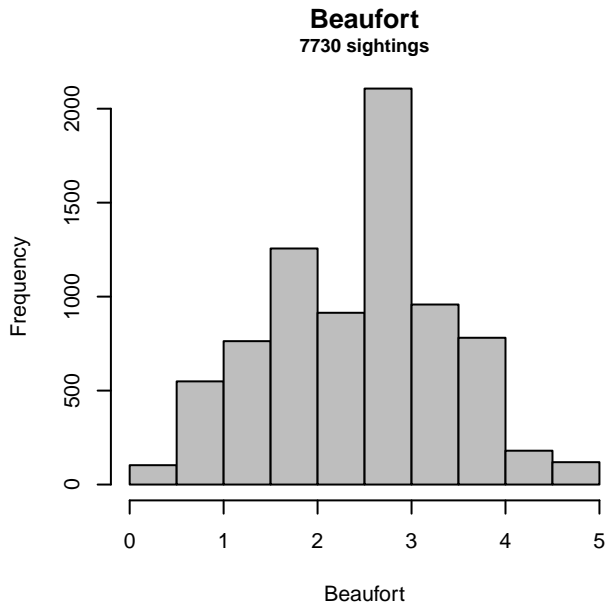


Figure 38: Distribution of the Beaufort covariate before (top row) and after (bottom row) observations were truncated to fit the NARWSS 2003-2016 detection function.



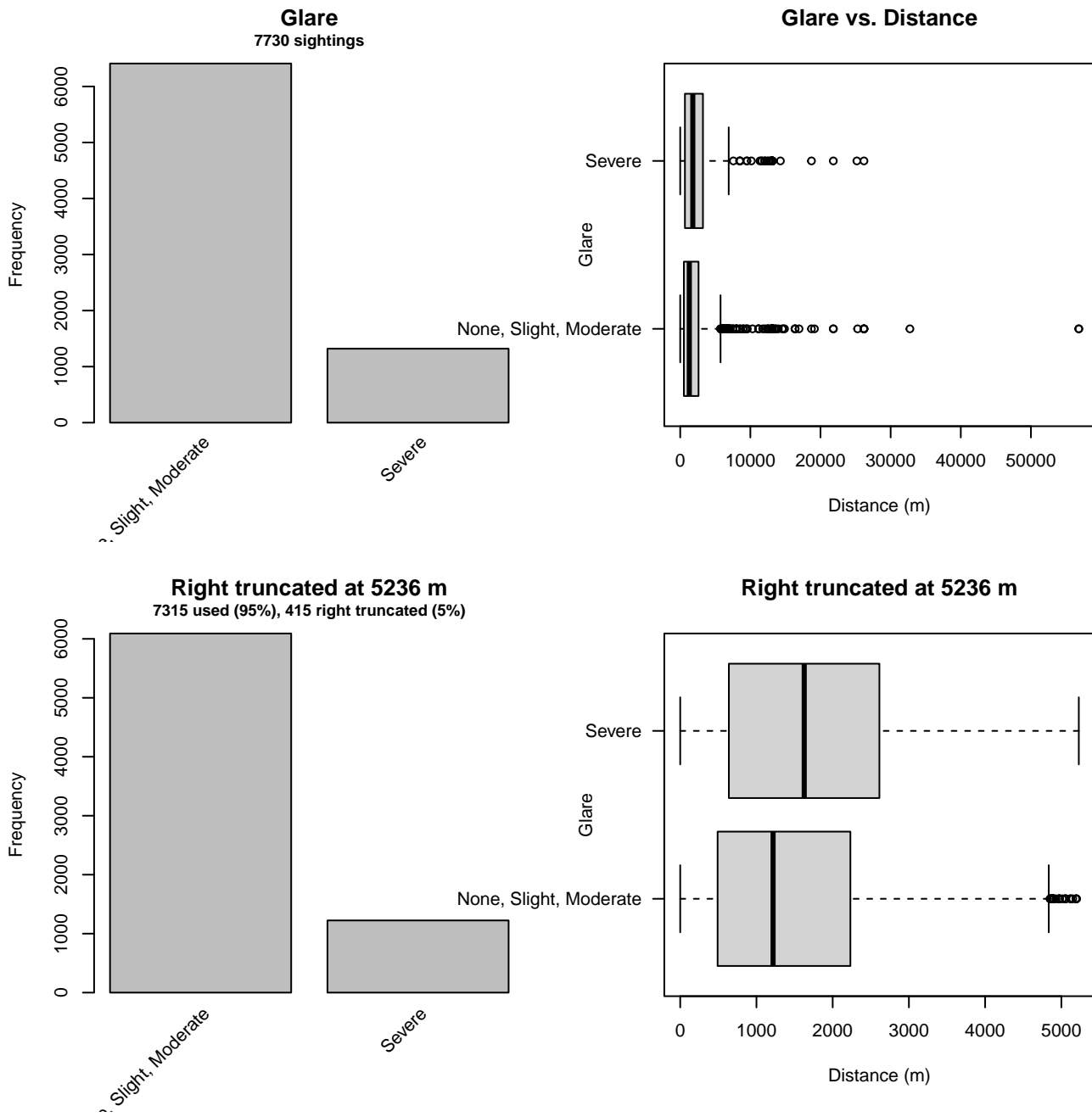


Figure 39: Distribution of the Glare covariate before (top row) and after (bottom row) observations were truncated to fit the NARWSS 2003-2016 detection function.

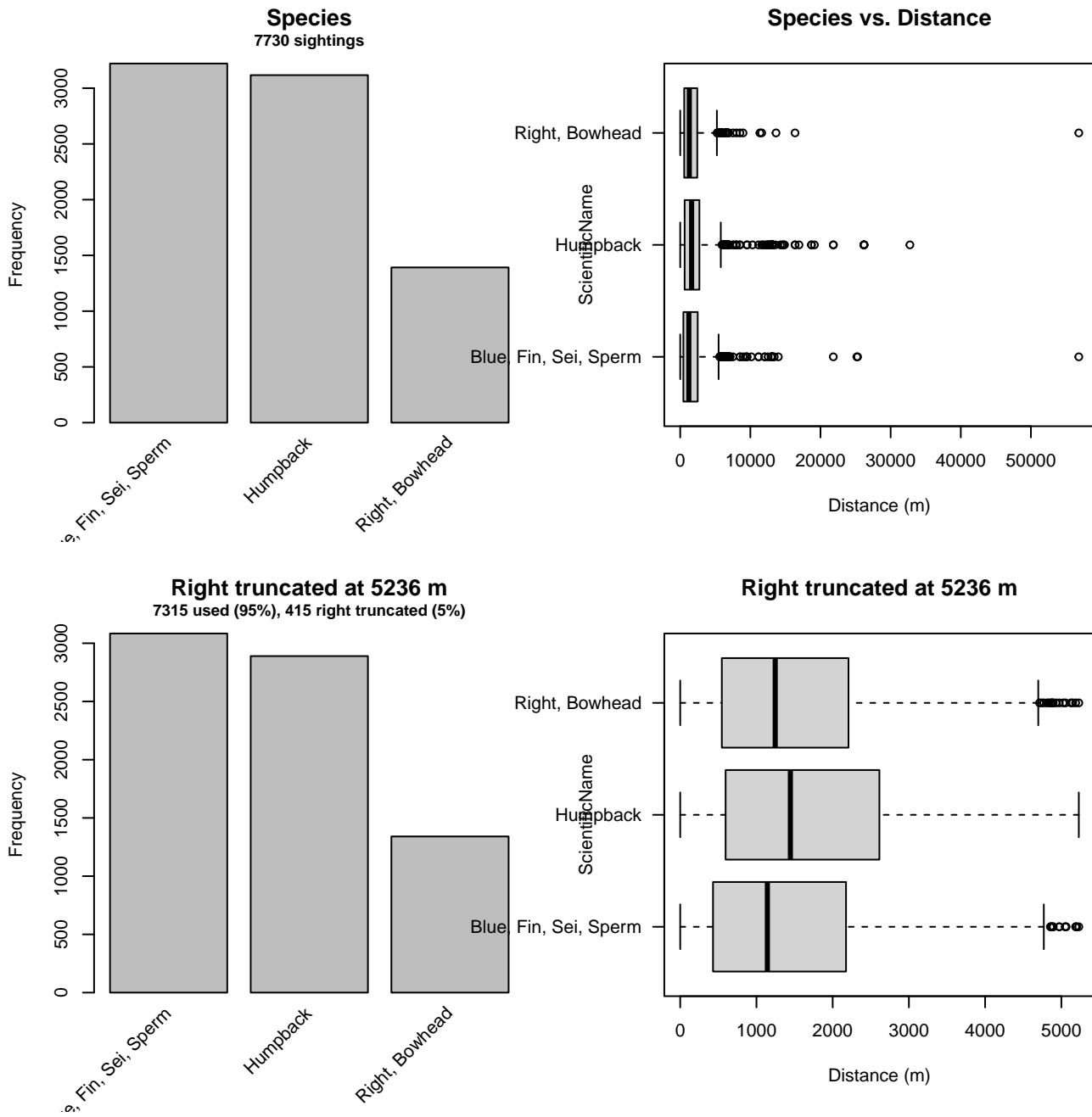


Figure 40: Distribution of the ScientificName covariate before (top row) and after (bottom row) observations were truncated to fit the NARWSS 2003-2016 detection function.

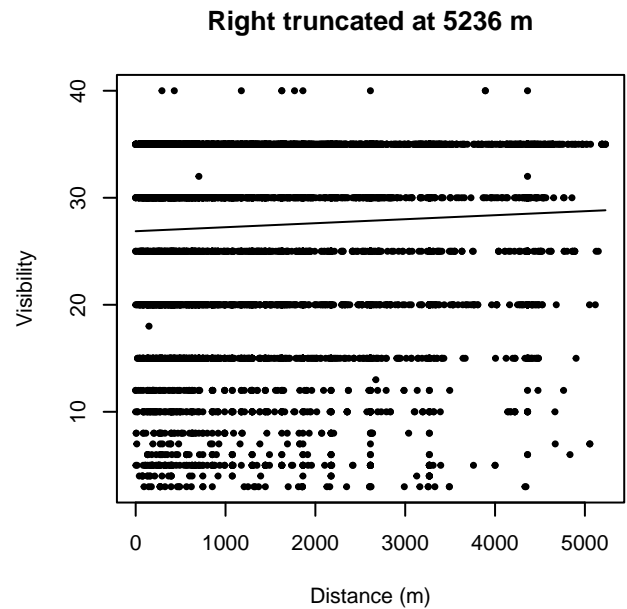
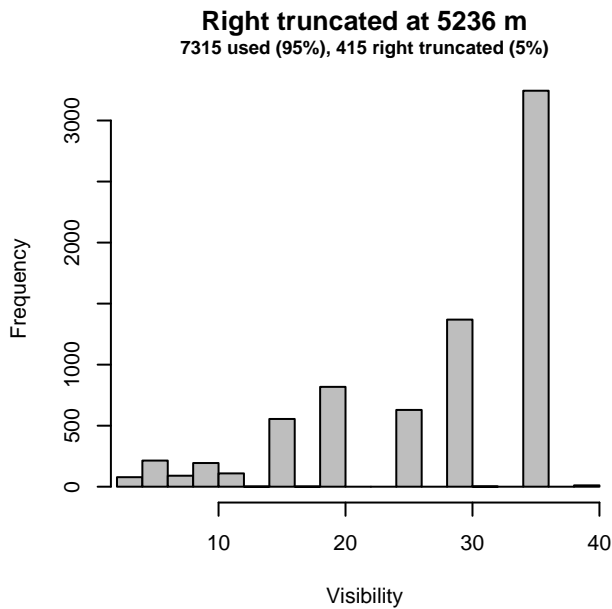
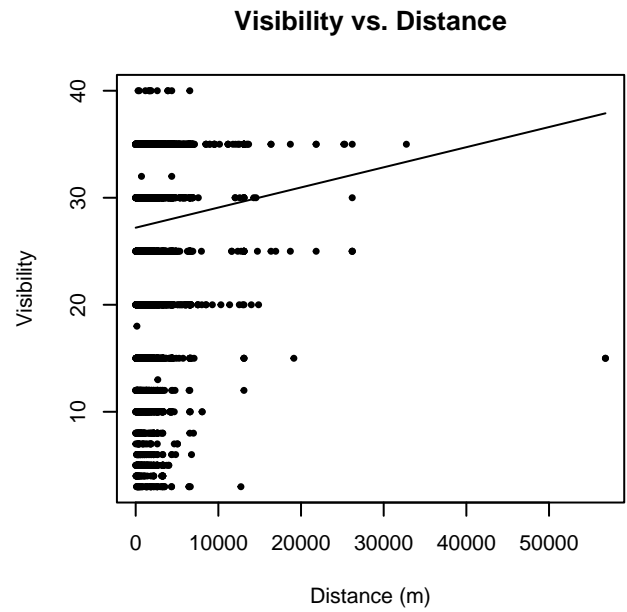
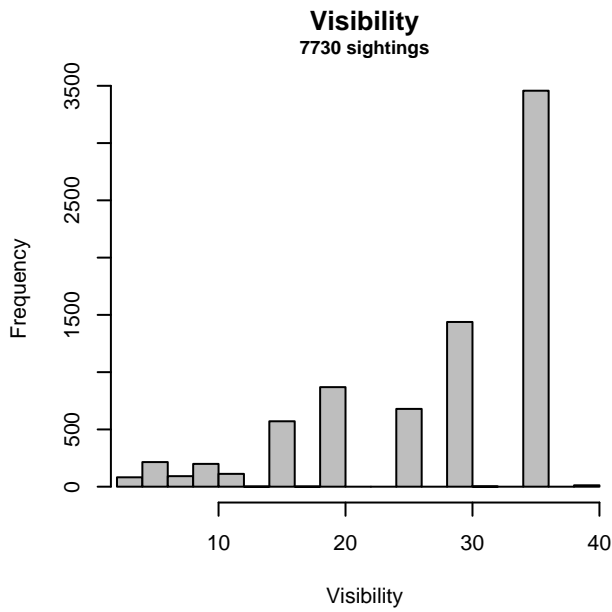


Figure 41: Distribution of the Visibility covariate before (top row) and after (bottom row) observations were truncated to fit the NARWSS 2003-2016 detection function.

### 3.1.2.1.5 NARWSS 2017-2020

After right-truncating observations greater than 5236 m, we fitted the detection function to the 1088 observations that remained (Table 15). The selected detection function (Figure 42) used a hazard rate key function with QualityCode (Figure 43) and ScientificName (Figure 44) as covariates.

Table 15: Observations used to fit the NARWSS 2017-2020 detection function.

| ScientificName                   | n           |
|----------------------------------|-------------|
| Blue, Bowhead, Fin, Right, Sperm | 510         |
| Humpback                         | 402         |
| Sei, Bryde's                     | 176         |
| <b>Total</b>                     | <b>1088</b> |

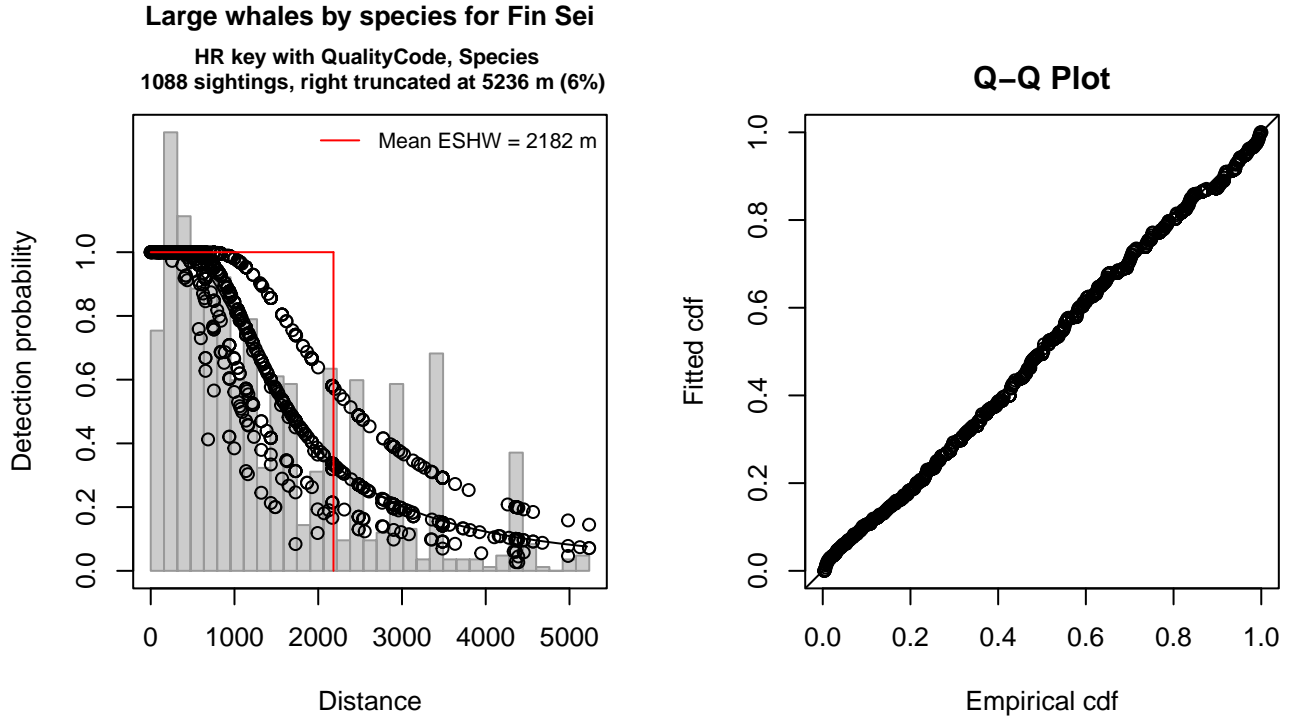


Figure 42: NARWSS 2017-2020 detection function and Q-Q plot showing its goodness of fit.

Statistical output for this detection function:

Summary for ds object

Number of observations : 1088  
 Distance range : 0 - 5236  
 AIC : 17919.96

Detection function:

Hazard-rate key function

Detection function parameters

Scale coefficient(s):

|                            | estimate   | se         |
|----------------------------|------------|------------|
| (Intercept)                | 7.2235234  | 0.08269456 |
| QualityCodeGood            | -0.4184817 | 0.11743936 |
| QualityCodeModerate        | -0.7472672 | 0.45781582 |
| ScientificNameHumpback     | 0.3855596  | 0.09754242 |
| ScientificNameSei, Bryde's | -0.2722542 | 0.12297203 |

Shape coefficient(s):

|             | estimate  | se         |
|-------------|-----------|------------|
| (Intercept) | 0.6646987 | 0.07157793 |

|                     | Estimate     | SE           | CV         |
|---------------------|--------------|--------------|------------|
| Average p           | 0.3945574    | 0.01634594   | 0.04142856 |
| N in covered region | 2757.5202964 | 132.04989012 | 0.04788719 |

Distance sampling Cramer-von Mises test (unweighted)  
 Test statistic = 0.162876 p = 0.352620

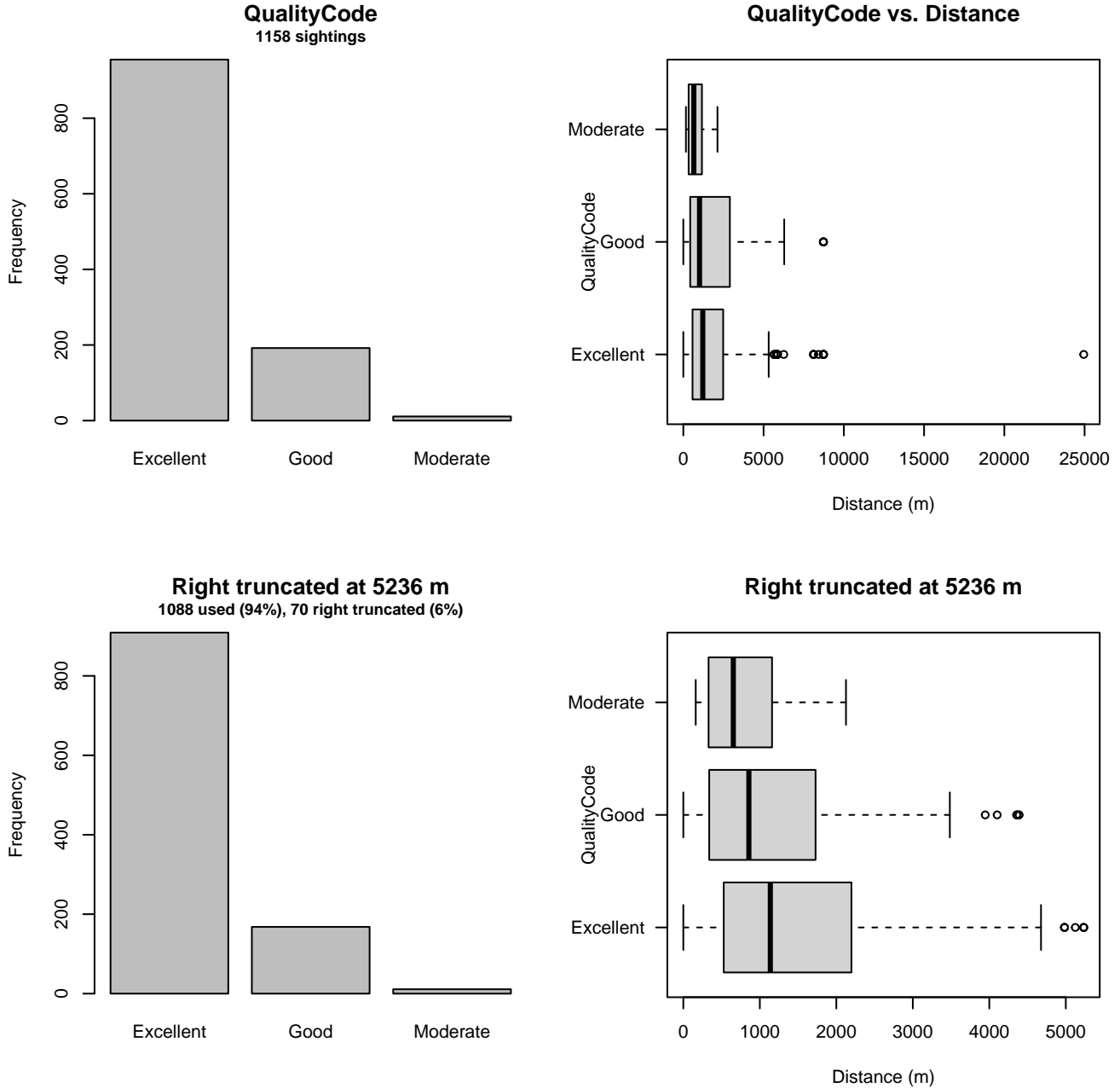


Figure 43: Distribution of the QualityCode covariate before (top row) and after (bottom row) observations were truncated to fit the NARWSS 2017-2020 detection function.

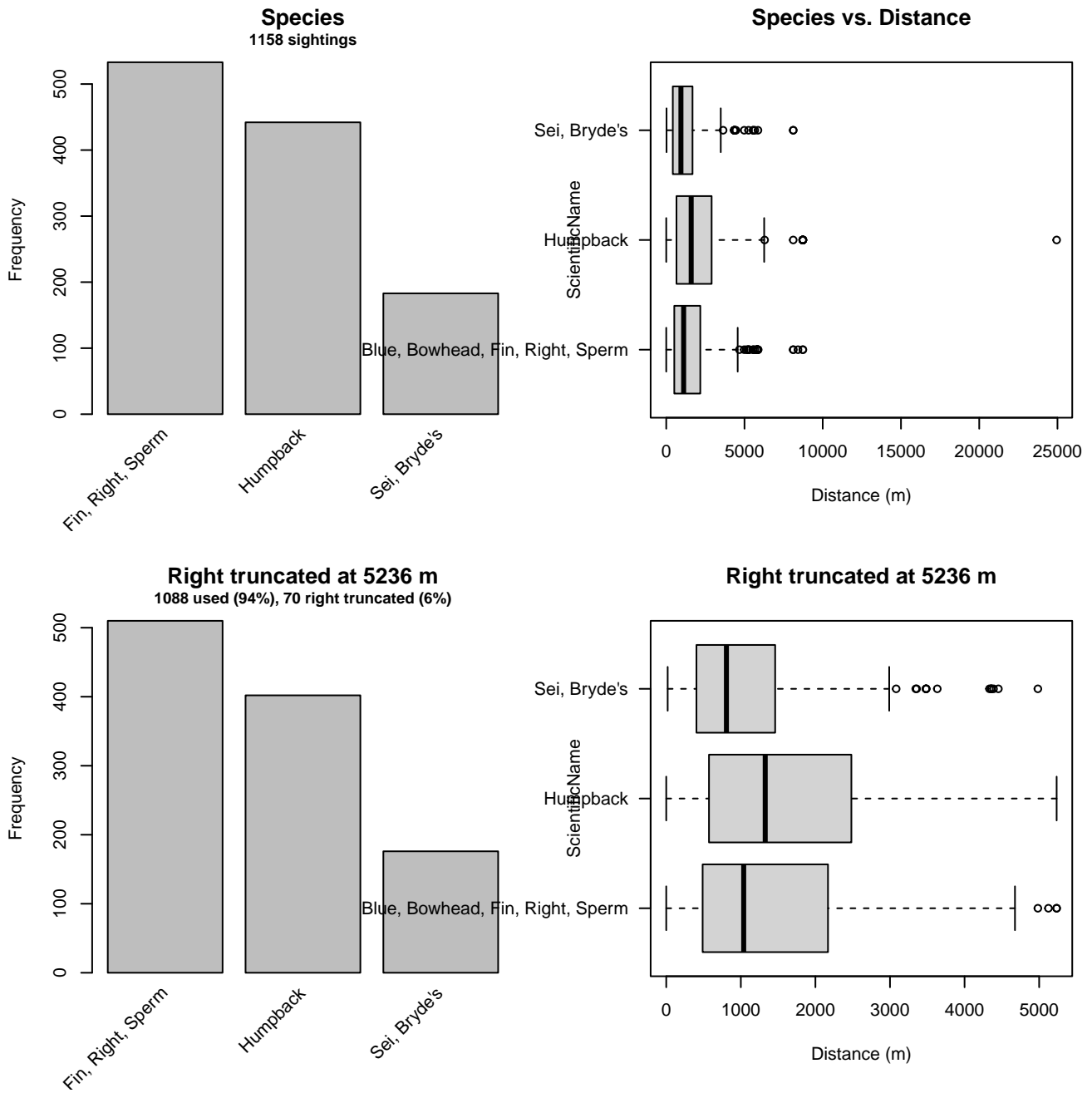


Figure 44: Distribution of the ScientificName covariate before (top row) and after (bottom row) observations were truncated to fit the NARWSS 2017-2020 detection function.

### 3.1.2.2 Shipboard Surveys

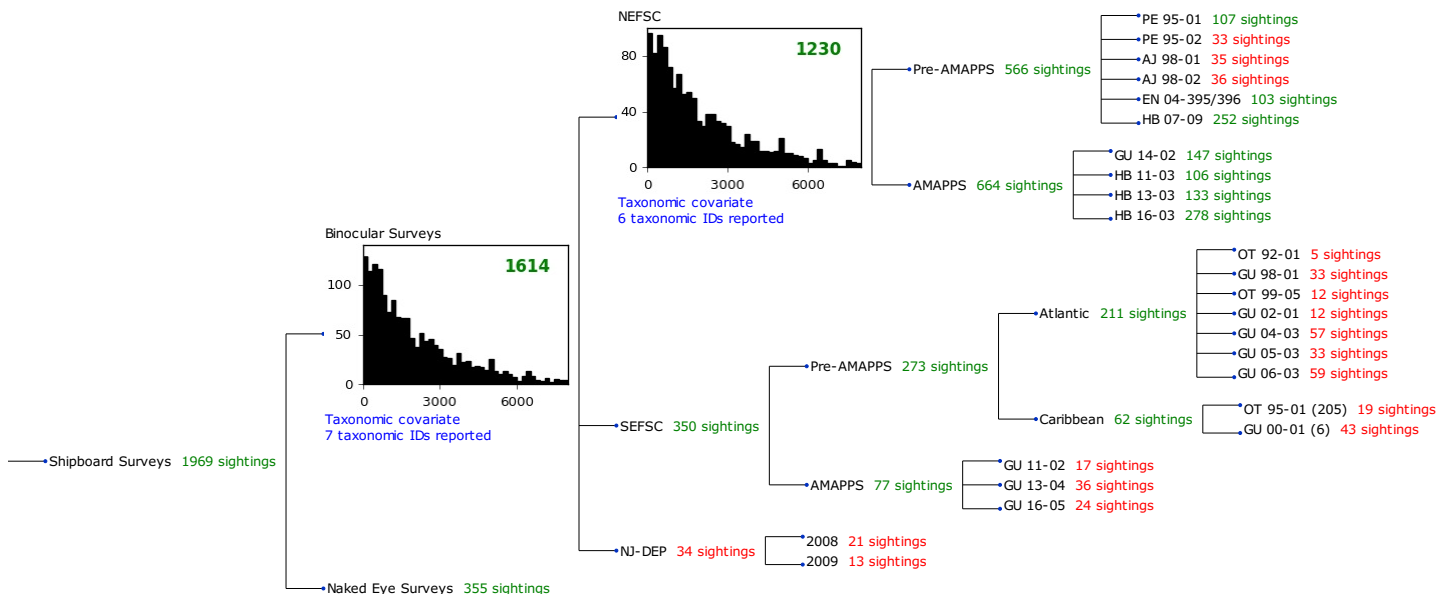


Figure 45: Detection hierarchy for shipboard surveys, showing how they were pooled during detectability modeling, for detection functions that pooled multiple taxa and used a taxonomic covariate to account for differences between them. Each histogram represents a detection function and summarizes the perpendicular distances of observations that were pooled to fit it, prior to truncation. Observation counts, also prior to truncation, are shown in green when they met the recommendation of Buckland et al. (2001) that detection functions utilize at least 60 sightings, and red otherwise. For rare taxa, it was not always possible to meet this recommendation, yielding higher statistical uncertainty. During the spatial modeling stage of the analysis, effective strip widths were computed for each survey using the closest detection function above it in the hierarchy (i.e. moving from right to left in the figure). Surveys that do not have a detection function above them in this figure were either addressed by a detection function presented in a different section of this report, or were omitted from the analysis.

#### 3.1.2.2.1 NEFSC

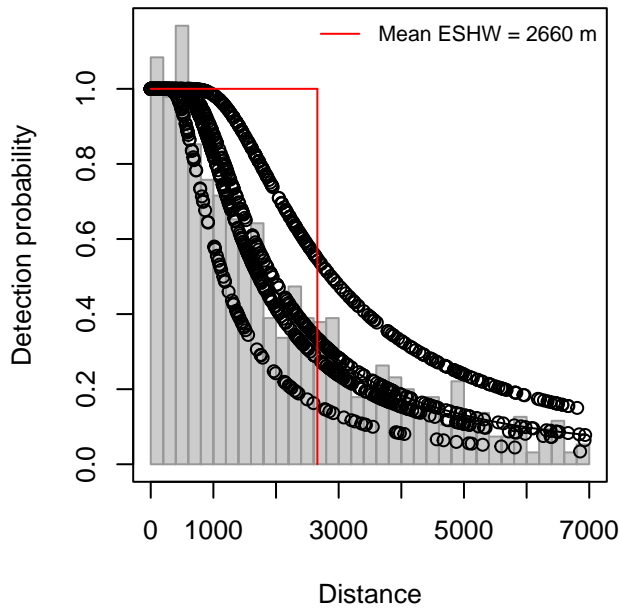
After right-truncating observations greater than 7000 m, we fitted the detection function to the 1201 observations that remained (Table 16). The selected detection function (Figure 46) used a hazard rate key function with Program (Figure 47) and ScientificName (Figure 48) as covariates.

Table 16: Observations used to fit the NEFSC detection function.

| ScientificName        | n           |
|-----------------------|-------------|
| Blue, Fin, Right, Sei | 452         |
| Humpback, Sperm       | 749         |
| <b>Total</b>          | <b>1201</b> |

## Large whales by species for Fin Sei

HR key with Program, Species  
1201 sightings, right truncated at 7000 m (2%)



## Q-Q Plot

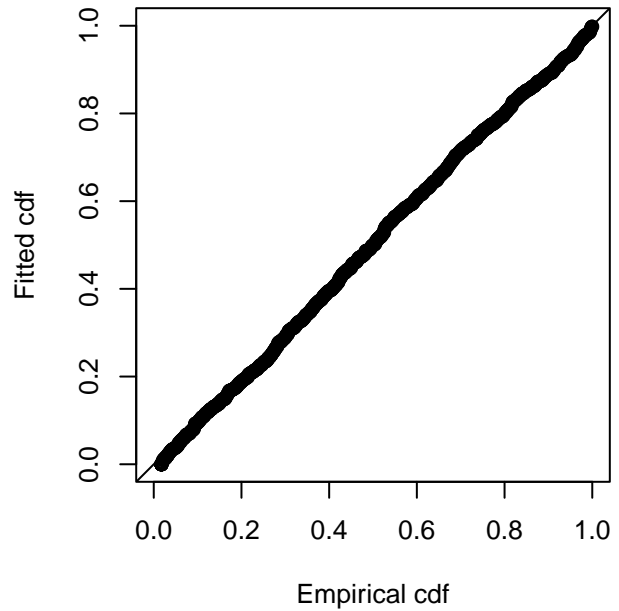


Figure 46: NEFSC detection function and Q-Q plot showing its goodness of fit.

Statistical output for this detection function:

Summary for ds object

Number of observations : 1201  
Distance range : 0 - 7000  
AIC : 20465.31

Detection function:

Hazard-rate key function

Detection function parameters

Scale coefficient(s):

|  | estimate   | se         |
|--|------------|------------|
| (Intercept)                            | 7.3545852  | 0.10172378 |
| ProgramMarine Mammal Abundance Surveys | -0.5171427 | 0.09909896 |
| ScientificNameHumpback, Sperm          | 0.3937321  | 0.10074438 |

Shape coefficient(s):

|             | estimate  | se         |
|-------------|-----------|------------|
| (Intercept) | 0.5222304 | 0.06599629 |

|                     | Estimate     | SE           | CV         |
|---------------------|--------------|--------------|------------|
| Average p           | 0.3611076    | 0.01603822   | 0.04441397 |
| N in covered region | 3325.8788088 | 166.96697837 | 0.05020236 |

Distance sampling Cramer-von Mises test (unweighted)

Test statistic = 0.099680 p = 0.586443



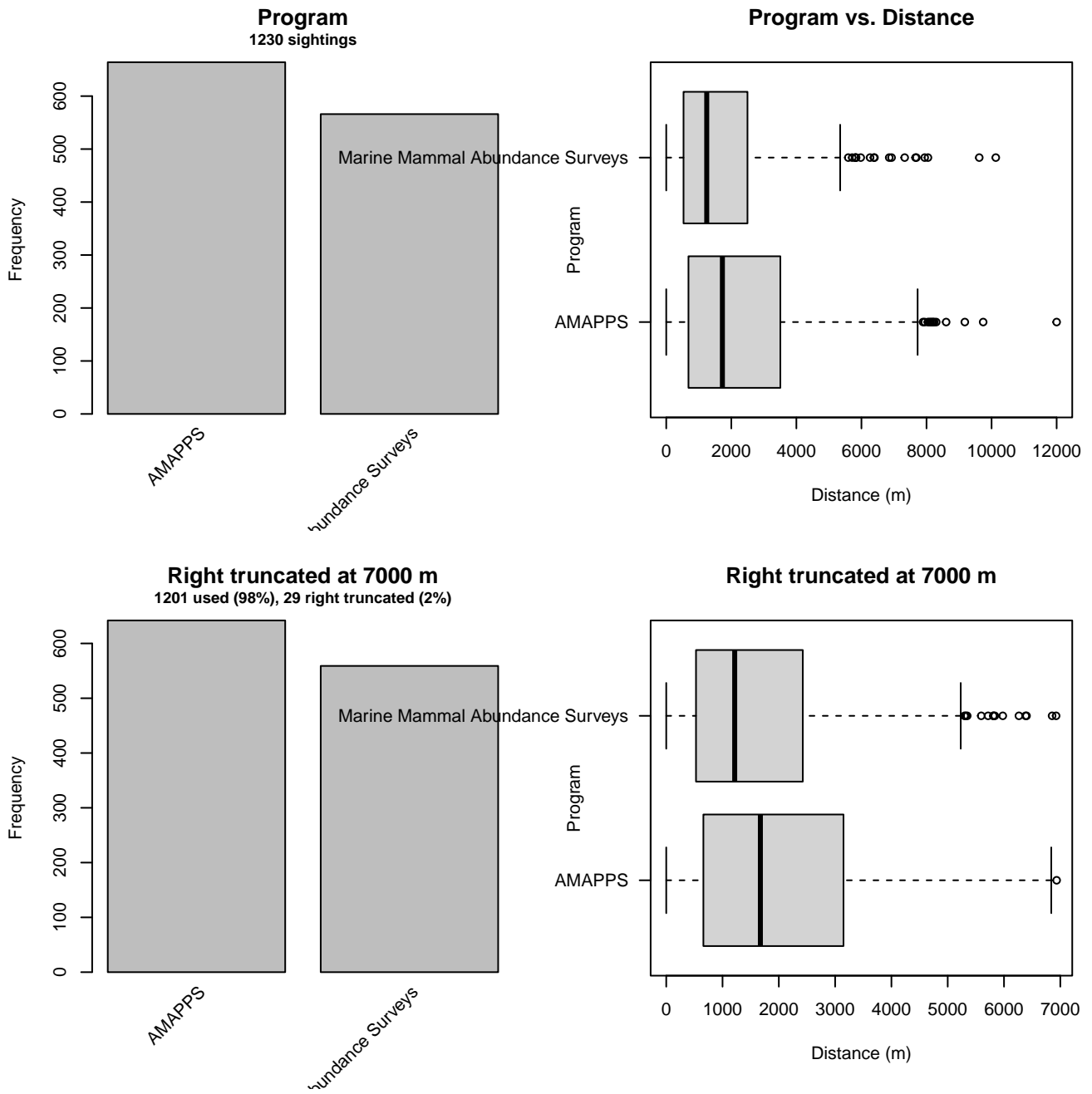


Figure 47: Distribution of the Program covariate before (top row) and after (bottom row) observations were truncated to fit the NEFSC detection function.

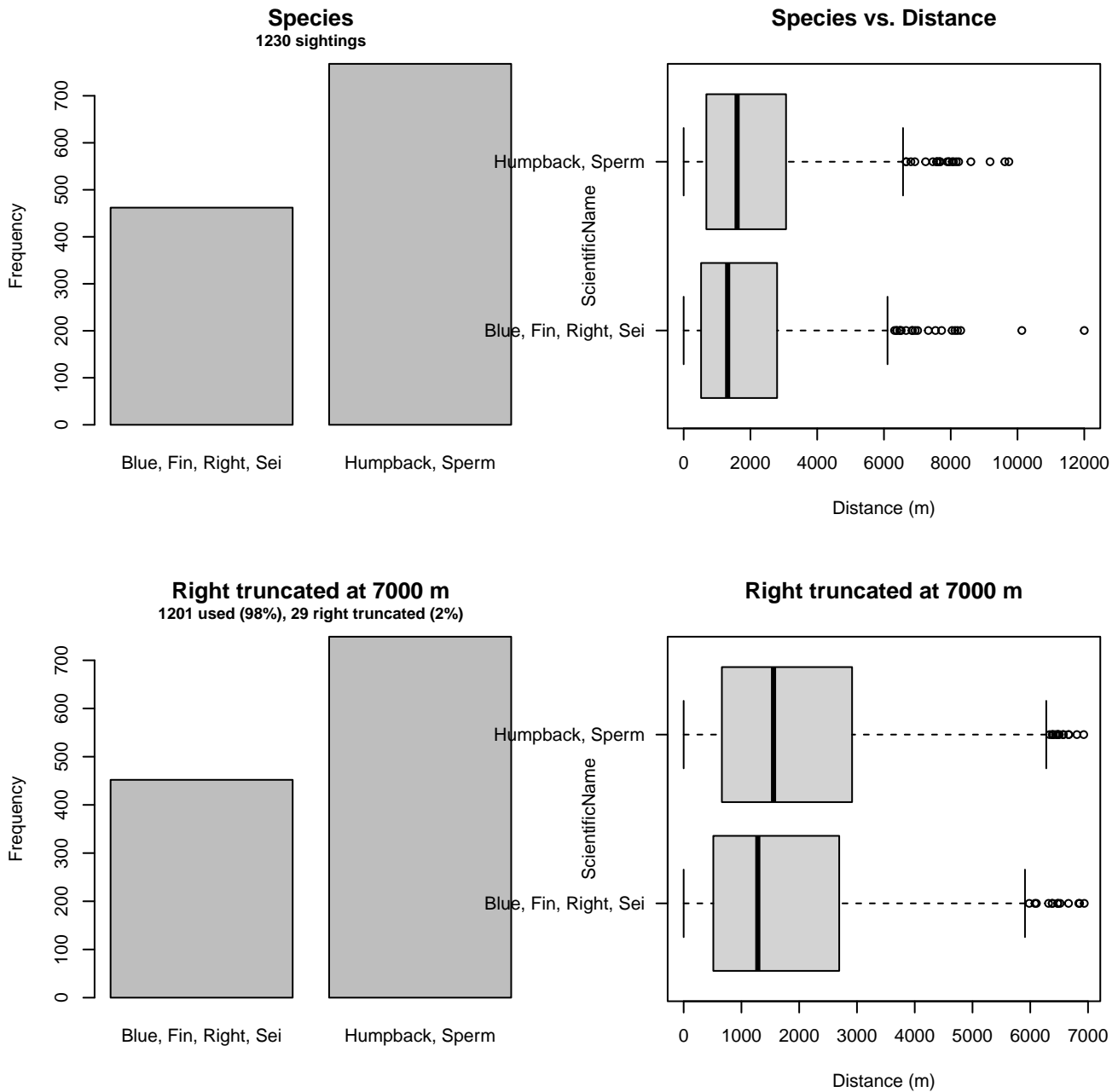


Figure 48: Distribution of the ScientificName covariate before (top row) and after (bottom row) observations were truncated to fit the NEFSC detection function.

### 3.1.2.2.2 Binocular Surveys

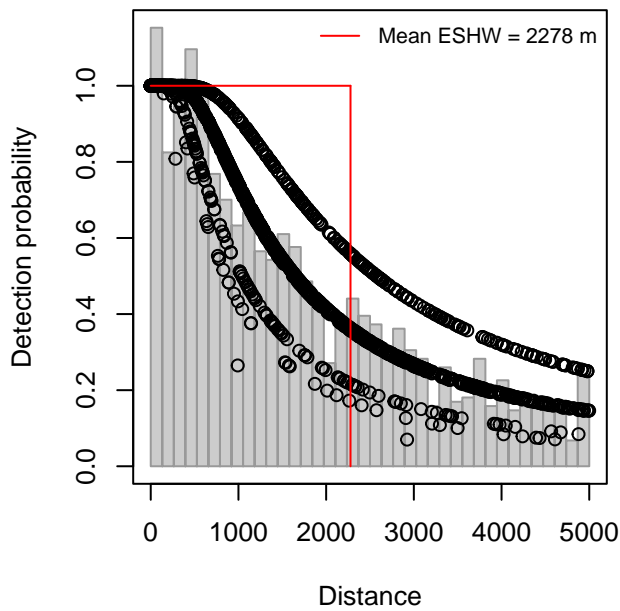
After right-truncating observations greater than 5000 m, we fitted the detection function to the 1471 observations that remained (Table 17). The selected detection function (Figure 49) used a hazard rate key function with Program (Figure 50) and ScientificName (Figure 51) as covariates.

Table 17: Observations used to fit the Binocular Surveys detection function.

| ScientificName                 | n           |
|--------------------------------|-------------|
| Blue, Bryde's, Fin, Right, Sei | 481         |
| Humpback, Sperm                | 990         |
| <b>Total</b>                   | <b>1471</b> |

## Large whales by species for Fin Sei

HR key with Program, Species  
1471 sightings, right truncated at 5000 m (9%)



## Q-Q Plot

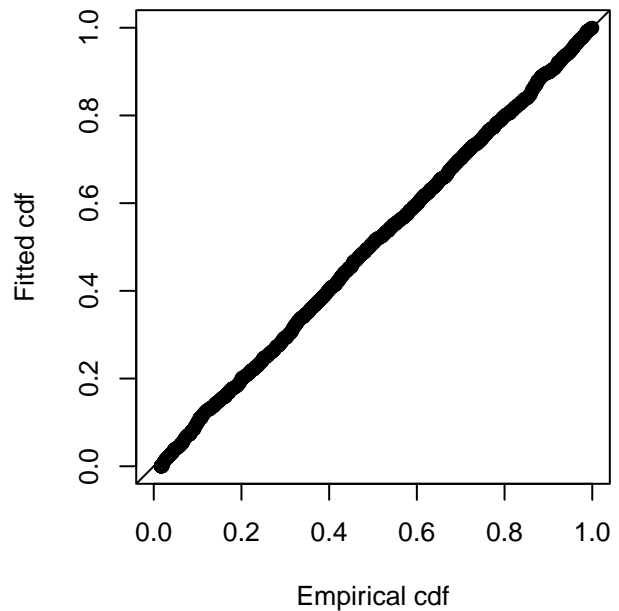


Figure 49: Binocular Surveys detection function and Q-Q plot showing its goodness of fit.

Statistical output for this detection function:

Summary for ds object

Number of observations : 1471  
Distance range : 0 - 5000  
AIC : 24501.67

Detection function:

Hazard-rate key function

Detection function parameters

Scale coefficient(s):

|                               | estimate   | se        |
|-------------------------------|------------|-----------|
| (Intercept)                   | 7.1184872  | 0.1313642 |
| ProgramAtlantic Pre-AMAPPS    | -0.4445467 | 0.1304985 |
| ProgramCaribbean              | -1.1012861 | 0.3025140 |
| ScientificNameHumpback, Sperm | 0.4613393  | 0.1338556 |

Shape coefficient(s):

|             | estimate  | se         |
|-------------|-----------|------------|
| (Intercept) | 0.2893248 | 0.07461625 |

|                     | Estimate     | SE           | CV         |
|---------------------|--------------|--------------|------------|
| Average p           | 0.4374109    | 0.02107636   | 0.04818435 |
| N in covered region | 3362.9703944 | 175.27854744 | 0.05212016 |

Distance sampling Cramer-von Mises test (unweighted)

Test statistic = 0.042713 p = 0.918683

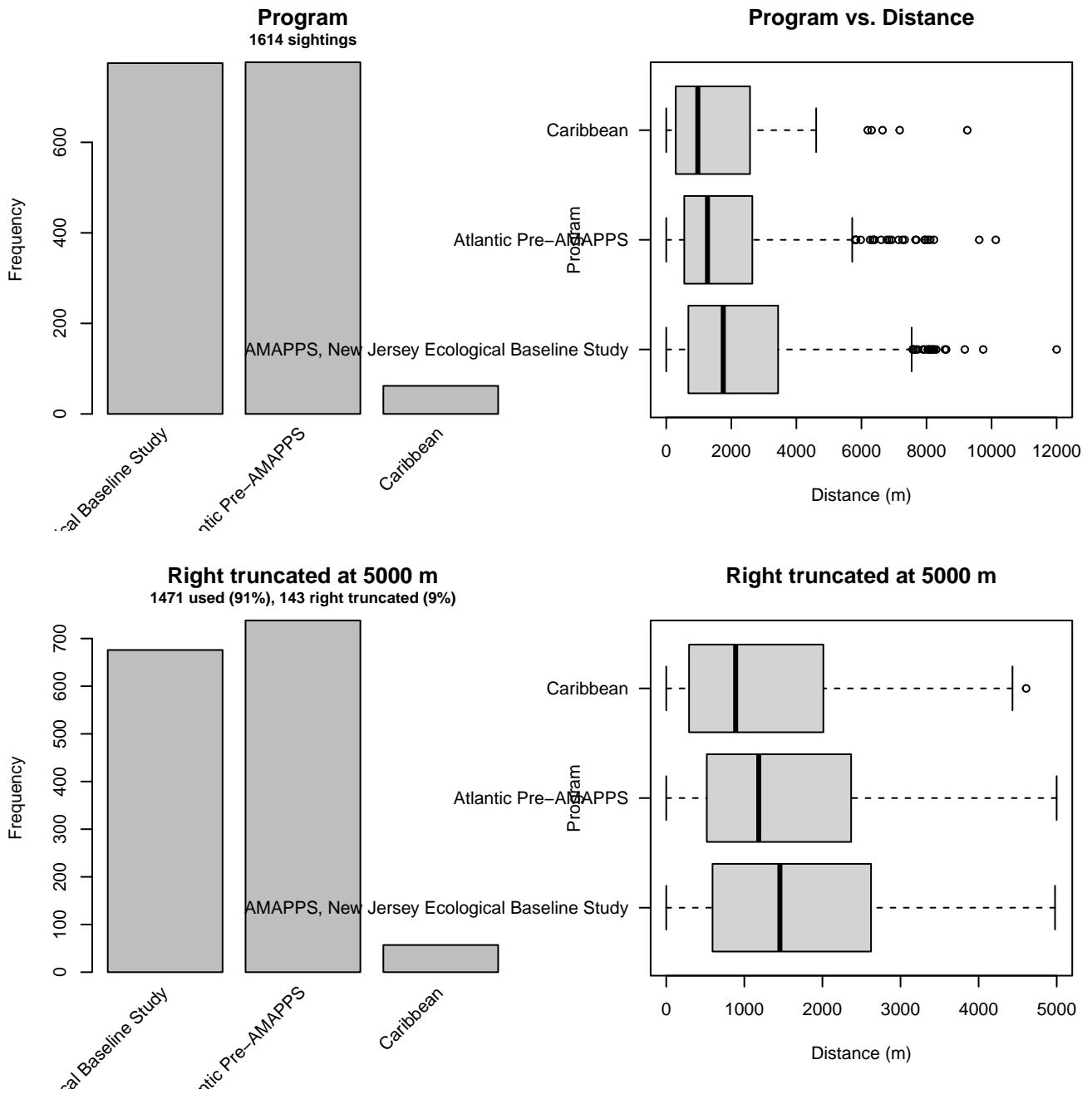


Figure 50: Distribution of the Program covariate before (top row) and after (bottom row) observations were truncated to fit the Binocular Surveys detection function.

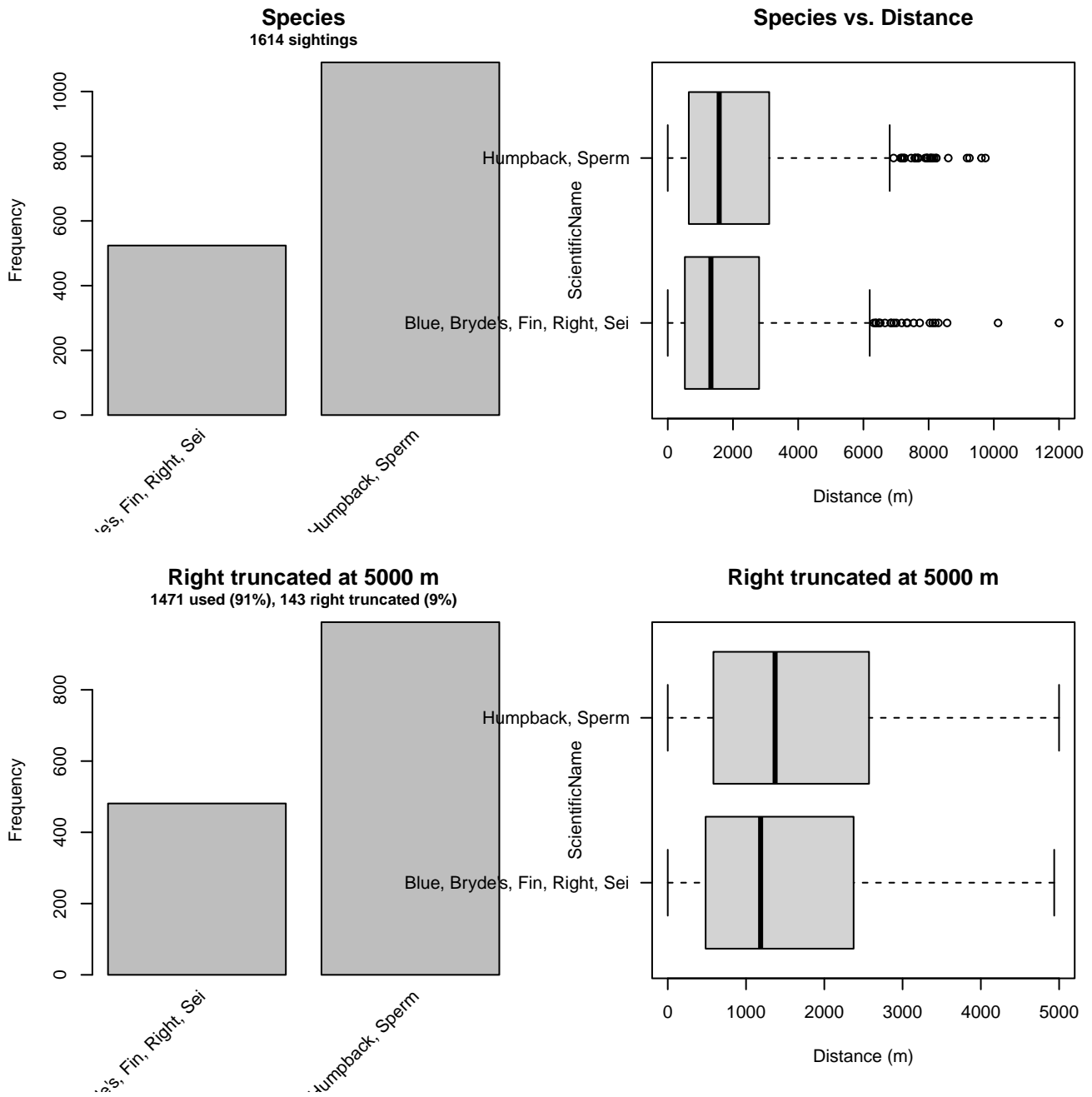


Figure 51: Distribution of the ScientificName covariate before (top row) and after (bottom row) observations were truncated to fit the Binocular Surveys detection function.

### 3.2 Without a Taxonomic Covariate

We fitted the detection functions in this section to pools of species with similar detectability characteristics but could not use a taxonomic identification as a covariate to account for differences between them. We usually took this approach after trying the taxonomic covariate and finding it had insufficient statistical power to be retained. We also resorted to it when the focal taxon being modeled had too few observations to be allocated its own taxonomic covariate level and was too poorly known for us to confidently determine which other taxa we could group it with.

### 3.2.1 Aerial Surveys

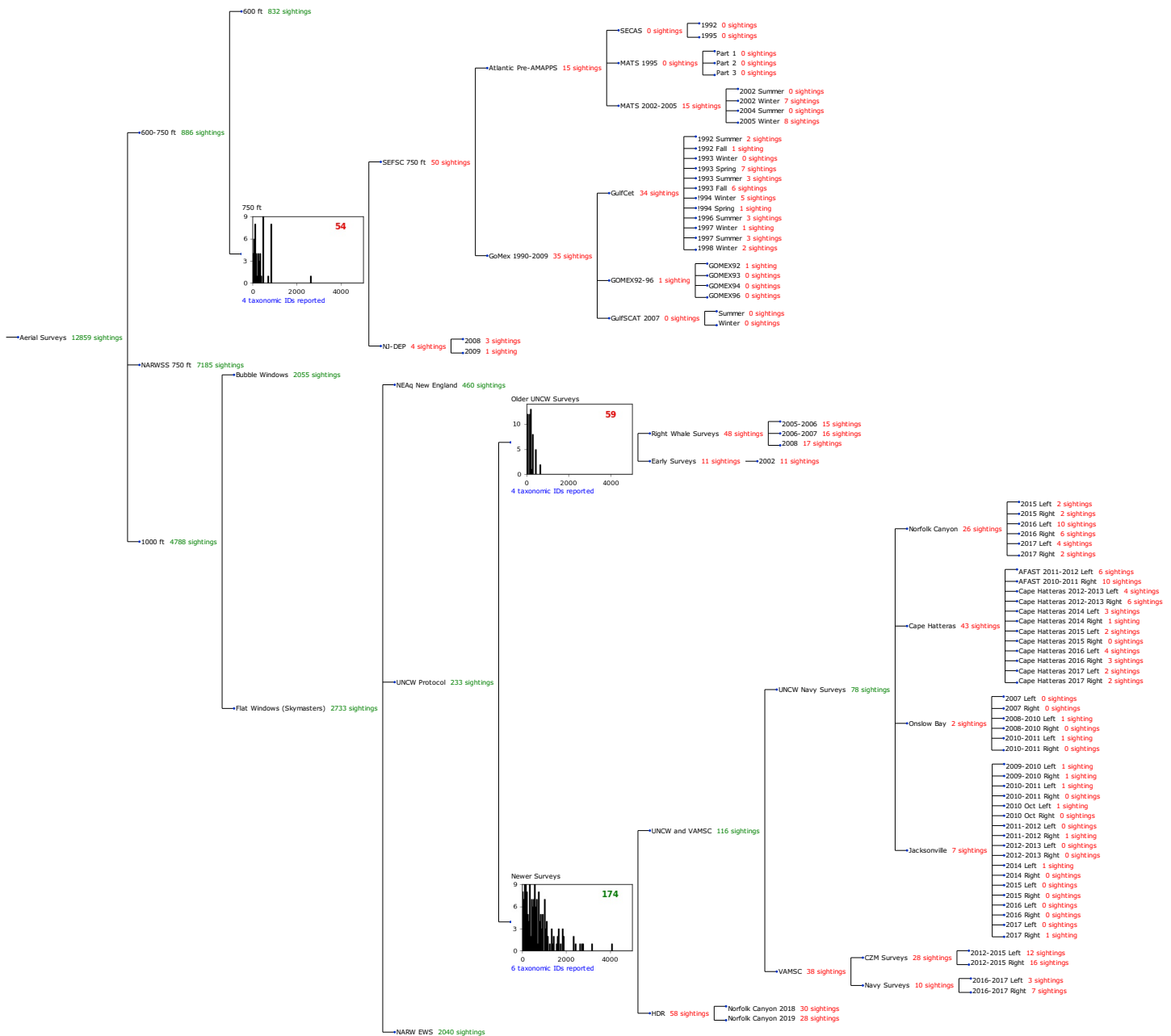


Figure 52: Detection hierarchy for aerial surveys, showing how they were pooled during detectability modeling, for detection functions that pooled multiple taxa but could not use a taxonomic covariate to account for differences between them. Each histogram represents a detection function and summarizes the perpendicular distances of observations that were pooled to fit it, prior to truncation. Observation counts, also prior to truncation, are shown in green when they met the recommendation of Buckland et al. (2001) that detection functions utilize at least 60 sightings, and red otherwise. For rare taxa, it was not always possible to meet this recommendation, yielding higher statistical uncertainty. During the spatial modeling stage of the analysis, effective strip widths were computed for each survey using the closest detection function above it in the hierarchy (i.e. moving from right to left in the figure). Surveys that do not have a detection function above them in this figure were either addressed by a detection function presented in a different section of this report, or were omitted from the analysis.

#### 3.2.1.1 750 ft

After right-truncating observations greater than 1297 m, we fitted the detection function to the 53 observations that remained (Table 18). The selected detection function (Figure 53) used a hazard rate key function with no covariates.

Table 18: Observations used to fit the 750 ft detection function.

| ScientificName         | n         |
|------------------------|-----------|
| Balaenoptera physalus  | 8         |
| Eubalaena glacialis    | 5         |
| Megaptera novaeangliae | 7         |
| Physeter macrocephalus | 33        |
| <b>Total</b>           | <b>53</b> |

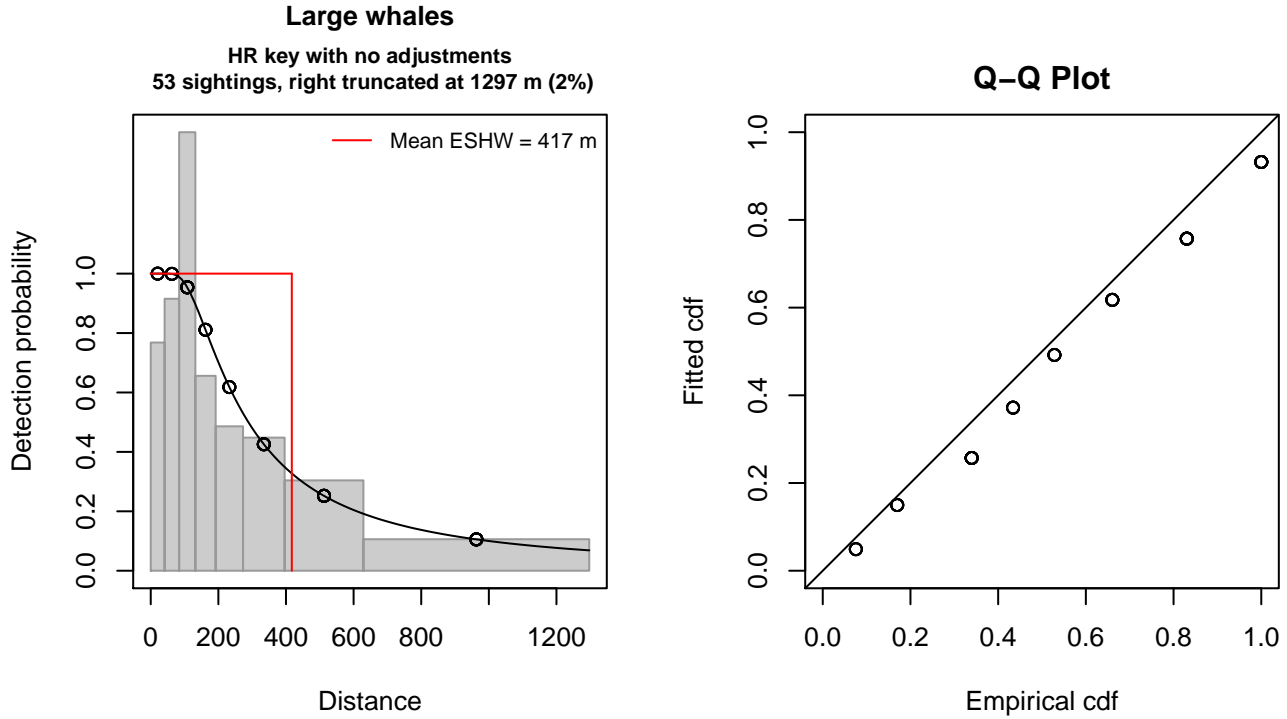


Figure 53: 750 ft detection function and Q-Q plot showing its goodness of fit.

Statistical output for this detection function:

Summary for ds object

Number of observations : 53  
 Distance range : 0 - 1297  
 AIC : 222.2921

Detection function:

Hazard-rate key function

Detection function parameters

Scale coefficient(s):

|             | estimate | se        |
|-------------|----------|-----------|
| (Intercept) | 5.423929 | 0.4460729 |

Shape coefficient(s):

|             | estimate  | se        |
|-------------|-----------|-----------|
| (Intercept) | 0.4163623 | 0.3128171 |

|                     | Estimate   | SE          | CV        |
|---------------------|------------|-------------|-----------|
| Average p           | 0.321688   | 0.07665669  | 0.2382951 |
| N in covered region | 164.755912 | 43.46025892 | 0.2637857 |

Distance sampling Cramer-von Mises test (unweighted)  
 Test statistic = 0.101698 p = 0.576612

### 3.2.1.2 Older UNCW Surveys

After right-truncating observations greater than 838 m, we fitted the detection function to the 59 observations that remained (Table 19). The selected detection function (Figure 54) used a hazard rate key function with Beaufort (Figure 55) as a covariate.

Table 19: Observations used to fit the Older UNCW Surveys detection function.

| ScientificName         | n         |
|------------------------|-----------|
| Balaenoptera physalus  | 13        |
| Eubalaena glacialis    | 24        |
| Megaptera novaeangliae | 13        |
| Physeter macrocephalus | 9         |
| <b>Total</b>           | <b>59</b> |

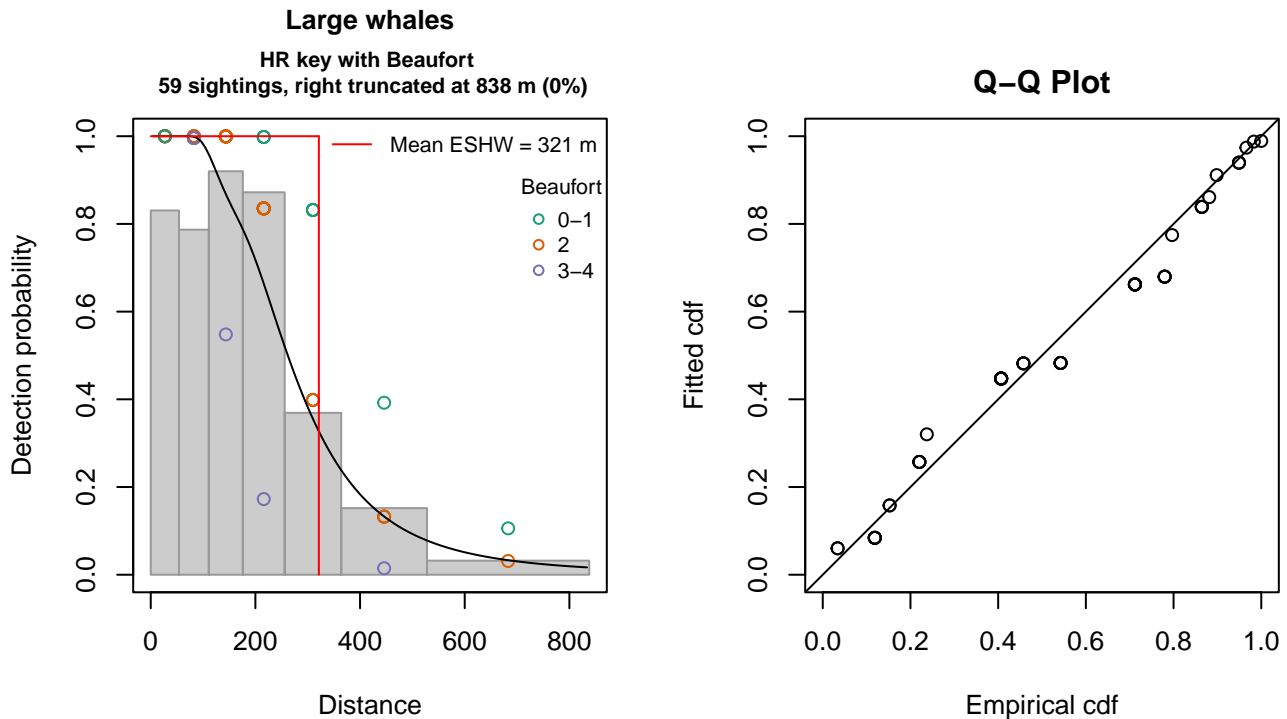


Figure 54: Older UNCW Surveys detection function and Q-Q plot showing its goodness of fit.

Statistical output for this detection function:

```
Summary for ds object
Number of observations : 59
Distance range       : 0 - 838
AIC                  : 218.1082
```

```
Detection function:
Hazard-rate key function
```

```
Detection function parameters
Scale coefficient(s):
```



|             | estimate   | se        |
|-------------|------------|-----------|
| (Intercept) | 5.9013957  | 0.2950158 |
| Beaufort2   | -0.3578033 | 0.3134356 |
| Beaufort3-4 | -1.0008354 | 0.3877033 |

Shape coefficient(s):

|             | estimate | se        |
|-------------|----------|-----------|
| (Intercept) | 1.254247 | 0.2627137 |

|                     | Estimate    | SE          | CV        |
|---------------------|-------------|-------------|-----------|
| Average p           | 0.3508662   | 0.04814793  | 0.1372259 |
| N in covered region | 168.1552636 | 29.31126242 | 0.1743107 |

Distance sampling Cramer-von Mises test (unweighted)  
Test statistic = 0.291522 p = 0.142842

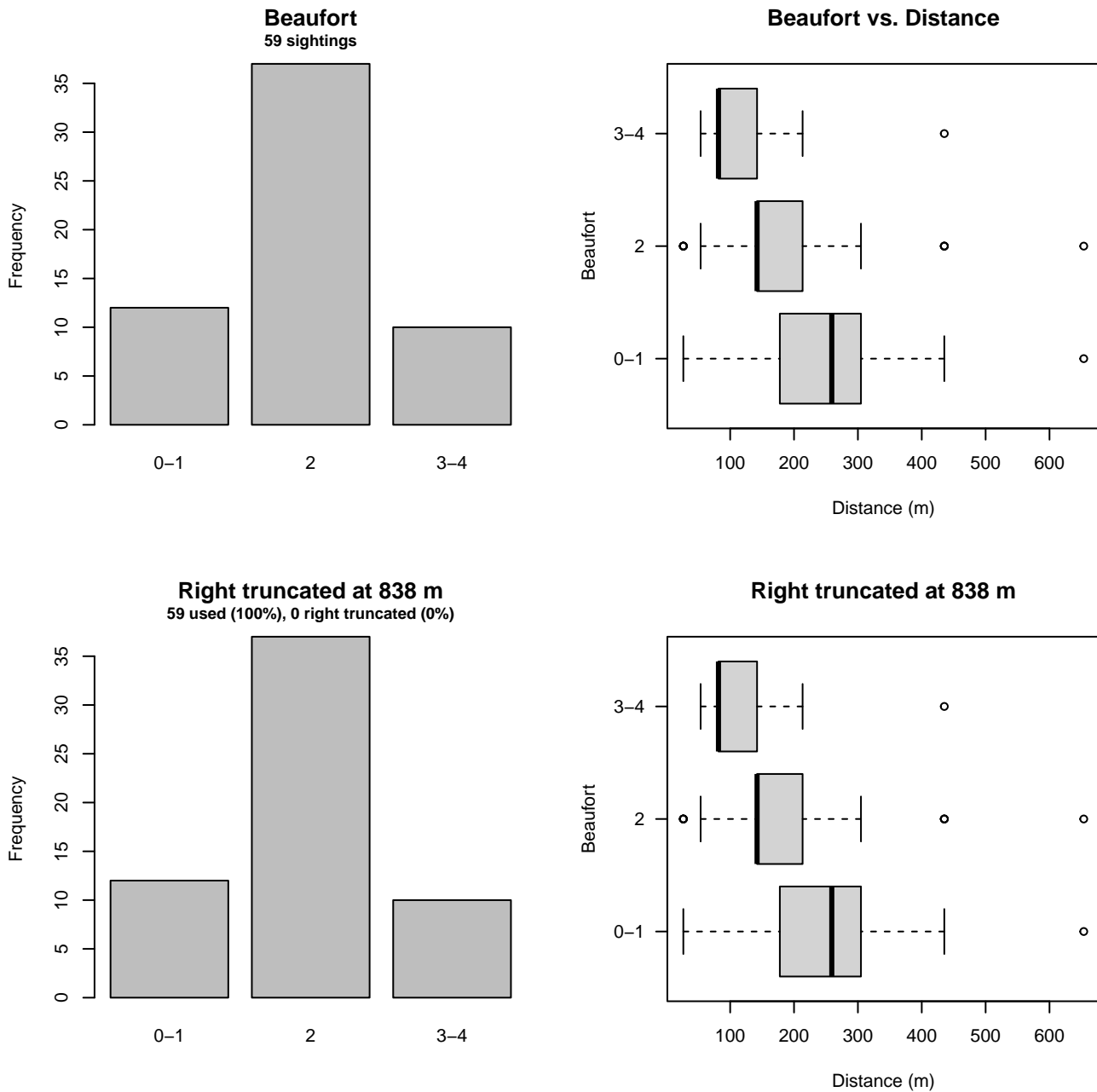


Figure 55: Distribution of the Beaufort covariate before (top row) and after (bottom row) observations were truncated to fit the Older UNCW Surveys detection function.

### 3.2.1.3 Newer Surveys

After right-truncating observations greater than 2000 m, we fitted the detection function to the 164 observations that remained (Table 20). The selected detection function (Figure 56) used a half normal key function with Beaufort (Figure 57) as a covariate.

Table 20: Observations used to fit the Newer Surveys detection function.

| ScientificName         | n          |
|------------------------|------------|
| Balaenoptera borealis  | 3          |
| Balaenoptera musculus  | 1          |
| Balaenoptera physalus  | 48         |
| Eubalaena glacialis    | 11         |
| Megaptera novaeangliae | 40         |
| Physeter macrocephalus | 61         |
| <b>Total</b>           | <b>164</b> |

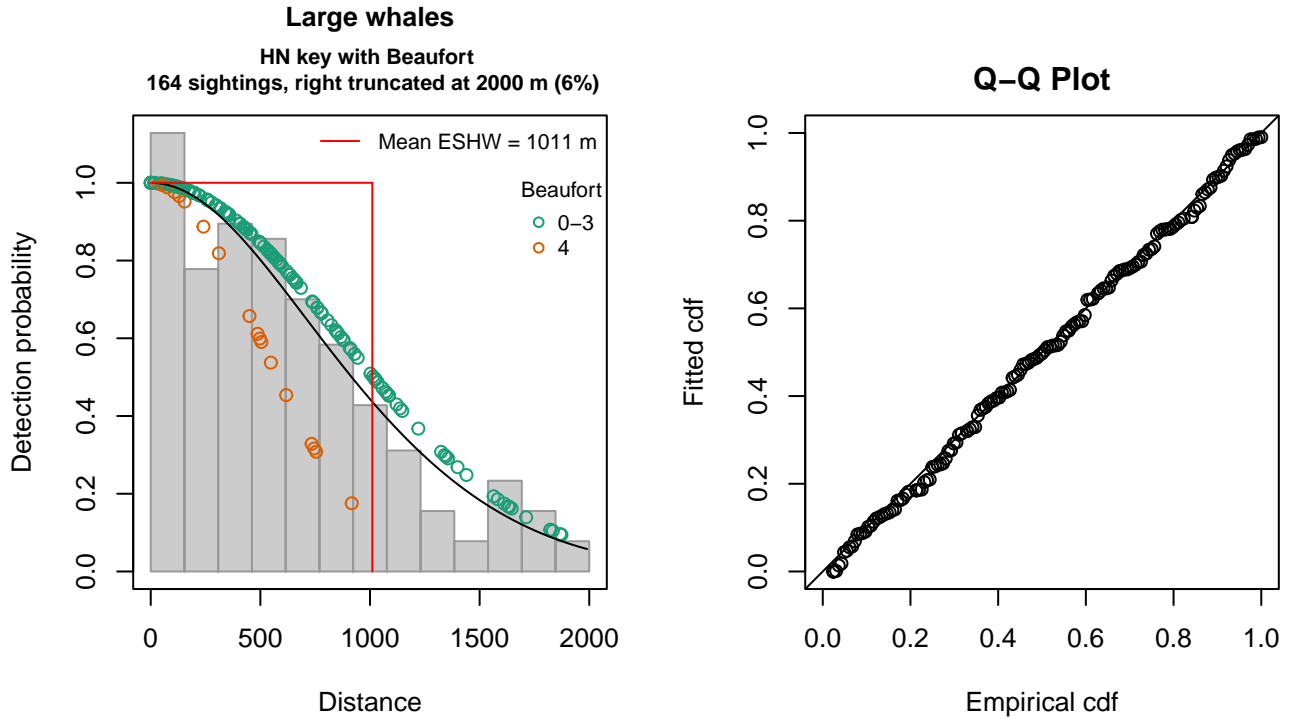


Figure 56: Newer Surveys detection function and Q-Q plot showing its goodness of fit.

Statistical output for this detection function:

Summary for ds object

Number of observations : 164  
 Distance range : 0 - 2000  
 AIC : 2414.311

Detection function:

Half-normal key function

Detection function parameters

Scale coefficient(s):

|             | estimate   | se         |
|-------------|------------|------------|
| (Intercept) | 6.7601346  | 0.07305226 |
| Beaufort4   | -0.5625984 | 0.24677736 |

|                     | Estimate    | SE          | CV         |
|---------------------|-------------|-------------|------------|
| Average p           | 0.4908118   | 0.03341248  | 0.06807595 |
| N in covered region | 334.1403290 | 29.56205574 | 0.08847198 |

Distance sampling Cramer-von Mises test (unweighted)  
 Test statistic = 0.025201 p = 0.989164

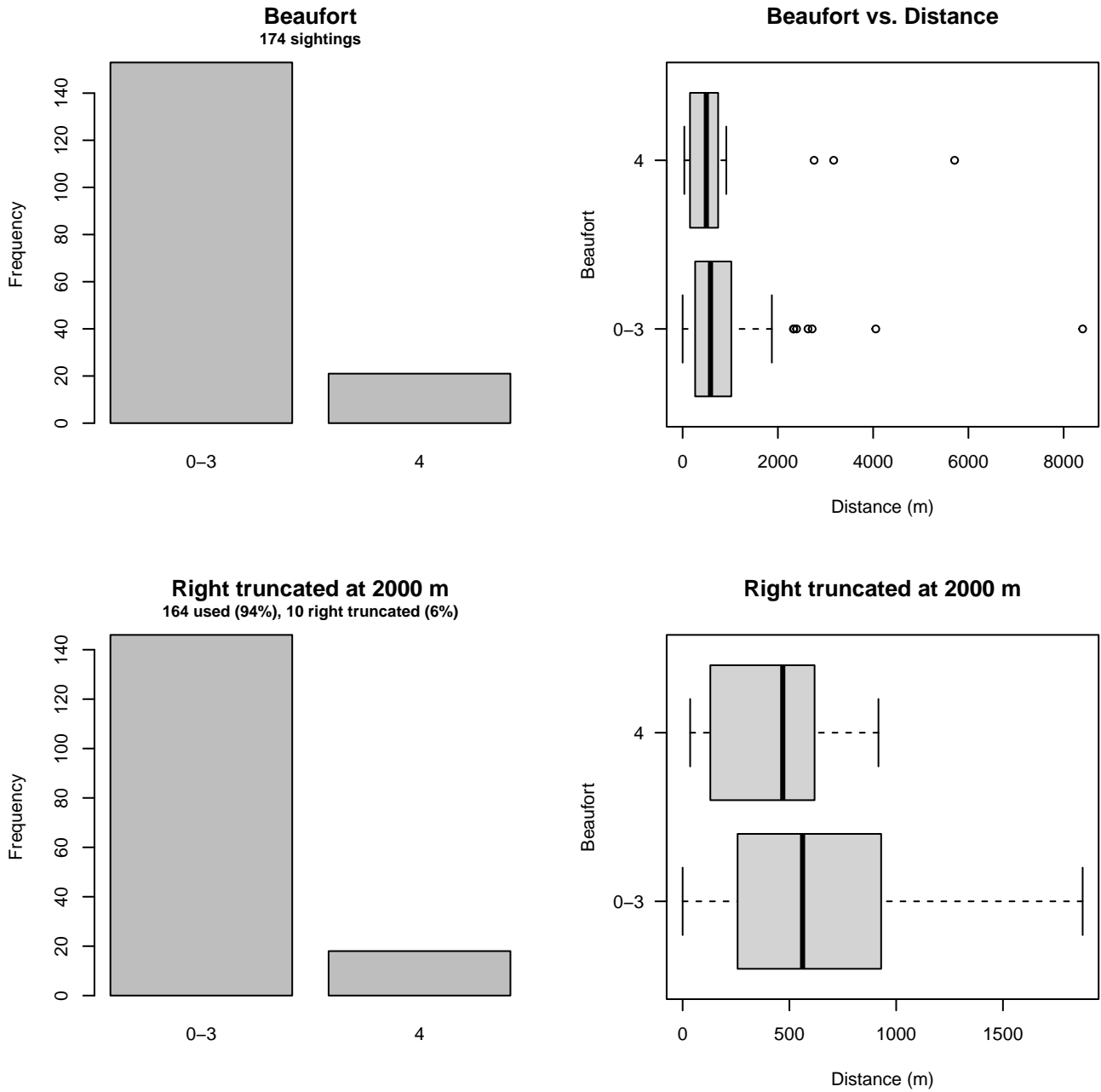


Figure 57: Distribution of the Beaufort covariate before (top row) and after (bottom row) observations were truncated to fit the Newer Surveys detection function.

### 3.2.2 Shipboard Surveys

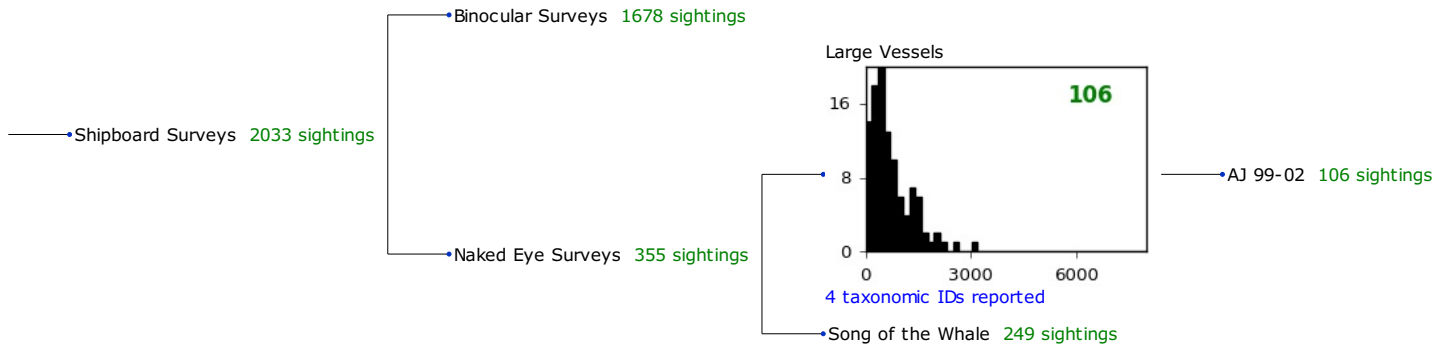


Figure 58: Detection hierarchy for shipboard surveys, showing how they were pooled during detectability modeling, for detection functions that pooled multiple taxa but could not use a taxonomic covariate to account for differences between them. Each histogram represents a detection function and summarizes the perpendicular distances of observations that were pooled to fit it, prior to truncation. Observation counts, also prior to truncation, are shown in green when they met the recommendation of Buckland et al. (2001) that detection functions utilize at least 60 sightings, and red otherwise. For rare taxa, it was not always possible to meet this recommendation, yielding higher statistical uncertainty. During the spatial modeling stage of the analysis, effective strip widths were computed for each survey using the closest detection function above it in the hierarchy (i.e. moving from right to left in the figure). Surveys that do not have a detection function above them in this figure were either addressed by a detection function presented in a different section of this report, or were omitted from the analysis.

#### 3.2.2.1 Large Vessels

After right-truncating observations greater than 2000 m, we fitted the detection function to the 102 observations that remained (Table 21). The selected detection function (Figure 59) used a hazard rate key function with no covariates.

Table 21: Observations used to fit the Large Vessels detection function.

| ScientificName                 | n          |
|--------------------------------|------------|
| Balaenoptera borealis          | 2          |
| Balaenoptera borealis/physalus | 53         |
| Eubalaena glacialis            | 10         |
| Megaptera novaeangliae         | 37         |
| <b>Total</b>                   | <b>102</b> |

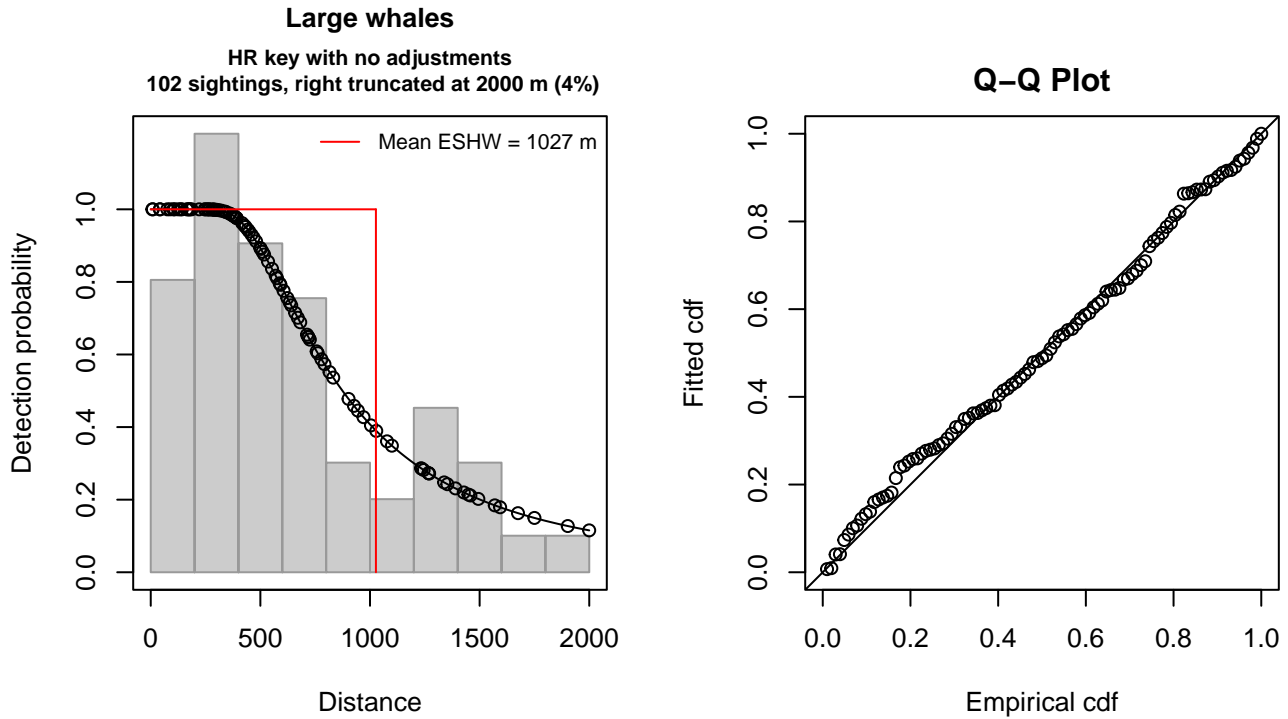


Figure 59: Large Vessels detection function and Q-Q plot showing its goodness of fit.

Statistical output for this detection function:

Summary for ds object

Number of observations : 102  
 Distance range : 0 - 2000  
 AIC : 1511.039

Detection function:

Hazard-rate key function

Detection function parameters

Scale coefficient(s):

|             | estimate | se        |
|-------------|----------|-----------|
| (Intercept) | 6.598567 | 0.2138084 |

Shape coefficient(s):

|             | estimate  | se        |
|-------------|-----------|-----------|
| (Intercept) | 0.7389469 | 0.2835546 |

|                     | Estimate    | SE          | CV        |
|---------------------|-------------|-------------|-----------|
| Average p           | 0.5134925   | 0.06353129  | 0.1237239 |
| N in covered region | 198.6396966 | 28.14611852 | 0.1416943 |

Distance sampling Cramer-von Mises test (unweighted)

Test statistic = 0.063071 p = 0.794652

## 4 Bias Corrections

Density surface modeling methodology uses *distance sampling* (Buckland et al. 2001) to model the probability that an observer on a line transect survey will detect an animal given the perpendicular distance to it from the transect line. Distance sampling assumes that detection probability is 1 when perpendicular distance is 0. When this assumption is not

met, detection probability is biased high, leading to an underestimation of density and abundance. This is known as the  $g_0 < 1$  problem, where  $g_0$  refers to the detection probability at distance 0. Modelers often try to address this problem by estimating  $g_0$  empirically and dividing it into estimated density or abundance, thereby correcting those estimates to account for the animals that were presumed missed.

Two important sources of bias for visual surveys are known as *availability bias*, in which an animal was present on the transect line but impossible to detect, e.g. because it was under water, and *perception bias*, in which an animal was present and available but not noticed, e.g. because of its small size or cryptic coloration or behavior (Marsh and Sinclair 1989). Modelers often estimate the influence of these two sources of bias on detection probability independently, yielding two estimates of  $g_0$ , hereafter referred to as  $g_{0A}$  and  $g_{0P}$ , and multiply them together to obtain a final, combined estimate:  $g_0 = g_{0A} \cdot g_{0P}$ .

Our overall approach was to perform this correction on a per-observation basis, to have the flexibility to account for many factors such as platform type, surveyor institution, group size, group composition (e.g. singleton, mother-calf pair, or surface active group), and geographic location (e.g. feeding grounds vs. calving grounds). The level of complexity of the corrections varied by species according to the amount of information available, with North Atlantic right whale having the most elaborate corrections, derived from a substantial set of publications documenting its behavior, and various lesser known odontocetes having corrections based only on platform type (aerial or shipboard), derived from comparatively sparse information. Here we document the corrections used for sei whale.

## 4.1 Aerial Surveys

Palka et al. (2021) developed perception bias corrections using two team, mark recapture distance sampling (MRDS) methodology (Burt et al. 2014) for aerial surveys conducted in 2010-2017 by NOAA NEFSC and SEFSC during the AMAPPS program. These were the only extant perception bias estimates developed from aerial surveys used in our analysis, aside from estimates developed earlier by Palka and colleagues (Palka 2006; Palka et al. 2017). Those earlier efforts utilized older methods and less data than their 2021 analysis, so we applied the Palka et al. (2021) estimates to all aerial survey programs (Table 22).

We applied Palka’s estimate for NEFSC to all programs other than SEFSC on the basis that those programs employed a similar visual scanning protocol that allowed observers to scan from the trackline up to the horizon, while SEFSC’s protocol generally limited scanning only up to  $50^\circ$  from the trackline, resulting in a smaller effective strip width. UNCW’s earlier surveys were an exception, for which detection distances were much closer to SEFSC’s for most species, so we applied Palka’s SEFSC estimate.

We caution that it is possible that perception bias was different on the other aerial programs, as they often used different aircraft, flew at different altitudes, and were staffed by different personnel. Of particular concern are that many programs flew Cessna 337 Skymasters, which had flat windows, while NOAA flew de Havilland Twin Otters, which had bubble windows, which likely afforded a better view of the transect line and therefore might have required less of a correction than the Skymasters. Correcting the other programs using NOAA’s estimate as we have done is likely to yield less bias than leaving them uncorrected, but we urge all programs to undertake their own efforts to estimate perception bias, as resources allow.

We estimated availability bias corrections using the Laake et al. (1997) estimator and dive intervals reported by Palka et al. (2017) (Table 23). To estimate time in view, needed by the Laake estimator, we used results reported by Robertson et al. (2015), rescaled linearly for each survey program according to its target altitude and speed. We caution that Robertson’s analysis was done for a de Havilland Twin Otter, which may have a different field of view than that of the other aircraft used here, which mainly comprised Cessna 337 Skymasters with flat windows but also a Partenavia P-68 with bubble windows (on the NYS-DEC/TT surveys). However, we note that McLellan et al. (2018) conducted a sensitivity analysis on the influence of the length of the “window of opportunity” to view beaked whales from a Cessna Skymaster on their final density estimates and found that they varied by only a few thousandths of an animal per kilometer when the window of opportunity more than doubled. Still, we urge additional program-specific research into estimation of availability bias.

To address the influence of group size on availability bias, we applied the group availability estimator of McLellan et al. (2018) on a per-observation basis. Following Palka et al. (2021), who also used that method, we assumed that individuals in the group dived asynchronously. The resulting  $g_{0A}$  corrections ranged from about 0.2 to 1 (Figure 60). We caution that the assumption of asynchronous diving can lead to an underestimation of density and abundance if diving is actually synchronous; see McLellan et al. (2018) for an exploration of this effect. However, if future research finds that this species conducts synchronous dives and characterizes the degree of synchronicity, the model can be updated to account for this knowledge.

Table 22: Perception bias corrections for sei whale applied to aerial surveys.

| Surveys               | Group Size | $g_{0P}$ | $g_{0P}$ Source            |
|-----------------------|------------|----------|----------------------------|
| SEFSC, UNCW 2002-2008 | < 3        | 0.86     | Palka et al. (2021): SEFSC |
| All others            | < 3        | 0.67     | Palka et al. (2021): NEFSC |
| All                   | $\geq 3$   | 1.00     | Assumed                    |

Table 23: Surface and dive intervals for sei whale used to estimate availability bias corrections.

| Surface Interval (s) | Dive Interval (s) | Source              |
|----------------------|-------------------|---------------------|
| 72.9                 | 331.5             | Palka et al. (2017) |

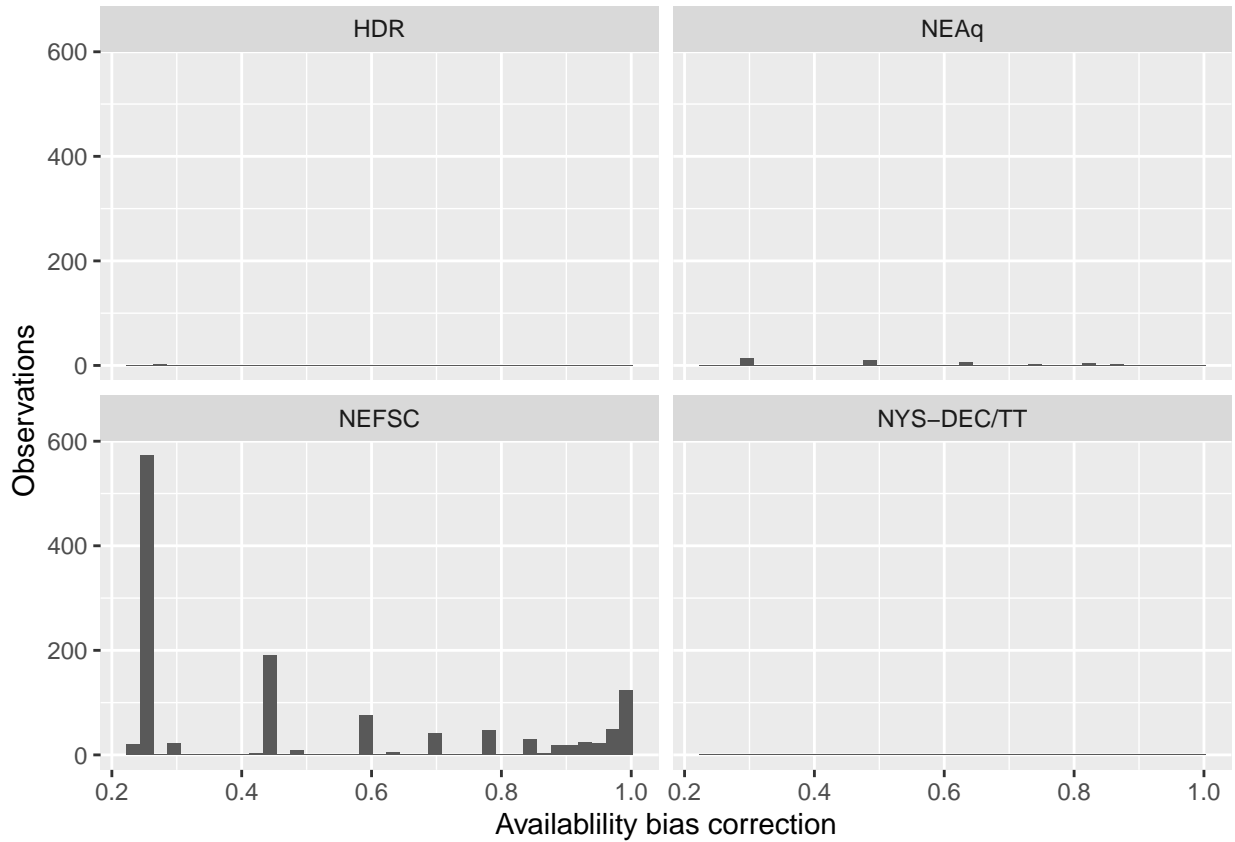


Figure 60: Availability bias corrections for sei whale for aerial surveys, by institution.

## 4.2 Shipboard Surveys

Most of the shipboard surveys in our analysis used high-power (25x150), pedestal-mounted binoculars. Similar to aerial surveys, Palka et al. (2021) developed perception bias corrections using two team, MRDS methodology (Burt et al. 2014) for high-power binocular surveys conducted in 2010-2017 by NOAA NEFSC and SEFSC during the AMAPPS program. These were the only extant perception bias estimates developed from high-power binocular surveys used in our analysis, aside from estimates developed earlier by Palka and colleagues (Palka 2006; Palka et al. 2017). Those earlier efforts utilized older methods and less data than their 2021 analysis, so we applied the Palka et al. (2021) estimates to all shipboard surveys that searched with high-power binoculars (Table 24).

A few surveys used naked eyes rather than high-power binoculars. For the one NEFSC naked eye survey (AJ 99-02) used in our analysis, we used the estimate developed for this survey by Palka (2006). For the surveys conducted by MCR on R/V Song of the Whale, for which a program-specific estimate was not available, we used the estimate from Cañadas et al. (2021). Given that the dive interval of this species (Table 23) was short relative to the amount of time a given patch of water remained



in view to shipboard observers, we assumed that no availability bias correction was needed ( $g_{0A} = 1$ ), following Palka et al. (2021) and Cañadas et al. (2021).

Table 24: Perception and availability bias corrections for sei whale applied to shipboard surveys.

| Surveys          | Searching Method | Group Size | $g_{0P}$ | $g_{0P}$ Source            | $g_{0A}$ | $g_{0A}$ Source       |
|------------------|------------------|------------|----------|----------------------------|----------|-----------------------|
| NEFSC, NJDEP     | Binoculars       | Any        | 0.48     | Palka et al. (2021): NEFSC | 1        | Assumed               |
| SEFSC            | Binoculars       | Any        | 0.57     | Palka et al. (2021): SEFSC | 1        | Assumed               |
| NEFSC (AJ 99-02) | Naked eye        | Any        | 0.48     | Palka et al. (2006)        | 1        | Assumed               |
| MCR              | Naked eye        | Any        | 0.72     | Cañadas et al. (2021)      | 1        | Cañadas et al. (2021) |

## 5 Density Model

Deemed the “forgotten whale”, the sei whale has received relatively little scientific study compared to the other baleen whales present in the western North Atlantic, and much of the knowledge of the sei whale’s distribution and movements is still based on whaling records (Prieto et al. 2012). Sei whales are thought to follow a typical baleen whale migration pattern, moving to high latitudes in summer to feed and low latitudes in winter to breed or calve. Mitchell (1975) analyzed whaling records from the Blandford, Nova Scotia whaling station and reported two “runs” of sei whales, and speculated that sei whales migrate northward from Cape Cod along the Scotian Shelf in June and July, and return again in September and October. Sightings from surveys used in our analysis were roughly consistent with this view, with a rapid influx of sightings into the Gulf of Maine in April, sustained high numbers in May and June, a decline in July and August, a single sighting in September, and a second rise in October and November, followed by a decline in December.

Prieto et al. (2014) tracked sei whales that migrated through the Azores in 2008 and 2009, arrived in the Labrador Sea starting in mid-May, performed movements consistent with feeding, and departed by mid-September. None of these whales visited the Gulf of Maine. After reviewing these results and other available evidence, these researchers concluded that the Gulf of Maine and the Labrador Sea seemed to comprise two discrete feeding grounds utilized simultaneously by sei whales, but that there was insufficient evidence to conclude that sei whales feeding at these locations belonged to distinct biological stocks. Huijser et al. (2018) analyzed mitochondrial control region DNA sequences and microsatellite genotypes from 87 samples collected in the Azores, Gulf of Maine, and Iceland and detected no statistically significant deviations from genetic homogeneity. However, they cautioned that this low level of genetic differentiation did not necessarily imply a single stock of sei whales in the North Atlantic because different breeding populations could have been mixing in these migration and feeding areas, and because their analysis could not rule out multiple stocks under the statistical confidence criterion they selected.

The breeding and calving grounds for sei whales in the North Atlantic are still unknown (Prieto et al. 2012). Stable isotope analysis indicated the whales tracked migrating through the Azores to the Labrador Sea in 2008 and 2009 likely overwintered off the Northwest African coast (Silva et al. 2019). In winter on the western side of the North Atlantic basin, two pairs and one singleton were sighted off the southeast U.S. over the Blake Plateau in January 1992 by the NOAA SEFSC OT-92 survey (Mullin and Ford 1992), and two sightings were reported in the vicinity of Puerto Rico in earlier years (Mignucci-Giannoni 1998). Davis et al. (2020) reported regular acoustic detections of sei whales over the western edge of the Blake Plateau from October through February from hydrophones deployed during various periods between 2009-2014. Kowarski et al. (2022) reported acoustic detections during November through February in the deeper waters of the eastern Blake Plateau from hydrophone deployed almost continuously between December 2017 and December 2020. Finally, on an aerial visual survey of the New York Bight, Rickard et al. (2022) observed a bout of possible socio-sexual behavior in April 2019 about 151 km southeast of Block Island.

We initially attempted to model sei whale with a single density surface model that spanned the entire study area, but this model proved problematic owing to the lack of survey effort beyond the shelf break in non-summer seasons. Instead, we split the study area at Cape Hatteras, an ecoregional boundary between distinct cetacean communities (Schick et al. 2011) where the Gulf Stream separates from the continental shelf and heads into the Atlantic, and we modeled the regions north and south of here separately. In the north (Figure 61, region A), we fitted a full density surface model that spanned the entire year (Section 5.1).

South of Cape Hatteras and the Gulf Stream we split the data into two seasons: “Winter”, which spanned October through February based on these months containing the all of the visual sightings reported by our collaborators and the bulk of acoustic detections reported by Davis et al. (2020) (in their areas 9 and 10), and “Summer”, which spanned March through September. In Summer, during which time no sei whale sightings were reported in the southern region, we assumed the

species was absent. In Winter, we further split the southern region into three sub-regions. Along the upper shelf, which was intensely surveyed by the North Atlantic Right Whale Early Warning System (NARW EWS) surveys since 2003 with no sei whale sightings, and in the Florida Gap south to the Straits of Florida (Figure 61, region D), we assumed the species was absent. (The NARW EWS surveys are not shown on this map.) In the region spanning the Blake Plateau and offshore waters for which some surveying was available and four sightings were reported (Figure 61, region C), as well as acoustic detections by Davis et al. (2020), we made a pseudo-stratified density estimate (Section 5.2). In the distant offshore region for which no surveying was available during the Winter months (Figure 61, region B), we did not estimate density, owing to a lack of data and our resulting low confidence in our ability to correctly guess whether sei whales are present in this area during these months.

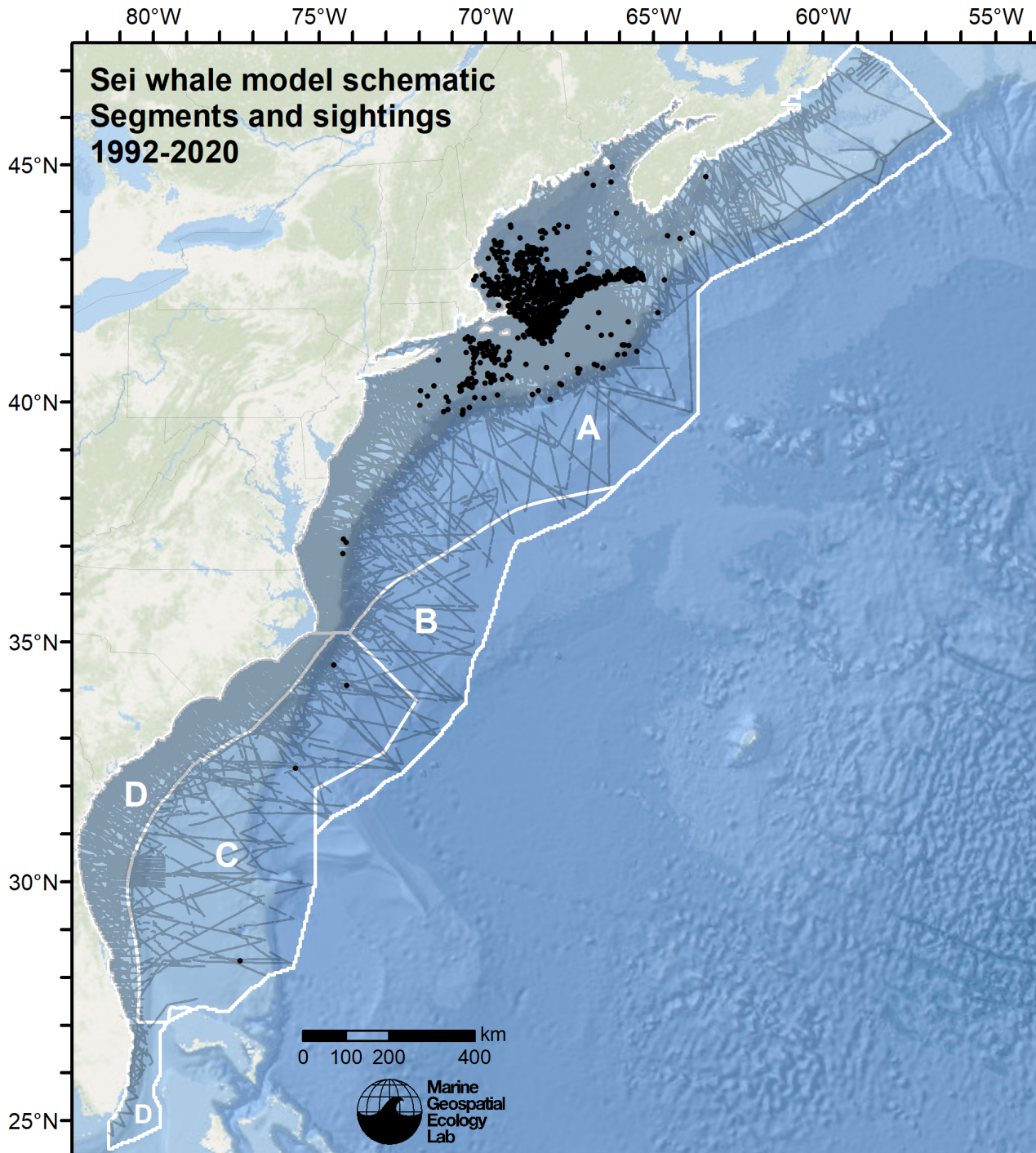


Figure 61: Schematic showing how we split the study area into regional models as described in the text above. Note that this figure shows data from year-round. Regions B, C, and D were only treated as separate regions in Winter (October-February). During Summer (March-September), they were treated as a single region.

## 5.1 North of the Gulf Stream

The surveys incorporated into the model for waters north of the Gulf Stream, spanning 1998-2020, reported over 1000 sightings (Figure 62). All were north of Hudson Canyon except for a small cluster east of Chesapeake Bay at the shelf break. The highest concentrations of sightings occurred in southern Gulf of Maine, especially the Great South Channel, and along the northern edge of Georges Bank. These concentrations reflected both a habitat preference of sei whales and a bias in survey effort by survey teams targeting North Atlantic right whales, which forage on the same zooplankton species (*Calanus finmarchicus*) as sei whales in the Gulf of Maine (Baumgartner et al. 2011).

The model selection procedure was straightforward. When ranked by REML score (Wood 2011), the highest ranked model with climatological covariates slightly outranked that with contemporaneous covariates and explained 0.2% more deviance. However, predictions from the best climatological-covariate model yielded very low densities across the Scotian Shelf in summer and fall, which did not accord with acoustic detections reported by Davis et al. (2020), nor with the large numbers of sightings available in the OBIS-SEAMAP system (Halpin et al. 2009) from surveys not able to be incorporated into our model. Given that the best contemporaneous-covariate model did not exhibit this problem and was only slightly outranked by the best climatological-covariate model, we selected it as our final choice.

The model included three static covariates and three dynamic covariates (Table 25). The functional relationship for depth (Figure 65) indicated a positive effect in waters deeper than 50 m (about 1.7 in  $\log_{10}$  scale), while hump-shaped relationships for distance to the 125 m and 300 m isobaths peaked just to the deep side of the 125 m isobath and about 150 km inshore of the 300 m isobath. Together, these static relationships reflect an avoidance of the shallowest waters, a broad distribution over the continental shelf and upper slope, and higher densities in the south and east Gulf of Maine.

Hump-shaped relationships for SST and sea surface salinity peaked at about 8 °C and 32 PSU, reflecting the species' preference for cooler, fresher waters found in the northern part of the study area. A hump-shaped relationship for primary productivity peaked at moderate values and then rose again for the highest values, although this part of the relationship was uncertain, as the confidence intervals enclosed zero. We interpret this relationship as selecting for the northern half of the study area, where primary productivity is higher than in the south.

The NT1 univariate extrapolation diagnostic indicated values of the primary productivity covariate were slightly beyond the sampled range at the northern Scotian Shelf in winter (Figure 72c-72f) and along the edge of the Gulf Stream in summer (Figure 72j-72l). In both cases, covariate values were slightly below the minimum sampled value and were Winsorized up to that minimum. Given that the relationship was trending sharply down on the left side, it is possible that densities were slightly overpredicted in these places in these months. However, the resulting densities, inclusive of this effect, were very low (Figures 80-83 and 87-89), so this is probably not a cause for concern for most users of the predictions.

5.1.1 Final Model

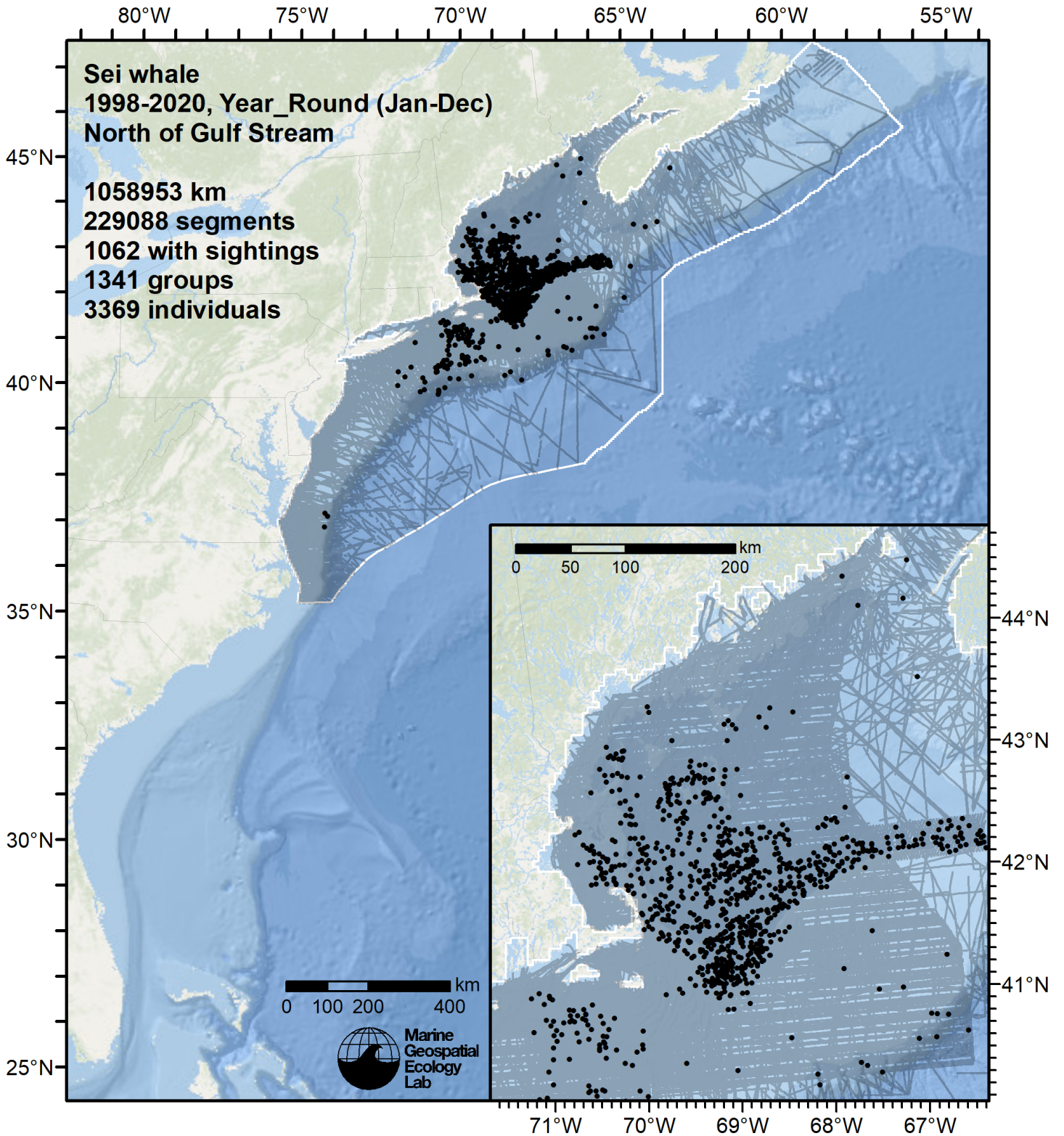


Figure 62: Survey segments used to fit the model for the region North of Gulf Stream. Black points indicate segments with observations.

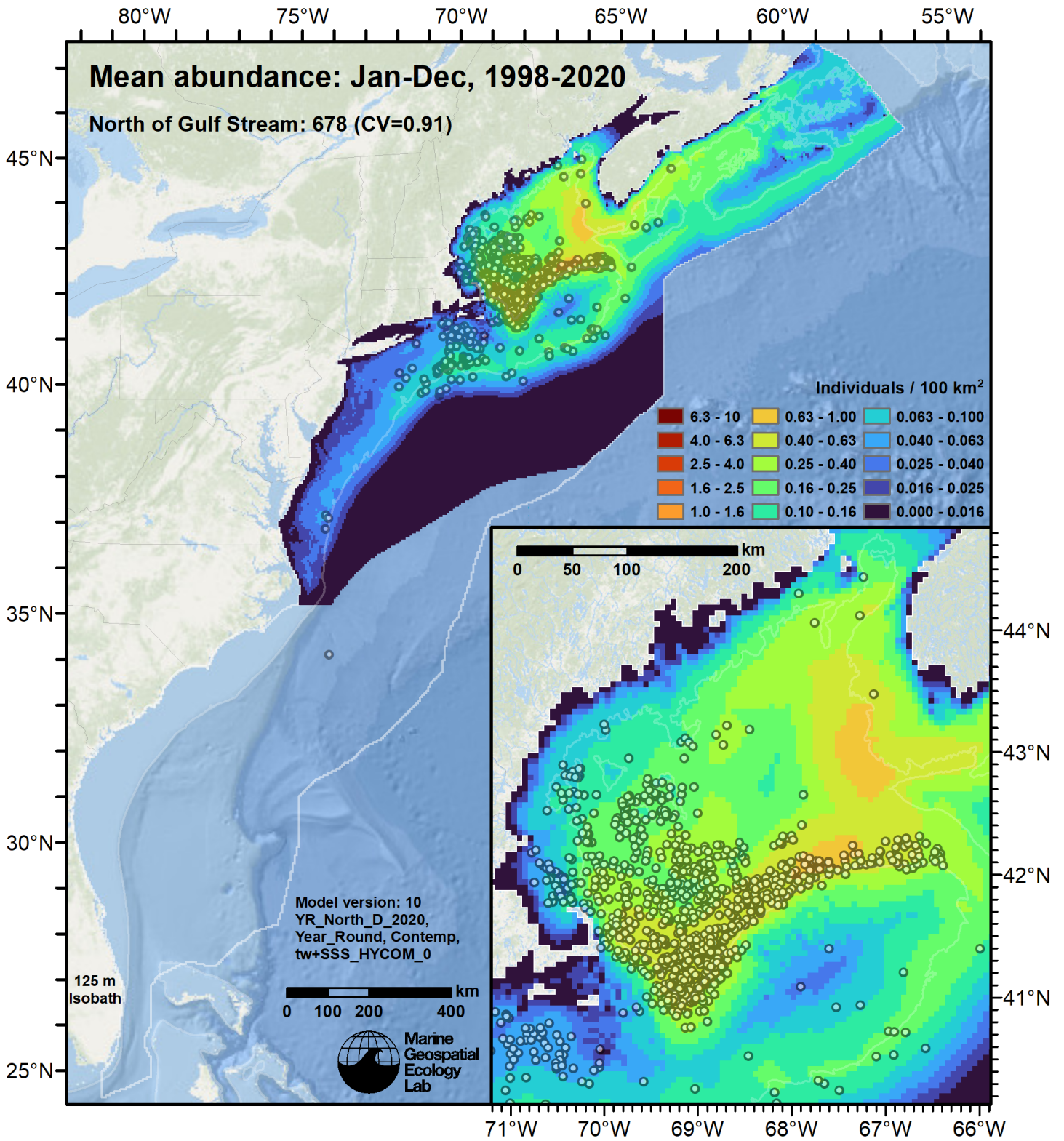


Figure 63: Sei whale mean density for the indicated period, as predicted by the model for the region North of Gulf Stream. Open circles indicate segments with observations. Mean total abundance and its coefficient of variation (CV) are given in the subtitle. Variance was estimated with the analytic approach given by Miller et al. (2022), Appendix S1, and accounts both for uncertainty in model parameter estimates and for seasonal and interannual variability in dynamic covariates.

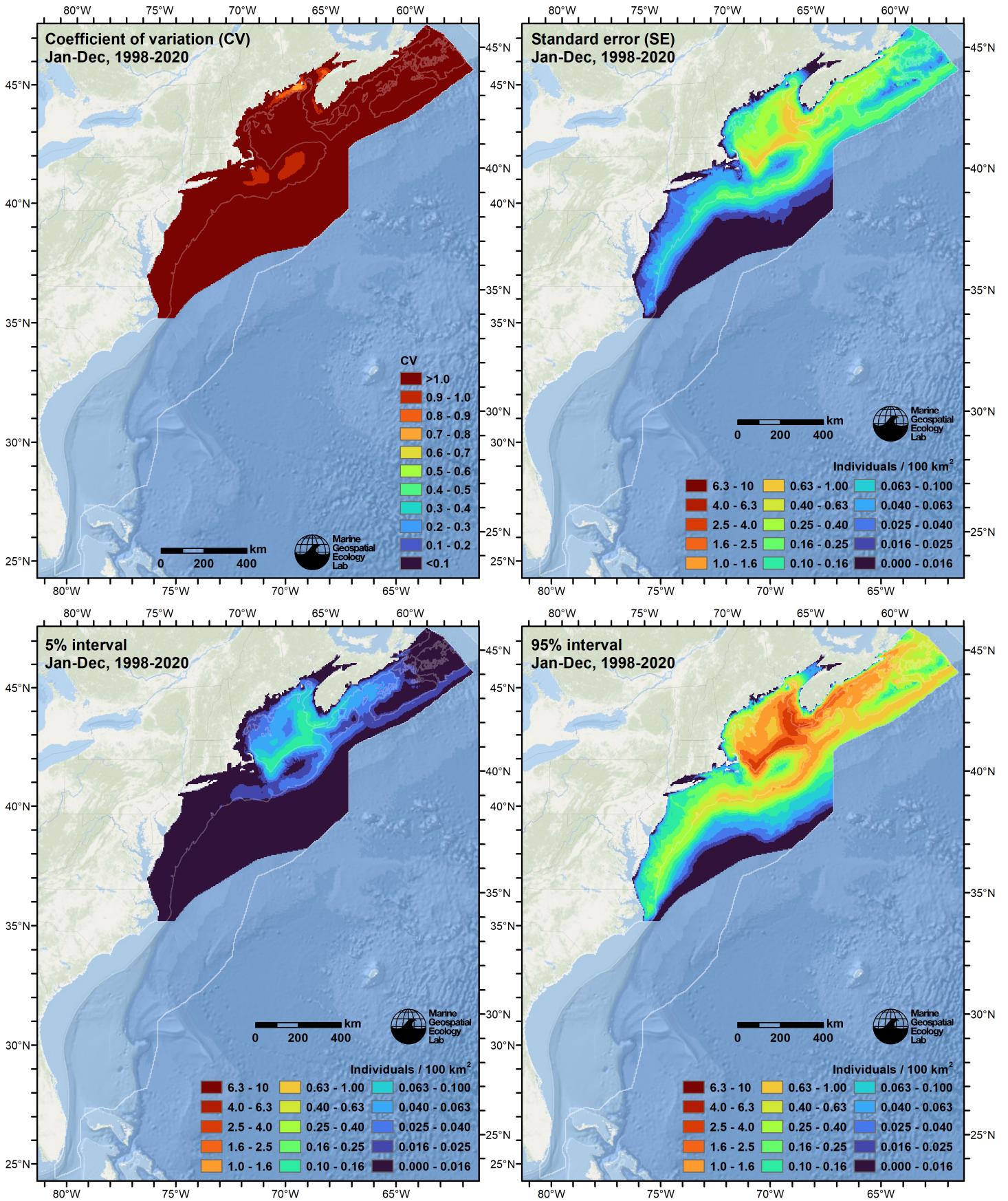


Figure 64: Uncertainty statistics for the sei whale mean density surface (Figure 63) predicted by the model for the region North of Gulf Stream. Variance was estimated with the analytic approach given by Miller et al. (2022), Appendix S1, and accounts both for uncertainty in model parameter estimates and for seasonal and interannual variability in dynamic covariates.

Statistical output for this model:

Family: Tweedie(p=1.216)

Link function: log

Formula:

```
IndividualsCorrected ~ offset(log(SegmentArea)) + s(log10(pmax(3,
  pmin(Depth, 2500))), bs = "ts", k = 5) + s(pmax(-75, pmin(I(DistTo125m/1000),
  75)), bs = "ts", k = 4) + s(pmax(-350, pmin(I(DistTo300m/1000),
  50)), bs = "ts", k = 5) + s(pmax(2, pmin(SST_CMC, 28)), bs = "ts",
  k = 5) + s(pmax(30.5, pmin(SSS_HYCOM, 36)), bs = "ts", k = 5) +
  s(pmax(200, pmin(PP_VGPM, 4000)), bs = "ts", k = 5)
```

Parametric coefficients:

```
      Estimate Std. Error t value Pr(>|t|)
(Intercept) -22.1111    0.1705  -129.7  <2e-16 ***
---
```

Signif. codes: 0 '\*\*\*' 0.001 '\*\*' 0.01 '\*' 0.05 '.' 0.1 ' ' 1

Approximate significance of smooth terms:

|   | edf   | Ref.df | F      | p-value    |
|---|-------|--------|--------|------------|
| s(log10(pmax(3, pmin(Depth, 2500))))        | 2.750 | 4      | 7.602  | <2e-16 *** |
| s(pmax(-75, pmin(I(DistTo125m/1000), 75)))  | 2.754 | 3      | 34.944 | <2e-16 *** |
| s(pmax(-350, pmin(I(DistTo300m/1000), 50))) | 3.272 | 4      | 32.170 | <2e-16 *** |
| s(pmax(2, pmin(SST_CMC, 28)))               | 3.720 | 4      | 61.055 | <2e-16 *** |
| s(pmax(30.5, pmin(SSS_HYCOM, 36)))          | 3.439 | 4      | 14.957 | <2e-16 *** |
| s(pmax(200, pmin(PP_VGPM, 4000)))           | 3.887 | 4      | 59.004 | <2e-16 *** |

---

Signif. codes: 0 '\*\*\*' 0.001 '\*\*' 0.01 '\*' 0.05 '.' 0.1 ' ' 1

R-sq.(adj) = 0.0153 Deviance explained = 25.7%

-REML = 8493.1 Scale est. = 14.357 n = 229088

Method: REML Optimizer: outer newton

full convergence after 12 iterations.

Gradient range [-0.002031122,0.0008515653]

(score 8493.096 & scale 14.35734).

Hessian positive definite, eigenvalue range [1.009104,6810.137].

Model rank = 24 / 24

Basis dimension (k) checking results. Low p-value (k-index<1) may indicate that k is too low, especially if edf is close to k'.

|   | k'   | edf  | k-index | p-value |
|---|------|------|---------|---------|
| s(log10(pmax(3, pmin(Depth, 2500))))        | 4.00 | 2.75 | 0.89    | 0.225   |
| s(pmax(-75, pmin(I(DistTo125m/1000), 75)))  | 3.00 | 2.75 | 0.91    | 0.885   |
| s(pmax(-350, pmin(I(DistTo300m/1000), 50))) | 4.00 | 3.27 | 0.89    | 0.160   |
| s(pmax(2, pmin(SST_CMC, 28)))               | 4.00 | 3.72 | 0.88    | 0.065 . |
| s(pmax(30.5, pmin(SSS_HYCOM, 36)))          | 4.00 | 3.44 | 0.90    | 0.525   |
| s(pmax(200, pmin(PP_VGPM, 4000)))           | 4.00 | 3.89 | 0.88    | 0.090 . |

---

Signif. codes: 0 '\*\*\*' 0.001 '\*\*' 0.01 '\*' 0.05 '.' 0.1 ' ' 1

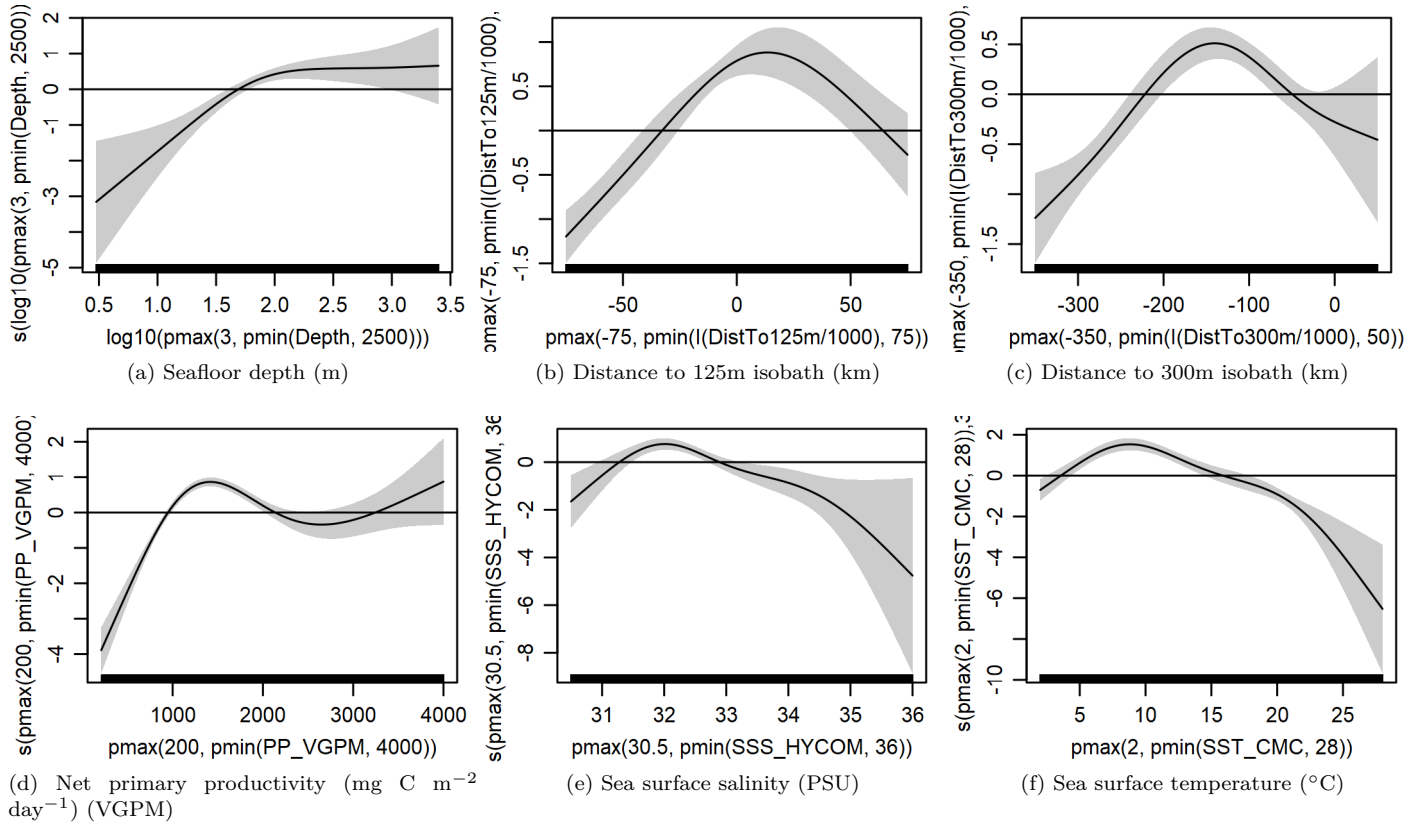


Figure 65: Functional plots for the final model for the region North of Gulf Stream. Transforms and other treatments are indicated in axis labels.  $\log_{10}$  indicates the covariate was  $\log_{10}$  transformed.  $pmax$  and  $pmin$  indicate the covariate's minimum and maximum values, respectively, were Winsorized to the values shown. Winsorization was used to prevent runaway extrapolations during prediction when covariates exceeded sampled ranges, or for ecological reasons, depending on the covariate.  $/1000$  indicates meters were transformed to kilometers for interpretation convenience.

Table 25: Covariates used in the final model for the region North of Gulf Stream.

| Covariate  | Description  |
|------------|--|
| Depth      | Depth (m) of the seafloor, from SRTM30_PLUS (Becker et al. (2009))   |
| DistTo125m | Distance (km) to the 125m isobath, derived from SRTM30_PLUS (Becker et al. (2009))   |
| DistTo300m | Distance (km) to the 300m isobath, derived from SRTM30_PLUS (Becker et al. (2009))   |
| PP_VGPM    | Monthly mean net primary productivity ( $\text{mg C m}^{-2} \text{ day}^{-1}$ ) from the Vertically Generalized Production Model (VGPM) (Behrenfeld and Falkowski (1997))  |
| SSS_HYCOM  | Monthly mean sea surface salinity (PSU) from the HYCOM GOFS 3.1 $1/12^{\circ}$ ocean model (Chassignet et al. (2009))  |
| SST_CMC    | Monthly mean sea surface temperature ( $^{\circ}\text{C}$ ) from GHRSSST Level 4 CMC0.2deg and CMC0.1deg (Brasnett (2008); Canada Meteorological Center (2012); Meissner et al. (2016); Canada Meteorological Center (2016)) |



### 5.1.2 Diagnostic Plots

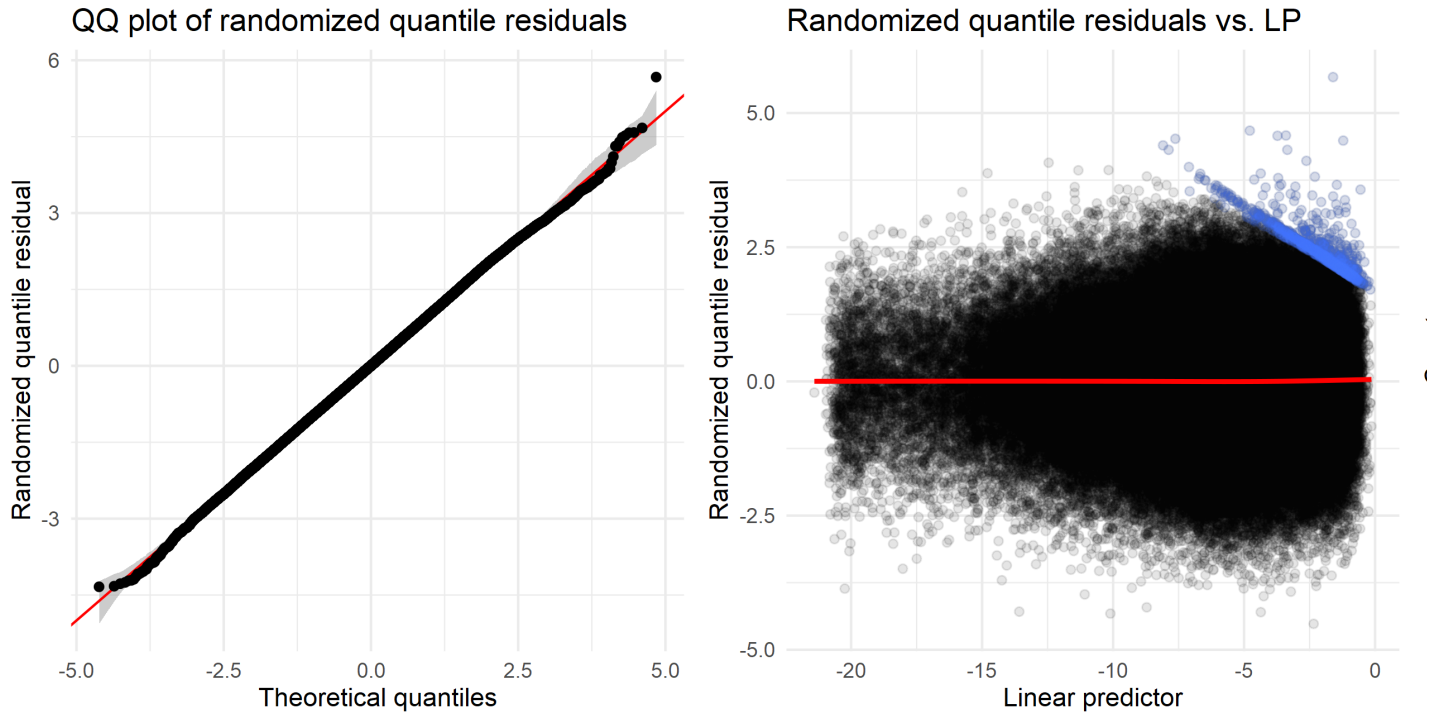


Figure 66: Residual plots for the final model for the region North of Gulf Stream.

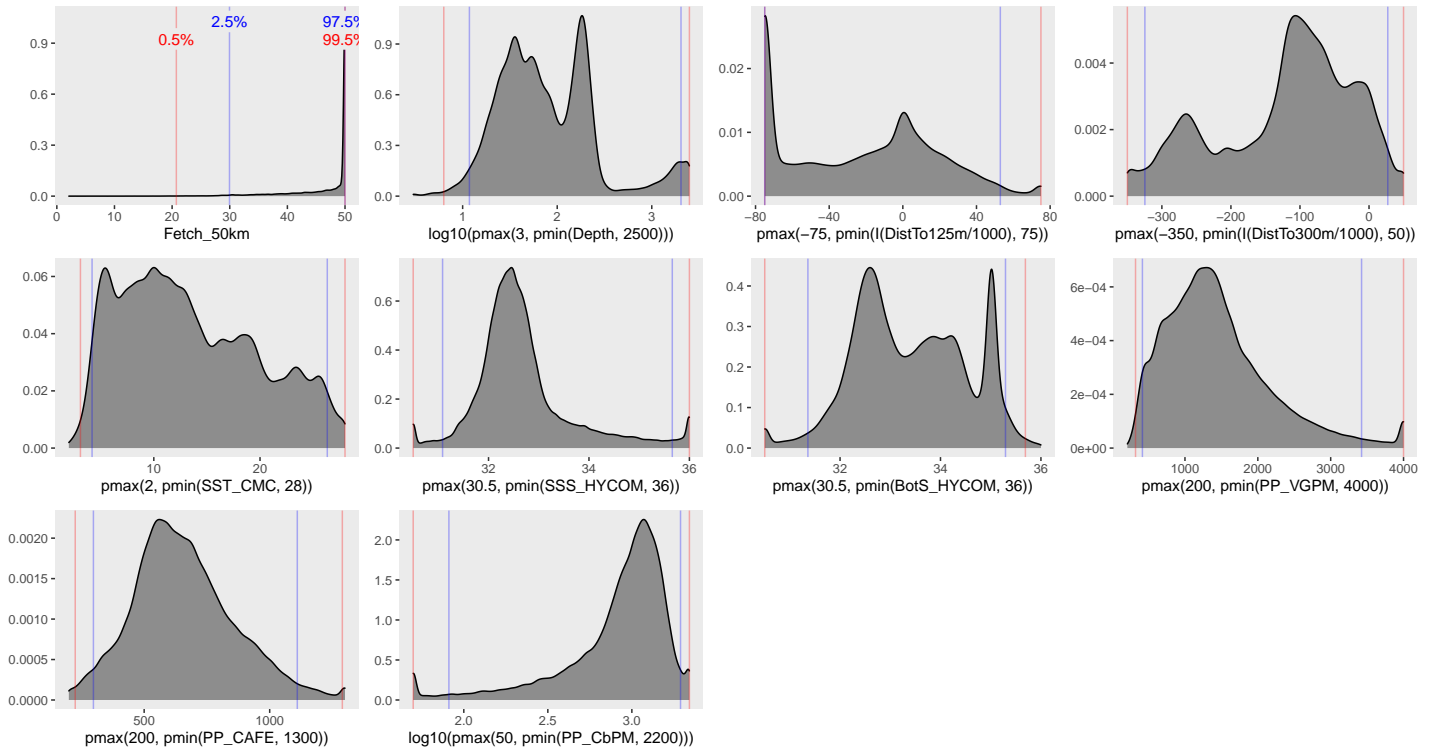


Figure 67: Density histograms showing the distributions of the covariates considered during the final model selection step. The final model may have included only a subset of the covariates shown here (see Figure 65), and additional covariates may have been considered in preceding selection steps. Red and blue lines enclose 99% and 95% of the distributions, respectively. Transforms and other treatments are indicated in axis labels.  $\log_{10}$  indicates the covariate was  $\log_{10}$  transformed.  $pmax$  and  $pmin$  indicate the covariate's minimum and maximum values, respectively, were Winsorized to the values shown. Winsorization was used to prevent runaway extrapolations during prediction when covariates exceeded sampled ranges, or for ecological reasons, depending on the covariate.  $/1000$  indicates meters were transformed to kilometers for interpretation convenience.

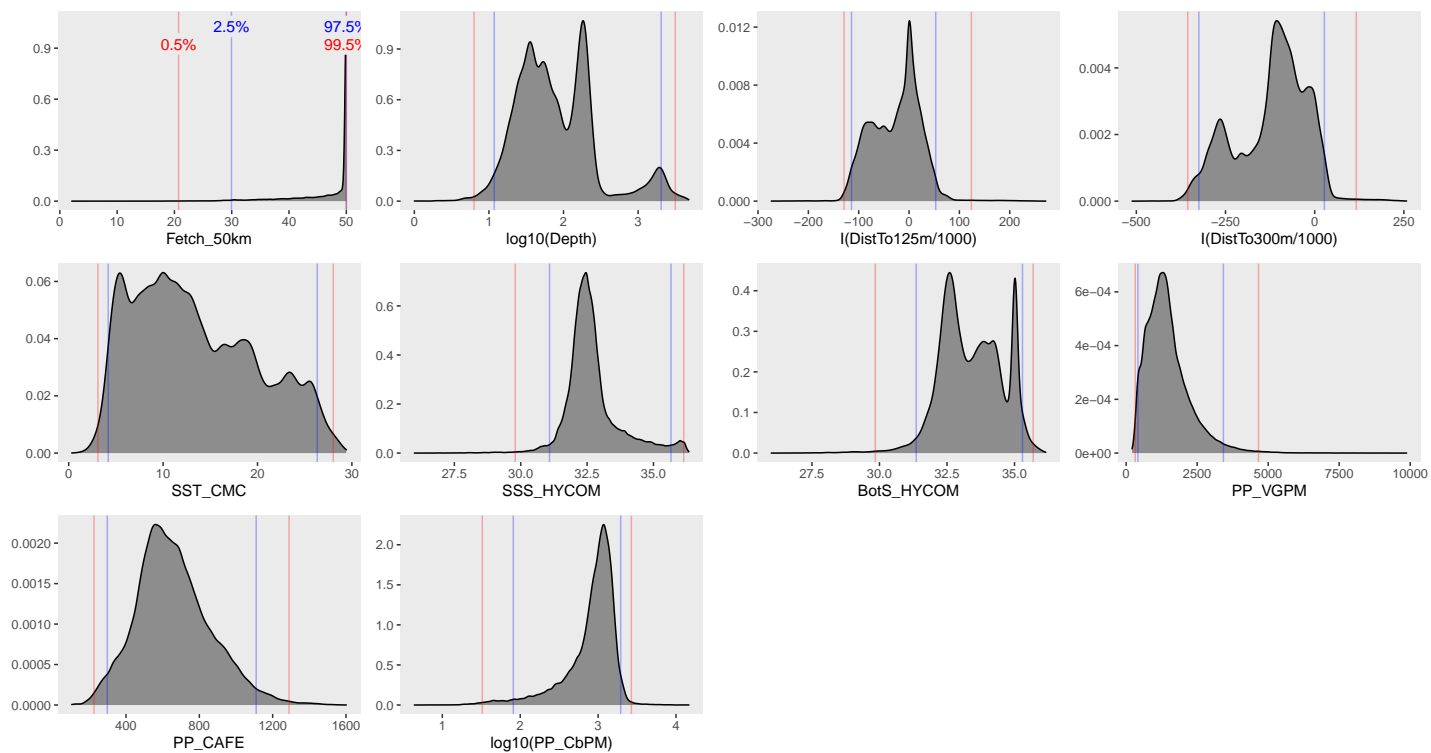


Figure 68: Density histograms shown in Figure 67 replotted without Winsorization, to show the full range of sampling represented by survey segments.

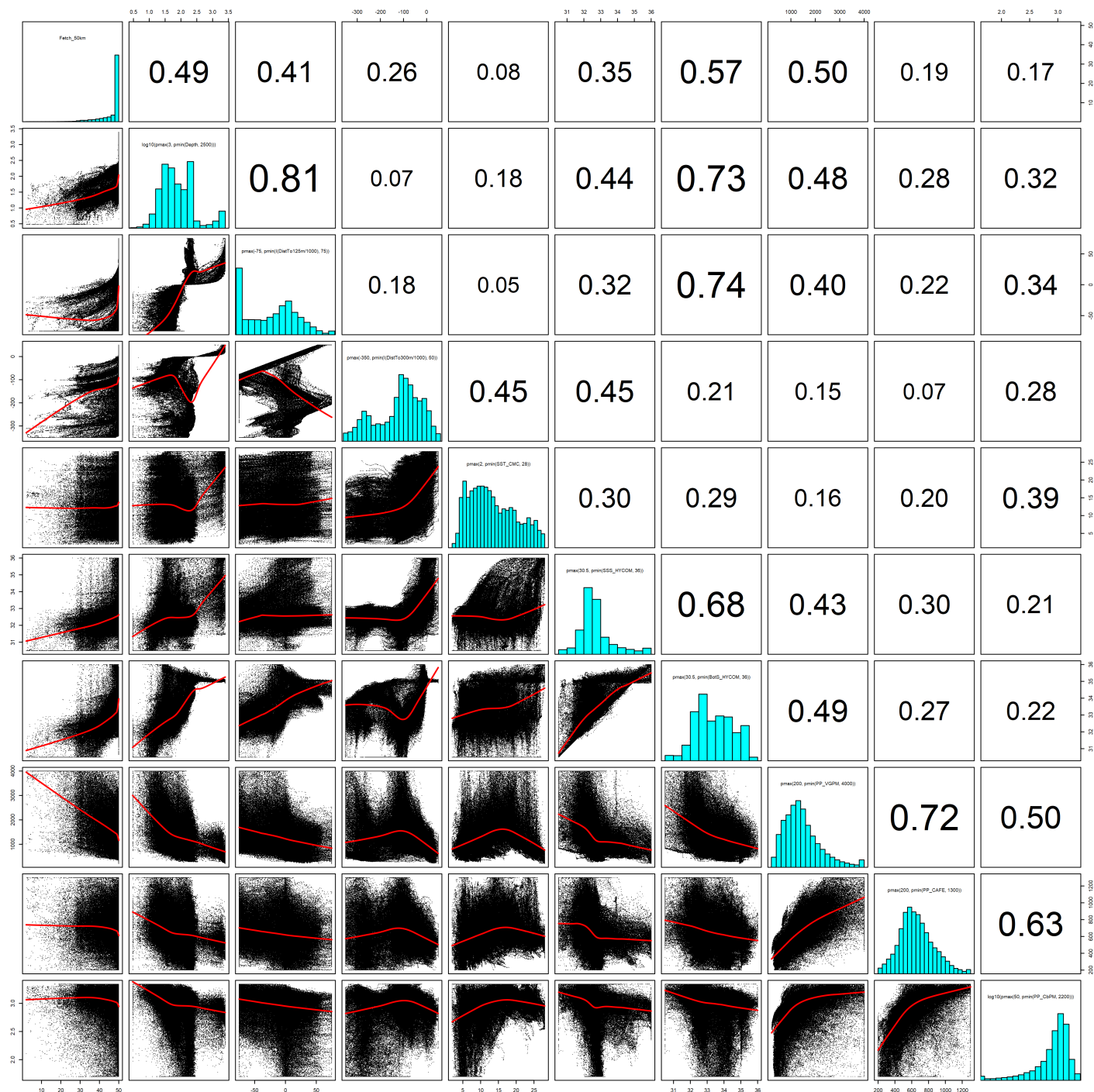


Figure 69: Scatterplot matrix of the covariates considered during the final model selection step. The final model may have included only a subset of the covariates shown here (see Figure 65), and additional covariates may have been considered in preceding selection steps. Covariates are transformed and Winsorized as shown in Figure 67. This plot is used to check simple correlations between covariates (via pairwise Pearson coefficients above the diagonal) and visually inspect for concurvity (via scatterplots and red loess curves below the diagonal).

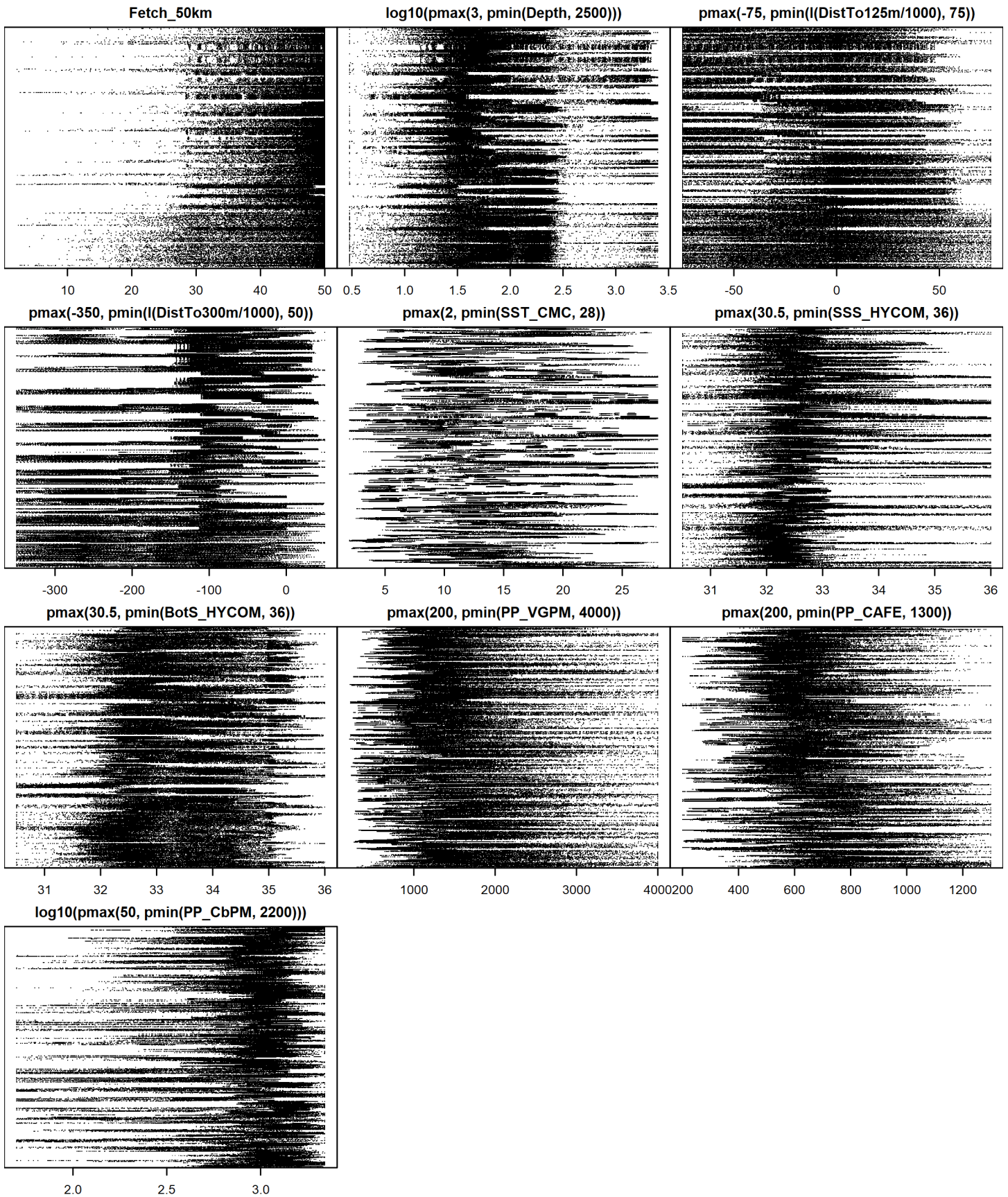


Figure 70: Dotplot of the covariates considered during the final model selection step. The final model may have included only a subset of the covariates shown here (see Figure 65), and additional covariates may have been considered in preceding selection steps. Covariates are transformed and Winsorized as shown in Figure 67. This plot is used to check for suspicious patterns and outliers in the data. Points are ordered vertically by segment ID, sequentially in time.

### 5.1.3 Extrapolation Diagnostics

#### 5.1.3.1 Univariate Extrapolation

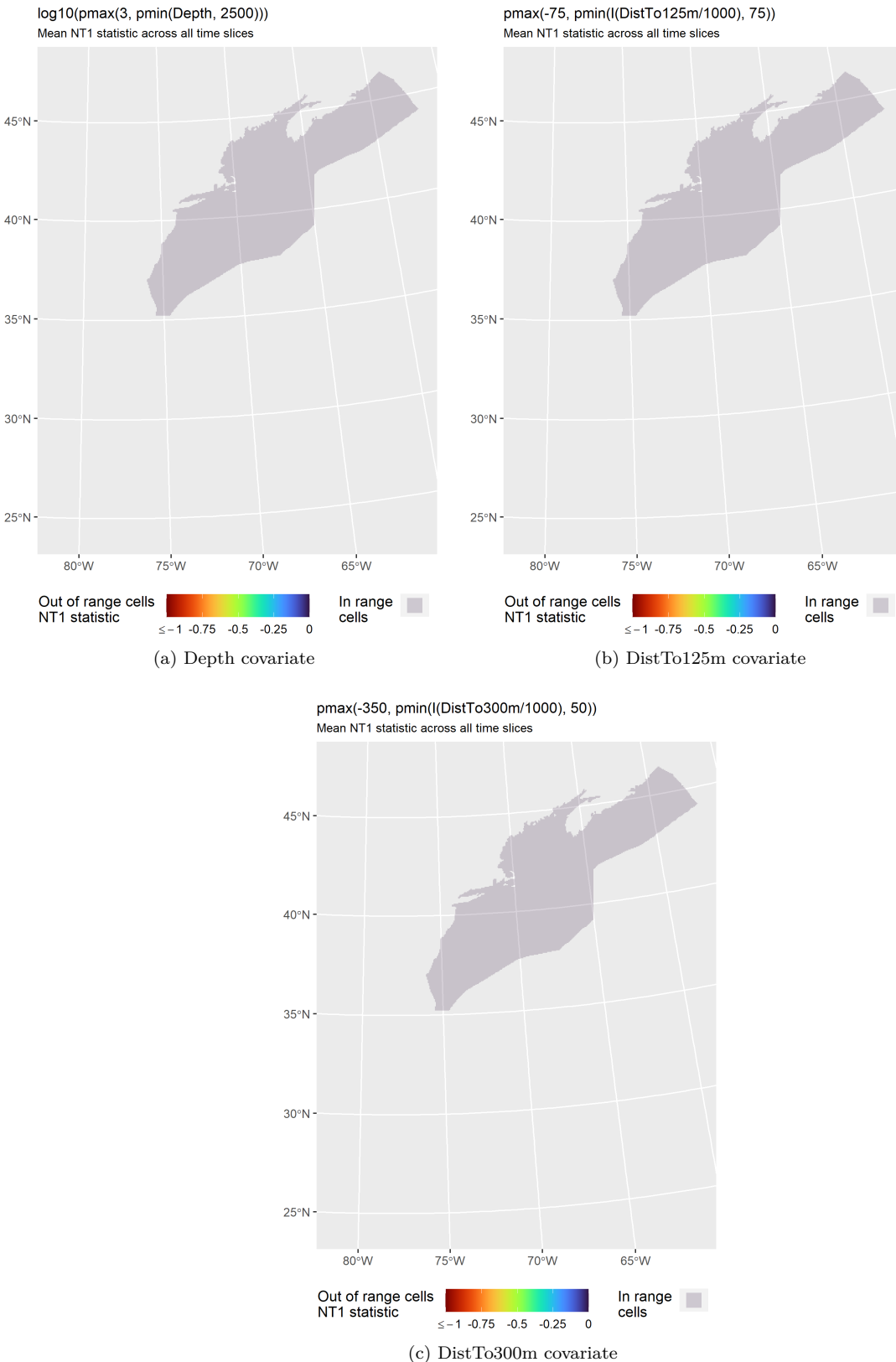


Figure 71: NT1 statistic (Mesgaran et al. (2014)) for static covariates used in the model for the region North of Gulf Stream. Areas outside the sampled range of a covariate appear in color, indicating univariate extrapolation of that covariate occurred there. Areas within the sampled range appear in gray, indicating it did not occur.

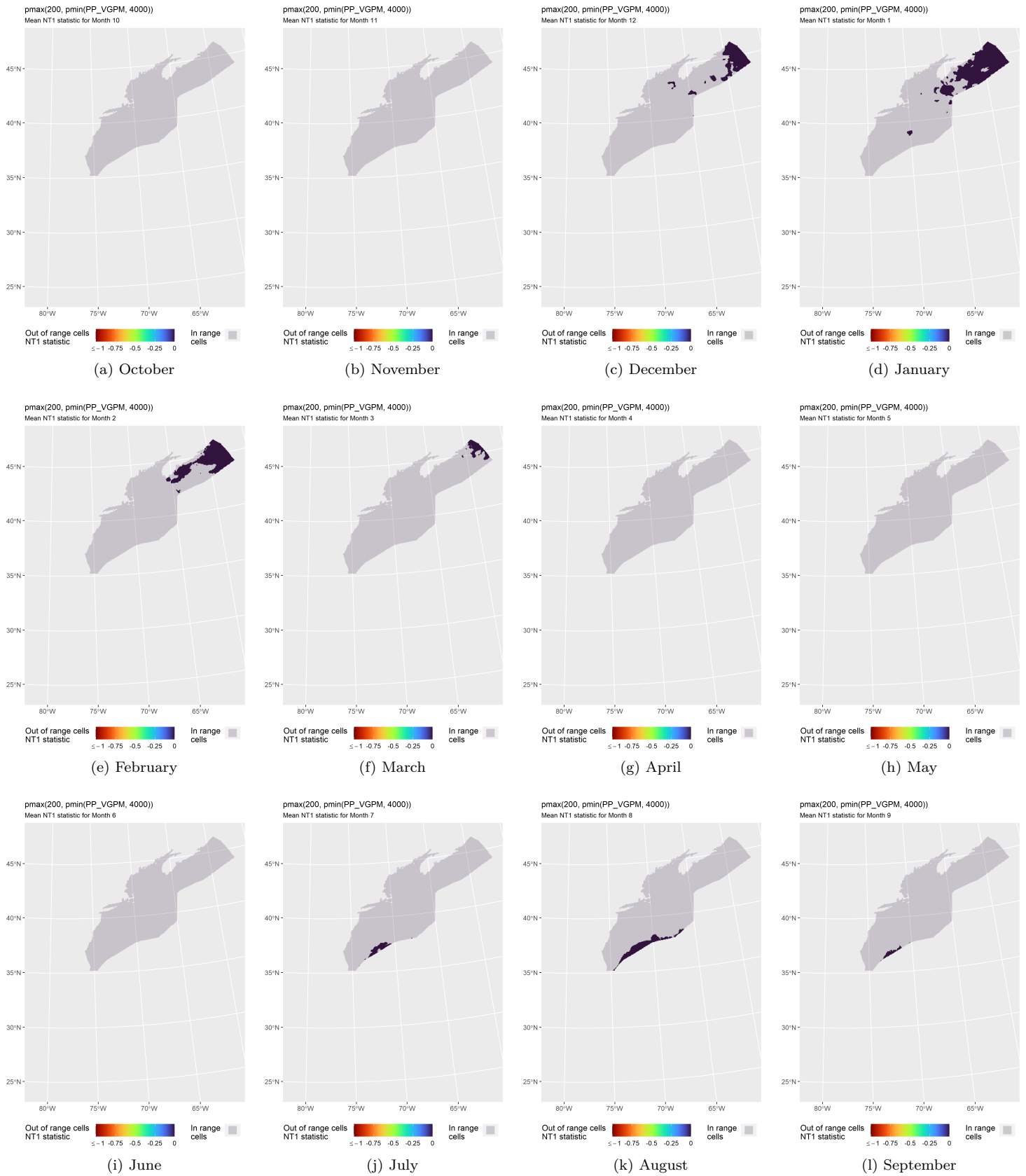


Figure 72: NT1 statistic (Mesgaran et al. (2014)) for the PP\_VGPM covariate in the model for the region North of Gulf Stream. Areas outside the sampled range of a covariate appear in color, indicating univariate extrapolation of that covariate occurred there during the month. Areas within the sampled range appear in gray, indicating it did not occur.

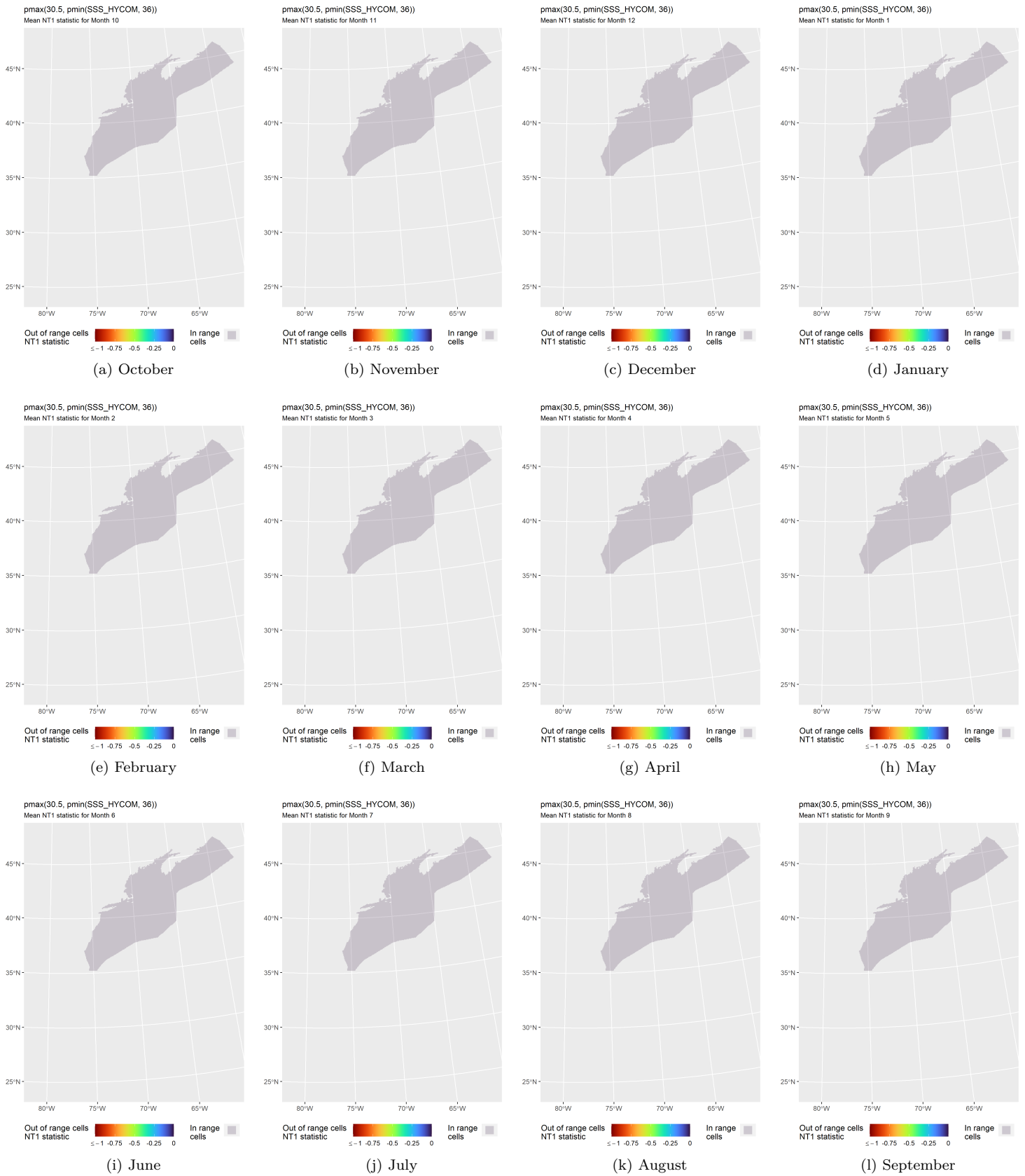


Figure 73: NT1 statistic (Mesgaran et al. (2014)) for the SSS\_HYCOM covariate in the model for the region North of Gulf Stream. Areas outside the sampled range of a covariate appear in color, indicating univariate extrapolation of that covariate occurred there during the month. Areas within the sampled range appear in gray, indicating it did not occur.



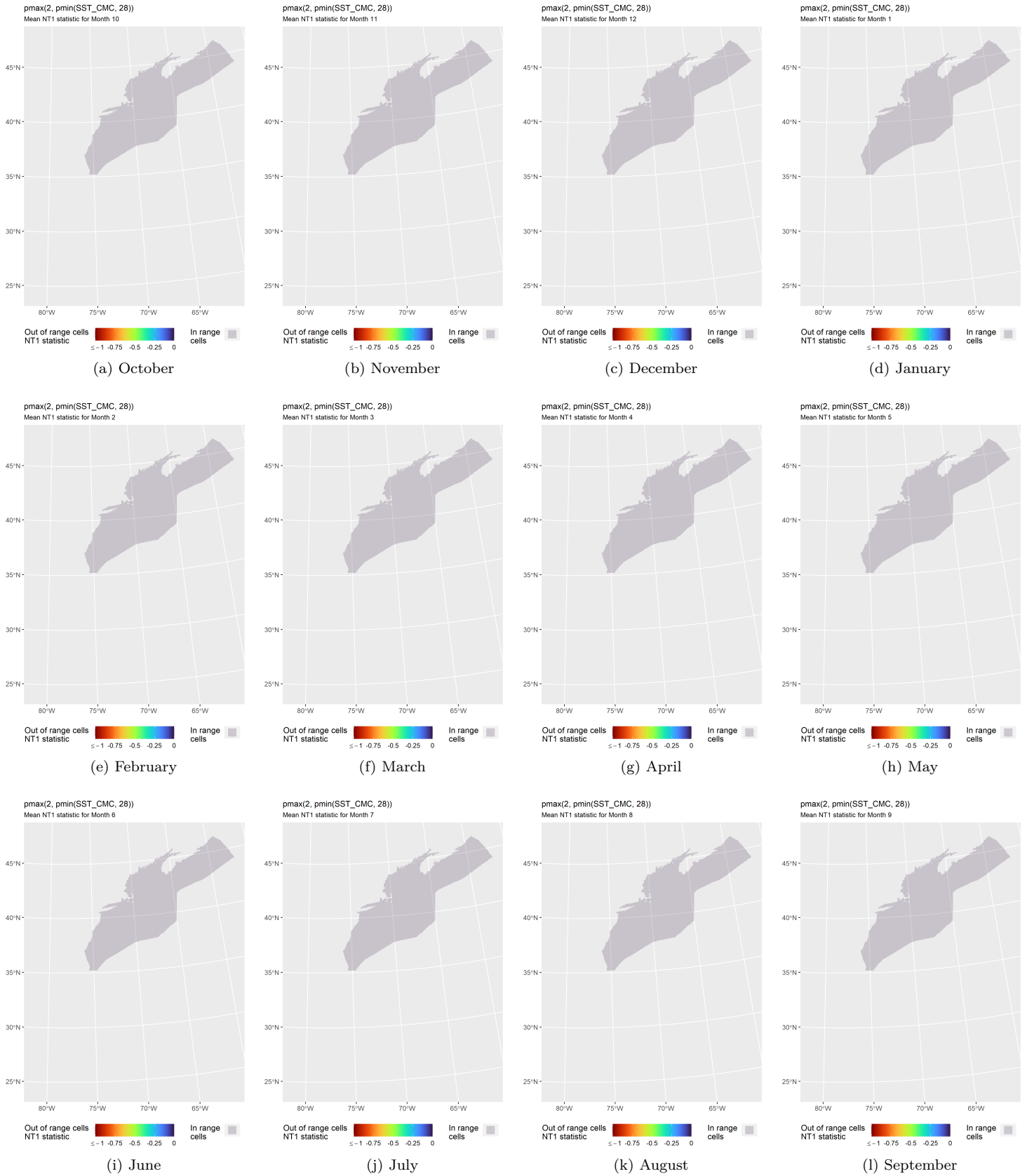


Figure 74: NT1 statistic (Mesgaran et al. (2014)) for the SST\_CMC covariate in the model for the region North of Gulf Stream. Areas outside the sampled range of a covariate appear in color, indicating univariate extrapolation of that covariate occurred there during the month. Areas within the sampled range appear in gray, indicating it did not occur.

### 5.1.3.2 Multivariate Extrapolation

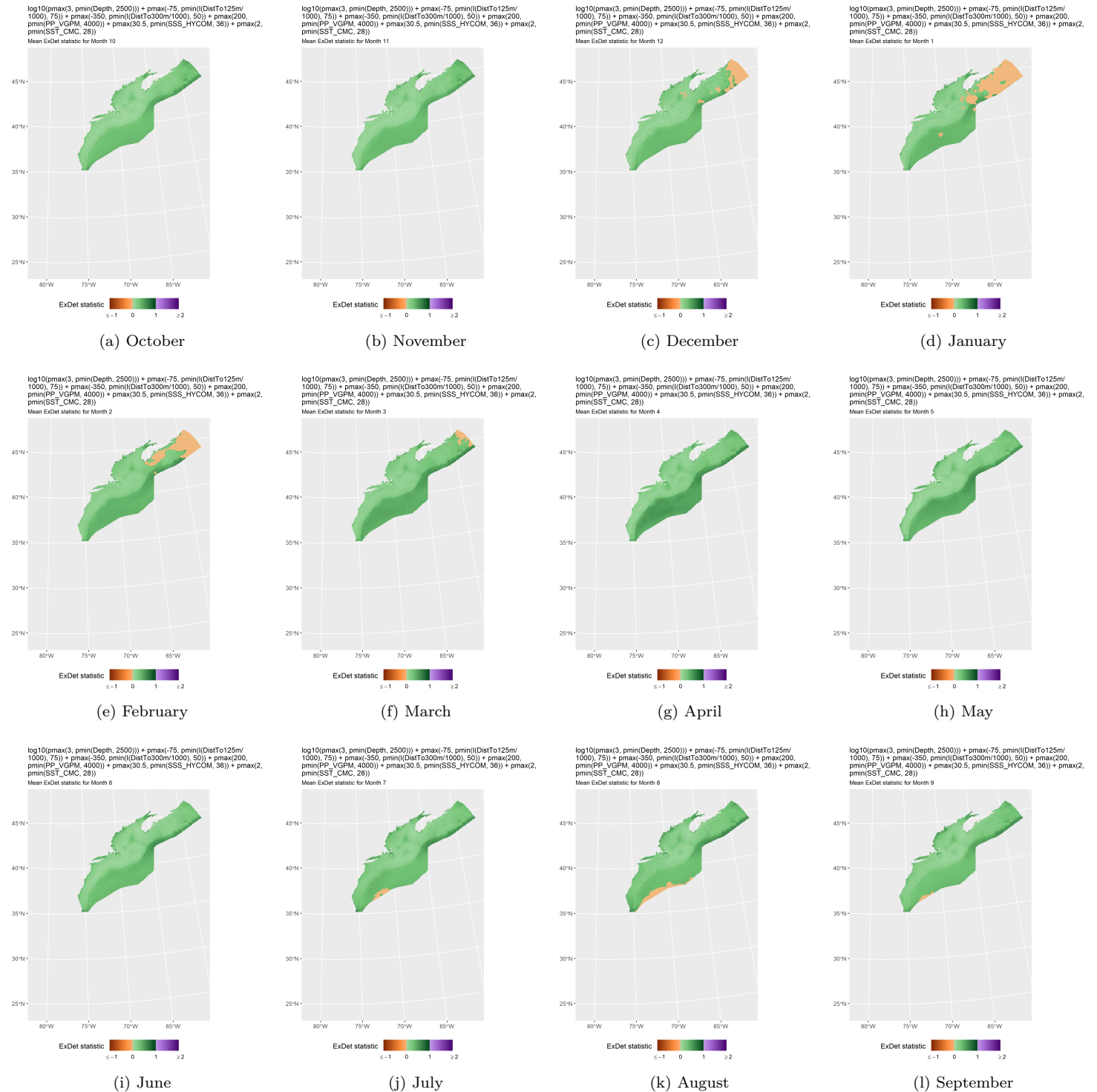


Figure 75: ExDet statistic (Mesgaran et al. (2014)) for all of the covariates used in the model for the region North of Gulf Stream. Areas in orange ( $ExDet < 0$ ) required univariate extrapolation of one or more covariates (see previous section). Areas in purple ( $ExDet > 1$ ), did not require univariate extrapolation but did require multivariate extrapolation, by virtue of having novel combinations of covariates not represented in the survey data, according to the NT2 statistic (Mesgaran et al. (2014)). Areas in green ( $0 \geq ExDet \leq 1$ ) did not require either type of extrapolation.

## 5.2 South of the Gulf Stream

South of the Gulf Stream, during the “Summer” season of March-September, no sei whale sightings were reported and very few sei whale calls were detected by Davis et al. (2020), and we assumed for the purpose of this model that the species was absent. In “Winter”, October-February, we estimated density in a region spanning the Blake Plateau and offshore waters for which some surveying was available and four sightings were reported (Figure 76). Davis et al. (2020) reported numerous acoustic detections during this period.

With so few sightings, it was not possible to fit a traditional density surface model that related density observed on survey segments to environmental covariates. Nor was it possible to make a proper design-based abundance estimate using traditional distance sampling (Buckland et al. 2001), because the aggregate surveys provided heterogeneous coverage that did not together constitute a proper systematic survey design.

To provide interested parties with at least a rough estimate of density for the region, we fitted a model with no covariates, under the assumption that density was distributed uniformly within it. This assumption, if true, would mean we could obtain similar density estimates under any sampling design, and therefore it would not matter if there was some heterogeneity in sampling. However, we strongly caution that this assumption of uniform density did not hold for models where we had sufficient data to build traditional density surface models—such as for sei whale in the region north of the Gulf Stream—as evidenced by the non-uniform patterns in density predicted by those models. In the region addressed here, waters beyond the upper continental shelf south of the Gulf Stream, sei whale density appears to be low, and additional surveying is required to properly characterize how it varies spatially. Until such data have been collected, we offer this simplified approach as a rough-and-ready substitute for a full density surface model.

In this section, we present a map and tallies of the survey effort and sightings (Figure 76). Section 6.1 gives the resulting map of density and the total abundance and coefficient of variation.

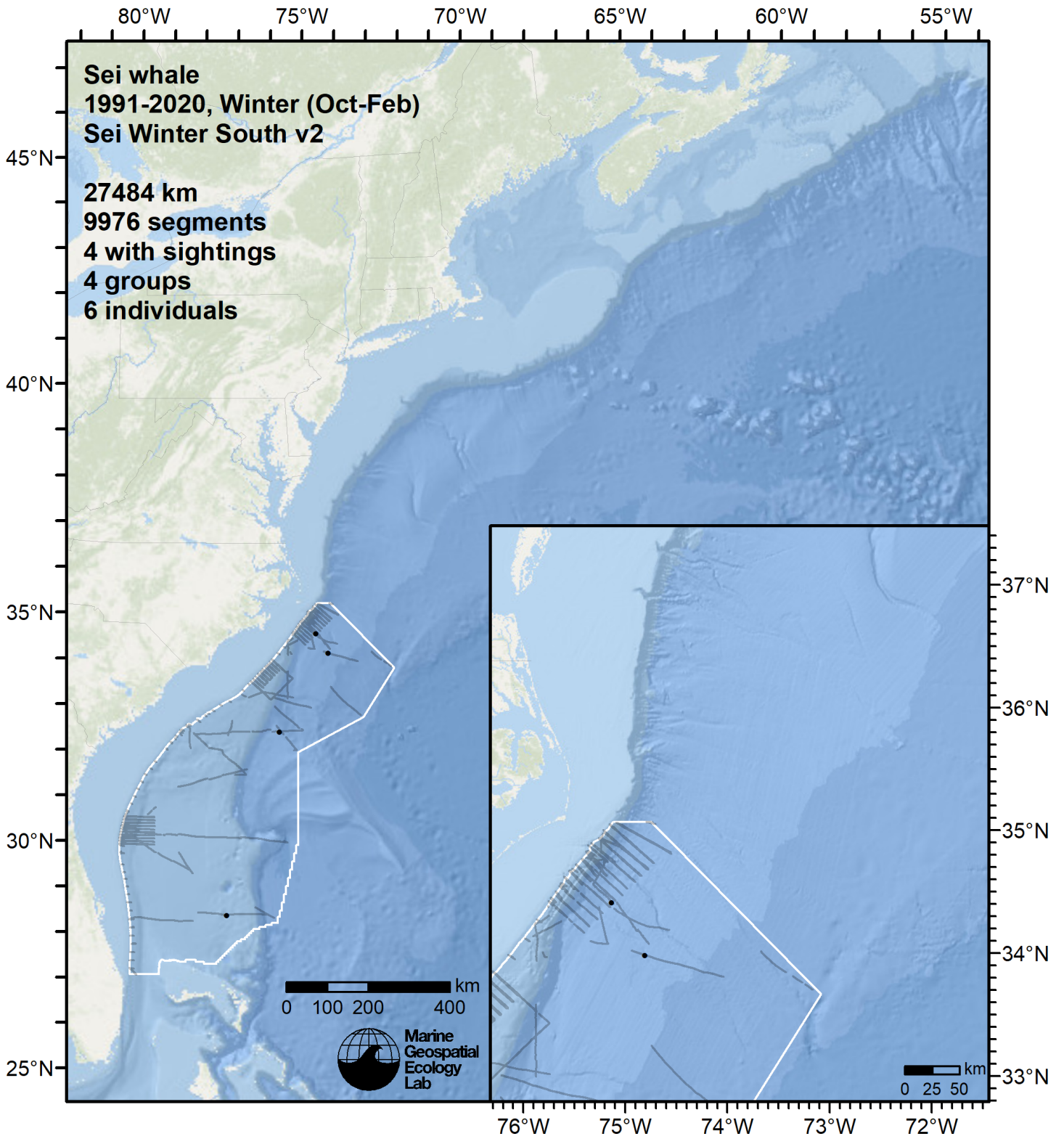


Figure 76: Survey segments and sightings used to estimate sei whale density for the off-shelf region south of Gulf Stream. Black points indicate segments with observations.

## 6 Predictions

Based on our evaluation of this model in the context of what is known of this species (see Section 7), we summarized its predictions into monthly climatological density and uncertainty surfaces, shown in the maps below.

### 6.1 Summarized Predictions

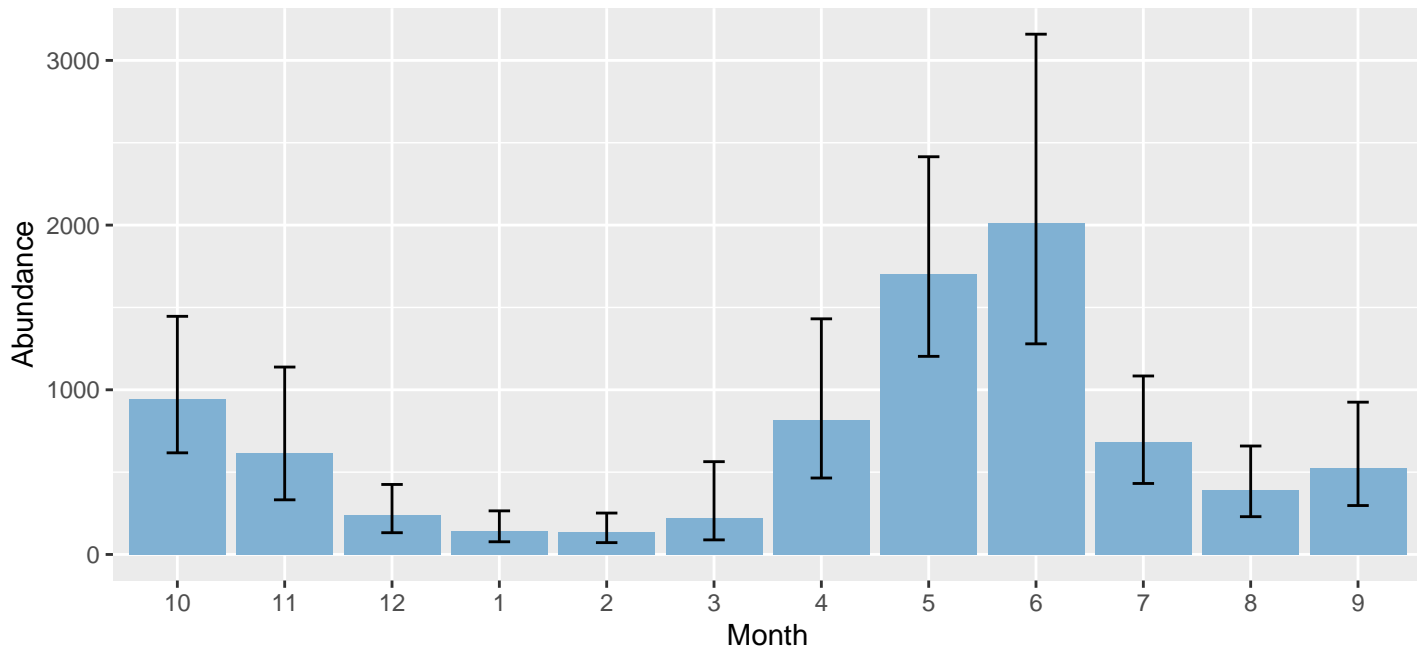


Figure 77: Mean monthly abundance for the prediction area for October 1998 - September 2020. Note that the prediction area was not the same for all months (see Table 26 below and maps following). Error bars are a 95% interval, made with a log-normal approximation using the prediction’s CV. The CV was estimated with the analytic approach given by Miller et al. (2022), Appendix S1, and accounts both for uncertainty in model parameter estimates and for temporal variability in dynamic covariates.

Table 26: Mean monthly abundance and density for the prediction area for October 1998 - September 2020. CV and intervals estimated as described for the previous figure.

| Month | Abundance | CV    | 95% Interval  | Area (km <sup>2</sup> ) | Density (individuals / 100 km <sup>2</sup> ) |
|-------|-----------|-------|---------------|-------------------------|--|
| 10    | 945       | 0.220 | 617 - 1,446   | 1,140,325               | 0.083  |
| 11    | 615       | 0.322 | 332 - 1,138   | 1,140,325               | 0.054  |
| 12    | 237       | 0.305 | 132 - 425     | 1,140,325               | 0.021  |
| 1     | 143       | 0.323 | 77 - 265      | 1,140,325               | 0.013  |
| 2     | 135       | 0.327 | 72 - 251      | 1,140,325               | 0.012  |
| 3     | 223       | 0.500 | 89 - 563      | 1,272,925               | 0.018  |
| 4     | 815       | 0.293 | 464 - 1,431   | 1,272,925               | 0.064  |
| 5     | 1,705     | 0.179 | 1,203 - 2,415 | 1,272,925               | 0.134  |
| 6     | 2,010     | 0.234 | 1,279 - 3,159 | 1,272,925               | 0.158  |
| 7     | 684       | 0.239 | 431 - 1,084   | 1,272,925               | 0.054  |
| 8     | 389       | 0.274 | 230 - 659     | 1,272,925               | 0.031  |
| 9     | 524       | 0.296 | 297 - 925     | 1,272,925               | 0.041  |

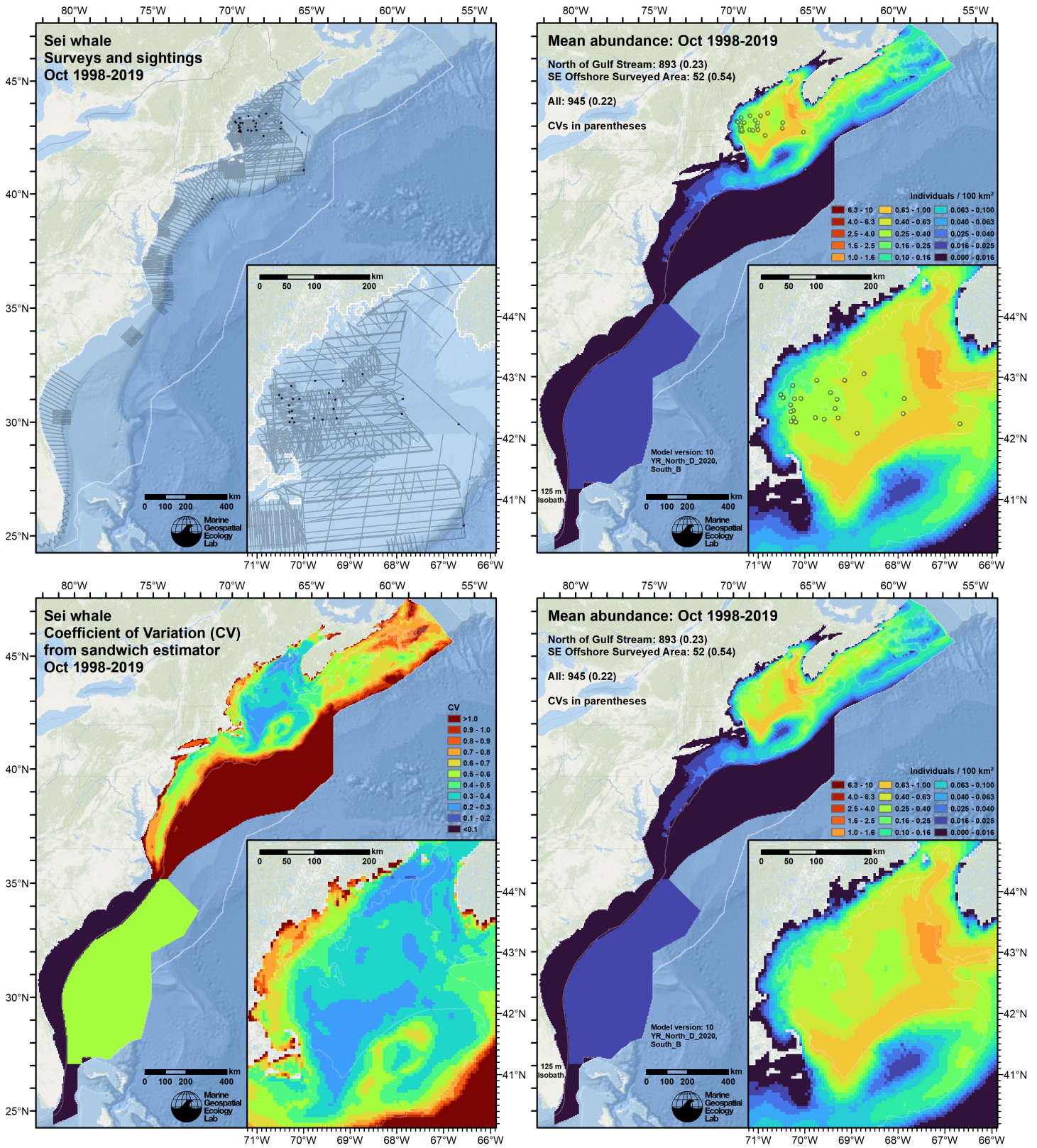


Figure 78: Survey effort and observations (top left), predicted density with observations (top right), predicted density without observations (bottom right), and coefficient of variation of predicted density (bottom left), for the month of October for the given era. Variance was estimated with the analytic approach given by Miller et al. (2022), Appendix S1, and accounts both for uncertainty in model parameter estimates and for temporal variability in dynamic covariates.

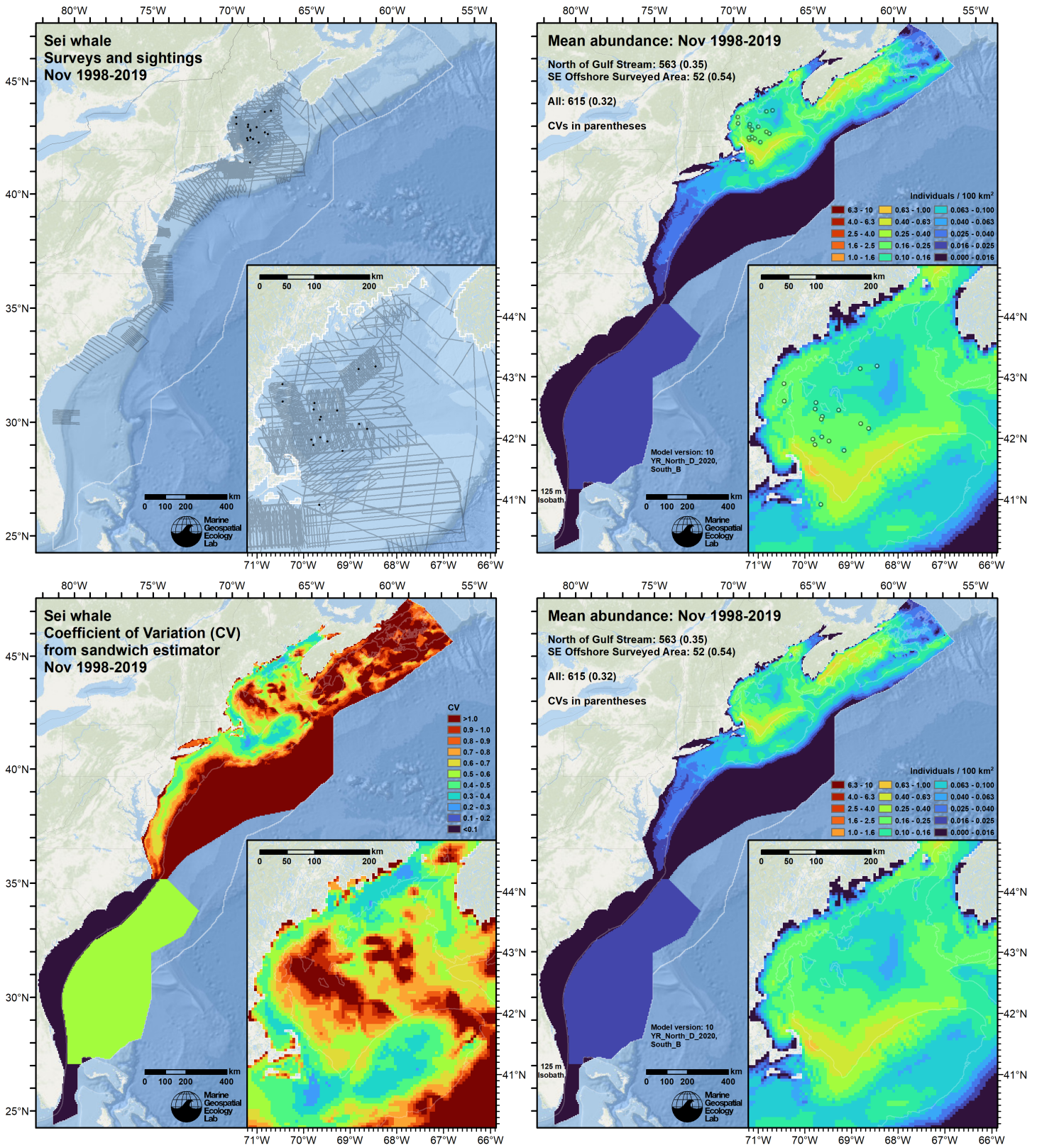


Figure 79: Survey effort and observations (top left), predicted density with observations (top right), predicted density without observations (bottom right), and coefficient of variation of predicted density (bottom left), for the month of November for the given era. Variance was estimated with the analytic approach given by Miller et al. (2022), Appendix S1, and accounts both for uncertainty in model parameter estimates and for temporal variability in dynamic covariates.

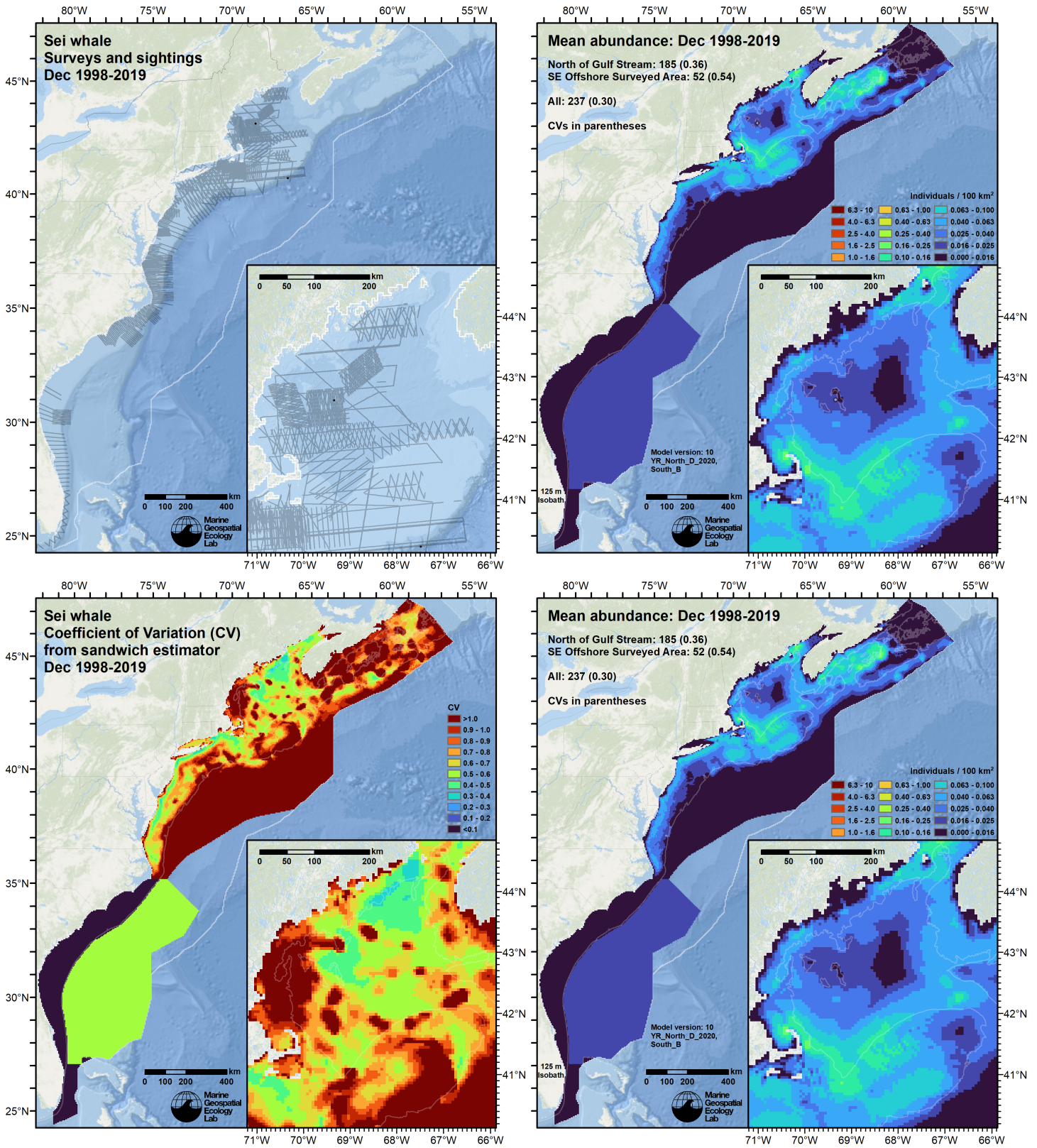


Figure 80: Survey effort and observations (top left), predicted density with observations (top right), predicted density without observations (bottom right), and coefficient of variation of predicted density (bottom left), for the month of December for the given era. Variance was estimated with the analytic approach given by Miller et al. (2022), Appendix S1, and accounts both for uncertainty in model parameter estimates and for temporal variability in dynamic covariates.



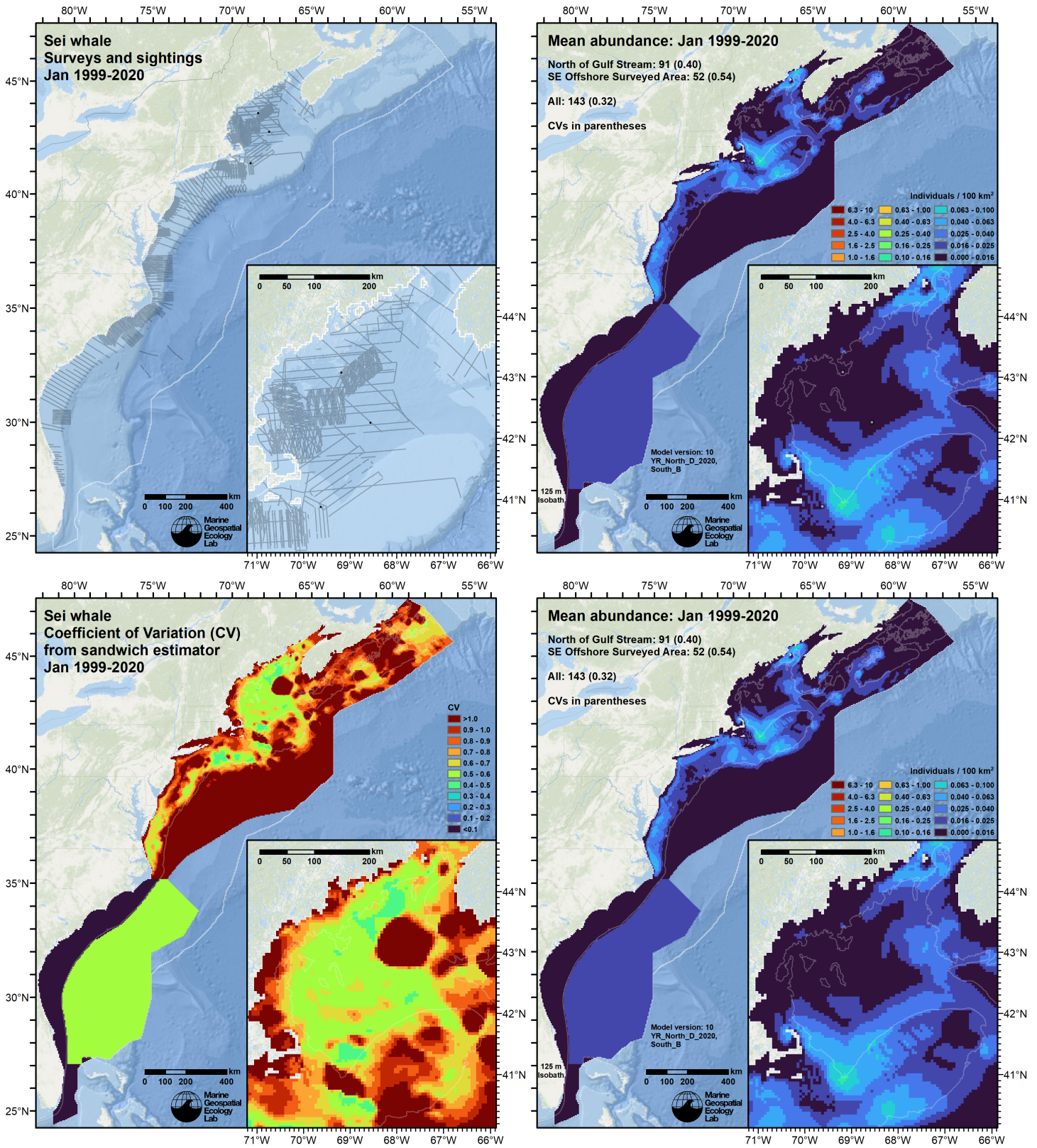


Figure 81: Survey effort and observations (top left), predicted density with observations (top right), predicted density without observations (bottom right), and coefficient of variation of predicted density (bottom left), for the month of January for the given era. Variance was estimated with the analytic approach given by Miller et al. (2022), Appendix S1, and accounts both for uncertainty in model parameter estimates and for temporal variability in dynamic covariates.

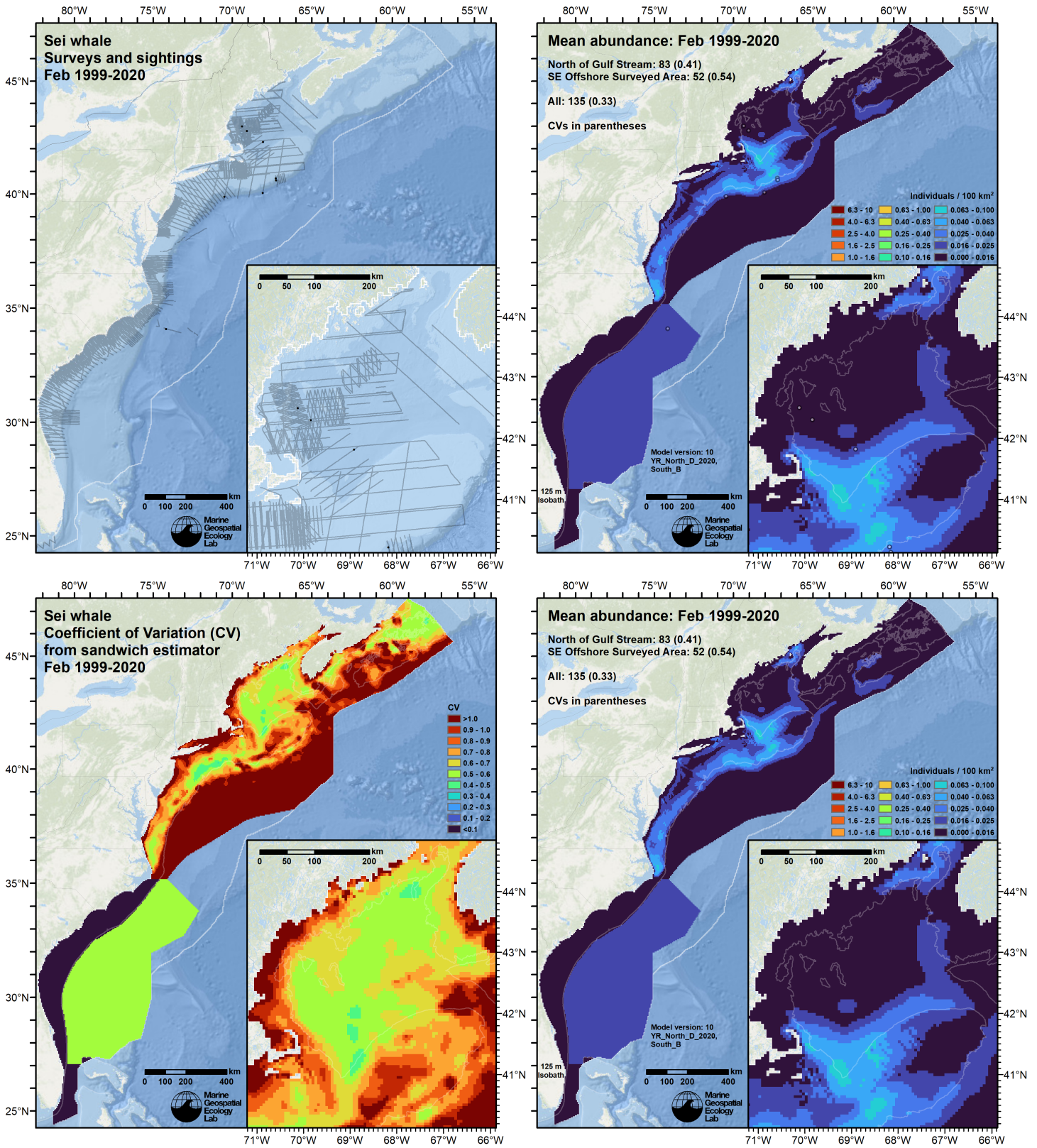


Figure 82: Survey effort and observations (top left), predicted density with observations (top right), predicted density without observations (bottom right), and coefficient of variation of predicted density (bottom left), for the month of February for the given era. Variance was estimated with the analytic approach given by Miller et al. (2022), Appendix S1, and accounts both for uncertainty in model parameter estimates and for temporal variability in dynamic covariates.

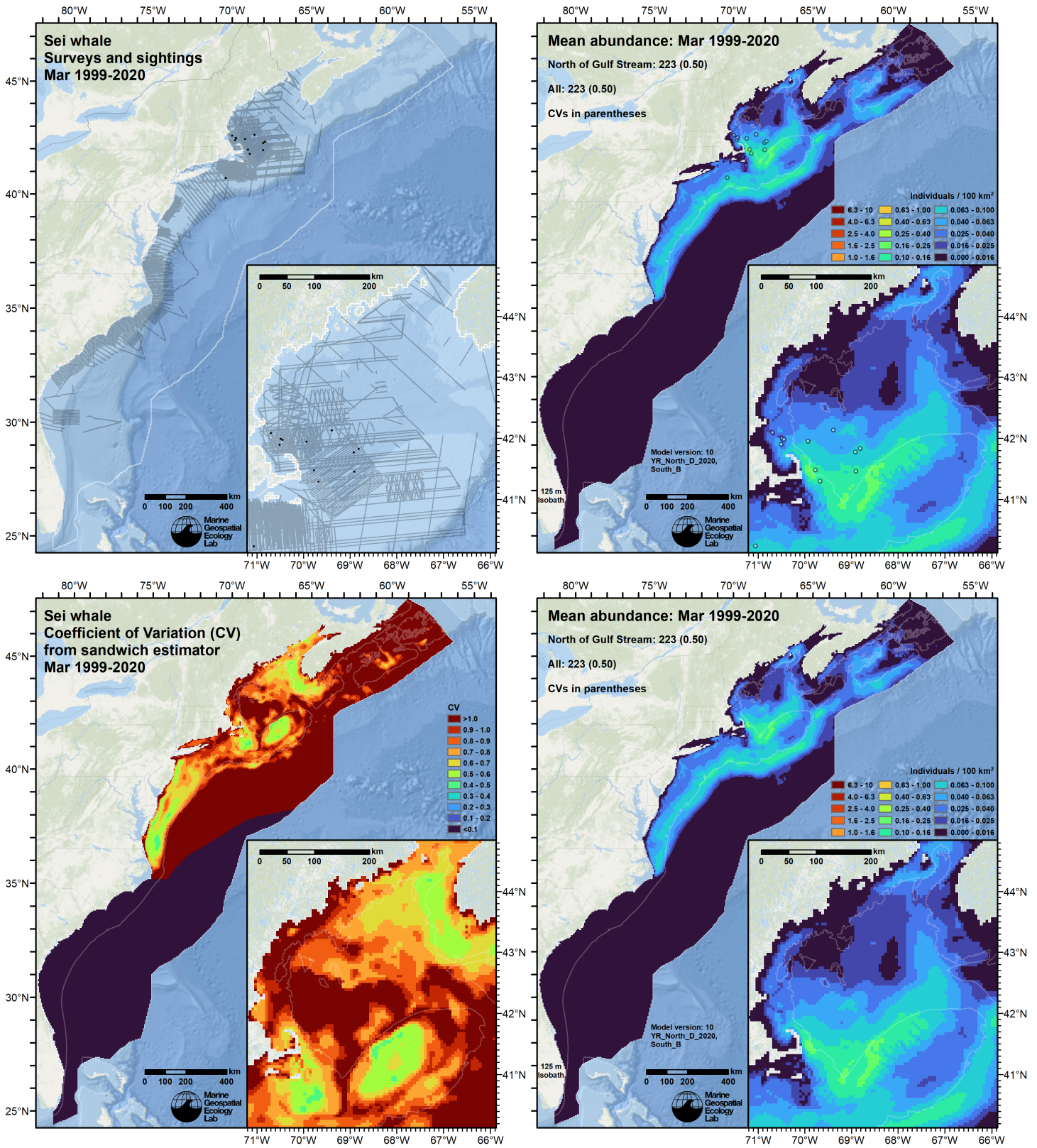


Figure 83: Survey effort and observations (top left), predicted density with observations (top right), predicted density without observations (bottom right), and coefficient of variation of predicted density (bottom left), for the month of March for the given era. Variance was estimated with the analytic approach given by Miller et al. (2022), Appendix S1, and accounts both for uncertainty in model parameter estimates and for temporal variability in dynamic covariates.

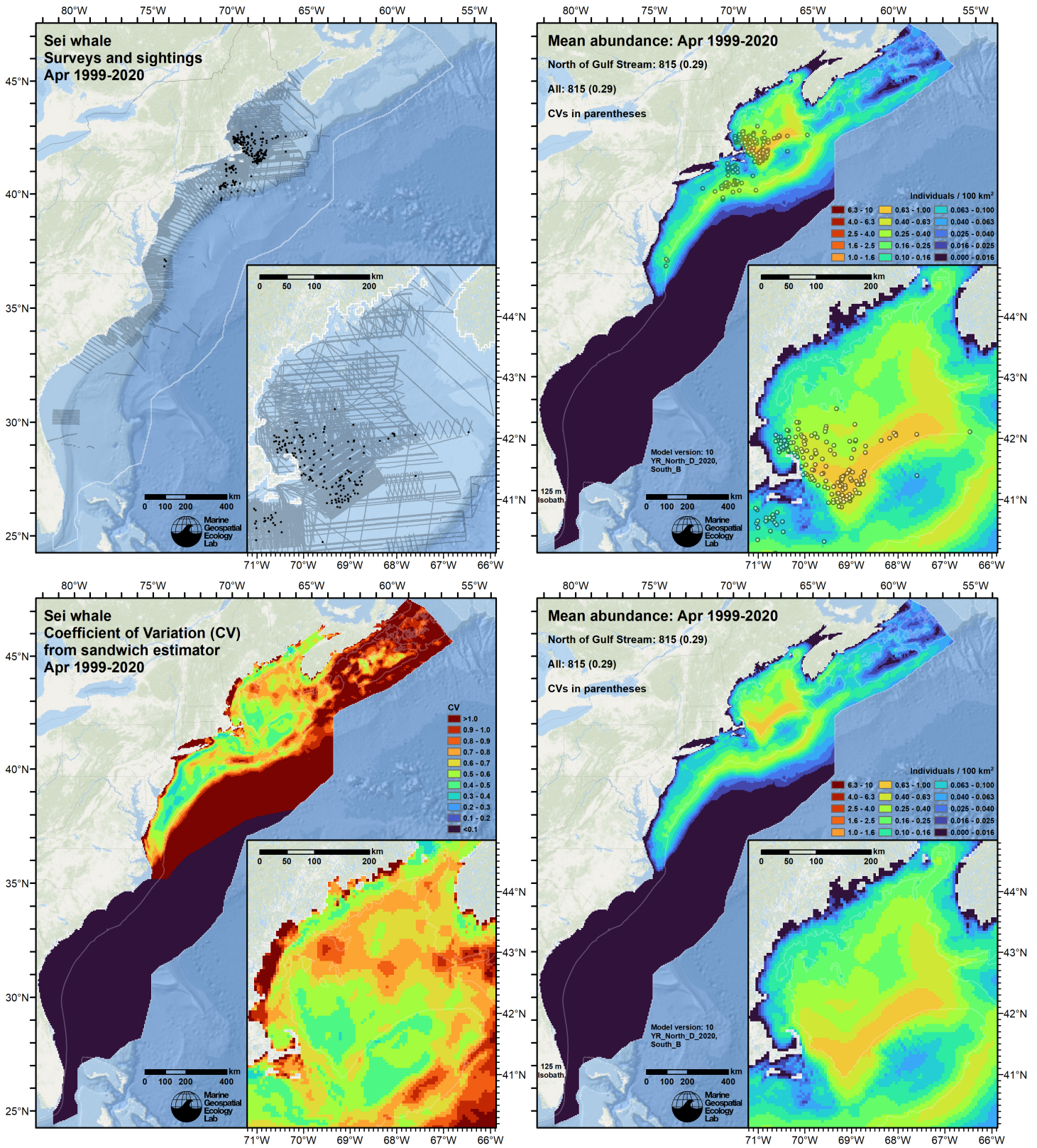


Figure 84: Survey effort and observations (top left), predicted density with observations (top right), predicted density without observations (bottom right), and coefficient of variation of predicted density (bottom left), for the month of April for the given era. Variance was estimated with the analytic approach given by Miller et al. (2022), Appendix S1, and accounts both for uncertainty in model parameter estimates and for temporal variability in dynamic covariates.

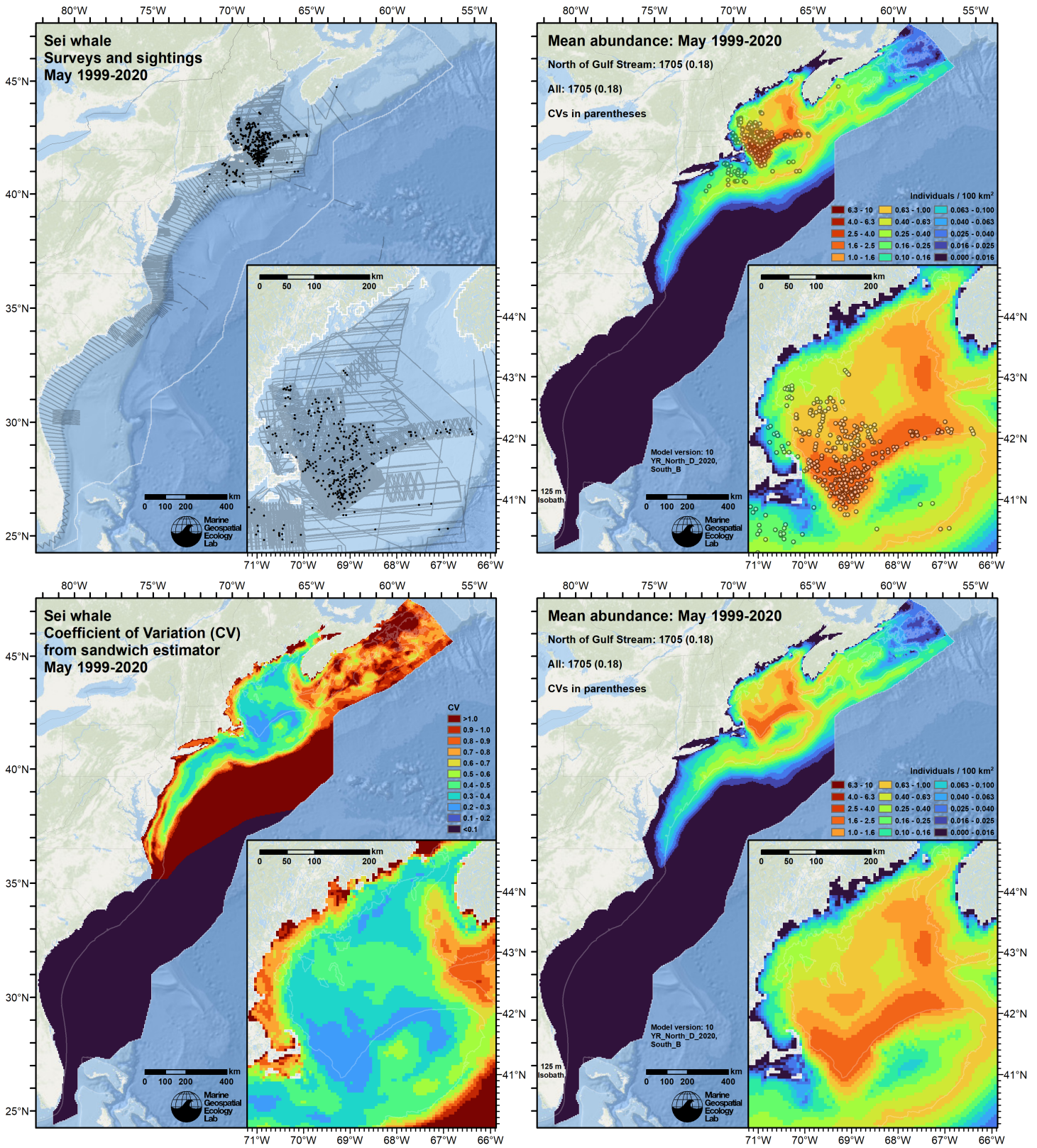


Figure 85: Survey effort and observations (top left), predicted density with observations (top right), predicted density without observations (bottom right), and coefficient of variation of predicted density (bottom left), for the month of May for the given era. Variance was estimated with the analytic approach given by Miller et al. (2022), Appendix S1, and accounts both for uncertainty in model parameter estimates and for temporal variability in dynamic covariates.

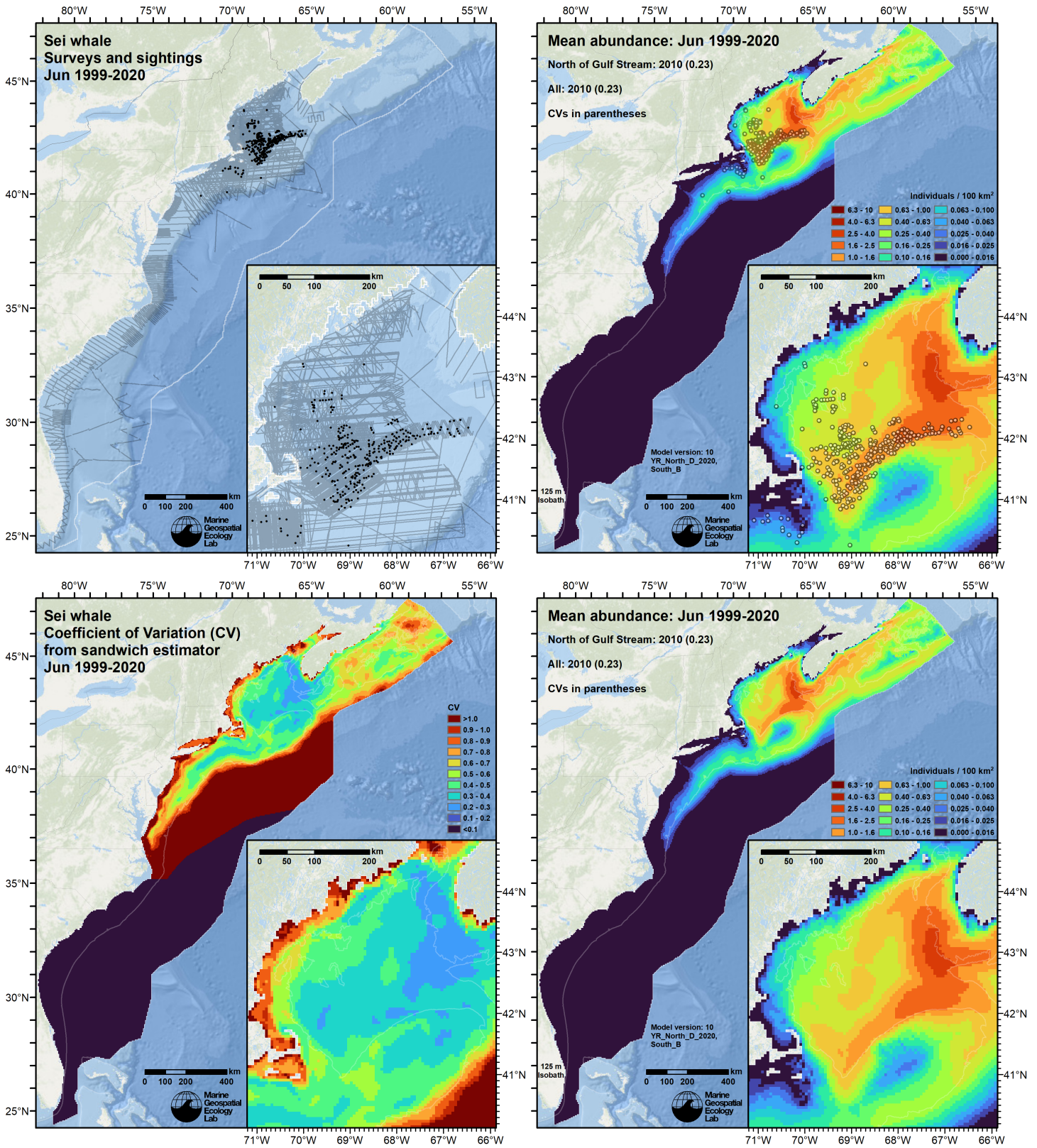


Figure 86: Survey effort and observations (top left), predicted density with observations (top right), predicted density without observations (bottom right), and coefficient of variation of predicted density (bottom left), for the month of June for the given era. Variance was estimated with the analytic approach given by Miller et al. (2022), Appendix S1, and accounts both for uncertainty in model parameter estimates and for temporal variability in dynamic covariates.

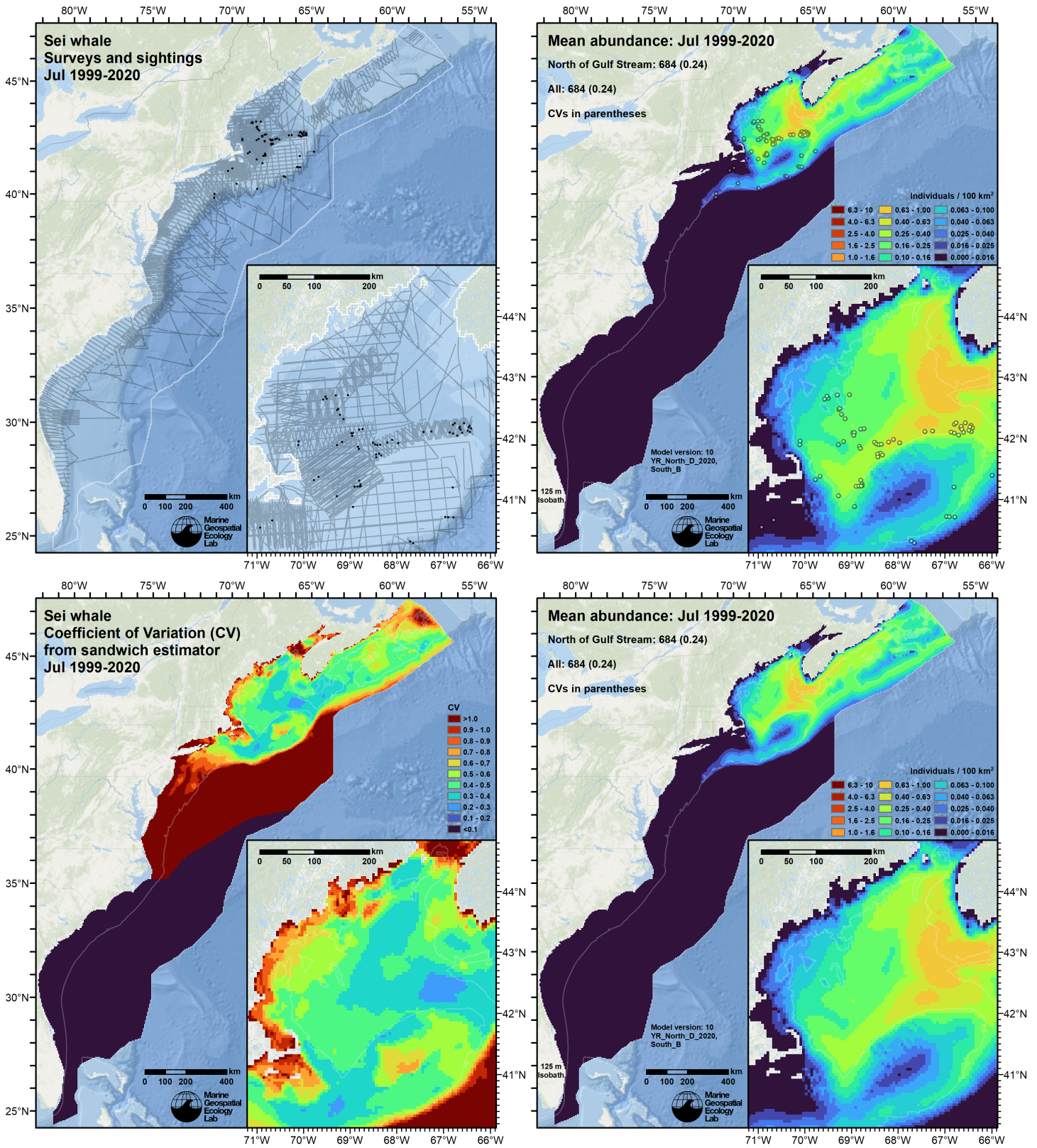


Figure 87: Survey effort and observations (top left), predicted density with observations (top right), predicted density without observations (bottom right), and coefficient of variation of predicted density (bottom left), for the month of July for the given era. Variance was estimated with the analytic approach given by Miller et al. (2022), Appendix S1, and accounts both for uncertainty in model parameter estimates and for temporal variability in dynamic covariates.

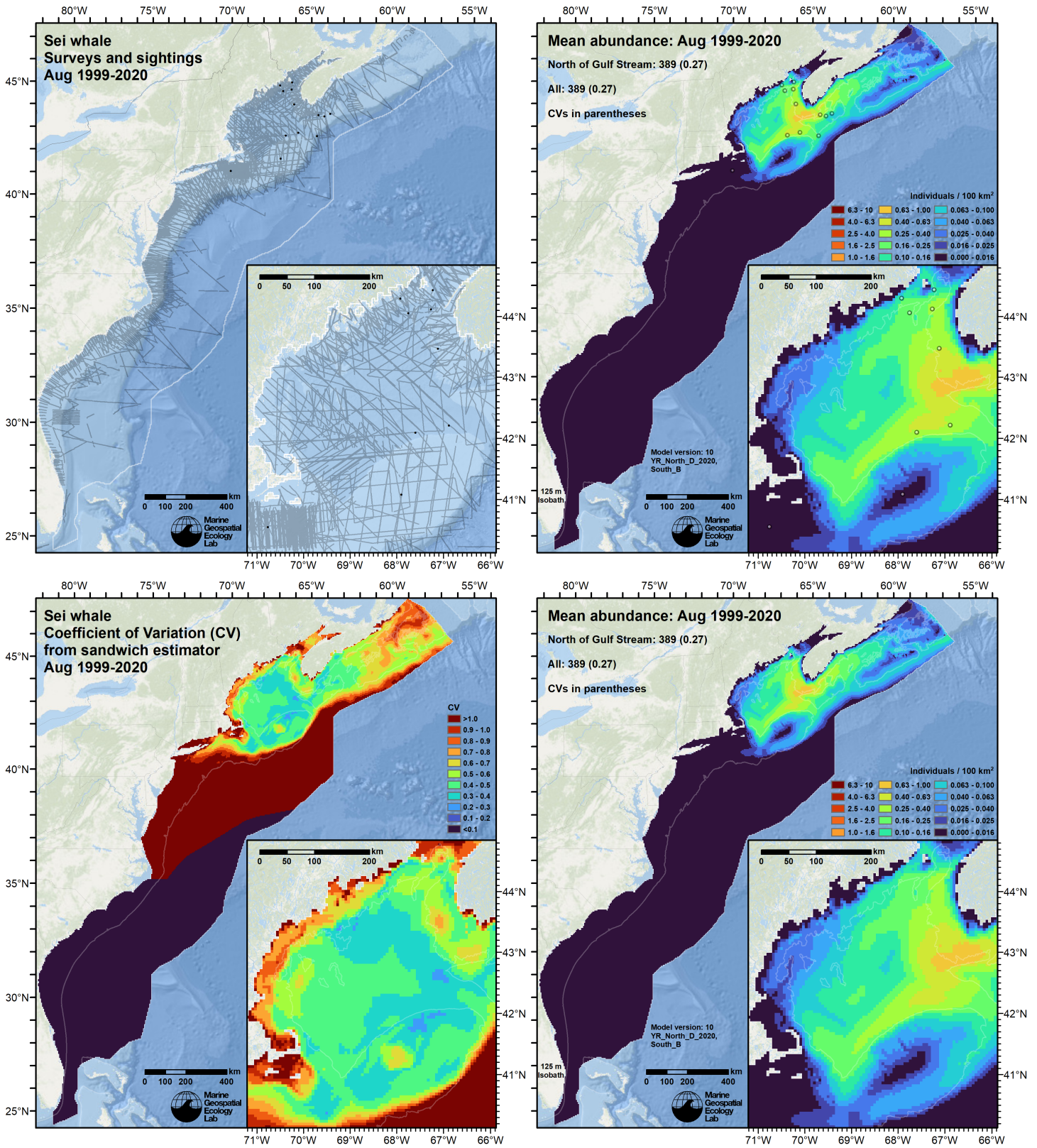


Figure 88: Survey effort and observations (top left), predicted density with observations (top right), predicted density without observations (bottom right), and coefficient of variation of predicted density (bottom left), for the month of August for the given era. Variance was estimated with the analytic approach given by Miller et al. (2022), Appendix S1, and accounts both for uncertainty in model parameter estimates and for temporal variability in dynamic covariates.



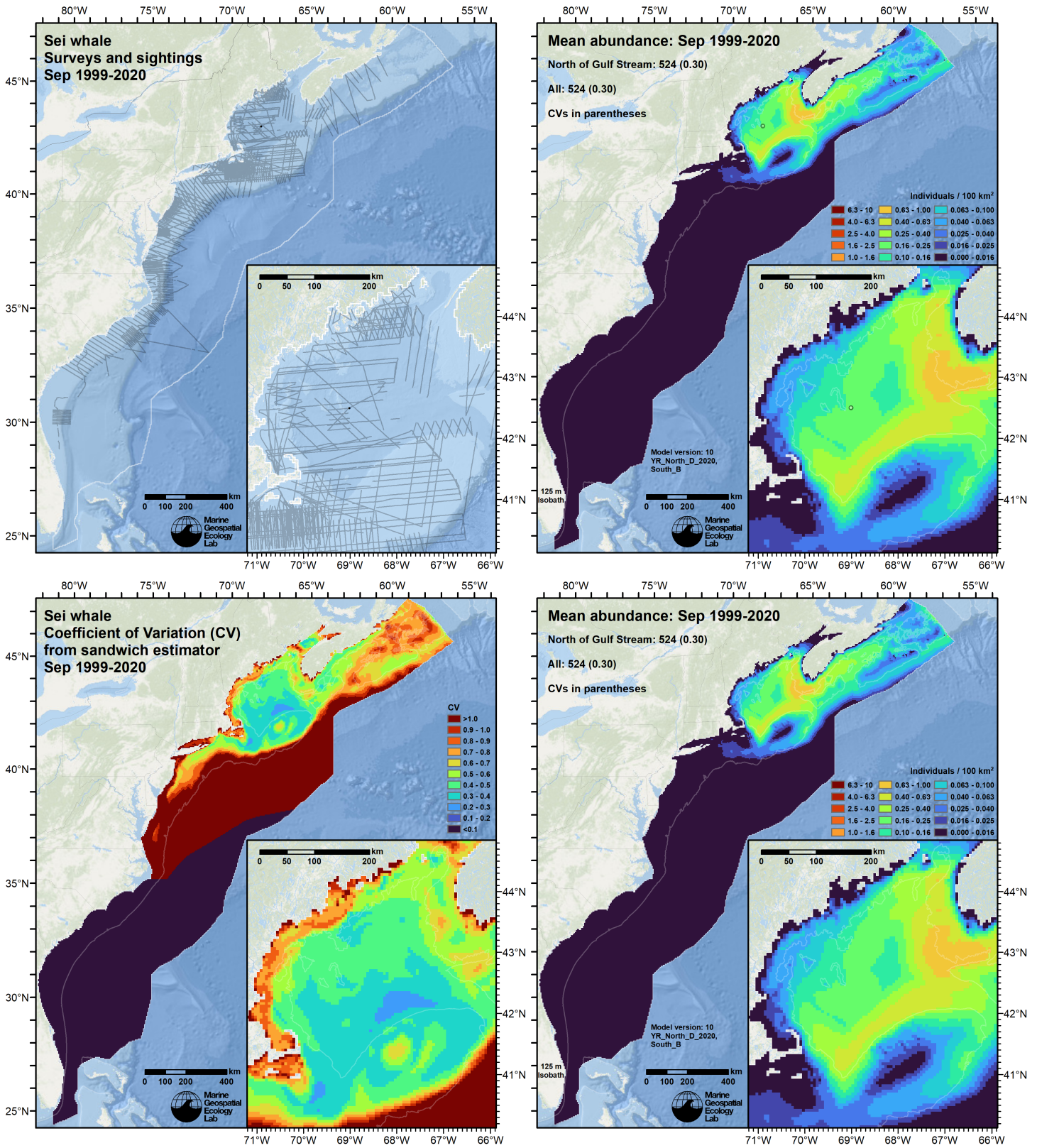


Figure 89: Survey effort and observations (top left), predicted density with observations (top right), predicted density without observations (bottom right), and coefficient of variation of predicted density (bottom left), for the month of September for the given era. Variance was estimated with the analytic approach given by Miller et al. (2022), Appendix S1, and accounts both for uncertainty in model parameter estimates and for temporal variability in dynamic covariates.

## 6.2 Abundance Comparisons

### 6.2.1 NOAA Stock Assessment Reports

Table 27: Comparison of the abundance estimate from the 2021 NOAA Stock Assessment Report (SAR) (Hayes et al. (2022)) to an estimate from this density model extracted from the same geographic zone.

| 2021 Stock Assessment Report |                                 |           | Density Model     |                                 |           |
|------------------------------|---------------------------------|-----------|-------------------|---------------------------------|-----------|
| Month/Year                   | Area                            | $N_{est}$ | Period            | Zone                            | Abundance |
| Mar-May 2010-2013            | Halifax to Florida <sup>a</sup> | 6,292     | Mar-May 1999-2020 | Halifax to Florida <sup>b</sup> | 859       |

<sup>a</sup> Estimate originally from the density surface model of Palka et al. (2017).

<sup>b</sup> Estimate extracted from our model using the polygon defined by Palka et al. (2017).

### 6.2.2 Previous Density Model

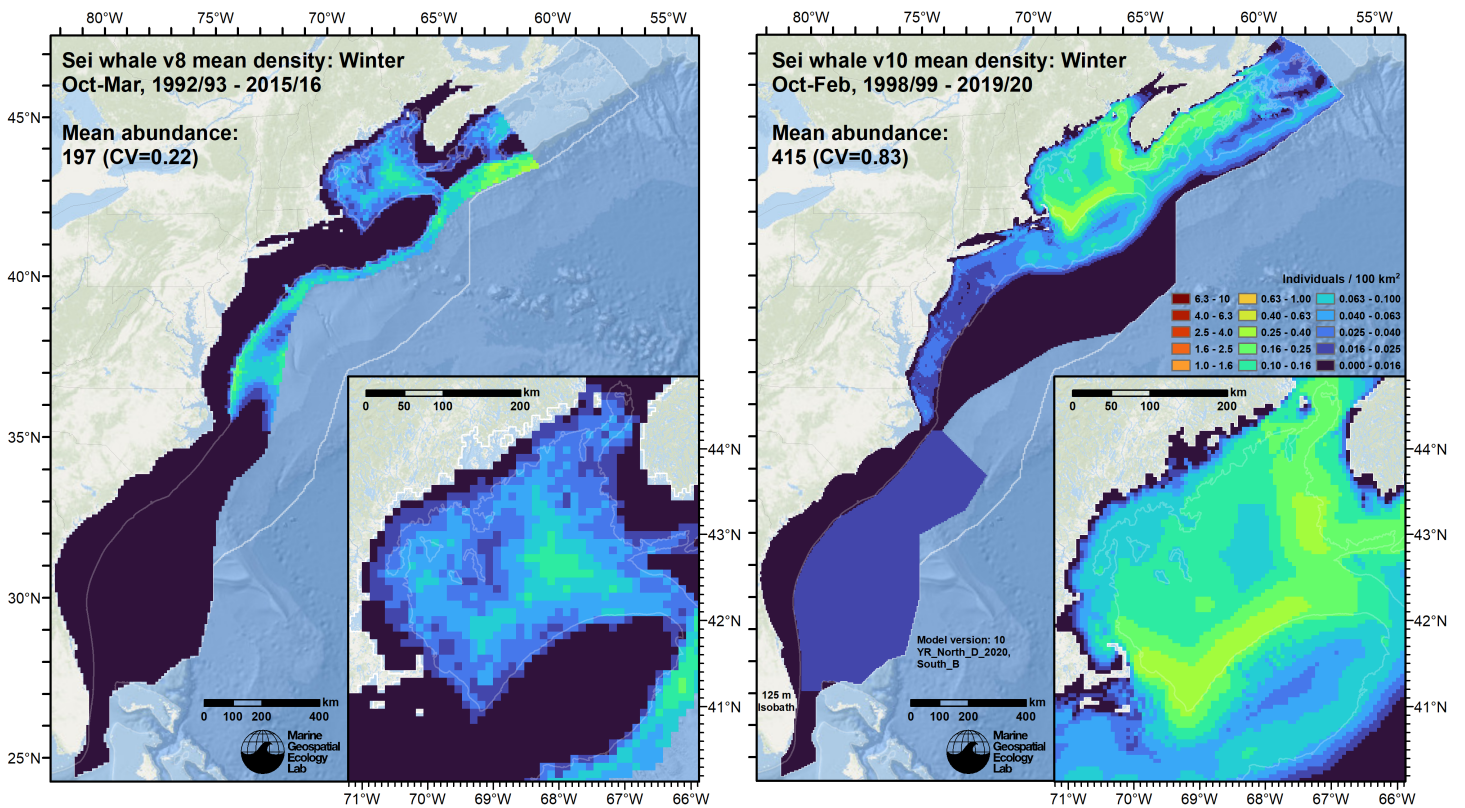


Figure 90: Comparison of the mean density predictions from the previous model (left) released by Roberts et al. (2018) to those from this model (right) for the Winter season. Note that the two models used slightly different seasonal definitions.

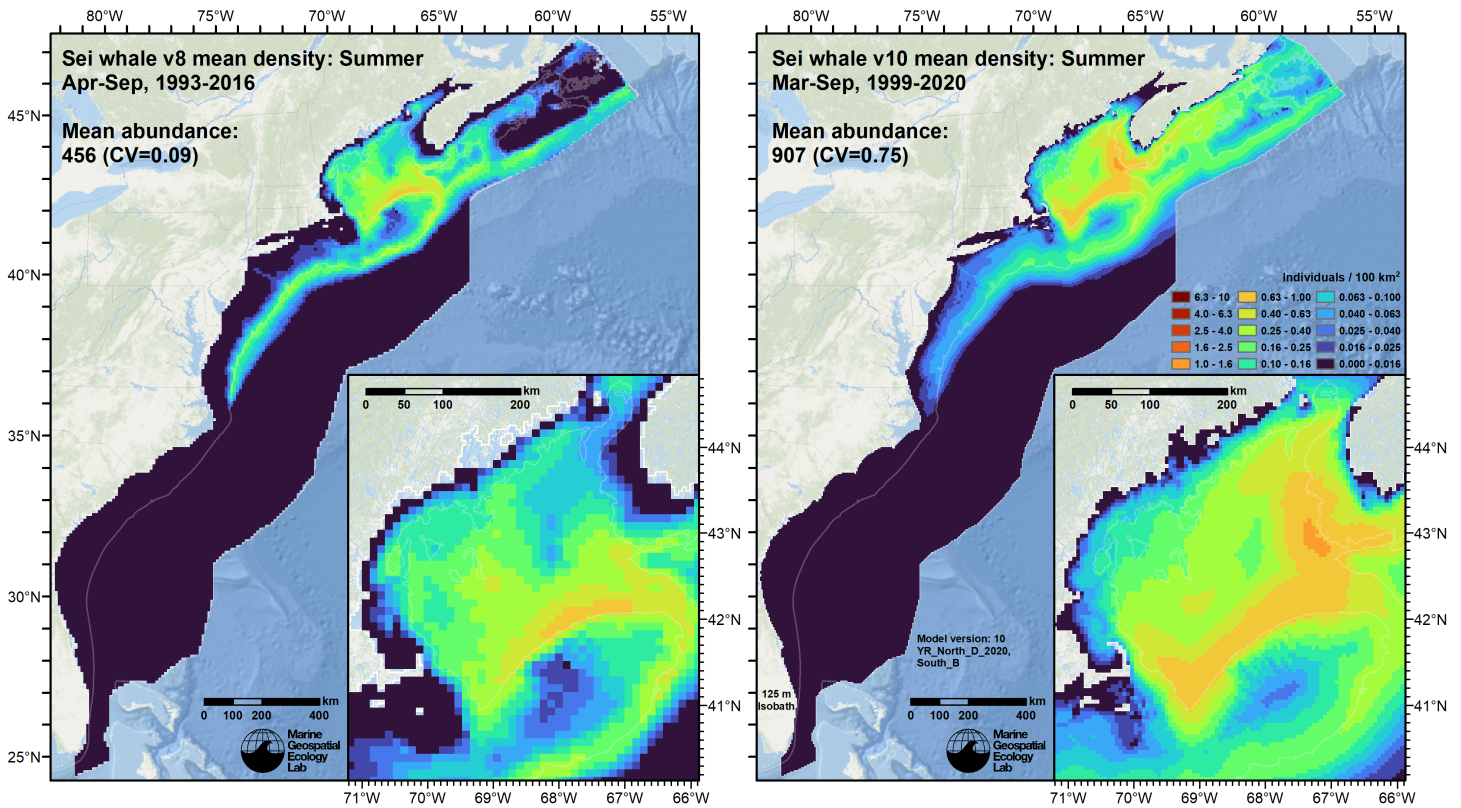


Figure 91: Comparison of the mean density predictions from the previous model (left) released by Roberts et al. (2018) to those from this model (right) for the Summer season. Note that the two models used slightly different seasonal definitions.

### 6.3 Comparison to Passive Acoustic Monitoring

To facilitate qualitative comparison of passive acoustic monitoring (PAM) detections to visual sightings and density predictions, we overlaid PAM results from Davis et al. (2020) on maps of visual segments and sightings and of density predictions. In each figure below, red circles and white dots represent PAM stations. White dots indicate that at that station, there were no days in which Davis et al. determined the species was acoustically present. Red circles indicate that the species was acoustically present, with the size of the circle indicating the percentage of days of the month it was present. The maps underlying the acoustic data are the effort segments and sightings (left side) used to fit the model, and the mean density prediction (right side), for the given month.

Note that each PAM station was usually only deployed for one of the years in the range listed. If a deployment was repeated in a subsequent year, it was treated as a separate station and allocated its own symbol. At such locations, the map may contain several different symbols, such as a white dot inside a red circle, or several red circles of different sizes, indicating interannual variability in acoustic presence at that location. Because both visual and acoustic surveys were very patchy across time, with multi-year coverage only occurring in a small number of specific areas, we urge caution in drawing firm conclusions about the species' distribution from the points and circles without considering the degree of interannual replication in coverage.

We gratefully acknowledge G. Davis and coauthors for making these data available for this comparison.

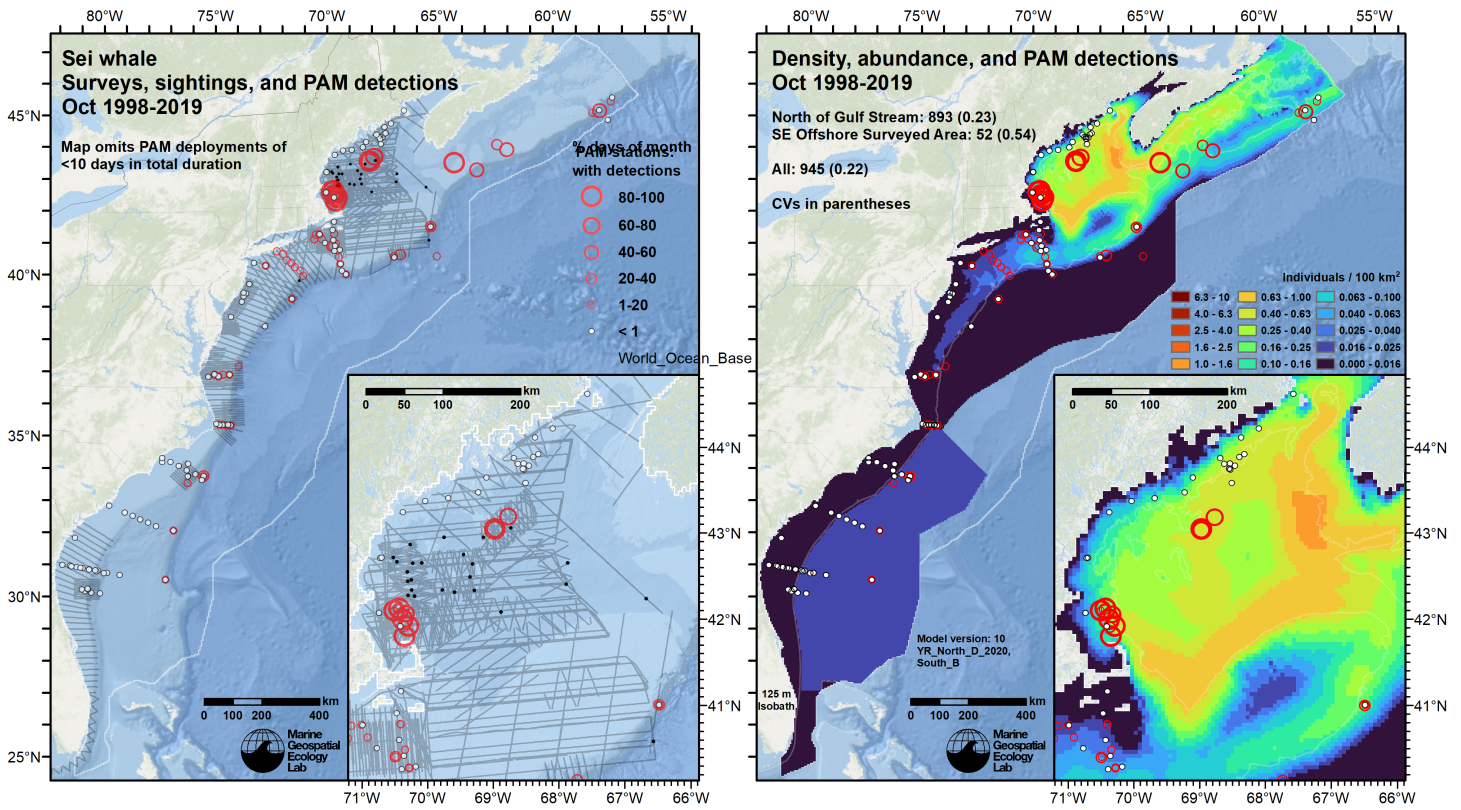


Figure 92: Passive acoustic monitoring stations (red circles and white dots) symbolized by detection rate, overlaid on visual segments and sightings (left) and predicted density (right), for the month of October for the given era.

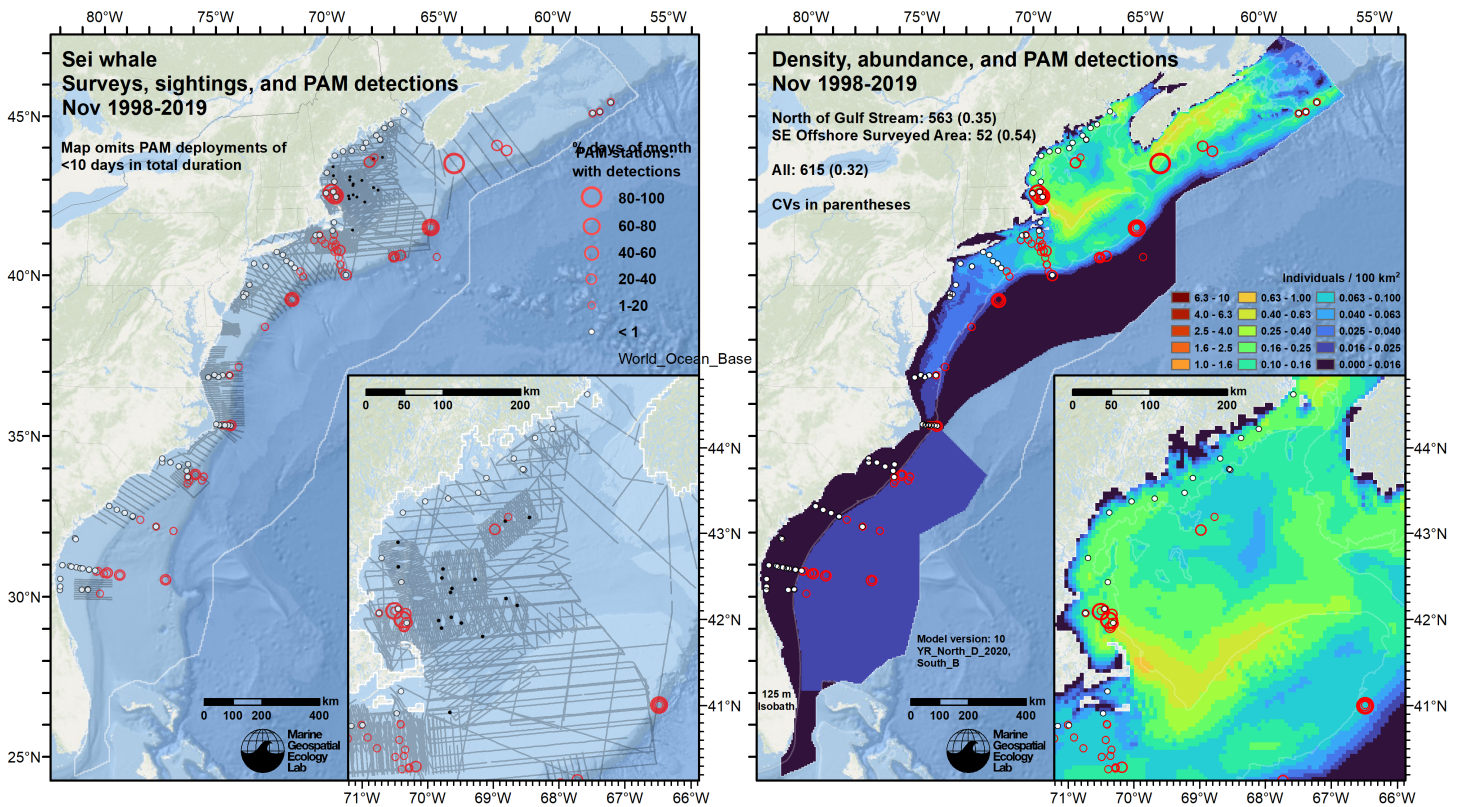


Figure 93: Passive acoustic monitoring stations (red circles and white dots) symbolized by detection rate, overlaid on visual segments and sightings (left) and predicted density (right), for the month of November for the given era.

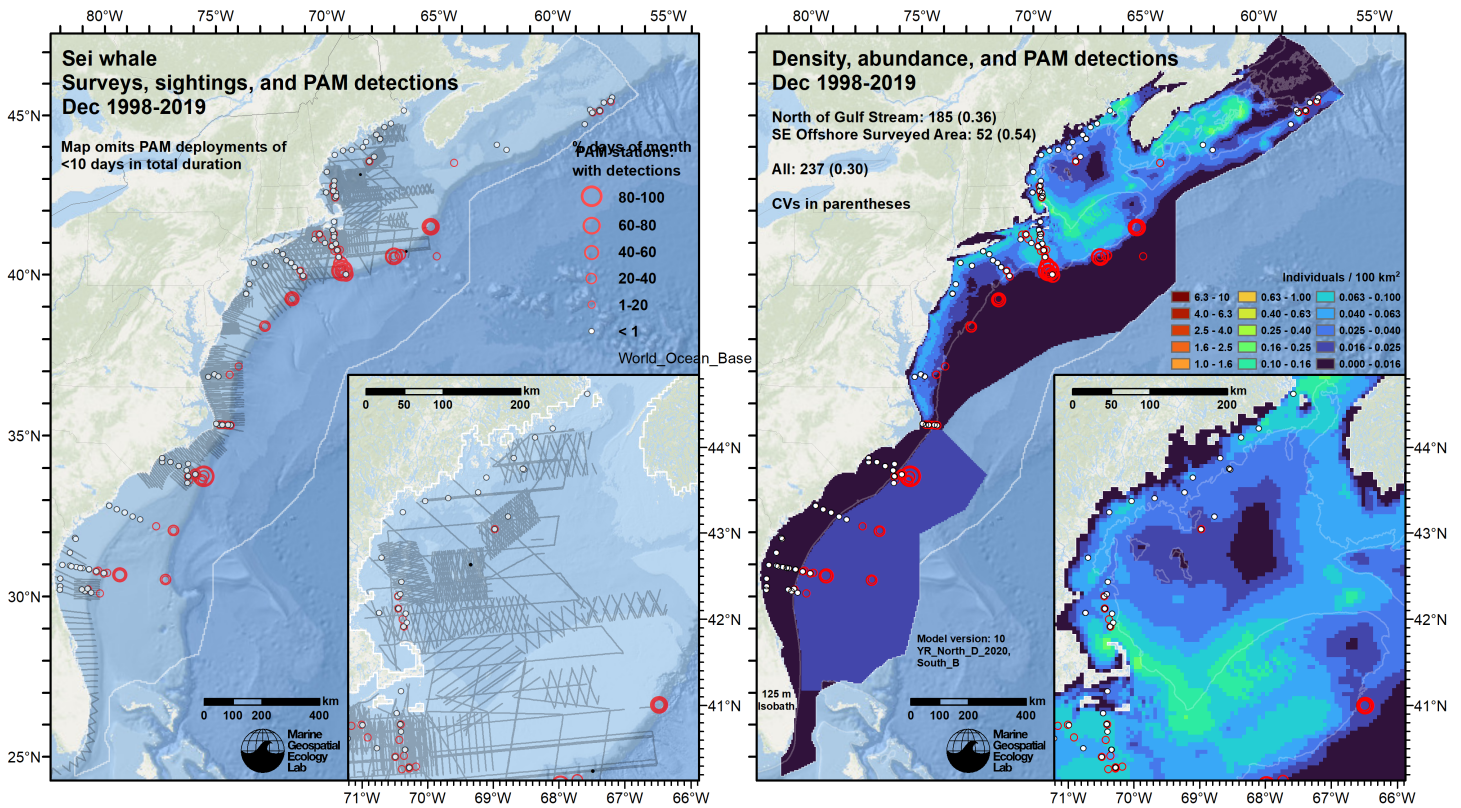


Figure 94: Passive acoustic monitoring stations (red circles and white dots) symbolized by detection rate, overlaid on visual segments and sightings (left) and predicted density (right), for the month of December for the given era.

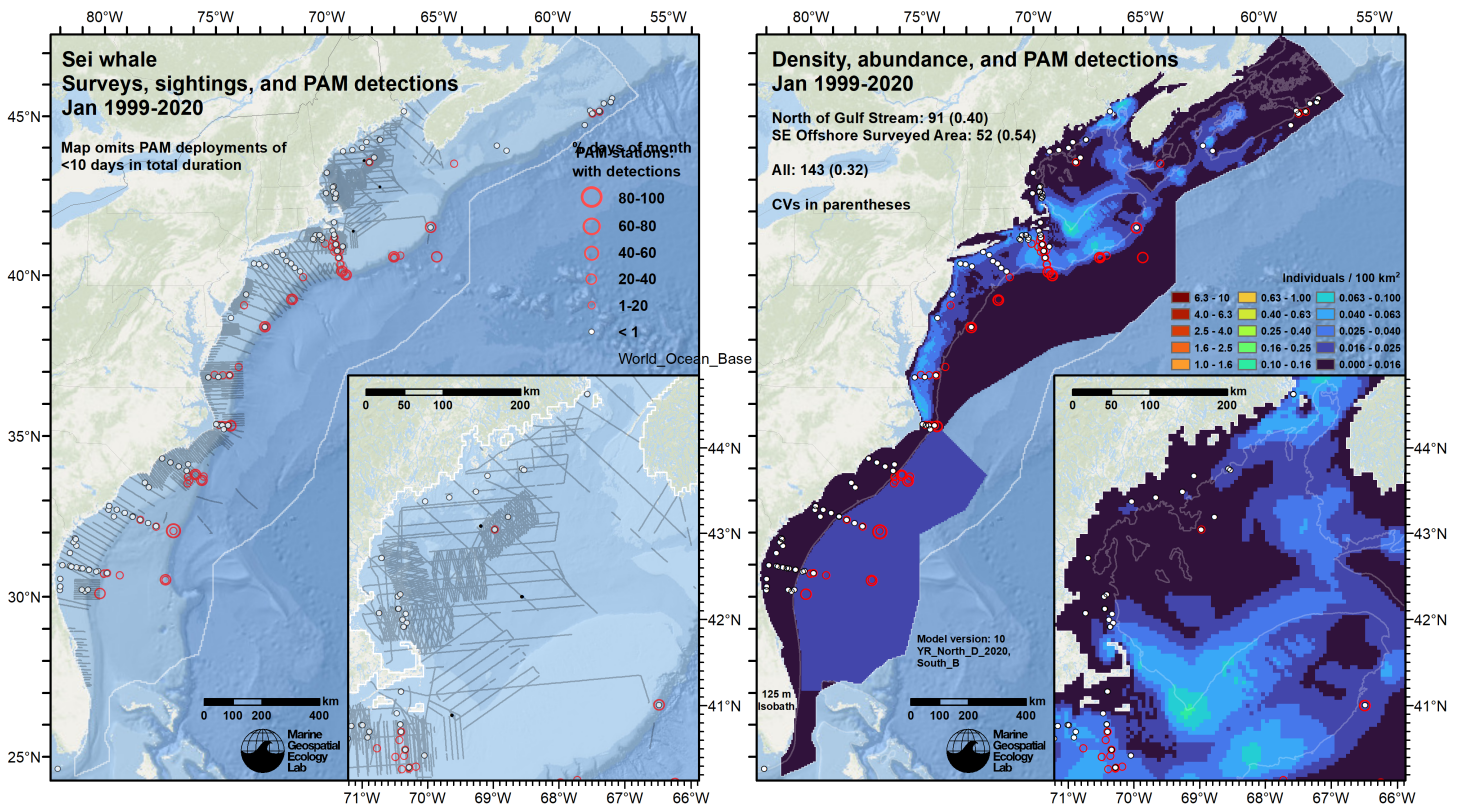


Figure 95: Passive acoustic monitoring stations (red circles and white dots) symbolized by detection rate, overlaid on visual segments and sightings (left) and predicted density (right), for the month of January for the given era.

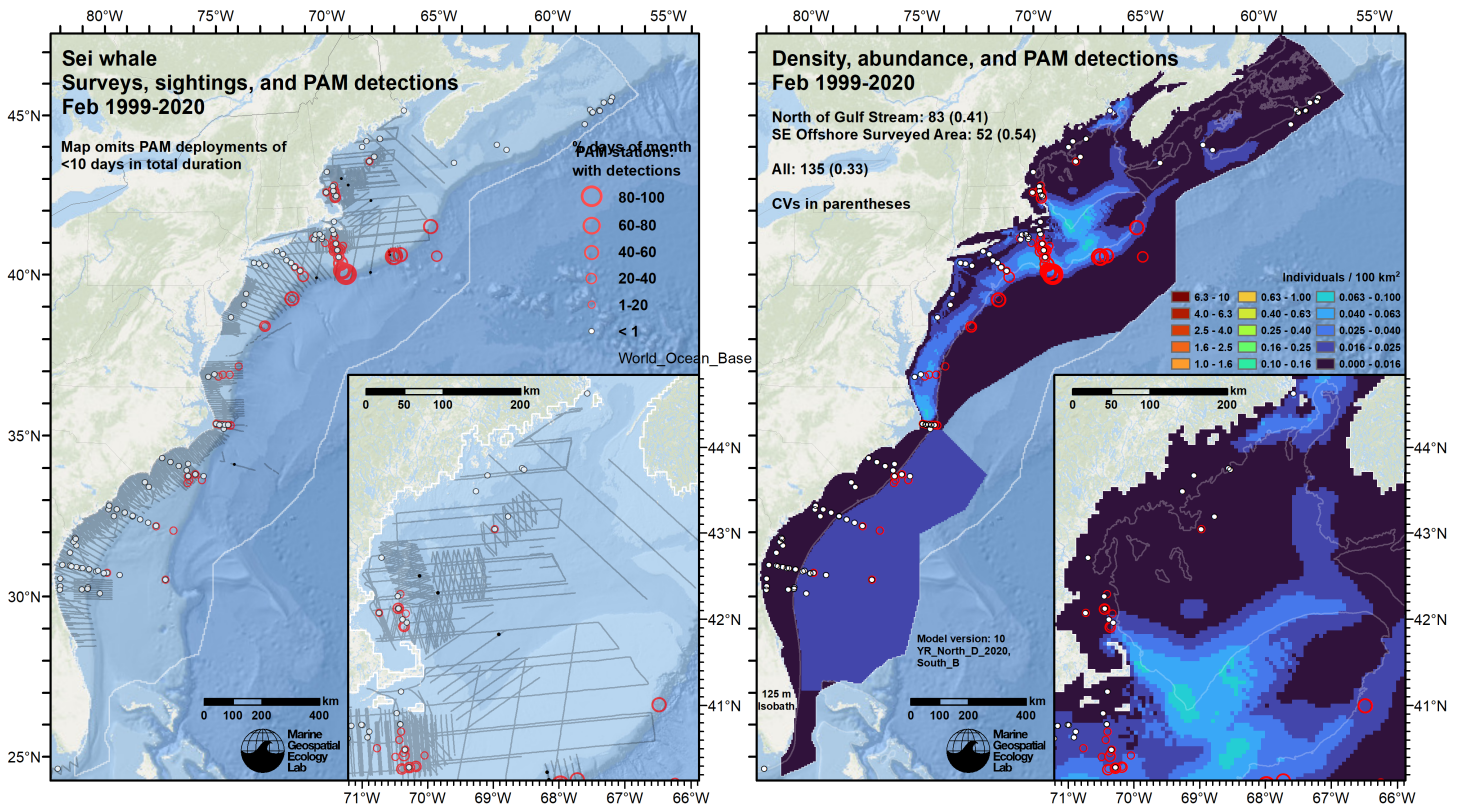


Figure 96: Passive acoustic monitoring stations (red circles and white dots) symbolized by detection rate, overlaid on visual segments and sightings (left) and predicted density (right), for the month of February for the given era.

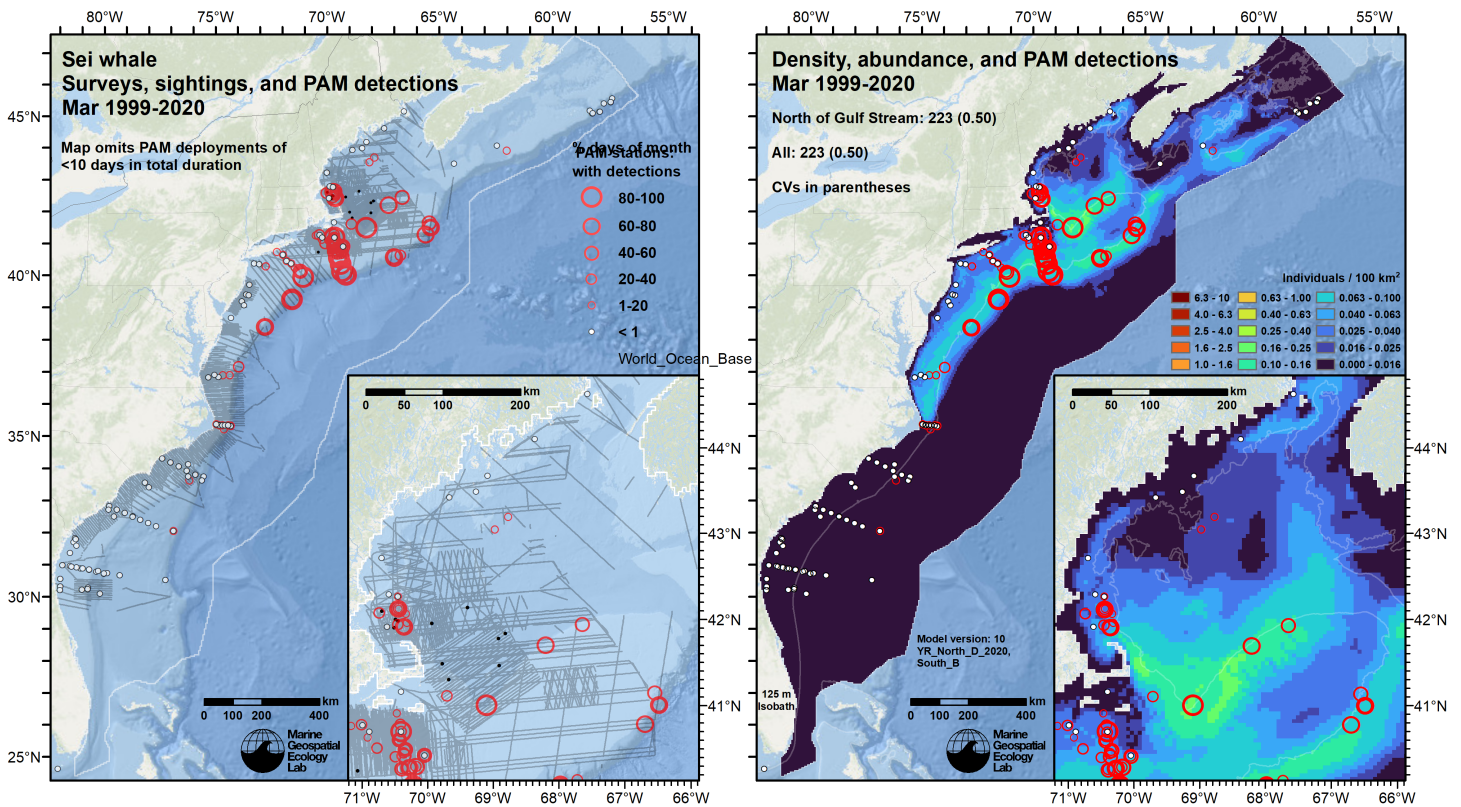


Figure 97: Passive acoustic monitoring stations (red circles and white dots) symbolized by detection rate, overlaid on visual segments and sightings (left) and predicted density (right), for the month of March for the given era.

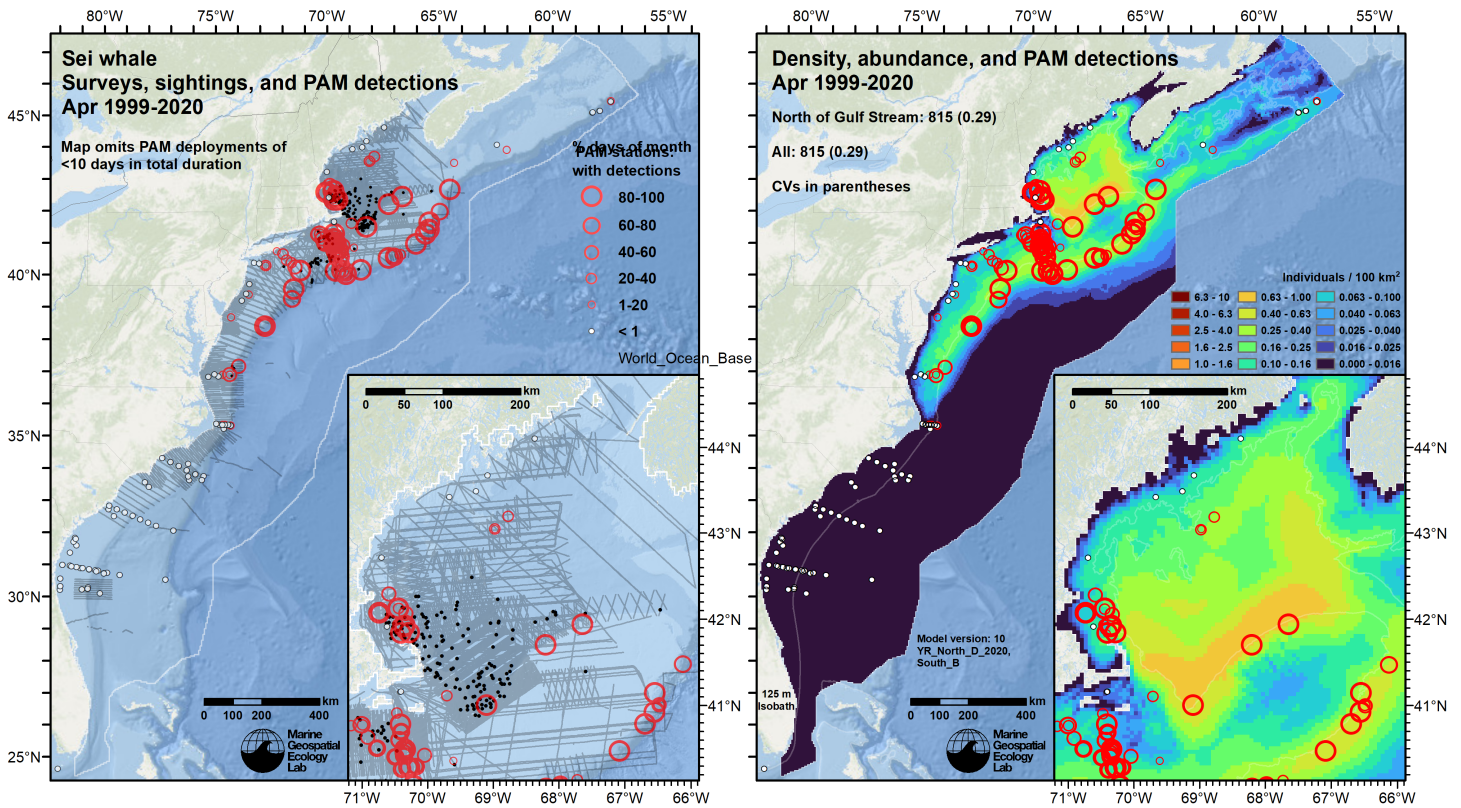


Figure 98: Passive acoustic monitoring stations (red circles and white dots) symbolized by detection rate, overlaid on visual segments and sightings (left) and predicted density (right), for the month of April for the given era.

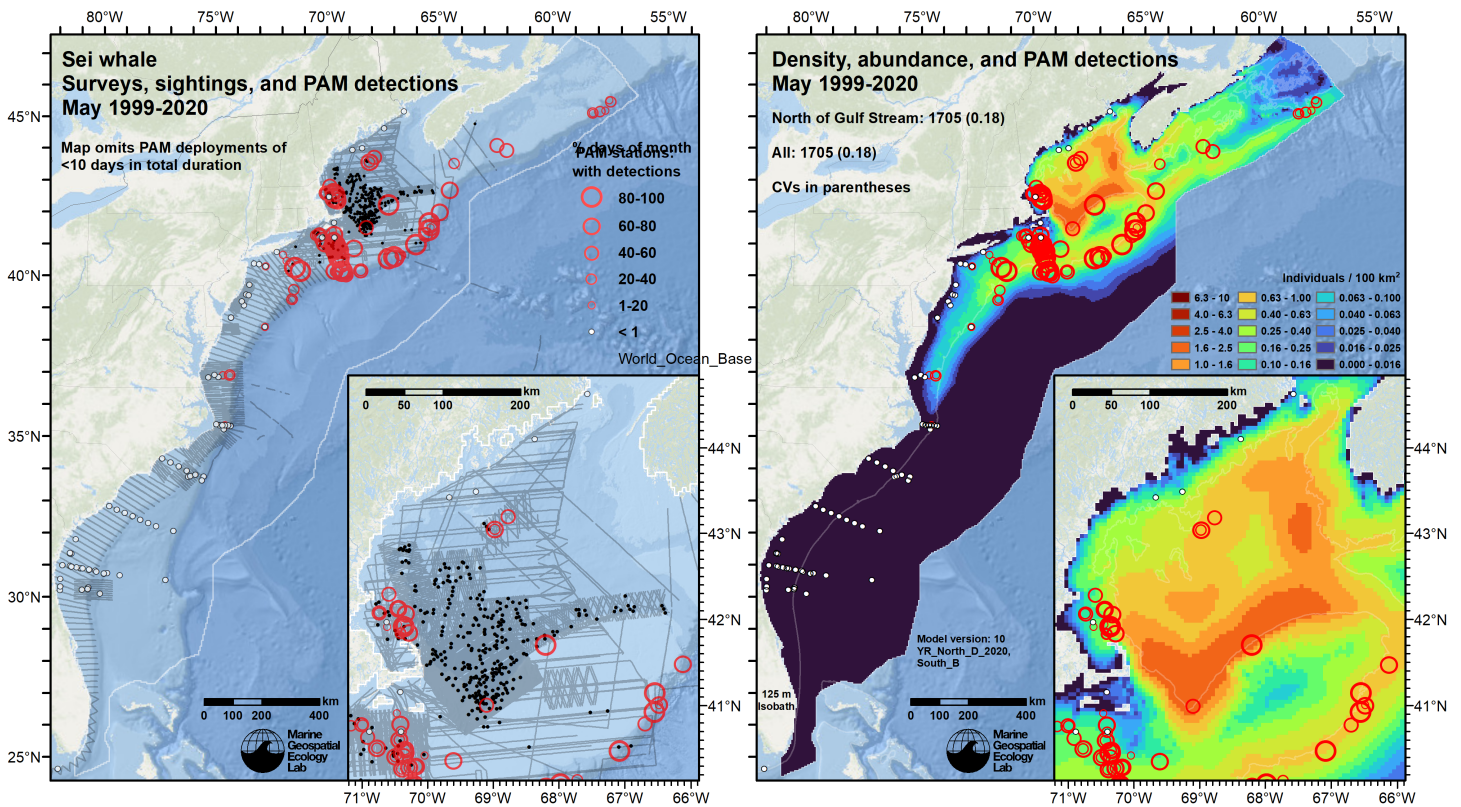


Figure 99: Passive acoustic monitoring stations (red circles and white dots) symbolized by detection rate, overlaid on visual segments and sightings (left) and predicted density (right), for the month of May for the given era.

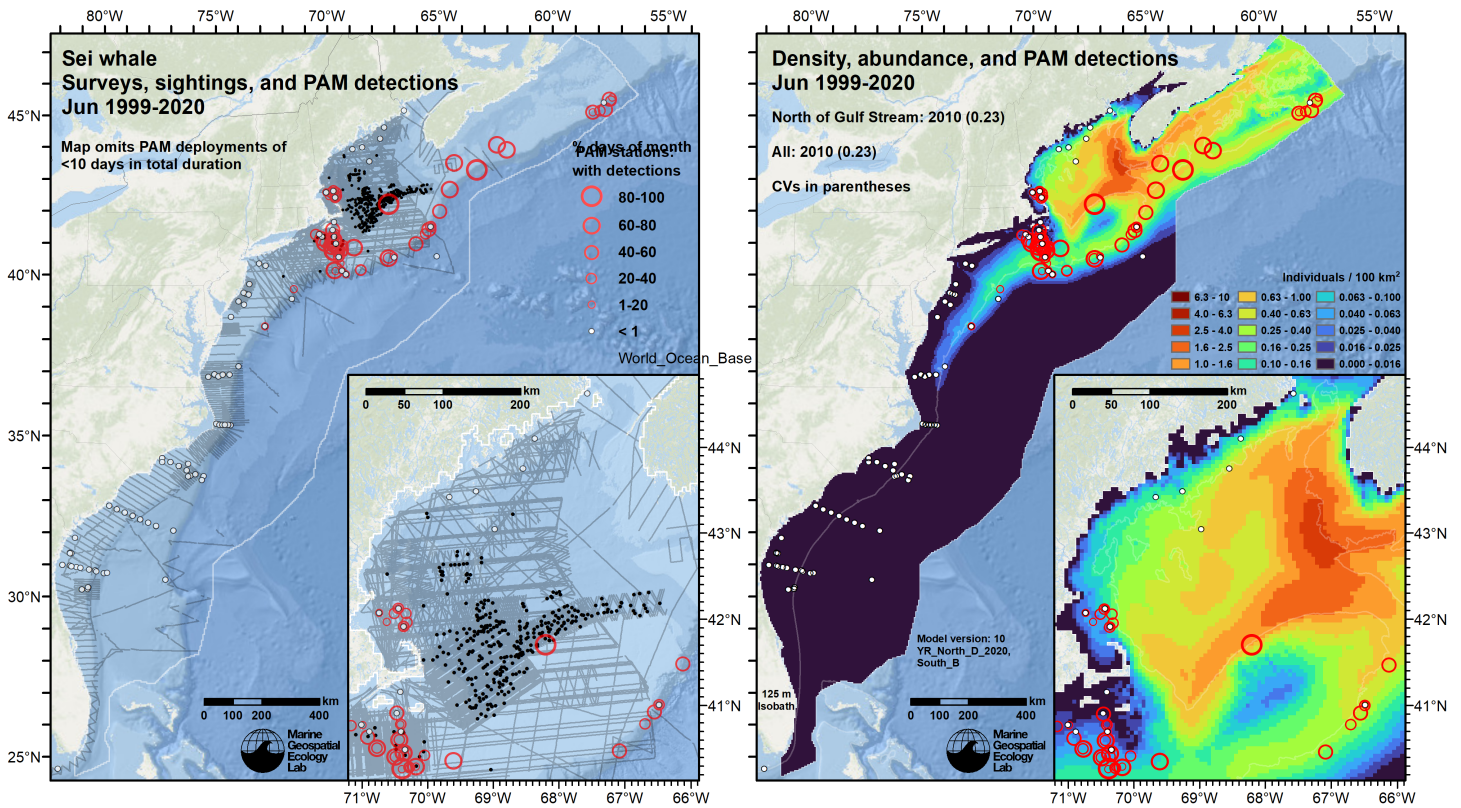


Figure 100: Passive acoustic monitoring stations (red circles and white dots) symbolized by detection rate, overlaid on visual segments and sightings (left) and predicted density (right), for the month of June for the given era.

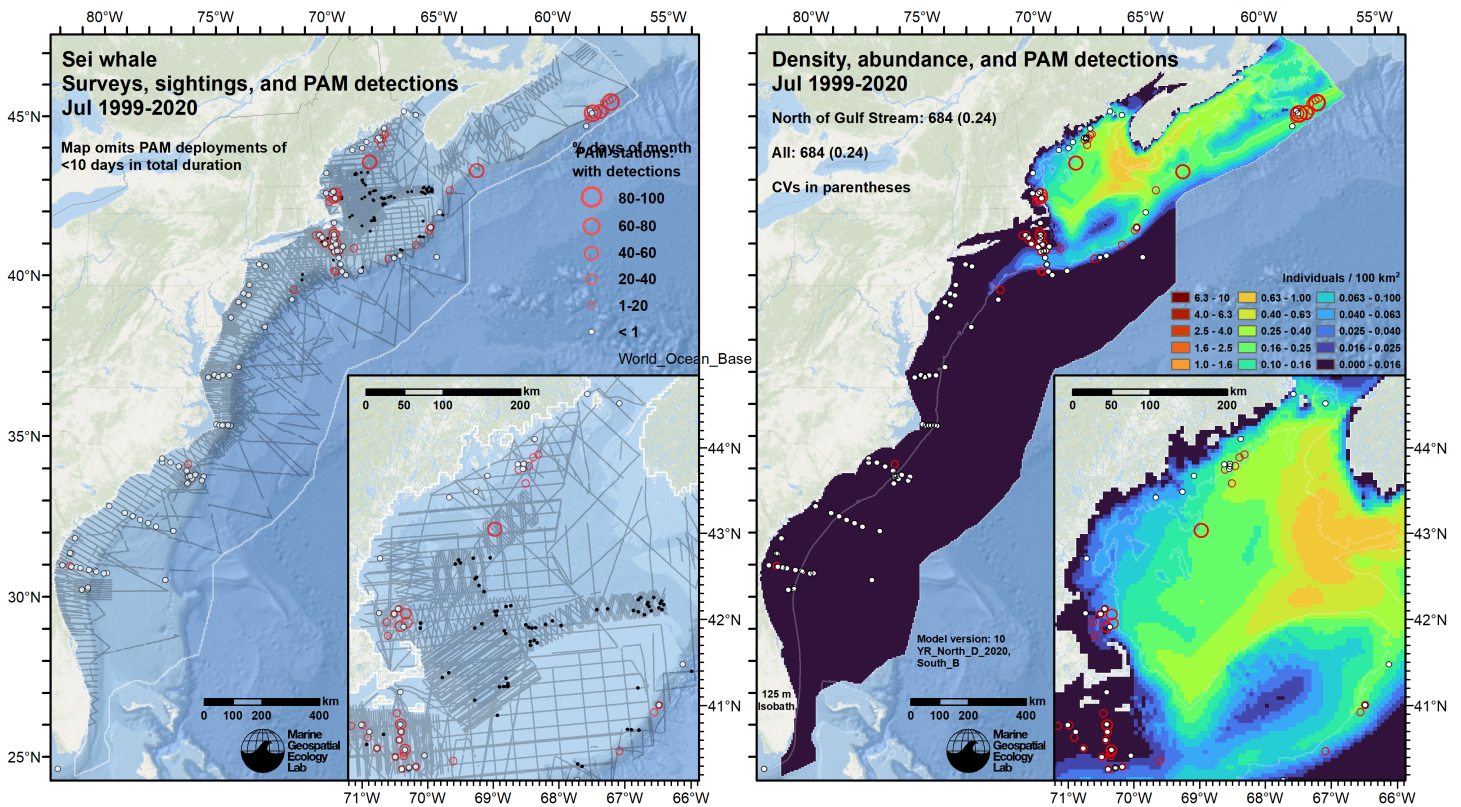


Figure 101: Passive acoustic monitoring stations (red circles and white dots) symbolized by detection rate, overlaid on visual segments and sightings (left) and predicted density (right), for the month of July for the given era.



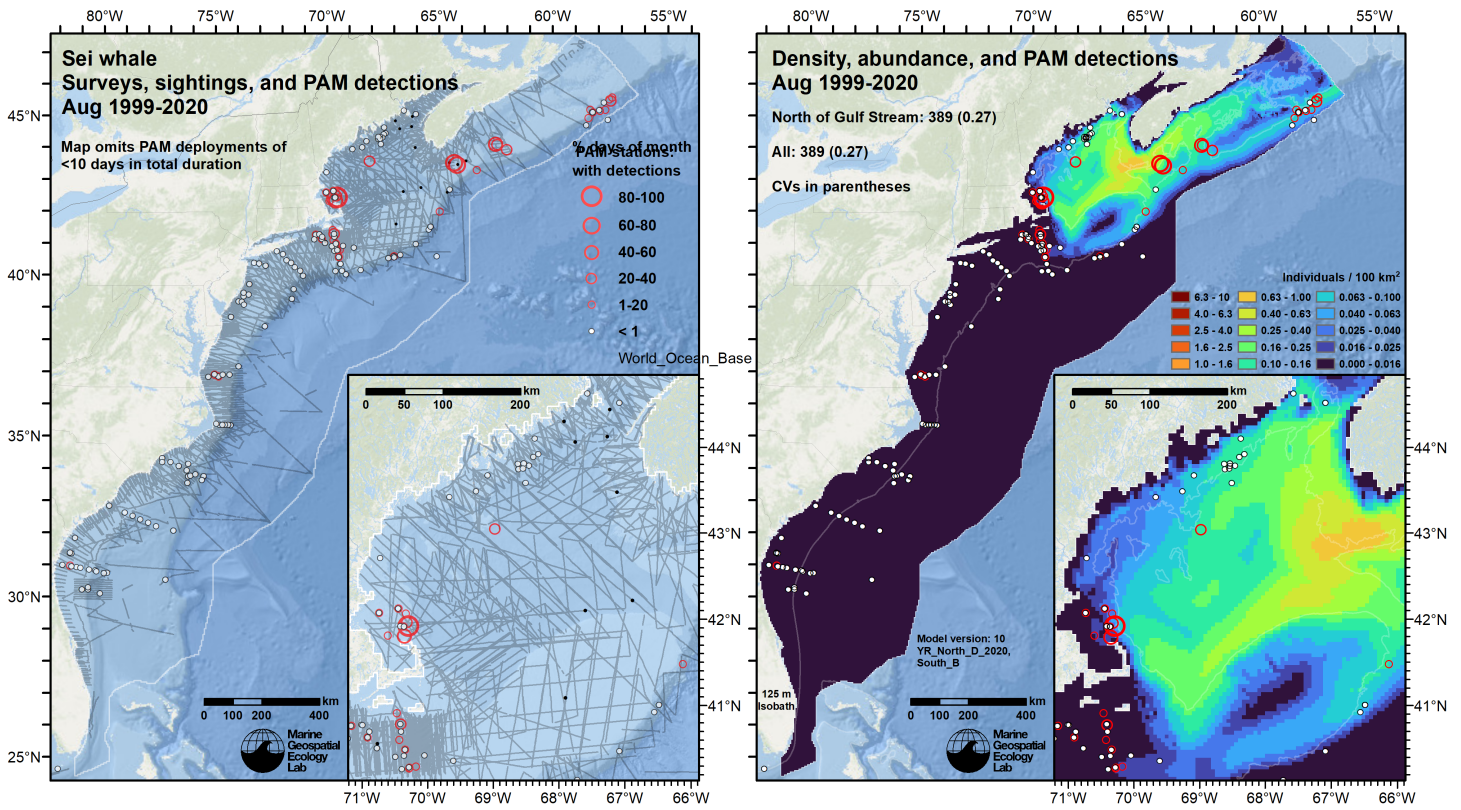


Figure 102: Passive acoustic monitoring stations (red circles and white dots) symbolized by detection rate, overlaid on visual segments and sightings (left) and predicted density (right), for the month of August for the given era.

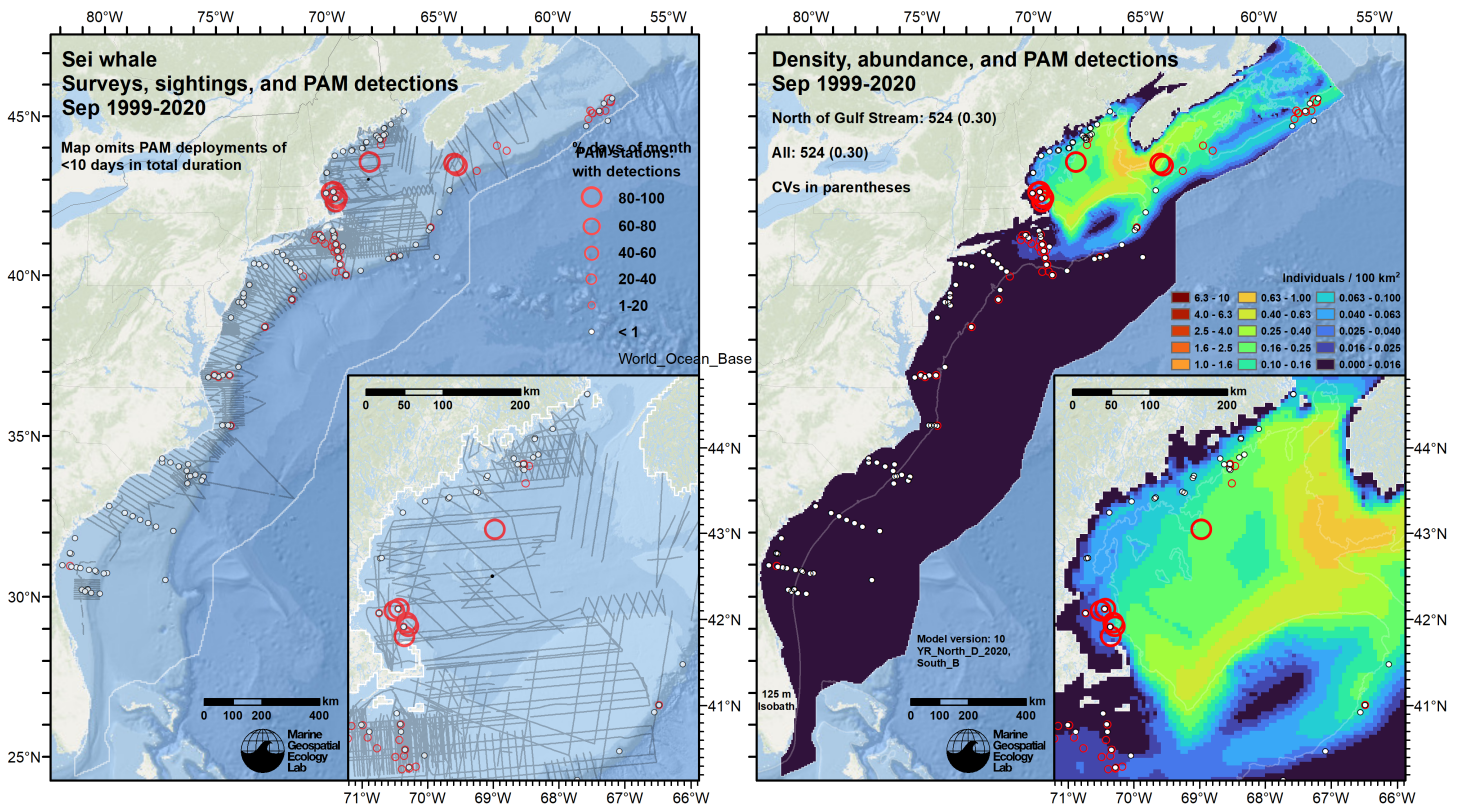


Figure 103: Passive acoustic monitoring stations (red circles and white dots) symbolized by detection rate, overlaid on visual segments and sightings (left) and predicted density (right), for the month of September for the given era.

## 7 Discussion

Comparatively little has been published about sei whales relative to other baleen whales (Prieto et al. 2012), especially regarding the details of their spatial distributions, but recent passive acoustic monitoring studies have helped fill in our understanding of their broad-scale seasonal and spatial dynamics (Davis et al. 2020; Weiss et al. 2021; Delarue et al. 2022; Kowarski et al. 2022). When summarized across the predicted period (October 1998 - September 2020), mean monthly density maps (Figures 78-89) broadly agreed with the overall spatial and seasonal patterns reported in these studies. The seasonal pattern in mean monthly abundance (Figure 77) agreed with Mitchell's (1975) report of a northward "run" of sei whales in spring and a southward "run" in fall. Given the general agreement between the model's predictions and these previous reports about the sei whale's seasonal dynamics in our study area, we elected to offer density predictions for this species at monthly temporal resolution.

Our model's estimated mean abundance for the months of March-May (859) was more than six times lower than that (6,292) of the most recent NOAA Stock Assessment Report (SAR) (Table 27). The SAR estimate was unusual in that it was based on a density surface model rather than a stratified design-based estimate traditionally used in the stock assessment process. The model was from Palka et al. (2017), who built it from the NOAA AMAPPS surveys conducted in 2010-2013. We presume the multi-year model-based estimate was used because NOAA's most recent single-year survey of the U.S. Atlantic, in 2016, was conducted in June-September, which was too far past the spring peak in sei whale abundance to sight many of them. Indeed, NOAA's design-based analysis from this survey estimated an abundance of only 52 sei whales (Palka 2020). (Note that the SAR only referenced the estimate of 28 whales for the "Shelf" stratum, while Palka (2020) also made an estimate of 24 whales for the "Gulf of Maine" stratum, yielding 52 in total. We do not know why the SAR only referenced one of the strata.)

We advise caution in utilizing the current SAR's estimate of 6,292. We believe it likely overestimates the sei whale population, at least in our study area. The model that it was taken from was built from only 22 sightings and thus exhibited a high CV (1.015) and a wide 95% confidence interval (1,209-32,733) (Palka et al. 2017 Appendix I, Tables 4-1 and 4-5). Chavez-Rosales et al. (2019) analyzed the same surveys with an updated methodology and estimated a lower March-May abundance of 4,500 (CV=0.42; 95% CI=2,042-9,915). Finally, Palka et al. (2021) expanded the analysis to the AMAPPS surveys of 2010-2017. These surveys recorded 74 sightings, included additional springtime effort, and yielded a March-May abundance estimate for 2010-2013 of 243 (CV=0.45; 95% CI=105-564), for 2014-2017 of 43 (CV=0.47; 95% CI=18-103), and for the full 2010-2017 period of 142 (CV=0.47; 95% CI=60-335).

The considerable variability in NOAA's model-based abundance estimates highlights the difficulty of modeling sei whales. In addition to the problems of handling ambiguous "fin or sei whale" sightings (Section 2) and strong seasonal variability (Figure 77), sei whales have previously been noted as exhibiting strong interannual fluctuations in distribution (Payne et al. 1990; Schilling et al. 1992; Kenney et al. 1996). Also, as a zooplanktivore that feeds on the same species (*Calanus finmarchicus*) as the North Atlantic right whale (Kenney et al. 1996; Baumgartner et al. 2011), it is possible that the sei whale has been affected by the same shifts in zooplankton distributions that appear to have strongly affected the right whale (Record et al. 2019; Meyer-Gutbrod et al. 2021; Meyer-Gutbrod et al. 2022).

A similar large difference in abundance estimates can be seen between this model and our prior model. In "Summer" months, this model's mean abundance (907, CV=0.75) was about twice that (456, CV=0.09) of our prior model (Figure 91). A similar overall pattern in density was predicted, with generally higher density everywhere but particularly in Canadian waters. CV was substantially higher for this model than our prior model because this model accounted both for seasonal and interannual variations in density predictions as well as uncertainty in model parameter estimates, while the prior model's CV only accounted for uncertainty in model parameter estimates. Given the strong rise in sei whale density from March-June and fall from June-September, the high CV of the new model for this March-September mean is appropriate. Monthly means, which did not suffer from seasonal variability but still accounted for interannual variability and model parameter uncertainty, showed lower CVs (Figures 83-89).

In "Winter" months, this model's mean abundance (415, CV=0.83) was also about twice that (197, CV=0.22) of our prior model, but also yielded important spatial differences in density (Figure 90). The new model predicted generally higher density in the Gulf of Maine and along the Scotian Shelf. While the prior model predicted moderate densities beyond the continental shelf break north of Cape Hatteras and near-zero density south of it, this model predicted the opposite. The new prediction south of Cape Hatteras is supported by acoustic monitoring, but north of Cape Hatteras the agreement is less certain. The new model does predict low to moderate density along the shelf break, but near zero density beyond it (Figures 92-96). A bottom-mounted recorder placed ~30 km north of Retriever Seamount at a depth of 3500 m recorded regular detections from October 29, 2014 through February 19, 2015 (PACM 2022). Additional visual surveying and acoustic monitoring is needed in deep waters north of Cape Hatteras to clarify sei whale density and presence there. The new model also predicted low densities north of Cape Hatteras on the shelf up through Georges Bank, while the prior model predicted near-zero density in these regions. The new model's prediction of some sei whales in these areas is supported by acoustic detections.

## References

- Barco SG, Burt L, DePerte A, Digiovanni R Jr. (2015) Marine Mammal and Sea Turtle Sightings in the Vicinity of the Maryland Wind Energy Area July 2013-June 2015, VAQF Scientific Report #2015-06. Virginia Aquarium & Marine Science Center Foundation, Virginia Beach, VA
- Baumgartner MF, Lysiak NS, Schuman C, Urban-Rich J, Wenzel FW (2011) Diel vertical migration behavior of *Calanus finmarchicus* and its influence on right and sei whale occurrence. *Marine Ecology Progress Series* 423:167–184. doi: [10.3354/meps08931](https://doi.org/10.3354/meps08931)
- Becker JJ, Sandwell DT, Smith WHF, Braud J, Binder B, Depner J, Fabre D, Factor J, Ingalls S, Kim S-H, Ladner R, Marks K, Nelson S, Pharaoh A, Trimmer R, Von Rosenberg J, Wallace G, Weatherall P (2009) Global Bathymetry and Elevation Data at 30 Arc Seconds Resolution: SRTM30\_PLUS. *Marine Geodesy* 32:355–371. doi: [10.1080/01490410903297766](https://doi.org/10.1080/01490410903297766)
- Behrenfeld MJ, Falkowski PG (1997) Photosynthetic rates derived from satellite-based chlorophyll concentration. *Limnology and oceanography* 42:1–20. doi: [10.4319/lo.1997.42.1.0001](https://doi.org/10.4319/lo.1997.42.1.0001)
- Brasnett B (2008) The impact of satellite retrievals in a global sea-surface-temperature analysis. *Quarterly Journal of the Royal Meteorological Society* 134:1745–1760. doi: [10.1002/qj.319](https://doi.org/10.1002/qj.319)
- Breiman L (2001) Random Forests. *Machine Learning* 45:5–32. doi: [10.1023/A:1010933404324](https://doi.org/10.1023/A:1010933404324)
- Buckland ST, Anderson DR, Burnham KP, Laake JL, Borchers DL, Thomas L (2001) *Introduction to Distance Sampling: Estimating Abundance of Biological Populations*. Oxford University Press, Oxford, UK
- Burt ML, Borchers DL, Jenkins KJ, Marques TA (2014) Using mark-recapture distance sampling methods on line transect surveys. *Methods in Ecology and Evolution* 5:1180–1191. doi: [10.1111/2041-210X.12294](https://doi.org/10.1111/2041-210X.12294)
- Canada Meteorological Center (2012) GHRSSST Level 4 CMC0.2deg Global Foundation Sea Surface Temperature Analysis Version 2.0. PODAAC, CA, USA. doi: [10.5067/GHCCMC-4FM02](https://doi.org/10.5067/GHCCMC-4FM02)
- Canada Meteorological Center (2016) GHRSSST Level 4 CMC0.1deg Global Foundation Sea Surface Temperature Analysis Version 3.0. PODAAC, CA, USA. doi: [10.5067/GHCCMC-4FM03](https://doi.org/10.5067/GHCCMC-4FM03)
- Cañadas A, Roberts JJ, Yack TM, Halpin PN (2021) Development of Exploratory Marine Species Density Models in the NAVEUR/C6F Study Area. Report prepared for Naval Facilities Engineering Command, Atlantic under Contract No. N62470-15-D-8006, Task Order 18F4048. Duke University Marine Geospatial Ecology Lab, Durham, NC
- Canny JF (1986) A computational approach to edge detection. *IEEE Transactions on Pattern Analysis and Machine Intelligence* 8:679–698. doi: [10.1016/B978-0-08-051581-6.50024-6](https://doi.org/10.1016/B978-0-08-051581-6.50024-6)
- Chassignet E, Hurlburt H, Metzger EJ, Smedstad O, Cummings J, Halliwell G, Bleck R, Baraille R, Wallcraft A, Lozano C, Tolman H, Srinivasan A, Hankin S, Cornillon P, Weisberg R, Barth A, He R, Werner F, Wilkin J (2009) US GODAE: Global Ocean Prediction with the HYbrid Coordinate Ocean Model (HYCOM). *Oceanog* 22:64–75. doi: [10.5670/oceanog.2009.39](https://doi.org/10.5670/oceanog.2009.39)
- Chavez-Rosales S, Palka DL, Garrison LP, Josephson EA (2019) Environmental predictors of habitat suitability and occurrence of cetaceans in the western North Atlantic Ocean. *Scientific Reports* 9:5833. doi: [10.1038/s41598-019-42288-6](https://doi.org/10.1038/s41598-019-42288-6)
- Cole T, Gerrior P, Merrick RL (2007) [Methodologies of the NOAA National Marine Fisheries Service Aerial Survey Program for Right Whales \(\*Eubalaena glacialis\*\) in the Northeast U.S., 1998-2006](#). U.S. Department of Commerce, Woods Hole, MA
- Cotter MP (2019) *Aerial Surveys for Protected Marine Species in the Norfolk Canyon Region: 2018–2019 Final Report*. HDR, Inc., Virginia Beach, VA
- Davis GE, Baumgartner MF, Corkeron PJ, Bell J, Berchok C, Bonnell JM, Bort Thornton J, Brault S, Buchanan GA, Cholewiak DM, Clark CW, Delarue J, Hatch LT, Klinck H, Kraus SD, Martin B, Mellinger DK, Moors-Murphy H, Nieu Kirk S, Nowacek DP, Parks SE, Parry D, Pegg N, Read AJ, Rice AN, Risch D, Scott A, Soldevilla MS, Stafford KM, Stanistreet JE, Summers E, Todd S, Van Parijs SM (2020) Exploring movement patterns and changing distributions of baleen whales in the western North Atlantic using a decade of passive acoustic data. *Glob Change Biol* gcb.15191. doi: [10.1111/gcb.15191](https://doi.org/10.1111/gcb.15191)
- Delarue JJ-Y, Moors-Murphy H, Kowarski KA, Davis GE, Urazghildiiev IR, Martin SB (2022) Acoustic occurrence of baleen whales, particularly blue, fin, and humpback whales, off eastern Canada, 2015–2017. *Endang Species Res* 47:265–289. doi: [10.3354/esr01176](https://doi.org/10.3354/esr01176)
- Foley HJ, Paxton CGM, McAlarney RJ, Pabst DA, Read AJ (2019) Occurrence, Distribution, and Density of Protected Species in the Jacksonville, Florida, Atlantic Fleet Training and Testing (AFTT) Study Area. Duke University Marine Lab, Beaufort, NC

- Garnesson P, Mangin A, Fanton d'Andon O, Demaria J, Bretagnon M (2019) The CMEMS GlobColour chlorophyll *a* product based on satellite observation: Multi-sensor merging and flagging strategies. *Ocean Science* 15:819–830. doi: [10.5194/os-15-819-2019](https://doi.org/10.5194/os-15-819-2019)
- Garrison LP, Martinez A, Maze-Foley K (2010) [Habitat and abundance of cetaceans in Atlantic Ocean continental slope waters off the eastern USA](#). *Journal of Cetacean Research and Management* 11:267–277.
- Geo-Marine, Inc. (2010) [New Jersey Department of Environmental Protection Baseline Studies Final Report Volume III: Marine Mammal and Sea Turtle Studies](#). Geo-Marine, Inc., Plano, TX
- Halpin P, Read A, Fujioka E, Best B, Donnelly B, Hazen L, Kot C, Urian K, LaBrecque E, Dimatteo A, Cleary J, Good C, Crowder L, Hyrenbach KD (2009) OBIS-SEAMAP: The World Data Center for Marine Mammal, Sea Bird, and Sea Turtle Distributions. *Oceanography* 22:104–115. doi: [10.5670/oceanog.2009.42](https://doi.org/10.5670/oceanog.2009.42)
- Hayes SA, Josephson E, Maze-Foley K, Rosel PE, Wallace J, Brossard A, Chavez-Rosales S, Cole TVN, Garrison LP, Hatch J, Henry A, Horstman SC, Litz J, Lyssikatos MC, Mullin KD, Murray K, Orphanides C, Ortega-Ortiz J, Pace RM, Palka DL, Powell J, Rappucci G, Soldevilla M, Wenzel FW (2022) [US Atlantic and Gulf of Mexico Marine Mammal Stock Assessments 2021](#). NOAA National Marine Fisheries Service, Northeast Fisheries Science Center, Woods Hole, MA
- Hothorn T, Hornik K, Zeileis A (2006) Unbiased Recursive Partitioning: A Conditional Inference Framework. *Journal of Computational and Graphical Statistics* 15:651–674. doi: [10.1198/106186006X133933](https://doi.org/10.1198/106186006X133933)
- Huijser LAE, Bérubé M, Cabrera AA, Prieto R, Silva MA, Robbins J, Kanda N, Pastene LA, Goto M, Yoshida H, Víkingsson GA, Palsbøll PJ (2018) Population structure of North Atlantic and North Pacific sei whales (*Balaenoptera borealis*) inferred from mitochondrial control region DNA sequences and microsatellite genotypes. *Conserv Genet* 19:1007–1024. doi: [10.1007/s10592-018-1076-5](https://doi.org/10.1007/s10592-018-1076-5)
- Kenney RD, Payne PM, Heinemann DW, Winn HE (1996) Shifts in Northeast shelf cetacean distributions relative to trends in Gulf of Maine/Georges Bank finfish abundance. In: *The Northeast Shelf Ecosystem: Assessment, Sustainability, and Management*. Blackwell Science, Cambridge, MA, pp 169–196
- Kowarski KA, Martin SB, Maxner EE, Lawrence CB, Delarue JJ-Y, Miksis-Olds JL (2022) Cetacean acoustic occurrence on the US Atlantic Outer Continental Shelf from 2017 to 2020. *Marine Mammal Science* mms.12962. doi: [10.1111/mms.12962](https://doi.org/10.1111/mms.12962)
- Laake JL, Calambokidis J, Osmek SD, Rugh DJ (1997) Probability of Detecting Harbor Porpoise From Aerial Surveys: Estimating  $g(0)$ . *Journal of Wildlife Management* 61:63–75. doi: [10.2307/3802415](https://doi.org/10.2307/3802415)
- Lehodey P, Senina I, Murtugudde R (2008) A spatial ecosystem and populations dynamics model (SEAPODYM)—Modeling of tuna and tuna-like populations. *Progress in Oceanography* 78:304–318. doi: [10.1016/j.pocean.2008.06.004](https://doi.org/10.1016/j.pocean.2008.06.004)
- Lehodey P, Conchon A, Senina I, Domokos R, Calmettes B, Jouanno J, Hernandez O, Kloster R (2015) Optimization of a micronekton model with acoustic data. *ICES Journal of Marine Science* 72:1399–1412. doi: [10.1093/icesjms/fsu233](https://doi.org/10.1093/icesjms/fsu233)
- Leiter S, Stone K, Thompson J, Accardo C, Wikgren B, Zani M, Cole T, Kenney R, Mayo C, Kraus S (2017) North Atlantic right whale *Eubalaena glacialis* occurrence in offshore wind energy areas near Massachusetts and Rhode Island, USA. *Endang Species Res* 34:45–59. doi: [10.3354/esr00827](https://doi.org/10.3354/esr00827)
- Mallette SD, Lockhart GG, McAlarney RJ, Cummings EW, McLellan WA, Pabst DA, Barco SG (2014) Documenting Whale Migration off Virginia's Coast for Use in Marine Spatial Planning: Aerial and Vessel Surveys in the Proximity of the Virginia Wind Energy Area (VA WEA), VAQF Scientific Report 2014-08. Virginia Aquarium & Marine Science Center Foundation, Virginia Beach, VA
- Mallette SD, Lockhart GG, McAlarney RJ, Cummings EW, McLellan WA, Pabst DA, Barco SG (2015) Documenting Whale Migration off Virginia's Coast for Use in Marine Spatial Planning: Aerial Surveys in the Proximity of the Virginia Wind Energy Area (VA WEA) Survey/Reporting Period: May 2014 - December 2014, VAQF Scientific Report 2015-02. Virginia Aquarium & Marine Science Center Foundation, Virginia Beach, VA
- Mallette SD, McAlarney RJ, Lockhart GG, Cummings EW, Pabst DA, McLellan WA, Barco SG (2017) [Aerial Survey Baseline Monitoring in the Continental Shelf Region of the VACAPES OPAREA: 2016 Annual Progress Report](#). Virginia Aquarium & Marine Science Center Foundation, Virginia Beach, VA
- Marsh H, Sinclair DF (1989) Correcting for Visibility Bias in Strip Transect Aerial Surveys of Aquatic Fauna. *The Journal of Wildlife Management* 53:1017. doi: [10.2307/3809604](https://doi.org/10.2307/3809604)
- McAlarney R, Cummings E, McLellan W, Pabst A (2018) Aerial Surveys for Protected Marine Species in the Norfolk Canyon Region: 2017 Annual Progress Report. University of North Carolina Wilmington, Wilmington, NC
- McLellan WA, McAlarney RJ, Cummings EW, Read AJ, Paxton CGM, Bell JT, Pabst DA (2018) Distribution and abundance of beaked whales (Family Ziphiidae) Off Cape Hatteras, North Carolina, U.S.A. *Marine Mammal Science*. doi: [10.1111/mms.12500](https://doi.org/10.1111/mms.12500)

- Meissner T, Wentz FJ, Scott J, Vazquez-Cuervo J (2016) Sensitivity of Ocean Surface Salinity Measurements From Spaceborne L-Band Radiometers to Ancillary Sea Surface Temperature. *IEEE Trans Geosci Remote Sensing* 54:7105–7111. doi: [10.1109/TGRS.2016.2596100](https://doi.org/10.1109/TGRS.2016.2596100)
- Mesgaran MB, Cousens RD, Webber BL (2014) Here be dragons: A tool for quantifying novelty due to covariate range and correlation change when projecting species distribution models. *Diversity Distrib* 20:1147–1159. doi: [10.1111/ddi.12209](https://doi.org/10.1111/ddi.12209)
- Meyer-Gutbrod E, Greene C, Davies K, Johns D (2021) Ocean Regime Shift is Driving Collapse of the North Atlantic Right Whale Population. *Oceanog* 34:22–31. doi: [10.5670/oceanog.2021.308](https://doi.org/10.5670/oceanog.2021.308)
- Meyer-Gutbrod EL, Davies KTA, Johnson CL, Plourde S, Sorochan KA, Kenney RD, Ramp C, Gosselin J, Lawson JW, Greene CH (2022) Redefining North Atlantic right whale habitat-use patterns under climate change. *Limnology & Oceanography* Ino.12242. doi: [10.1002/lno.12242](https://doi.org/10.1002/lno.12242)
- Mignucci-Giannoni AA (1998) *Zoogeography of cetaceans off Puerto Rico and the Virgin Islands*. *Caribbean Journal of Science* 34:173–190.
- Miller DL, Becker EA, Forney KA, Roberts JJ, Cañadas A, Schick RS (2022) Estimating uncertainty in density surface models. *PeerJ* 10:e13950. doi: [10.7717/peerj.13950](https://doi.org/10.7717/peerj.13950)
- Mitchell E (1975) Preliminary report on Nova Scotia fishery for sei whales (*Balaenoptera borealis*). *Rep Int Whal Comm* 25:218–225.
- Mullin K, Ford R (1992) *Oregon II Cruise 92-01 (198): Exploratory Cruise for Marine Mammals and Longline Sampling of Pelagic Apex Predators*. NOAA National Marine Fisheries Service, Southeast Fisheries Science Center, Pascagoula, MS
- Mullin KD, Fulling GL (2003) *Abundance of cetaceans in the southern U.S. North Atlantic Ocean during summer 1998*. *Fishery Bulletin* 101:603–613.
- O'Brien O, Pendleton DE, Ganley LC, McKenna KR, Kenney RD, Quintana-Rizzo E, Mayo CA, Kraus SD, Redfern JV (2022) Repatriation of a historical North Atlantic right whale habitat during an era of rapid climate change. *Sci Rep* 12:12407. doi: [10.1038/s41598-022-16200-8](https://doi.org/10.1038/s41598-022-16200-8)
- PACM (2022) *Passive acoustic cetacean map, v1.1.3, accessed 2022-12-14*. NOAA Northeast Fisheries Science Center, Woods Hole, MA
- Palka D (2020) *Cetacean Abundance in the US Northwestern Atlantic Ocean Summer 2016. Northeast Fish Sci Cent Ref Doc. 20-05*. NOAA National Marine Fisheries Service, Northeast Fisheries Science Center, Woods Hole, MA
- Palka D, Aichinger Dias L, Broughton E, Chavez-Rosales S, Cholewiak D, Davis G, DeAngelis A, Garrison L, Haas H, Hatch J, Hyde K, Jech M, Josephson E, Mueller-Brennan L, Orphanides C, Pegg N, Sasso C, Sigourney D, Soldevilla M, Walsh H (2021) *Atlantic Marine Assessment Program for Protected Species: FY15 – FY19 (OCS Study BOEM 2021-051)*. U.S. Department of the Interior, Bureau of Ocean Energy Management, Washington, DC
- Palka DL (2006) *Summer abundance estimates of cetaceans in US North Atlantic navy operating areas (NEFSC Reference Document 06-03)*. U.S. Department of Commerce, Northeast Fisheries Science Center, Woods Hole, MA
- Palka DL, Chavez-Rosales S, Josephson E, Cholewiak D, Haas HL, Garrison L, Jones M, Sigourney D, Waring G, Jech M, Broughton E, Soldevilla M, Davis G, DeAngelis A, Sasso CR, Winton MV, Smolowitz RJ, Fay G, LaBrecque E, Leiness JB, Dettloff K, Warden M, Murray K, Orphanides C (2017) *Atlantic Marine Assessment Program for Protected Species: 2010-2014 (OCS Study BOEM 2017-071)*. U.S. Department of the Interior, Bureau of Ocean Energy Management, Washington, DC
- Payne PM, Wiley DN, Young SB, Pittman S, Clapham PJ, Jossi JW (1990) Recent fluctuations in the abundance of baleen whales in the southern Gulf of Maine in relation to changes in selected prey. *Fishery Bulletin* 88:687–696.
- Perkins NJ, Schisterman EF (2006) The Inconsistency of "Optimal" Cutpoints Obtained using Two Criteria based on the Receiver Operating Characteristic Curve. *American Journal of Epidemiology* 670–675.
- Prieto R, Janiger D, Silva MA, Waring GT, GonçAlves JM (2012) The forgotten whale: A bibliometric analysis and literature review of the North Atlantic sei whale *Balaenoptera borealis*: North Atlantic sei whale review. *Mammal Review* 42:235–272. doi: [10.1111/j.1365-2907.2011.00195.x](https://doi.org/10.1111/j.1365-2907.2011.00195.x)
- Prieto R, Silva MA, Waring GT, Gonalves JMA (2014) Sei whale movements and behaviour in the North Atlantic inferred from satellite telemetry. *Endang Species Res* 26:103–113. doi: [10.3354/esr00630](https://doi.org/10.3354/esr00630)
- Quintana-Rizzo E, Leiter S, Cole T, Hagbloom M, Knowlton A, Nagelkirk P, O'Brien O, Khan C, Henry A, Duley P, Crowe L, Mayo C, Kraus S (2021) Residency, demographics, and movement patterns of North Atlantic right whales *Eubalaena glacialis* in an offshore wind energy development area in southern New England, USA. *Endang Species Res* 45:251–268. doi: [10.3354/esr01137](https://doi.org/10.3354/esr01137)

- Read AJ, Barco S, Bell J, Borchers DL, Burt ML, Cummings EW, Dunn J, Fougères EM, Hazen L, Hodge LEW, Laura A-M, McAlarney RJ, Peter N, Pabst DA, Paxton CGM, Schneider SZ, Urian KW, Waples DM, McLellan WA (2014) [Occurrence, distribution and abundance of cetaceans in Onslow Bay, North Carolina, USA](#). *Journal of Cetacean Research and Management* 14:23–35.
- Record N, Runge J, Pendleton D, Balch W, Davies K, Pershing A, Johnson C, Stamieszkin K, Ji R, Feng Z, Kraus S, Kenney R, Hudak C, Mayo C, Chen C, Salisbury J, Thompson C (2019) Rapid Climate-Driven Circulation Changes Threaten Conservation of Endangered North Atlantic Right Whales. *Oceanog*. doi: [10.5670/oceanog.2019.201](#)
- Redfern JV, Kryc KA, Weiss L, Hodge BC, O'Brien O, Kraus SD, Quintana-Rizzo E, Auster PJ (2021) Opening a Marine Monument to Commercial Fishing Compromises Species Protections. *Front Mar Sci* 8:645314. doi: [10.3389/fmars.2021.645314](#)
- Rickard ME, Lomac-MacNair KS, Ireland DS, Leiter SM, Poster MD, Zoidis AM (2022) Evidence of Large Whale Socio-Sexual Behavior in the New York Bight. *Aquat Mamm* 48:401–417. doi: [10.1578/AM.48.5.2022.401](#)
- Roberts JJ, Best BD, Dunn DC, Treml EA, Halpin PN (2010) Marine Geospatial Ecology Tools: An integrated framework for ecological geoprocessing with ArcGIS, Python, R, MATLAB, and C++. *Environmental Modelling & Software* 25:1197–1207. doi: [10.1016/j.envsoft.2010.03.029](#)
- Roberts JJ, Best BD, Mannocci L, Fujioka E, Halpin PN, Palka DL, Garrison LP, Mullin KD, Cole TVN, Khan CB, McLellan WA, Pabst DA, Lockhart GG (2016) Habitat-based cetacean density models for the U.S. Atlantic and Gulf of Mexico. *Scientific Reports* 6:22615. doi: [10.1038/srep22615](#)
- Roberts JJ, Mannocci L, Schick RS, Halpin PN (2018) Final Project Report: Marine Species Density Data Gap Assessments and Update for the AFTT Study Area, 2017-2018 (Opt. Year 2), Document Version 1.2. Duke University Marine Geospatial Ecology Lab, Durham, NC
- Roberts JJ, Yack TM, Halpin PN (2023) Marine mammal density models for the U.S. Navy Atlantic Fleet Training and Testing (AFTT) study area for the Phase IV Navy Marine Species Density Database (NMSDD), Document Version 1.3. Duke University Marine Geospatial Ecology Lab, Durham, NC
- Robertson FC, Koski WR, Brandon JR, Thomas TA, Trites AW (2015) [Correction factors account for the availability of bowhead whales exposed to seismic operations in the Beaufort Sea](#). *Journal of Cetacean Research and Management* 15:35–44.
- Rosel PE, Wilcox LA, Yamada TK, Mullin KD (2021) A new species of baleen whale ( *Balaenoptera* ) from the Gulf of Mexico, with a review of its geographic distribution. *Marine Mammal Science* 37:577–610. doi: [10.1111/mms.12776](#)
- Ryan C, Boisseau O, Cucknell A, Romagosa M, Moscrop A, McLanaghan R (2013) [Final report for trans-Atlantic research passages between the UK and USA via the Azores and Iceland, conducted from R/V Song of the Whale 26 March to 28 September 2012](#). Marine Conservation Research International, Essex, UK
- Schick R, Halpin P, Read A, Urban D, Best B, Good C, Roberts J, LaBrecque E, Dunn C, Garrison L, Hyrenbach K, McLellan W, Pabst D, Palka D, Stevick P (2011) Community structure in pelagic marine mammals at large spatial scales. *Marine Ecology Progress Series* 434:165–181. doi: [10.3354/meps09183](#)
- Schilling MR, Seipt I, Weinrich MT, Frohock SE, Kuhlberg AE, Clapham PJ (1992) Behavior of individually-identified sei whales *Balaenoptera borealis* during an episodic influx into the southern Gulf of Maine in 1986. *FISHERY BULLETIN-NATIONAL OCEANIC AND ATMOSPHERIC ADMINISTRATION* 90:749–755.
- Silsbe GM, Behrenfeld MJ, Halsey KH, Milligan AJ, Westberry TK (2016) The CAFE model: A net production model for global ocean phytoplankton. *Global Biogeochemical Cycles* 30:1756–1777. doi: [10.1002/2016GB005521](#)
- Silva MA, Borrell A, Prieto R, Gauffier P, Bérubé M, Palsbøl PJ, Colaço A (2019) Stable isotopes reveal winter feeding in different habitats in blue, fin and sei whales migrating through the Azores. *R Soc open sci* 6:181800. doi: [10.1098/rsos.181800](#)
- Stone KM, Leiter SM, Kenney RD, Wikgren BC, Thompson JL, Taylor JKD, Kraus SD (2017) Distribution and abundance of cetaceans in a wind energy development area offshore of Massachusetts and Rhode Island. *J Coast Conserv* 21:527–543. doi: [10.1007/s11852-017-0526-4](#)
- Torres LG, McLellan WA, Meagher E, Pabst DA (2005) [Seasonal distribution and relative abundance of bottlenose dolphins, \*Tursiops truncatus\*, along the US mid-Atlantic coast](#). *Journal of Cetacean Research and Management* 7:153.
- Weiss SG, Cholewiak D, Frasier KE, Trickey JS, Baumann-Pickering S, Hildebrand JA, Van Parijs SM (2021) Monitoring the acoustic ecology of the shelf break of Georges Bank, Northwestern Atlantic Ocean: New approaches to visualizing complex acoustic data. *Marine Policy* 130:104570. doi: [10.1016/j.marpol.2021.104570](#)
- Whitt AD, Powell JA, Richardson AG, Bosyk JR (2015) [Abundance and distribution of marine mammals in nearshore waters off New Jersey, USA](#). *Journal of Cetacean Research and Management* 15:45–59.

- Wood SN (2011) Fast stable restricted maximum likelihood and marginal likelihood estimation of semiparametric generalized linear models. *Journal of the Royal Statistical Society: Series B (Statistical Methodology)* 73:3–36. doi: [10.1111/j.1467-9868.2010.00749.x](https://doi.org/10.1111/j.1467-9868.2010.00749.x)
- Zoidis AM, Lomac-MacNair KS, Ireland DS, Rickard ME, McKown KA, Schlesinger MD (2021) Distribution and density of six large whale species in the New York Bight from monthly aerial surveys 2017 to 2020. *Continental Shelf Research* 230:104572. doi: [10.1016/j.csr.2021.104572](https://doi.org/10.1016/j.csr.2021.104572)